

Department of Applied Chemistry

An Investigation of Polyacrylate Adsorption onto Hematite

Luke J Kirwan


**This thesis is presented as part of the requirements for
the award of the Degree of Doctor of Philosophy
of the Curtin University of Technology**

September 2002

DECLARATION

This thesis contains no material which has been accepted for the award of any other degree or diploma in any university.

To the best of my knowledge and belief this thesis contains no material previously published by any other person except where due acknowledgment has been made.

Signature: ... 

Date: ...30/9/02.....

ACKNOWLEDGEMENTS

First and foremost I would like to thank my supervisors, Associate Professor Bill van Bronswijk (Curtin University) and Doctor Phillip Fawell (CSIRO Minerals). Throughout the course of my PhD, they have always been generous with their time, encouraging, patient, and have offered a wealth of constructive feedback. I believe I could not have had two better supervisors and their support has been a major factor in this thesis coming to fruition. To both of them I owe a huge debt of gratitude, thank you so much.

There have been many other people that have contributed to this thesis. I would therefore like to thank Peter Chapman (Curtin University) for his technical and practical support in use of the FTIR spectrometer, Ian Davies (CSIRO) for XRD scans, Jason Scott (UNSW) for zeta potential measurements, Manijeh Reyhani (Curtin University) for her help with the AFM, and Phil for his assistance in the MALLS measurements.

In addition, I would like to thank the Centre for Microscopy and Microanalysis (UWA) for their assistance with TEM. In characterising materials used throughout this PhD many thanks must go to the Particle Analysis Service (CSIRO) and the Analytical Group (CSIRO).

I gratefully acknowledge the AJ Parker CRC for Hydrometallurgy (in particular the Alumina Production Program), and Curtin University of Technology (School of Applied Chemistry) for the opportunity to undertake this PhD. Special thanks to CSIRO Minerals, where I had my office and carried out most of my lab work.

Finally, I would like to thank the AJ Parker CRC for Hydrometallurgy and the Australian Research Council who supplied financial support throughout this PhD.

ABSTRACT

For the majority of tailings substrates, flocculant adsorption proceeds through hydrogen bonding of the amide functionalities with neutral surfaces. However, flocculation of Bayer process residue solids takes place in highly caustic liquors, typically using high molecular weight polyacrylates. This represents an almost unique situation, and implies a totally different adsorption mechanism. Direct examination of polyacrylate adsorption within the complex matrix of real liquors and a mixture of residue phases is difficult, making it necessary to focus on a model substrate (hematite) and synthetic liquors (pH 13 at high ionic strength).

Previous spectral studies have used *ex situ* techniques, with sample drying potentially altering the adsorbed species, leading to inconclusive results. This study presents for the first time direct *in situ* evidence of polyacrylate adsorption onto hematite obtained by Fourier Transform Infrared-Attenuated Total Reflection (FTIR-ATR) Spectroscopy. Adsorption and hence concentration of dilute polyacrylate solutions onto hematite-coated zinc selenide optics has provided spectra of adsorbed polymer under a range of conditions, unbiased by any contribution from the bulk polymer solution.

Analysis of the polyacrylate carbon-oxygen stretching frequencies established differing modes of adsorption at low and high pH conditions. At pH 2 adsorption proceeded through bidentate chelation of the carboxylate to a surface ferric ion, facilitated through deprotonation of a carboxylic acid group and removal of a hematite surface hydroxyl group, i.e. chemisorption. Unshifted carboxyl peaks in the spectrum enabled the unadsorbed 'loops' and 'tails' to be distinguished from the adsorbed polymer, and represented at least 70% of the total polymer chain length.

In contrast, at pH 13 adsorption of polyacrylate occurs via physisorption and was only possible with the addition of electrolyte. This adsorption was enhanced with increasing electrolyte concentrations up to 1 M NaCl. The hematite surface charge was negative at high pH, however with increasing ionic strength the specific adsorption of Na^+ ions decreased the negative surface charge, and at very high salt concentrations the surface became positively charged. For electrolyte with different monovalent cations, polymer adsorption increased in the order $\text{Li}^+ > \text{Na}^+ > \text{Cs}^+$.

The identity of the monovalent cation had no effect on the polymer solution dimensions but the ability to reduce the magnitude of the hematite surface charge followed the same trend. This finding is consistent with the 'structure making - structure breaking' model proposed by Berube and de Bruyn.

At both high and low pH, polyacrylate exhibited adsorption isotherms that are best described by the Langmuir expression. Surface coverage was greatest at low pH due to more available surface sites and the adsorbed polymer conformation (a greater fraction of loops and tails). Adsorbed conformation and hence maximum adsorption was independent of molecular weight at low pH, however at high pH maximum adsorption increased with increased molecular weight, indicating an adsorbed polymer configuration exhibiting a greater degree of loops and tails.

While the individual carboxylate-surface interaction was stronger at low pH than high pH, both were relatively weak. Despite this, none of the polymers could be removed by washing, demonstrating the strength and irreversibility of the multi-attached polymer molecules. The stronger individual carboxylate-surface interactions at low pH is indicative of a higher activation energy of formation, and may be a contributing factor to the slower rate of adsorption at low pH.

The rate of polyacrylate adsorption was dominated by mass transport limitations in all cases. The initial rate of adsorption was greater at lower polymer molecular weight, consistent with the relative polymer diffusion coefficients. This rate of adsorption was much less dependent on polymer molecular weight at high pH than at low pH, suggesting significantly different polymer-solvent interactions.

It was clearly demonstrated that the sodium ion concentration within the high ionic strength Bayer liquors is more than sufficient to facilitate polyacrylate adsorption on bauxite residue. There is no need to postulate calcium bridging between the polymer and surface, as has been suggested in previous studies. Improved settling and clarity associated with the presence of calcium on residue surfaces is more likely due to enhanced particle coagulation prior to flocculation. FTIR-ATR has been shown to be an excellent tool for the *in situ* examination of polyacrylate adsorption onto hematite, and will be a powerful technique for the characterisation and subsequent comparison of the adsorption behaviour of other systems.

TABLE OF CONTENTS

1.	INTRODUCTION	1
2.	LITERATURE REVIEW	3
2.1	Surface and Colloid Chemistry	3
2.2	Flocculants and Flocculation Processes	8
2.2.1	Flocculant Structure	8
2.2.2	Flocculation	8
2.2.2.1	Polymer Adsorption	9
2.2.2.2	Aggregate Formation	10
2.3	Studies of Relevance to Bayer Residue Flocculation	11
2.3.1	Surface Chemistry of Hematite	13
2.3.2	Solution Properties of Polyacrylate	18
2.3.3	Surface Chemistry of Polymer Adsorption	19
2.4	Techniques for Evaluating Flocculation Processes	24
2.4.1	Fourier Transform Infrared (FTIR) Spectroscopy	24
2.4.1.1	Carboxylate Adsorption Modes	25
2.4.1.2	Attenuated Total Reflection (ATR) Spectroscopy	27
2.4.1.3	FTIR-ATR Adsorption Studies	29
2.4.2	Adsorption Isotherms and Adsorption Kinetics	34
2.4.3	Quantitation of Adsorbed Species by FTIR-ATR	39
2.4.4	Multi-Angle Laser Light Scattering (MALLS)	41
2.4.5	Electrophoretic Mobility	44
3.	OBJECTIVES	50
4.	MATERIALS AND METHODS	52
4.1	Samples and Reagents	52
4.1.1	General Reagents	52
4.1.2	Aqueous Solutions	52
4.1.3	Colloidal Hematite Preparation	53
4.1.4	Adsorbates and Adsorbate Solutions	54

4.2	FTIR-ATR Spectroscopy	55
4.2.1	Instrumentation.....	55
4.2.2	Spectra of Concentrated Adsorbate Solution Species and Adsorbed Species on Hematite	56
4.2.3	Optical Parameters Study for FTIR-ATR Spectroscopy	57
4.2.4	Peak Area Determination	58
4.3	Multi-Angle Laser Light Scattering (MALLS)	58
4.4	Electrophoretic Mobility	60
4.5	Other Techniques	60
5.	MATERIALS CHARACTERISATION	61
5.1	Colloidal Hematite Characterisation	61
5.1.1	Chemical and Physical Properties.....	61
5.1.2	Transmission Electron Microscopy (TEM)	63
5.2	Concentrated Polymer Solution Characterisation.....	64
6.	ADSORPTION MODE OF POLYACRYLATES ON HEMATITE.....	66
6.1	Adsorption Mode at pH 2.....	66
6.2	Adsorption Mode at pH 13	75
7.	COLLOID DEPOSITION AND CHARACTERISATION.....	82
7.1	Infrared Analysis Area	82
7.2	Cast Hematite Film Deposition and Characterisation	83
7.3	Effect of Flowrate and Film Reproducibility	87
8.	FACTORS AFFECTING ADSORPTION AT HIGH pH	91
8.1	Effect of Electrolyte (NaCl) at pH 13	91
8.1.1	Effect of Electrolyte (NaCl) on Polyacrylate at pH 13	94
8.1.2	Effect of Electrolyte (NaCl) on the Hematite Surface at pH 13	98

8.2	Effect of Cation Type at pH 13	102
8.2.1	Effect of Cation Type on Polyacrylate at pH 13	103
8.2.2	Effect of Cation Type on the Hematite Surface at pH 12	104
9.	QUANTIFICATION OF ADSORPTION	109
9.1	Determining Adsorption Density from Peak Area	109
9.1.1	Characterisation of the ATR Solid-Liquid Interface	109
9.1.1.1	Polarisation Ratio Characterisation.....	112
9.1.1.2	Effect of Hematite Coated Optics	116
9.1.1.3	Effect of Adsorbed Polymer	118
9.1.2	Adsorbed Polymer Quantification	121
9.2	Adsorption Isotherms	125
9.2.1	Langmuir Isotherm Fit	128
9.2.2	Maximum Adsorption Densities	129
9.2.3	Interpreting the Langmuir ' <i>K</i> ' Value	139
9.3	Adsorption Kinetics.....	140
9.3.1	Effect of Flowrate.....	141
9.3.2	Effect of Polymer Concentration and Molecular Weight	146
9.3.3	Factors Affecting Subsequent Flocculation	153
10.	SUMMARY AND CONCLUSIONS.....	157
10.1	FTIR-ATR.....	157
10.2	Characterisation of the ATR Solid-Liquid Interface	158
10.3	Adsorption Mode at pH 2.....	159
10.4	Adsorption Mode at pH 13.....	160
10.5	Adsorption Isotherms and Adsorption Kinetics	164
10.6	Bayer Process Implications	167
10.6.1	Factors Affecting Flocculation.....	167
10.6.2	Aggregation Kinetics.....	169
11.	FUTURE WORK.....	171
11.1	Studies of Bayer Systems.....	171

11.2	Studies of Other Systems	175
12.	REFERENCES.....	177
APPENDIX A		cxcii
APPENDIX B		cxcii

LIST OF FIGURES

Figure 2.1: Schematic representations of (a and b) a diffuse double layer, and (c) surface potential as a function of distance from surface.....	3
Figure 2.2: The Stern model - schematic representation of (a and b) an electric double layer, and (c) reversal of charge due to specific counter-ion adsorption.....	5
Figure 2.3: Molecular structures of (a) polyacrylamide, and (b) polyacrylate.....	8
Figure 2.4: Schematic view of flocculant adsorbed onto a surface.....	9
Figure 2.5: Diagrammatic representation of the bridging mechanism of flocculation.....	11
Figure 2.6: Types of proposed adsorption mechanisms for polyacrylate onto an iron oxide surface; (a) asymmetric bidentate bridging complexation (Jones, Farrow and van Bronswijk, 1998c); (b) a possible calcium ion bridging structure as speculated by Connelly, Owen and Richardson (1986); (c) monodentate complexation, (d) coordination via sodium ion, (e) and (f) hydrogen bonding structures (Basu, Nitowski and The, 1986).....	23
Figure 2.7: Modes of carboxylate-metal complexation; (I) monodentate, (II) bidentate chelating, and (III) bidentate bridging.....	25
Figure 2.8: Schematic showing technical aspects of ATR spectroscopy.....	28
Figure 2.9: FTIR-ATR technique – adsorption onto a coated IRE.....	30
Figure 2.10: Typical Debye plot for a high molecular weight polymer.....	42
Figure 2.11: Relationship between r.m.s radius of gyration and hydrodynamic size.....	43
Figure 2.12: Schematic representation of the Brookhaven ZetaPlus instrument (Brookhaven Instrument Corporation internet site).....	47
Figure 4.1: Schematic representation of FTIR-ATR experimental set-up.....	55
Figure 4.2: Schematic representation of the Harrick ‘Seagull’ variable angle reflection accessory, showing the mirrors M1 to M8.....	56

Figure 4.3:	Diagram of the peak areas determined in this study. Type 1 (valley-valley) includes: 1720 cm^{-1} ($1630 - 1805\text{ cm}^{-1}$) and 1560 cm^{-1} peaks ($1484 - 1636\text{ cm}^{-1}$); and Type 2 (three-valley, perpendicular drop) includes: 1410 cm^{-1} peak ($1362, 1436$ and 1488 cm^{-1}).....	58
Figure 4.4:	Schematic representation of DAWN DSP photometer flowcell, showing relationship between (a) observed angle and scattering angle, and (b) the detectors array around the flowcell. Detectors 1, 2 and 3 can not be used with aqueous solutions due the solvent scattering.....	59
Figure 5.1	TEM images of colloidal hematite particles.....	63
Figure 5.2:	Spectra of concentrated PAA450K (1 wt%) solution species at pH 2 and pH 13 (1 M NaCl).....	64
Figure 6.1:	Adsorption of PAA450K (50 ppm) onto hematite at pH 2 as a function of time.....	67
Figure 6.2:	Schematic representation of the proposed mode of adsorption of polyacrylic acid onto hematite at pH 2.....	68
Figure 6.3:	Schematic representation of pimelic acid molecule.....	70
Figure 6.4:	Adsorption of pimelic acid (100 ppm) onto hematite at pH 2 as a function of time.....	70
Figure 6.5:	Spectra of concentrated pimelic acid (3 wt%) solution species at pH 2 and pH 13.....	71
Figure 6.6:	Diagrammatic representation of the large volume occupied by adsorbed polyacrylic acid in the measured interaction volume of the evanescent wave resulting in detection of solvent displacement. In comparison, adsorbed pimelic acid occupies a small volume and no solvent displacement is detected.....	74
Figure 6.7:	Adsorption of PAA13M (50 ppm) onto hematite at pH 13 (no added salt) for 30 minutes.....	75
Figure 6.8:	Adsorption of PAA450K (50 ppm) onto hematite at pH 13 (1 M NaCl) as a function of time.....	76
Figure 6.9:	Schematic representation of the proposed mode of adsorption of polyacrylate onto hematite at pH 13 in the presence of excess Na^+ ions.....	78

Figure 6.10: Desorption experiment for PAA5K (50 ppm) adsorbed onto hematite at pH 13 (1 M NaCl).....	79
Figure 6.11: Adsorption of pimelic acid (100 ppm) onto hematite at pH 13 (1 M NaCl) for 20 minutes.....	80
Figure 7.1: Determination of infrared analysis area: 3300 cm^{-1} water peak area versus water droplet diameter.....	82
Figure 7.2: Adsorption of PAA2K (50 ppm) onto hematite after 20 mins (monitored by the 1720 cm^{-1} peak area) as a function of colloid volume used to cast the hematite film (flowrate 1 mL min^{-1}).....	84
Figure 7.3: Adsorption of PAA450K (50 ppm) onto hematite after 30 minutes (monitored by the 1720 cm^{-1} peak area) as a function of colloid volume used to cast the hematite film (flowrate 1 mL min^{-1}).....	84
Figure 7.4: Cast hematite film: (a) optical microscopy; and (b) AFM scan data.....	85
Figure 7.5: Image analysis of hematite film cross-section, showing the grey value and corresponding film thickness.....	87
Figure 7.6: Adsorption of PAA450K (50 ppm) at pH 2 as a function of time and flowrate (monitored by the 1720 cm^{-1} peak area).....	88
Figure 7.7: Adsorption of polyacrylic acid at pH 2 as monitored by the area of the carbonyl stretching peak (1720 cm^{-1}) as a function of time and polymer molecular weight.....	88
Figure 7.8: Ratio of the unadsorbed carbonyl stretching peak (1720 cm^{-1}) area to the adsorbed symmetric carboxylate ion stretching peak (1410 cm^{-1}) area for polymers adsorbed with varying molecular weight at pH 2, as shown in Figure 7.7.....	90
Figure 8.1: Adsorption of PAA450K (50 ppm) onto hematite at pH 13, as a function of NaCl concentration and monitored by the 1560 cm^{-1} peak area.....	91
Figure 8.2: The plateau adsorption of polyacrylate (PAA450K) at pH 13 from Figure 8.1 as a function of NaCl concentration.....	92
Figure 8.3: Schematic representation of how increasing the electrolyte concentration affects both the dimensions of polyacrylate in solution and the hematite surface at pH 13. The electrolyte shields the negative charge of both the hematite surface and the carboxylate groups on the polymer.....	93

Figure 8.4: Adsorption of PAA13M (50 ppm) at pH 14.....	94
Figure 8.5: The radius of gyration (r_g) of PAA450K (200 ppm) as a function of solution pH.....	95
Figure 8.6: The radius of gyration (r_g) of: (a) PAA13M (40 ppm) as a function of pH, and (b) as a function of NaCl concentration at pH 13.....	97
Figure 8.7: Zeta potential of hematite measured as a function of pH.....	99
Figure 8.8: Zeta potential of hematite at pH 13 measured as a function of NaNO ₃ concentration.....	99
Figure 8.9: Adsorption of PAA450K (50 ppm) at pH 13 (LiOH, NaOH or CsOH) and 0.2 M added electrolyte (LiCl, NaCl or CsCl) as monitored by the area of the 1560 cm ⁻¹ peak area.....	102
Figure 8.10: The radius of gyration (r_g) of PAA450K (200 ppm) at pH 13 and 0.2 M added salt as a function of cation type.....	103
Figure 8.11: Zeta potential of hematite at pH 12 measured as a function of electrolyte (LiNO ₃ or NaNO ₃) concentration.....	105
Figure 9.1: Decay of the evanescent wave intensity. Area under curve for $x(0 \rightarrow 1) = 0.633$. Total area under curve is 1.0.....	111
Figure 9.2: Intensity of the evanescent wave, assuming a box car function.....	111
Figure 9.3: The 1560 cm ⁻¹ peak area as a function of polymer solution concentration (wt%) for PAA450K at pH 13 (1 M NaCl).....	123
Figure 9.4: The 1560 cm ⁻¹ peak area as a function of polymer solution concentration (wt%) for PAA13M at pH 13 (1 M NaCl).....	123
Figure 9.5: The 1720 cm ⁻¹ peak area as a function of polymer solution concentration (wt%) for PAA450K at pH 2.....	124
Figure 9.6: PAA450K adsorption at pH 2 (monitored by the 1720 cm ⁻¹ peak area), demonstrating equivalent adsorption achieved by either direct application of 50 ppm polymer solution or by sequential addition of increasing polymer solution concentration up to 50 ppm.....	126

Figure 9.7: Adsorption of PAA450K at pH 2 (monitored by 1720 cm^{-1} peak area) and at pH 13 and 1 M NaCl (monitored by 1560 cm^{-1} peak area) at polymer concentrations of 5, 10, 20 and 50 ppm.....	127
Figure 9.8: Adsorption of PAA13M at pH 13 and 1 M NaCl (monitored by 1560 cm^{-1} peak area) at polymer concentrations of 6, 11, 23 and 56 ppm.....	127
Figure 9.9: Plot of plateau absorbance values as a function of polymer concentration in Figure 9.7 for PAA450K adsorption at both pH 2 and pH 13 (1 M NaCl) and the subsequent Langmuir adsorption isotherm fit to the data.....	128
Figure 9.10: Plot of plateau absorbance values as a function of polymer concentration in Figure 9.8 for PAA13M adsorption at pH 13 (1 M NaCl) and the subsequent Langmuir adsorption isotherm fit to the data.....	129
Figure 9.11: Close packed arrangement of spherical particles.....	131
Figure 9.12: The 1410 cm^{-1} peak area as a function of polymer solution concentration (wt%) for PAA450K at pH 13 (1 M NaCl).....	133
Figure 9.13: Adsorption of 50 ppm PAA450K at pH 2 (monitored by 1720 cm^{-1} peak area) and at a flowrate of 0.17 mL min^{-1} , together with the predicted response, as determined using Equation 9.8, for the initial relative rate of reaction. Also shown is the relative rate as determined from the slope of the plot of $\ln(A_{\infty}/(A_{\infty} - A))$ as a function of time. Both the fast relative rate of adsorption at initial times and the slower relative rate of adsorption at longer times are given.....	143
Figure 9.14: Adsorption of 50 ppm PAA450K at pH 2 (monitored by 1720 cm^{-1} peak area) and at a flowrate of 0.5 mL min^{-1} , together with the predicted response, as determined using Equation 9.8, for the initial relative rate of reaction. Also shown is the relative rate as determined from the slope of the plot of $\ln(A_{\infty}/(A_{\infty} - A))$ as a function of time. Both the fast relative rate of adsorption at initial times and the slower relative rate of adsorption at longer times are given.....	143
Figure 9.15: Adsorption of 50 ppm PAA450K at pH 2 (monitored by 1720 cm^{-1} peak area) and at a flowrate of 1.0 mL min^{-1} , together with the predicted response, as determined using Equation 9.8, for the initial relative rate of reaction. Also shown is the relative rate as determined from the slope of the plot of $\ln(A_{\infty}/(A_{\infty} - A))$ as a function of time. Both the fast relative rate of adsorption at initial times and the slower relative rate of adsorption at longer times are given.....	144

- Figure 9.16: Adsorption of 50 ppm PAA450K at pH 2 (monitored by 1720 cm^{-1} peak area) and at a flowrate of 2.0 mL min^{-1} , together with the predicted response, as determined using Equation 9.8, for the initial relative rate of reaction. Also shown is the relative rate as determined from the slope of the plot of $\ln(A_{\infty}/(A_{\infty} - A))$ as a function of time. Both the fast relative rate of adsorption at initial times and the slower relative rate of adsorption at longer times are given.....144
- Figure 9.17: Relative rate of adsorption of PAA450K at pH 2 as a function of flowrate up to 1 mL min^{-1} from Table 9.8.....146
- Figure 9.18: Adsorption of 5 ppm PAA450K at pH 2 (monitored by 1720 cm^{-1} peak area), together with the predicted response, as determined using Equation 9.8, for the initial relative rate of reaction. Also shown is the relative rate as determined from the slope of the plot of $\ln(A_{\infty}/(A_{\infty} - A))$ as a function of time. Both the fast relative rate of adsorption at initial times and the slower relative rate of adsorption at longer times are given.....147
- Figure 9.19: Adsorption of 50 ppm PAA450K at pH 2 (monitored by 1720 cm^{-1} peak area), together with the predicted response, as determined using Equation 9.8, for the initial relative rate of reaction. Also shown is the relative rate as determined from the slope of the plot of $\ln(A_{\infty}/(A_{\infty} - A))$ as a function of time. Both the fast relative rate of adsorption at initial times and the slower relative rates of adsorption at longer times are given.....147
- Figure 9.20: Adsorption of 5 ppm PAA450K at pH 13 (1 M NaCl) (monitored by 1560 cm^{-1} peak area), together with the predicted response, as determined using Equation 9.8, for the initial relative rate of reaction. Also shown is the relative rate as determined from the slope of the plot of $\ln(A_{\infty}/(A_{\infty} - A))$ as a function of time. Both the fast relative rate of adsorption at initial times and the slower relative rate of adsorption at longer times are given.....148
- Figure 9.21: Adsorption of 50 ppm PAA450K at pH 13 (1 M NaCl) (monitored by 1560 cm^{-1} peak area), together with the predicted response, as determined using Equation 9.8, for the initial relative rate of reaction. Also shown is the relative rate as determined from the slope of the plot of $\ln(A_{\infty}/(A_{\infty} - A))$ as a function of time. Both the fast relative rate of adsorption at initial times and the slower relative rates of adsorption at longer times are given.....148
- Figure 9.22: Adsorption of 50 ppm PAA13M at pH 13 (1 M NaCl) (monitored by 1560 cm^{-1} peak area), together with the predicted response, as determined using Equation 9.8, for the initial relative rate of reaction. Also shown is the relative rate as determined from the slope of the plot of $\ln(A_{\infty}/(A_{\infty} - A))$ as a function of time. Both the fast relative rate of adsorption at initial times and the slower relative rate of adsorption at longer times are given.....149

Figure 9.23: Adsorption of 50 ppm PAA13M at pH 2 (monitored by 1720 cm^{-1} peak area), together with the predicted response, as determined using Equation 9.8, for the initial relative rate of reaction. Also shown is the relative rate as determined from the slope of the plot of $\ln(A_{\infty}/(A_{\infty} - A))$ as a function of time. Both the fast relative rate of adsorption at initial times and the slower relative rate of adsorption at longer times are given.....149

Figure 9.24: Adsorption of 5 ppm PAA450K at pH 13 (1 M NaCl) (monitored by the 1560 cm^{-1} peak) onto hematite, with the first order fit as determined using Equation 9.8.....154

Figure 10.1: Schematic representation of the proposed adsorption mode of polyacrylic acid onto hematite at pH 2.....157

Figure 10.2: Schematic representation of the proposed adsorption mode of polyacrylate onto hematite at pH 13 with and without added electrolyte.....163

Figure A: Typical X-ray Diffractogram obtained for the colloidal hematite samples prepared in this study. The red lines represent peak positions obtained for a synthetic hematite reference sample (PDF number 33, 664).....xcxi

Figure B: Particle size distribution obtained for second hematite colloid prepared (typical of all colloids prepared).....xcxii

LIST OF TABLES

Table 2.1:	Some selected iep and pzc values for hematite.....	14
Table 2.2:	Selected spectroscopic studies determining the bonding mechanism of carboxylates onto mineral surfaces.....	24
Table 2.3:	Solution size and molecular weight of some selected polyacrylate and hydrolysed polyacrylamide polymers.....	44
Table 4.1:	Adsorbates used in this study.....	54
Table 5.1:	Physical and chemical properties of prepared hematite colloids.....	62
Table 6.1:	Comparison of FTIR-ATR peak assignments for PAA450K (1 wt% - 10 000 ppm) at pH 2 and pH 13 (1 M NaCl), and after adsorption of PAA450K (50 ppm) at pH 2.....	67
Table 6.2:	Comparison of spectral peak position for adsorption of pimelic acid at pH 2.....	72
Table 6.3:	Comparison of spectral peak positions for polyacrylate (PAA450K) at pH 13 (1 M NaCl) in solution and after adsorption onto hematite at pH 13 (1 M NaCl).....	77
Table 9.1:	Determination of the fraction of parallel (X) and perpendicular ($1-X$) polarised infrared radiation at 45° and 50° incident angles.....	114
Table 9.2:	Effective thickness (d_e) calculation for 1 wt% polymer ($n_2 = 1.360$) and ZnSe ($n_1 = 2.426$ at 1720 cm^{-1} and 2.424 at 1560 cm^{-1}) interface. d_e was determined at 1720 cm^{-1} for adsorption at pH 2 and 1560 cm^{-1} for adsorption at pH 13 (1 M NaCl).....	122
Table 9.3:	Calculated absorptivity (ϵ) for the 1720 cm^{-1} integrated peak area of PAA450K at pH 2 and the 1560 cm^{-1} integrated peak areas of PAA450K and PAA13M at pH 13 (1 M NaCl).....	125
Table 9.4:	The maximum integrated peak area and K as determined by Langmuir isotherm fit of the data in Figures 9.9 and 9.10.....	129

Table 9.5:	The maximum adsorption of PAA450K at pH 2 and at pH 13 (1 M NaCl) and PAA13M at pH 13 (1 M NaCl) onto hematite, expressed as an equivalent solution concentration.....	130
Table 9.6:	Adsorption densities determined using porous hematite film model and by applying the FTIR-ATR adsorption density equation (Sperline, Muralidharan and Freiser, 1987).....	132
Table 9.7:	Adsorption density values for PAA450K at pH 2 and PAA450K and PAA13M at pH 13 (1 M NaCl), and the number of equivalent monolayer coverages that these adsorption densities represent.....	135
Table 9.8:	Relative rates of 50 ppm PAA450K adsorption at pH 2 as a function of flowrate and derived from the slope of the graph of $\ln(A_{\infty}/(A_{\infty} - A))$ versus time (t) (Equation 9.9) for initial adsorption times as shown in Figures 9.13 to 9.16.....	145
Table 9.9:	Relative rates of adsorption (k') for polymer adsorption at varying concentration.....	150
Table 9.10:	Rate constants for the adsorption of polyacrylate onto hematite at a flow rate of 1 mL min ⁻¹ and diffusional fluxes that correspond to 50 ppm bulk polymer solution concentration.....	151
Table 9.11:	The time taken to achieve 50% maximum surface coverage ($t_{0.5A_{max}}$) for the adsorption profiles shown in Figures 9.18 to 9.22, determined by a first order fit of the data.....	155

1. INTRODUCTION

The Bayer process was patented over 110 years ago by Karl Bayer as a method to refine alumina from bauxite (Bayer, 1888). To this day the general principles of this process remain unchanged, and are used extensively in alumina refineries throughout the world. Refining of bauxite to alumina is arguably the most important example of hydrometallurgy in Australia, with the alumina industry being the second largest mineral earning industry within Australia, and Australia the largest producer of alumina worldwide.

Bauxitic ore from the Darling escarpment in Western Australia is mined to a depth of 10 to 20 metres and is crushed before processing. The top few metres of earth mined is overburden material and contains primarily topsoil and vegetation. Contained within the ore are clay materials such as kaolinite and halloysite, which are referred to as reactive silicas. They will dissolve in Bayer liquor and can react with solution species, contributing to scale formation. Commonly, these dissolved silicas are controlled by precipitation prior to digestion (desilication) to form insoluble desilication products (DSPs). The bauxite ore is then digested in hot caustic (~5 M) until the liquor becomes supersaturated with dissolved alumina. Vegetation introduced with the bauxite becomes a source of dissolved organic contamination and is present mainly as a variety of uncharacterised humic acids and sodium oxalate. The remaining solid residue is removed and the supersaturated liquor is cooled and seeded so that the available alumina can precipitate as hydrated alumina (gibbsite – $\text{Al}(\text{OH})_3$). Once the gibbsite is reclaimed it is calcined at high temperature to remove water of crystallisation and dehydroxlate it, giving the commercial alumina (Al_2O_3) product.

The Bayer process generates large volumes of waste residue in alkaline liquors. This residue has a small particle size, which contributes to its very poor settling behaviour. The residue is removed by solid-liquid separation, which is typically achieved through flocculation in a series of gravity thickeners, with significant quantities of flocculant being consumed at each stage. Throughput and clarity are the critical factors, and the small amount of solids left in the clarified liquor are removed by filtration. The solid residue waste generally consists of silica, sodium aluminosilicates (DSPs) and iron oxides (hematite, goethite), and is aptly named ‘red

mud'. The flocculants used are generally high molecular weight polyacrylates or acrylate/acrylamide copolymers. More recently the hydroxamate functionality has been introduced into the polymer structure, offering the potential for improved flocculation efficiency.

While there have been significant advances in the nature of flocculants used to treat bauxite residue, comparatively little fundamental research has been carried out to characterise the flocculant adsorption process. Refinery liquors are highly caustic, have a very high ionic strength and contain a wide range of inorganic and organic impurities, many at much higher concentrations than added flocculants, which greatly complicates any experimental study. For this study, hematite was chosen as the most appropriate model substrate, as it is the dominant mineral found in Bayer residue solids in Australia. The work has sought to examine the fundamental aspects of how the carboxylate functionality, which is dominant in Bayer-process flocculants, interacts with hematite during the adsorption process. A better understanding of this process may allow more efficient application of flocculants and ultimately lead to the development of improved flocculation products.

Chapter 2 presents an overview of the literature in relation to flocculation and surface chemistry in general, followed by a comprehensive review of studies dealing with residue flocculation in the Bayer process. An examination of the surface chemistry of hematite and the solution properties of polyacrylate along with the instruments and techniques that were used to achieve the goals of this study are also reviewed. The specific objectives of this study are covered in Chapter 3, with the materials, instrumentation, experimental design and methods outlined in Chapter 4. The results for the characterisation of the materials used in this study are presented and discussed in Chapter 5. The mode of polyacrylate adsorption onto hematite is dealt with in Chapter 6, and the reproducibility of the FTIR-ATR measurements of adsorption are examined in Chapter 7, enabling the factors affecting adsorption at high pH to be investigated in Chapter 8. Kinetic and equilibria factors affecting the adsorption process are presented and discussed in Chapter 9. A summary of the results and the conclusions drawn from the study are given in Chapter 10 along with the implications these results have to residue flocculation within the Bayer process. Future work that could stem from the results of the study is presented in Chapter 11.

2. LITERATURE REVIEW

2.1 Surface and Colloid Chemistry

When brought into contact with an aqueous medium, most minerals acquire a surface charge. This surface charge has an influence on the distribution of nearby ions in solution. Ions of opposite charge are attracted to the surface and ions of like charge are repelled, with the ions distributed in a diffuse manner throughout the aqueous medium (Figure 2.1a). This phenomenon, in addition to mixing due to thermal motion, is described as the electric double layer (Shaw, 1992, pp174). The electric double layer can be regarded as consisting of two regions, an inner region which may include specifically adsorbed ions, and an outer diffuse region where the ions are distributed according to the influence of electrostatic forces and thermal motion.

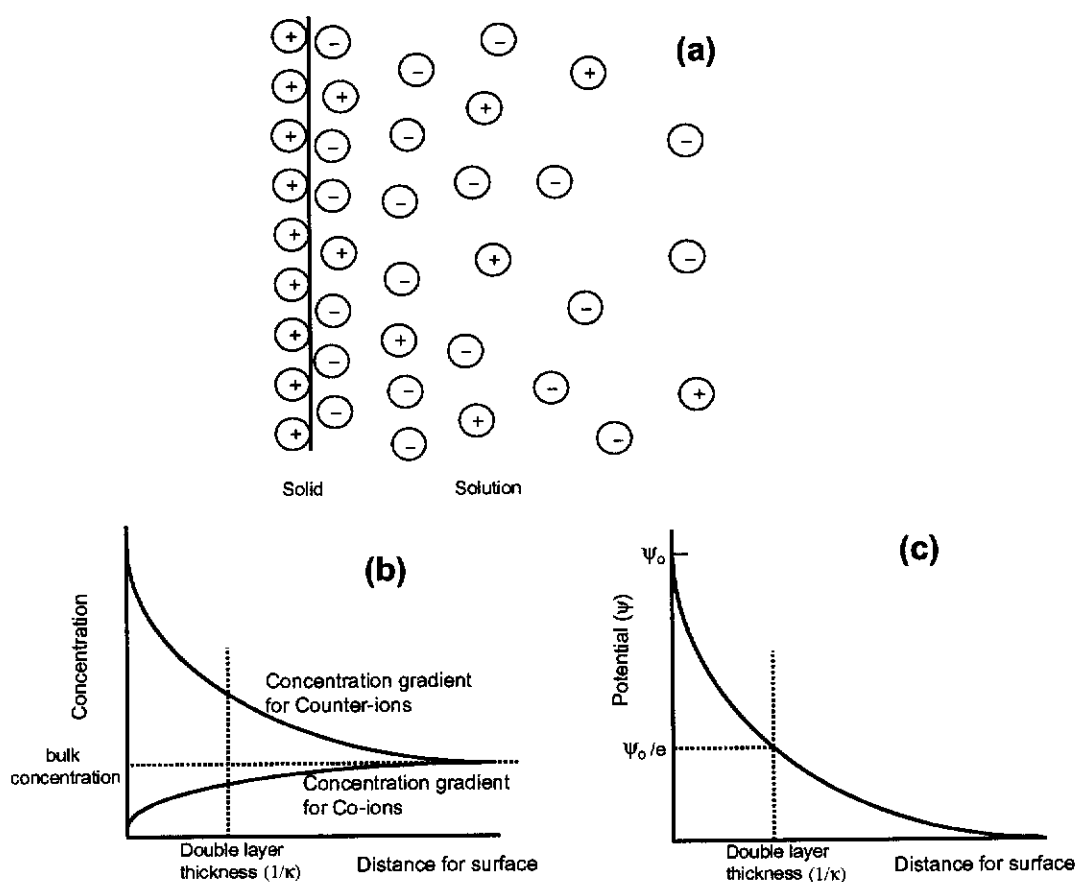


Figure 2.1: Schematic representations of (a and b) a diffuse double layer, and (c) surface potential as a function of distance from surface.

The Gouy-Chapman model of the diffuse part of the double layer is perhaps the simplest quantitative treatment of the diffuse region and is based on several assumptions. The model assumes that the surface is flat, infinite and uniform in charge; the ions in the diffuse region are point charges and are distributed according to the Boltzmann distribution; and the only influence of the solvent is through its dielectric constant, which remains a constant value throughout the diffuse region (Hunter, 1981, pp22).

The double layer thickness ($1/\kappa$ as shown in Figures 2.1b and c) depends on the surface potential (ψ_0) and the surface charge (σ_0) as shown by Equation 2.1:

$$\sigma_0 = \epsilon \kappa \psi_0 \quad (\text{Equation 2.1})$$

where κ is related to the ionic composition of the medium and ϵ the permittivity.

When the surface potential is relatively low, there is an exponential decrease in potential with distance from the surface and the double layer thickness ($1/\kappa$) is at a surface potential of (ψ_0/e) (Figure 2.1c). At charged surfaces, where the potential is likely to be relatively high, the potential will decrease at a greater than exponential rate (Shaw, 1992, pp180).

While the diffuse region of the electrical double layer can be modelled using point charges, the finite size of ions will have an influence on the inner part of the diffuse double layer. The Stern model (represented schematically in Figures 2.2a and b) considers the possibility of specifically adsorbed ions and divides the double layer into two parts that are separated by the Stern plane, which is located at approximately one hydrated ion radius from the surface. Ions are specifically adsorbed by electrostatic and/or van der Waals forces that are strong enough to overcome thermal agitation and may be dehydrated. These specifically adsorbed ions are located in what is known as the Stern layer, with ions located beyond the Stern plane being described by the Gouy-Chapman model (Shaw, 1992, pp182).

The potential at the Stern plane is referred to as the Stern potential (ψ_d in Figure 2.2b). When specific adsorption takes place, counter-ion adsorption usually predominates (as represented schematically in Figure 2.2a) and it is possible for reversal of charge to take place (Figure 2.2c). It is assumed that the surface of shear

(Figure 2.2a) is located a small distance further out from the particle surface than the Stern plane and separates the liquid adhering to the particle and the mobile liquid phase.

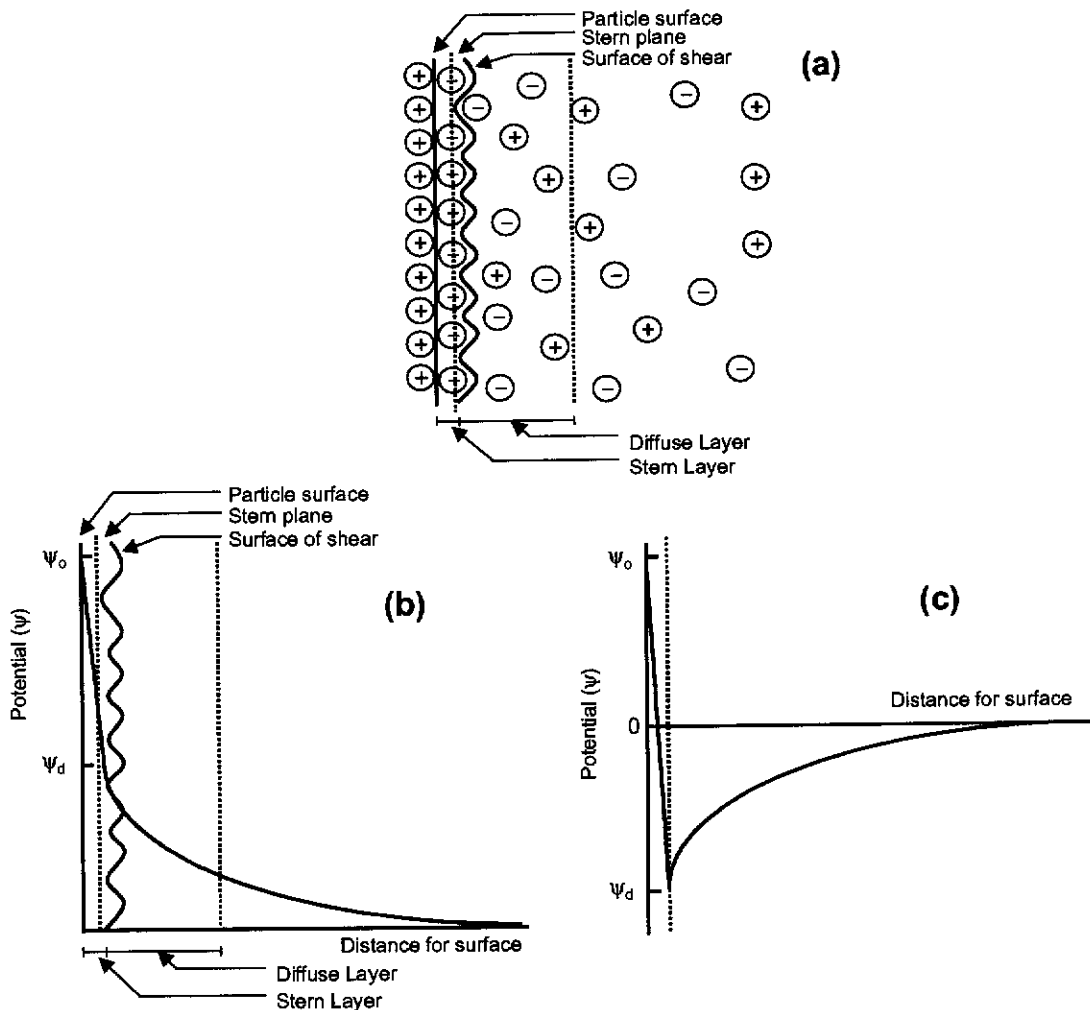


Figure 2.2: The Stern model - schematic representation of (a and b) an electric double layer, and (c) reversal of charge due to specific counter-ion adsorption.

The Stern model has been further refined to include an outer Helmholtz plane, which is the same as the Stern plane, and an inner Helmholtz plane. The inner Helmholtz plane describes the region of specifically adsorbed ions that are dehydrated (at least in the direction of the surface). In addition, instead of the surface being treated as uniform in charge, the refined model treats the surface charge as being located at discrete sites on the surface, affecting the ions adsorbed in the inner Helmholtz plane and rearranging neighbouring surface charges (Shaw, 1992, pp188).

The point at which the surface charge density (σ) is zero is referred to as the point of zero charge (pzc). For substrates such as AgI it is possible to estimate the surface potential (ψ_0) from a knowledge of the pzc and the concentration of the potential-determining ion in solution, because they obey the Nernst equation (Equation 2.2):

$$\psi_0 = (RT / F)[pAg_{pzc} - pAg] \quad (\text{Equation 2.2})$$

where R is the gas constant, T is the temperature in Kelvin, F is Faraday's constant, pAg is $-\log_{10}[Ag^+]$ and pAg_{pzc} is the concentration of silver ions when σ is zero.

It is not possible to determine the surface potential for oxide materials because they do not obey the Nernst equation. This is due to the presence of surface hydroxyl groups and the way they affect the surface charge behaviour (Hunter, 1993, pp231).

Even if the surface potential can be reasonably estimated, this may be of little assistance in predicting colloidal behaviour. It is the apparent surface charge of a particle and the distribution of ions near the surface that affect the way that discrete particles interact. They are particularly important physical properties of colloidal suspensions, as they determine the tendency for the particles to aggregate or coagulate. For example, a lyophobic sol such as a colloidal hematite suspension will tend to aggregate by the addition of electrolyte. The added electrolyte compresses the diffuse parts of the particle's double layers and may also specifically adsorb to the particle surface. Depending on the strength of attractive and repulsive forces, the sol may destabilise, leading to coagulation.

The Derjaguin-Landau and Verwey-Overbeek (DLVO) theory describes the stability of lyophobic sols, particularly in relation to added electrolyte (Derjaguin and Landau, 1941; Verwey and Overbeek, 1948). In relation to the stability of dispersions, application of this theory has enabled calculations to be made for the interaction between spheres, which estimate the energy due to the overlap of the electric double layers (usually repulsive) and the van der Waals energy (usually attractive) in terms of distance between approaching particles. This is normally interpreted by the total interaction energy in terms of the distance between the particles and stability of the colloid, and is represented by an interaction energy-distance diagram (Shaw, 1992, pp212).

In a more practical sense, observations of coagulation experiments have shown that the concentration of electrolyte required to induce coagulation of a charged, stabilised colloid is inversely dependent on the valency of the electrolyte counter-ion. This is referred to as the Schulze-Hardy rule (Hunter, 1993, pp51, 52). Also, there has been shown to be little dependence on the character of the counter-ion, charge number of the co-ion, and concentration and nature of the sol. With regards to the character of the counter-ion, it has generally been found that the larger the counter-ion, the smaller the radius of hydration and therefore the closer the counter-ion can get to the surface of the colloid. Therefore, larger counter-ions have a greater destabilising effect than smaller counter-ions that have larger radii of hydration (Verrall, Warwick and Fairhurst, 1999).

To determine the way in which charged particles interact, the obvious relevant measure in predicting colloidal behaviour is a knowledge of the Stern potential (ψ_d). Practically, this is not possible and it must be estimated from the zeta potential (ζ). The zeta potential is the potential difference between the surface of shear and the bulk phase. In addition to ions in the Stern layer, it is possible that a small amount of solvent will be bound to the charged particle surface and hence form part of the measured zeta potential. For these reasons the zeta potential is marginally smaller in value than the Stern potential (Stumm, 1992, pp50). Generally these values are assumed to be the same, although differences will be most clearly pronounced at high potentials and at high ionic strength (Shaw, 1992, pp185). The magnitude and sign of the zeta potential is indicative of the magnitude and sign of the electrokinetic charge, which is the charge on the shear plane, not the charge at the particle surface. The pH at which the zeta potential is zero is called the iso-electric point (iep) (Stumm, 1992, pp50).

In the case of oxide materials, for which hydrogen ions are the potential-determining ion, the point of zero charge density (σ) can be determined by potentiometric titration. This provides a 'point of zero salt effect' value, which is the intersection of the surface charge-pH curve obtained at various concentrations of indifferent electrolyte (e.g. using NaCl or KNO₃ as the electrolyte). This 'point of zero salt effect' value is indicative of the pzc as long as the only exchange reaction between the solution and surface is proton adsorption/desorption, there is an absence of a

permanent charge, and there is no surface dissolution/precipitation reactions (Chvedov, Ostap and Le, 2001). If there is no specific adsorption of ions to the particle surface then the iep and the pzc of the surface will be the same. This fact can be used as a measure of the validity of using potentiometric titration to determine the pzc of oxide materials (Hunter, 1993, pp255).

2.2 Flocculants and Flocculation Processes

2.2.1 Flocculant Structure

Polyacrylamide (Figure 2.3a) is a water-soluble polymer widely used in the mining industry as a flocculant to aid solid-liquid separation. The advantages of polyacrylamide include its very high molecular weight ($1-3 \times 10^7$ Dalton), strong hydrogen bonding with mineral particles, and its ability to be modified to acrylamide/acrylate copolymers by partial hydrolysis (Rangaraj, Vangani and Rakshit, 1997). Partial hydrolysis of the acrylamide polymer is achieved with strong alkali at elevated temperatures, converting the amide groups of the polymer to carboxylates. Due to the high caustic levels found in the Bayer-process thickeners, the flocculants most commonly used are polyacrylates (Figure 2.3b) or highly anionic acrylamide/acrylate copolymers (Connelly, Owen and Richardson, 1986).

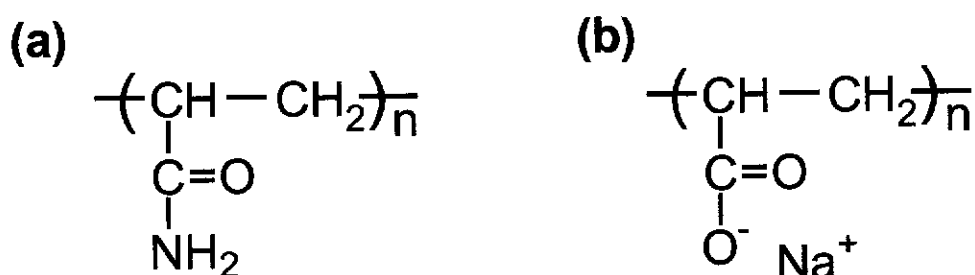


Figure 2.3: Molecular structures of (a) polyacrylamide, and (b) polyacrylate.

2.2.2 Flocculation

The process of flocculation consists of two main steps. The first is the adsorption of the flocculant onto the particles within a slurry. The second is the actual aggregation of the particles, either through bridging or charge neutralisation.

2.2.2.1 Polymer Adsorption

Polymer adsorption onto mineral particles is typically characterised by ‘trains’ of adsorbed polymer with ‘loops’ and ‘tails’ of unadsorbed polymer (Figure 2.4) that extend into the solution. Hence, flocculant adsorption characteristically reaches a limiting value, corresponding to a large excess over that expected for monolayer coverage of polymer adsorbed flat on the solid surface (Eirich, 1977; Misra, 1996).

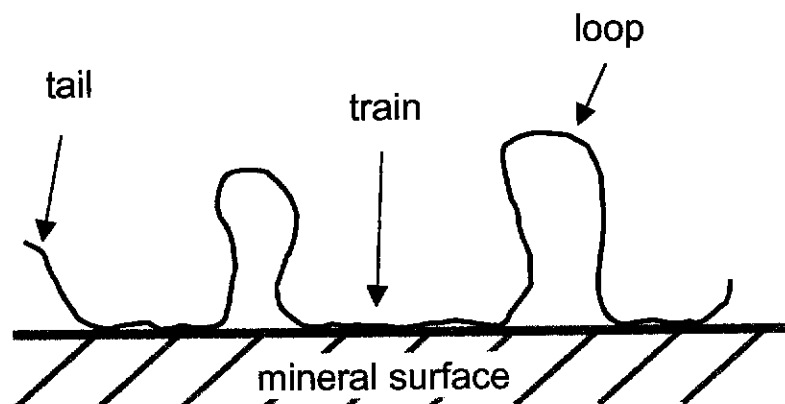


Figure 2.4: Schematic view of flocculant adsorbed onto a surface.

Polymer adsorption onto a substrate is usually attributed to electrostatic interactions or hydrogen bonding. Cationic or anionic polyelectrolytes adsorb onto particles of opposite charge resulting in a charge neutralisation bonding mechanism (Laird, 1997; Vermohlen *et al.*, 2000). Bonding of nonionic polymers such as polyethylene oxide and polyacrylamide is attributed to hydrogen bond formation between surface hydroxyls of the substrate and the ether oxygen in polyethylene oxide or the amide group in polyacrylamide (Drzymala and Fuerstenau, 1987; Mathur and Moudgil, 1998; Lee and Somasundaran, 1989).

In acrylamide/acrylate copolymers, while both amide and carboxylate groups have the capacity to adsorb onto mineral surfaces, they have different primary roles. In weakly alkaline solutions the primary role of the amide group is adsorption by hydrogen bonding, whilst interactions of the negatively charged carboxylate groups extend the conformation of the polymer chain, enabling bridging to take place more easily and improve the flocculation effectiveness (Connelly, Owen and Richardson, 1986).

In contrast to this, flocculants commonly utilised within the Bayer process are 100% anionic (i.e. polyacrylate, containing no acrylamide functionality), being used in liquor that is strongly alkaline and having high ionic strength. Thus, with the absence of the amide functionality, the primary role of the carboxylate group becomes adsorption.

Generally, flocculant adsorption processes are rapid and while the individual bond strengths are relatively low, the sheer number of bonds results in the overall bonding force being high. Adsorption of flocculant is considered virtually irreversible, as desorption would require all adsorbed polymer segments to detach simultaneously (Kitchener, 1972). Thermodynamically, loss of conformational entropy when a polymer adsorbs is compensated by the gain in interaction energy due to the large number of contacts to the substrate. The conformation in the adsorbed state adjusts itself until the overall free energy change is zero, as required for equilibrium, resulting in high standard free energies of adsorption (Lyklema, 1985).

2.2.2.2 Aggregate Formation

The second step in the flocculation process is the formation of aggregates, which most often occurs via polymer bridging. Collision of flocculant-adsorbed particles and the interaction of the loops and tails projecting from the surface of the particles may lead to bridge formation (Figure 2.5). At high polymer concentrations it is possible that the polymer may completely adsorb onto individual particles before bridging formation can occur. At such concentrations, flocculation may decrease and the repulsion of the charges on the polymer can even lead to particle dispersion (Moss and Dymond, 1978). In practice this almost never occurs in tailings flocculation, mainly due to the concentration of solids used, the amount of flocculant needed to achieve this, and the mixing conditions required. Most often, over-dosing of flocculant leads to over-flocculation, whereby large independent flocs that exhibit no hindered settling behaviour are formed. The overdosing of flocculant in this way is not advantageous and is generally avoided in tailings flocculation.

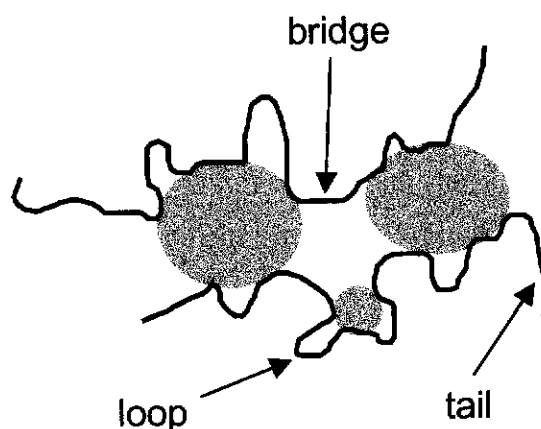


Figure 2.5: Diagrammatic representation of the bridging mechanism of flocculation.

Aggregation is a dynamic process involving polymer adsorption and particle-particle collision, which results in floc formation and growth. Due to the irreversible nature of polymer adsorption, the kinetics of adsorption has a major impact on the distribution of adsorbed polymer among slurry particles and the formation of the polymer bridges between particles necessary for flocculation. While Hogg (1999) has described a simplified model for polymer adsorption kinetics, recent work by Swift *et al.* (2002) has used a linear pipe reactor and examined aggregation by polymer flocculants *in situ* using a focussed beam reflectance measurement probe. They found that after a very short induction period (flocculant and slurry mixing, flocculant adsorption), aggregate size increased rapidly (flocculation), achieved a maximum value and then decreased at a slower rate than the initial aggregation rate (aggregate rupture). Though in their study they found the induction period to be very rapid (<0.5 s), it highlights the importance of understanding adsorption properties in developing kinetic models of aggregation by polymeric flocculation.

2.3 Studies of Relevance to Bayer Residue Flocculation

While the amount of available alumina and organic contaminating matter within bauxite deposits varies quite markedly throughout the world, most bauxite deposits are generally classified as goethite or hematite rich, with these mineral phases being a major component of the residue separated during clarification. Bauxite deposits within Australia are generally regarded as hematite rich.

Solid-liquid separation of residue following digestion can be a major bottleneck in the Bayer process. It is critical to remove the residue solids from the saturated

aluminate liquors as rapidly as possible to avoid premature precipitation of product. The slow settling nature of the residue solids meant that in the absence of flocculant it was necessary to filter the large volumes of slurry to achieve both separation and clarity.

Starch or flour (which contains starch) were found to be successful at flocculating bauxite residue (Brown, 1942) and were used almost exclusively in residue thickeners for many decades. While generally achieving good clarities and liquor stability, the amount needed combined with the significant desorption rate during settling meant that starch based flocculants were actually a major contributor to the organic contaminants found in the liquor. Synthetic flocculants were found to be as effective at lower dosages, with most flocculant remaining irreversibly adsorbed and hence reducing the amount of residual flocculant contaminating the liquor (Sibert, 1968; Pearse and Sartowski, 1984; and Bublik *et al.*, 1986). The use of synthetic flocculants gained acceptance in the 1970's (Connelly, Owen and Richardson, 1986) and has largely replaced that of natural products over the last 20 years, although flour is still used in a few plants around the world. Synthetic flocculants generally give better settling rates and compaction, leading to increased caustic recovery from counter-current residue washing (Hunter, Moody and Tran, 1990).

Since the inception of synthetic flocculants, many laboratory and plants trials have been carried out to optimise flocculant dosages so that clarities in overflow liquors and density of underflow solids can be maximised, increasing the throughput of the liquor filtration (Sibert, 1968; Yamada, Harato and Shiozaki, 1980; Pearse and Sartowski, 1984; Sankey and Schwarz, 1984; Bublik *et al.*, 1986, Hood and Willemon, 1987; Kahane, 1992; and Perrier *et al.*, 1999). In contrast, there have been relatively few laboratory-based fundamental studies of flocculation within the Bayer process. Li (1998, 2001) has extensively studied the effect that digestion conditions may have on residue mineralogy, particle size, surface area and therefore subsequent settling behaviour, but gave no consideration to flocculant interactions.

Many fundamental studies of flocculant adsorption have been carried out in systems at mild acid/base conditions and low ionic strength, rarely deviating far from the point of zero charge of the substrate being studied. Examining the adsorption of

Bayer flocculants onto bauxite residue solids is much more difficult, due to the complex nature of Bayer liquor and the variability of mineral phases found in residue and hence simplified (model) systems are more commonly studied.

Model liquors used are commonly solutions of high pH with added electrolyte, while more typically synthetic Bayer liquors are used, which are sodium aluminate solutions where the measured caustic and aluminate concentration is comparable to that found in a refinery liquor (Jones, Farrow and van Bronswijk, 1998a, 1998b). These solutions avoid the organics and other dissolved salts found in Bayer liquor, but simulate the high caustic and ionic strength environment. Often well-characterised goethite or hematite are used as models for residue solids.

2.3.1 Surface Chemistry of Hematite

In understanding how solution species may associate with the surface of a substrate, it is imperative to have an understanding of the surface chemistry. In solution environments, this is often related to the surface charge of the substrate.

The iso-electric point (iep) and point of zero charge (pzc) for synthetic hematite is typically reported to lie between 8 and 9, although values for natural hematite samples have been reported in a range of 2 to 10 (Pugh and Lundström, 1987). Table 2.1 gives an example of some iep and pzc values for hematite that are given in the literature.

The results of Drzymala and Fuerstenau (1987) and Golikova *et al.* (1998) in Table 2.1 show that the iep and pzc of hematite are very similar, as one may expect. The low value of iep found by Khangaonkar and Bala Subramani (1993) and Subramanian and Natarajan (1989) can most likely be explained by the presence of silicate impurities in the hematite used by these authors. This is an explanation given by many authors when low iep values are obtained for naturally occurring hematite samples.

Table 2.1: Some selected iep and pzc values for hematite.

Reference	Measurement Type	Sample Type	Value
Bajpai and Bajpai (1995a, 1995b)	pzc	reagent	6.8
Drzymala and Fuerstenau (1987)	pzc	reagent	8.1
Drzymala and Fuerstenau (1987)	iep	reagent	8.1
Golikova <i>et al.</i> (1998)	pzc	synthetic	7.8
Golikova <i>et al.</i> (1998)	iep	synthetic	8.0
Zhang and Buffle (1995)	iep	synthetic	9.2
Lee and Somasundaran (1989)	iep	synthetic	7.5
Khangaonkar and Bala Subramani (1993)	iep	natural	4.5
Subramanian and Natarajan (1989)	iep	natural	4.1

The surface of hematite becomes more negative with increasing pH above the iep. Jones, Marwood and Horsley (1994) attributed this to the binding of hydroxyl anions to the surface. While this may be a contributing factor, infrared spectroscopy has identified both surface hydroxyl groups and molecularly-bound water molecules on the virginal hematite surface formed by hydration (Rochester and Topham, 1979; Lorenzelli, Busca and Sheppard, 1980). This has led many authors to describe the formation of surface charge via proton transfer reactions of surface hydroxyl and water groups (Drzymala and Fuerstenau, 1987; Jones, Farrow and van Bronswijk, 1998a).

The increase in surface charge of hematite with increasing pH inhibits the flocculant from interacting with the surface of the hematite by hydrogen bonding (amide functionality) or electrostatic interactions (carboxylate functionality). This may only hold true for pH values near the iep, as there is some conjecture as to the surface charge/pH relationship in more forcing caustic and higher ionic strength environments. Jones, Marwood and Horsley (1994) found that for an iron (III) oxide sample with a iep at pH 7, the zeta potential reached a minimum (negative voltage) at around pH 10 and then began to increase at higher pH's. Their zeta potential measurements could not be recorded past pH 11.5 due to the high concentrations of

alkali involved. The authors concluded that the increase in zeta potential at the higher pH region was due to the large concentration of sodium cations accumulating at the double layer screening the negatively charged iron (III) oxide surface.

Jones, Farrow and van Bronswijk (1998a) obtained similar results when they measured the stability of hematite suspensions. They were able to carry out settling measurements in more forcing caustic conditions and found that the hindered settling rate decreased beyond 1 M caustic solution. This did not indicate dispersion of hematite but rather a significant increase in liquor viscosity. The authors concluded that in high strength caustic synthetic Bayer liquor, the hematite would be expected to be weakly aggregated due to coagulation.

While not providing any experimental evidence, Sankey and Schwartz (1984) similarly suggest that in Bayer conditions the zeta potential of the iron oxide particles will essentially be zero due to the extremely high ionic conductivity of the solution.

Although there is little literature on the evaluation of surface properties of particles in high ionic strength environments, Rowlands *et al.* (1997) have published results on the surface properties of aluminium hydroxide in up to 3 M NaCl electrolyte using electroacoustic measurements. They found that in 0.5 M NaCl the iep shifted from 9.1 to approximately 11, while in 3 M NaCl there was no iep. The authors suggested that under such forcing conditions, the normal picture of the diffuse double layer is no longer valid and hence the absolute value of the zeta potentials is no longer accurate. However, they did suggest that the measured trends in the zeta potential as a function of pH and electrolyte concentration are significant. They concluded that in alkaline, high ionic strength solution, sodium ions adsorb close to the particle surface so that the net charge at the surface where liquid flow begins to develop is positive.

Breeuwsma and Lyklema (1971) investigated the surface charge of hematite as a function of Li^+ , K^+ and Cs^+ , and found that at high LiCl concentrations the surface charge-pH curves were very steep on the negative side of pzc (8.5) and there was a shift in pzc to lower values. This indicated to the authors that there was specific adsorption of Li^+ . At low concentrations of KCl and CsCl, there was a trend for the

surface charge in the presence of K^+ to be higher than Cs^+ , although no difference was observed in concentrated solutions. These results are obviously contrary to what would be expected and the authors attribute this behaviour predominantly to the porosity of the hematite and the ability of the cations to penetrate the surface. The results indicate that little penetration of K^+ and Cs^+ takes place whereas Li^+ penetrates easily. This behaviour was attributed to the fact that the crystal ionic radii of Li^+ and Fe^{3+} are almost identical, enabling Li^+ to penetrate easily and occupy a vacant Fe^{3+} site. Their explanation was also corroborated by the bivalent series where only Mg^{2+} , which also has a very similar crystal ionic radius compared to Fe^{3+} , showed substantial penetration.

Using a similar experimental set-up to that of Rowlands *et al.* (1997), Johnson, Scales and Healy (1999) monitored the binding of monovalent electrolyte ions on the surface of α -alumina as a function of pH and ionic strength and observed a similar trend to that of Breeuwsma and Lyklema (1971). The authors found that for nitrate salts at high pH (12) and high ionic strength, adsorption to the α -alumina surface took the order $Li^+ > Na^+ > K^+ \approx Cs^+$.

Contrary to the explanation offered by Breeuwsma and Lyklema (1971), Johnson, Scales and Healy (1999) have described the similar monovalent adsorption series for an α -alumina substrate using the 'structure making - structure breaking' model. This has been previously described by Berube and de Bruyn (1968), whereby the structure-inducing behaviour of each ionic species is closely related to its hydration enthalpy. For alkali monovalent cations, Li^+ is the smallest and most heavily hydrated cation, it has the highest hydration enthalpy and hence the greatest water ordering ability. Therefore the structure-inducing behaviour or the water ordering properties is promoted in the sequence $Li^+ > Na^+ > K^+ > Cs^+$. The sequence of cation adsorption to the negative α -alumina surface can then only be consistent with this model if the surface is also classified as structure-making.

Structure-making refers to the water structuring capabilities of surfaces with the strength of the water-solid interaction indicative of the degree of ordering of the water molecules on the surface of the substrate. Dumont, Dang Van Tan, and Watillon (1976) suggested that if the structuring properties of ions are directly

related to their heat of hydration, then the structuring properties of the substrate should be related to the heat of immersion. Therefore the 'structure making - structure breaking' model is related to the hydration enthalpy of the ion (water ordering properties of ions) and the heat of hydration or the heat of immersion of the substrate (water structuring capability). Therefore the above cation adsorption sequence makes sense due to the large heat of immersion that the α -alumina surface possesses.

Amhamdi, Dumont and Buess-Herman (1997) found from coagulation experiments with a hematite sol that the adsorption sequence observed for cations at pH values greater than the pzc (8.2) is $\text{Li}^+ > \text{Na}^+ > \text{K}^+$. Using a similar argument to the above, the authors stated that as the ferric oxide water interface is a structure promoter for water molecules, the surface will preferentially adsorb structure-making ions such as Li^+ and Na^+ and reject ions such as K^+ and Cs^+ when the surface is negatively charged.

Perhaps due to the diversity of various mineral phases found in bauxite residues from different refineries throughout the world, there has been little research directed specifically at investigating the effect of pH and ionic strength on the surface charge of bauxite residue. An exception is the study by Chvedov, Ostap and Le (2001), which characterised the surface charge of red muds generated from different bauxite sources. While their testing conditions were relatively benign and not particularly related to the Bayer process, they found that the pzc of the muds ranged from 6.5 to 7.8 depending on the amount of sodalite in the muds, which they suggested lowered the pzc. They also found that the surface charge of the muds became increasingly negative up to the maximum pH value tested (12.5). When comparing the affinity of Na^+ and K^+ to the negatively charged mud surface, the difference in pzc values obtained suggested that the specific adsorption of K^+ ions on the surface of the mud particles made the surface less negative.

In examining the surface properties of hematite in this study, both the porous model described by Breeuwsma and Lyklema (1971) and the 'structure making - structure breaking' model described by Berube and de Bruyn (1968) need to be considered, particularly if the substrate exhibits a high degree of porosity. Generally though, it

would appear that the 'structure making - structure breaking' model has become more widely accepted in explaining the inverse lyotropic adsorption sequence ($\text{Li}^+ > \text{Na}^+ > \text{K}^+ > \text{Cs}^+$) exhibited by some oxide surfaces.

2.3.2 Solution Properties of Polyacrylate

The dominant functional group of Bayer-process flocculants is the carboxylate functionality. Due to the ionisable nature of the carboxylate functional group, the pH and ionic strength affects the characteristics of the polymer in solution. Lee, Condrate and Reed (1996) have stated that the pK_a for polyacrylate is approximately 4.5, although Boisvert *et al.* (2002) found that polyacrylate neutralised through a pH range of 3-9, indicating a pK_a of approximately 6. Therefore at pH values below the pK_a , the majority of the carboxylate functional groups will be protonated, decreasing repulsion between polymer segments, resulting in the polymer having a coiled conformation. Increasing the ionic strength of such a solution will have no significant effect on the conformation of the polymer. At pH values above the pK_a the carboxylate functional groups will become increasingly deprotonated, causing repulsion between the polymer segments, resulting in a polymer with an extended conformation and a solution with increased viscosity. Increasing the ionic strength of this solution will result in the added cations screening the negative charge of the deprotonated carboxylate functional groups, causing the polymer to once again assume a coiled conformation and the solution viscosity to decrease.

Pochard *et al.* (2001) carried out a study to determine the effect of ionic strength (NaCl) on the effective charge of polyacrylate in a pH range of 6-9. The effective charge was described with respect to the theory of ionic condensation. Counter-ions near the functional groups of the polyelectrolyte are condensed and it is the excess uncondensed ions that attribute to the effective charge. The authors found that the effective charge was proportional to the square root of the ionic strength, and explained this trend on the decrease in electrostatic repulsion between neighbouring charges enabling more counter-ions to decondense. In clarifying this finding, they suggested that the addition of salt to increase the effective charge would not increase the electrostatic interaction of the polyelectrolyte with a charged surface because any

charge increase of the polymer promoted by salt addition would be compensated by the high extent of screening of the polymer.

Boisvert *et al.* (2002) examined the interaction of monovalent cations and polyacrylate using osmotic pressure measurements. The authors studied the effect of the Li^+ , Na^+ and tetramethyl ammonium (TMA^+) ions on the effective charge of polyacrylic acid through a pH range of 4 to 9. They observed that the effective charge was not dependent on the nature of the monovalent cation and that the interaction between cation and carboxylate functionality was non-specific and purely electrostatic. Contrary to this, they found that the interaction of the polymer with divalent cations showed specific interactions. Their results suggested that this interaction was inversely related to the energy of hydration of the cation. This resulted in Ba^{2+} , which is the largest and least hydrated cation, exhibiting the lowest energy of hydration, having a higher tendency than Ca^{2+} and Mg^{2+} to precipitate the polymer from solution.

Due to the highly caustic nature of Bayer liquor, all the carboxylate groups of the polymer are expected to be ionised and the polymer to have an extended conformation. However, due to the high ionic strength of the liquor the repulsion between the carboxylate groups is reduced by their association with sodium ions, restricting the extended polymer conformation.

2.3.3 Surface Chemistry of Polymer Adsorption

Several workers have developed conceptual theories for the adsorption of polymers onto surfaces and in particular for the adsorption of polyelectrolytes onto oxide surfaces (Papenhuijzen, van der Schee and Fler, 1985a; Bohmer, Evers and Scheutjens, 1990; Au *et al.*, 1999). While most have predicted trends that follow those of laboratory experiments (Papenhuijzen, van der Schee and Fler, 1985b), the studies have had little quantitative success due to the complexity and large number of variables associated with the adsorption process.

Polyelectrolytes have been found to be spherically shaped in solution both in the presence and absence of electrolyte (Rangaraj, Vangani and Rakshit, 1997). For

adsorption of a polyelectrolyte to a surface of opposite charge it has been found that at very low ionic strength the polymer takes on an extended conformation and hence will adsorb in a flat configuration on the particle surface. With increasing electrolyte, the polymer takes a more tightly coiled conformation in solution, with the adsorbed configuration exhibiting more loops and tails and enabling more polymer to adsorb onto the particle. At high ionic strength, the charges on both the polyelectrolyte and the particle are heavily screened, decreasing the attractive interaction between the two and adsorption decreases (Lyklema and Fleer, 1987; Greenwood and Kendall, 2000).

The pH will also influence adsorption as it affects the charge of both the polyelectrolyte and the particle surface. Hence, for the electrostatic interaction of a negatively charge polyelectrolyte with a positively charged surface, adsorption will decrease with increasing pH. This has been demonstrated by Au *et al.* (1999) who modelled the adsorption of a weak polyelectrolyte onto the surface of hematite. They assumed the charge of the polyelectrolyte to be negative and found that when the hematite surface was positive, adsorption increased with decreasing pH and increasing ionic strength. When the hematite surface was negative, adsorption increased with decreasing pH (i.e. as the pH approaches the iep/pzc).

When polyelectrolytes adsorb onto uncharged surfaces or those of the same charge, then adsorption can no longer be described by the simple electrostatic interaction. Quite often polyelectrolytes are copolymers containing other functional groups such as the amide functionality in anionic and cationic polyacrylamide. In these types of polyelectrolytes adsorption is often be attributed to hydrogen bonding of the amide functional groups of the polymer to surface hydroxyl groups on the substrate, rather than by electrostatic interactions (Drzymala and Fuerstenau, 1987).

Other polyelectrolytes exhibit a charge that is pH dependant, such as polyacrylic acid, which can behave as a neutral homopolymer ($< \text{pH } 3$), a polyelectrolyte copolymer ($\text{pH } 3$ to $\text{pH } 9$) or a polyelectrolyte homopolymer ($> \text{pH } 9$). For polyacrylic acid at solution pH less than 9, interaction with substrate surfaces is not always strictly electrostatic. This has been demonstrated by Vermohlen *et al.* (2000) in a study of the adsorption of an anionic polyelectrolyte onto alumina (pzc 8.7) at

pH 5.2. They found that adsorption increased with increasing ionic strength of the solution. The authors noted that if the interaction was electrostatic; i.e. positive substrate surface and negatively charged polyelectrolyte, then at high ionic strength the adsorption should decrease, but found it continued to increase. This indicated to them that there was a specific non-electrostatic interaction between the surface and the polyelectrolyte and suggested that in the case of polyacrylic acid, this could only exist between the carboxylic group and the surface. At pH 5.2, greater than half the carboxylic acid groups on the polymer would be protonated and this would suggest that the interaction would most likely be through a carboxylic acid group and the surface rather than through an ionised carboxylate group on the polymer chain.

Flocculation of residue material within the Bayer process represents a special situation, where the surface charge of the substrate is expected to be negative due to the highly caustic environment, and where flocculation is achieved commonly with 100% anionic polyacrylate. This is an example of where both the polyelectrolyte and substrate exhibit the same charge.

In a similar system, Cosgrove, Obey and Vincent (1986) observed no adsorption for a negative poly(styrene sulfonate) onto a negatively charge polystyrene latex in zero added salt, but found adsorption increased with increasing salt. While they did not specify an adsorption mechanism, it is assumed that the added electrolyte facilitated an electrostatic interaction between polymer and substrate that increased with increasing electrolyte concentration. The increase in adsorption with ionic strength was also attributed to a change in the polymer adsorbed conformation, with the development of loops made possible by the suppression in the intersegmental electrostatic repulsions associated with high ionic strength media.

In characterising polymer adsorption in the Bayer process, Jones, Farrow and van Bronswijk (1998a) studied the adsorption of a polyacrylate flocculant onto hematite in synthetic Bayer liquor. The results suggested that the polyacrylate flocculant had a very low affinity for the hematite surface and this is discussed further in Section 2.4.2.

Jones, Farrow and van Bronswijk (1998b) also observed that increasing caustic strength did not have an effect on the polyacrylate flocculant adsorption density onto hematite or the flocculant size in solution. Despite this, it was found that it did significantly reduce flocculation efficiency. While this could not be fully explained by the physical effects of increasing liquor viscosity, the authors proposed that the increasing liquor viscosity affected the rate of flocculant adsorption and interparticle collision, hence decreasing the degree of bridging between particles.

There has only ever been speculation as to the mechanism of adsorption of polyacrylates onto residue material in the Bayer process. For example, Connelly, Owen and Richardson (1986) speculated that the adsorption process is facilitated by a Ca^{2+} ion bridge between substrate and adsorbate (Figure 2.6b). Basu, Nitowski and The (1986) suggested several possible interactions, including hydrogen bonding (Figures 2.6e and 2.6f), monodentate coordination of the carboxylate directly to a surface iron atom (Figure 2.6c), and coordination through a sodium ion to a surface oxygen atom (Figure 2.6d).

The only spectroscopic study of note was carried out by Jones, Farrow and van Bronswijk (1998c), who used diffuse reflectance infrared Fourier transform spectroscopy (DRIFT) to examine polyacrylate flocculant adsorption onto hematite from pure sodium hydroxide solutions of varying pH (up to pH 14). They found that the carboxylate functionality of the polyacrylate was bound directly to a surface ferric ion of the hematite via an asymmetric bidentate bridging complexation (Figure 2.6a). The results of that study are discussed further in Section 2.4.1.1.

The contradictory views expressed in the literature cannot be resolved with confidence on the basis of currently published data. In a study of the adsorption of polyacrylate onto hematite, an integrated approach that takes into account the way in which the solution conditions affect both the structure of the hematite surface and the properties of the polymer in solution is needed. In this way, all factors are assessed and quantified in order to elucidate the adsorption process.

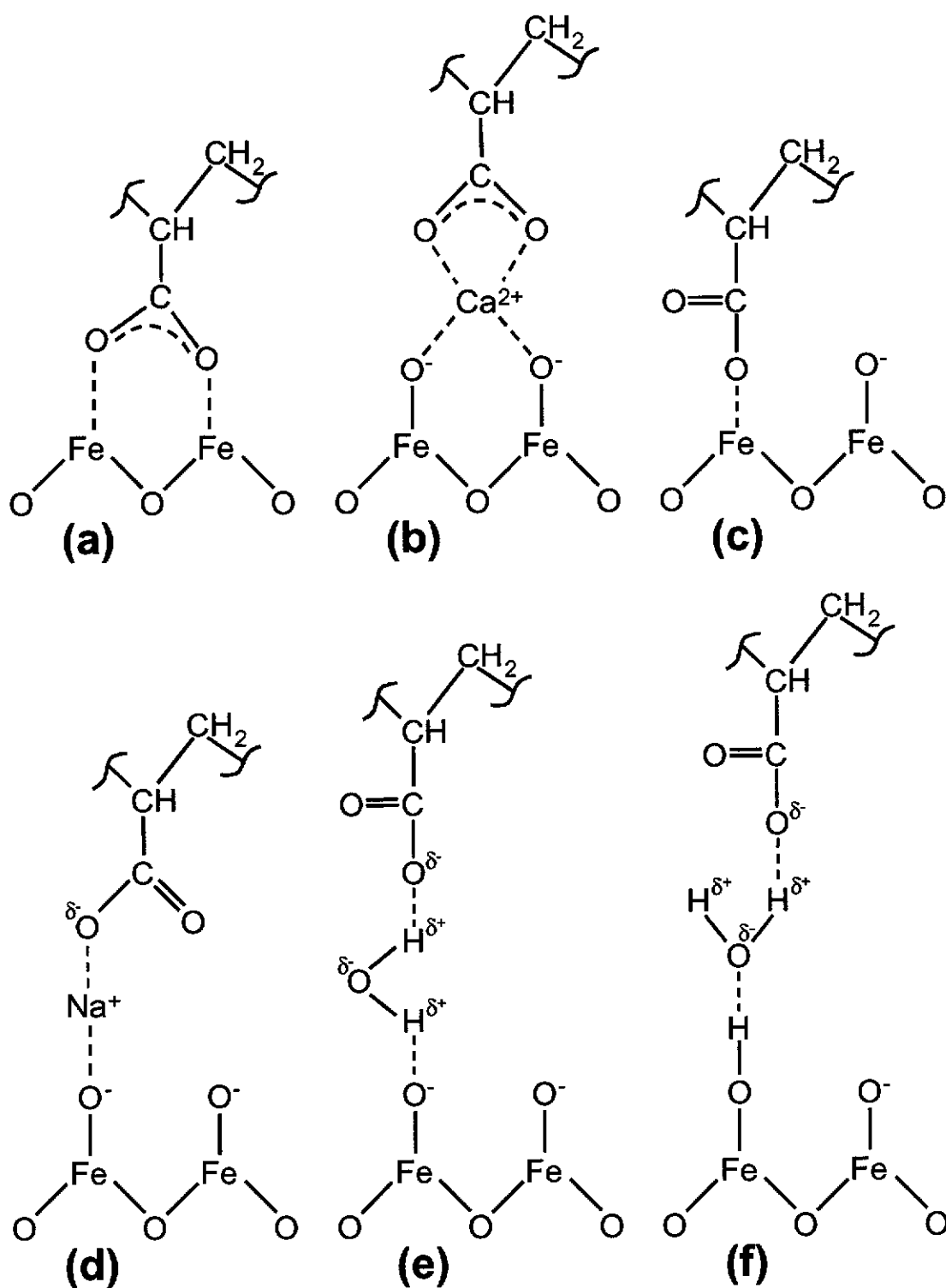


Figure 2.6: Types of proposed adsorption mechanisms for polyacrylate onto an iron oxide surface; (a) asymmetric bidentate bridging complexation (Jones, Farrow and van Bronswijk, 1998c); (b) a possible calcium ion bridging structure as speculated by Connelly, Owen and Richardson (1986); (c) monodentate complexation, (d) coordination via sodium ion, (e) and (f) hydrogen bonding structures (Basu, Nitowski and The, 1986).

2.4 Techniques for Evaluating Flocculation Processes

The bonding mechanism of carboxylic acids and their corresponding polymers onto mineral surfaces has been studied extensively using many spectroscopic techniques, as outlined in Table 2.2. All these techniques have the potential to produce information on the adsorbed functionalities and their interactions with oxide surfaces and have generally found that the interaction between the carboxylic acid functional group and substrate is chemisorption. However, they also suffer from being *ex situ* techniques, requiring samples to be removed from contact with solutions and then dried prior to spectroscopic examination.

Table 2.2: Selected spectroscopic studies determining the bonding mechanism of carboxylates onto mineral surfaces.

Reference	Spectroscopic Technique	Adsorbate/Substrate System
Alexander <i>et al.</i> (2001)	X-ray photoelectron	Polyacrylic acid/pseudoboehmite
Leadley and Watts (1997)		Polyacrylic acid/various metals
Underhill and Timsit (1992)		Propionic acid/oxidised aluminium
Coast <i>et al.</i> (1996)	Inelastic electron tunneling	Acrylic acid/oxidised aluminium
Zhou <i>et al.</i> (1994)	Mössbauer	Oxalic acid/hematite
Jones, Farrow and van Bronswijk (1998c)	(Diffuse Reflectance Infrared –DRIFT)	Polyacrylate/hematite
Vermohlen <i>et al.</i> (2000b)		Polyacrylic acid/alumina
Parker and Frost (1996)		Propionic acid/montmorillonite
Gong <i>et al.</i> (1991)		Oleate/hematite

2.4.1 Fourier Transform Infrared (FTIR) Spectroscopy

Infrared spectroscopy offers the advantage of being applicable to the direct study of the solid-liquid interface, and is therefore discussed in detail. Infrared spectroscopy

is a very powerful technique whereby molecular vibrations absorb infrared radiation and the subsequent interpretation of the absorption frequencies can give information as to the chemical environment of atoms within a molecule. The molecular vibrations associated with the carboxylate functionality present in polyacrylate flocculants offer considerable potential for adsorbed species characterisation by FTIR.

2.4.1.1 Carboxylate Adsorption Modes

Deacon and Phillips (1980) correlated transmission infrared spectroscopic and X-ray crystallographic data of acetato transition metal complexes to determine the relationship between the carbon-oxygen stretching frequencies of carboxylato complexes and the type of carboxylate coordination. By comparing the separation of the antisymmetric and symmetric stretching frequencies of the carboxylate ion (ΔCOO^-) bound to transition metals to that of the sodium salt, they were able to propose a set of rules for identifying the bonding mechanism in complex ions.

These are summarised as follows, and relate to the schematic views of bonding shown in Figure 2.7:

- i) If there is C=O character in the spectrum and $\Delta\text{COO}^-_{(\text{complex})}$ is greater than $\Delta\text{COO}^-_{(\text{salt})}$ then the adsorbed structure is monodentate (I).
- ii) If there is no C=O character in the spectrum and $\Delta\text{COO}^-_{(\text{complex})}$ is smaller than $\Delta\text{COO}^-_{(\text{salt})}$ then the adsorbed structure is bidentate chelating (II).
- iii) If there is no C=O character in the spectrum and $\Delta\text{COO}^-_{(\text{complex})}$ is similar to $\Delta\text{COO}^-_{(\text{salt})}$ then the adsorbed structure is bidentate bridging (III).

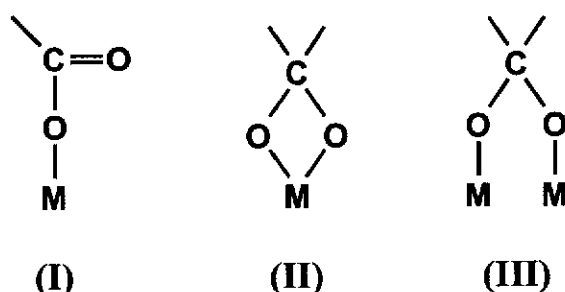


Figure 2.7: Modes of carboxylate-metal complexation; (I) monodentate, (II) bidentate chelating, and (III) bidentate bridging.

It would be reasonable to expect that these rules would apply to adsorbed carboxylates, and in doing so, additional adsorbed structures have been proposed. An asymmetric bidentate bridging structure (Figure 2.6a) was suggested by Jones, Farrow and van Bronswijk (1998c) for a high molecular weight polyacrylate adsorbed on hematite in caustic media. The structure was based on the fact that in their DRIFT spectra $\Delta\text{COO}^-_{(\text{complex})}$ was much greater than $\Delta\text{COO}^-_{(\text{salt})}$, but with a lack of substantial C=O character. The evidence was thought to indicate that one C-O-M bond was longer and weaker than the other. Allara and Nuzzo (1985) proposed a similar structure, based on Polarised Grazing Angle (PGA) infrared spectroscopy, in their study of the adsorption of *n*-alkanoic acids on oxidised aluminium substrates.

Also utilising DRIFT, Vermohlen *et al.* (2000) examined polyacrylic acid coated alumina. The occurrence of peaks associated with the symmetric and antisymmetric stretch of the carboxylate ion in the adsorbed species spectra indicated that the polymer was coordinated to the alumina, but poor resolution of the peaks inhibited the ability to distinguish bidentate bridging coordination from bidentate chelation. Their results also showed a peak attributable to the carboxyl stretch and hence indicated that not all of the polymer chain was adsorbed, however no evidence was given to suggest the coating thickness and whether it was significantly less, significantly more, or representative of monolayer coverage.

The disadvantage of many FTIR studies, in particular those utilising DRIFT or PGA, is that the analysis is carried out *ex situ*. When we consider polymer adsorption, only a fraction of the molecule is assumed to be adsorbed, with the remainder forming loops and tails that extend into solution. Therefore, it is highly likely that any *ex situ* examination of such samples may be hindered by potential binding changes during the washing and drying process. In particular, the polymer tails and loops that were unadsorbed while in solution may collapse onto the surface, distorting the true binding behaviour.

In situ surface studies are much more challenging, as information pertaining to surface adsorption is commonly flooded by that of the bulk solution. Fourier transform infrared – attenuated total reflection (FTIR-ATR) spectroscopy offers the possibility of *in situ* examinations of the solid-liquid interface. By utilising this

shallow penetration reflection technique, stretching and bending frequencies that give information as to the molecular interactions between the adsorbate functional groups and the surface of the substrate can be obtained. Hence, it is thus possible that the adsorbed fraction of the polymer may be able to be distinguished from that of the unadsorbed fraction.

2.4.1.2 Attenuated Total Reflection (ATR) Spectroscopy

When radiation is travelling through a medium with a refractive index of n_1 (ATR element) and it strikes the boundary of an interface with a medium of lower refractive index n_2 (sample) with an incident angle greater than the critical angle ($\theta_c = \sin^{-1}[n_2/n_1]$), then the radiation will be totally internally reflected at the interface. With this reflection, an exponentially decaying evanescent wave is set up in the medium of lower refractive index. This penetrates to a small distance, depending on the refractive indices of the two media, the incident angle, and the wavelength of the radiation. The depth of this penetration is commonly represented by d_p , which is not a measure of the total depth of penetration of the evanescent wave but rather the thickness within which the intensity of the evanescent wave decreases to $1/e$ of the intensity at the boundary. Mathematically, d_p represents the depth of penetration if it were a box car function and not an exponential decay (Figure 2.8). ATR thus acts as a short path length sampling cell able to measure the attenuation associated with a solution-substrate interface, provided there is intimate contact between the ATR element and the solution-substrate sample.

The depth of penetration (d_p) is given by Equation 2.3 (Harrick, 1987, pp30):

$$d_p = \frac{\lambda}{2\pi n_1 (\sin^2 \theta - n_{21}^2)^{1/2}} \quad (\text{Equation 2.3})$$

- where: n_1 = refractive index of optically denser medium
 n_2 = refractive index of optically rarer medium
 $n_{21} = n_2/n_1$
 θ = incidence angle of infrared radiation
 λ = wavelength of infrared radiation

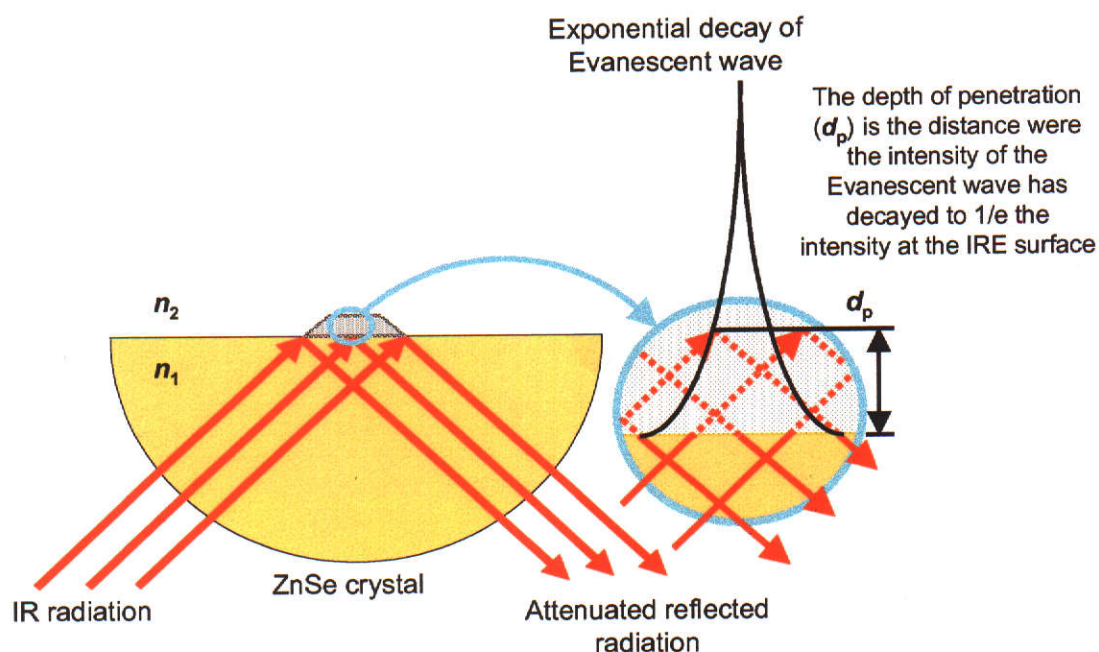


Figure 2.8: Schematic showing technical aspects of ATR spectroscopy.

For transmission infrared, the absorbance (A) is proportional to the molar absorption coefficient (ϵ), the concentration (c) and the path length (ℓ), i.e. Beer's Law (Equation 2.4):

$$A = \epsilon \cdot c \cdot \ell \quad (\text{Equation 2.4})$$

For ATR spectroscopy the path length (ℓ) is the effective thickness (d_e) (Equation 2.5):

$$A = \epsilon \cdot c \cdot d_e \quad (\text{Equation 2.5})$$

The effective thickness (d_e) is the thickness required in normal transmission measurements to achieve the same absorbance as measured by one internal reflection and is proportional to the penetration depth (Equation 2.6, Lentz, 1995, pp605):

$$d_e = \frac{n_{21} \cos \theta}{1 - n_{21}^2} \left(1 + \frac{2 \sin^2 \theta - n_{21}^2}{(1 + n_{21}^2) \sin^2 \theta - n_{21}^2} \right) d_p \quad (\text{Equation 2.6})$$

Both the parallel and perpendicular polarised components of the radiations contribute to the effective thickness (Equation 2.7):

$$d_e = X \cdot d_{e||} + (1 - X) \cdot d_{e\perp} \quad (\text{Equation 2.7})$$

where X represents the fraction of parallel polarised and $(1-X)$ the fraction of perpendicular polarised infrared radiation.

The individual components are given by Equations 2.8 and 2.9 (Harrick, 1987, pp43):

$$d_{e||} = \frac{n_{21} \lambda (2 \sin^2 \theta - n_{21}^2) \cos \theta}{n_1 \pi (1 - n_{21}^2) [(1 + n_{21}^2) \sin^2 \theta - n_{21}^2] (\sin^2 \theta - n_{21}^2)^{1/2}} \quad (\text{Equation 2.8})$$

and

$$d_{e\perp} = \frac{n_{21} \lambda \cos \theta}{n_1 \pi (1 - n_{21}^2) (\sin^2 \theta - n_{21}^2)^{1/2}} \quad (\text{Equation 2.9})$$

2.4.1.3 FTIR-ATR Adsorption Studies

Hind, Bhargava and McKinnon (2001) and Sperline and Freiser (1995) have given comprehensive reviews of the FTIR-ATR technique and how it can be utilised as a tool to examine the solid/liquid interface. They also discuss the different cell geometries that can be utilised and several different strategies that have been employed, such as adsorption directly onto the infrared element (IRE), adsorption onto particulate matter and subsequent contact with the IRE, and adsorption to coated IREs.

Utilising the adsorption onto particulate matter and subsequent contact with the IRE strategy, Hind, Bhargava and Grocott (1997a, 1997b) and Hind and Bhargava (2000) have successfully used FTIR-ATR to examine the adsorption of quaternary ammonium compounds on solid sodium oxalate and gibbsite in synthetic Bayer liquors. However, they only used the spectra to quantify the relative amounts of different chain length compounds that adsorbed under selected conditions. This suggests that peak positions in the spectra of their quaternary ammonium compounds

were insensitive to the adsorption state, and therefore did not lend themselves to mechanistic interpretation.

When the substrate of interest cannot be constructed to be an IRE, the adsorption to a coated IRE strategy offers the greatest advantage, as adsorption gives quantitative surface excess results equivalent to those obtained by solution depletion (Sperline and Freiser, 1995). The limitation of the technique is that the substrate must be relatively insoluble and be able to be applied to the IRE as a very thin film with uniform contact.

This strategy has been the choice of many researchers (e.g. Connor and McQuillan, 1999; Hug, 1997, Hug and Sulzberger, 1994; Kuys and Roberts, 1987). A solid sample is placed in contact with a polished crystal of high refractive index, with infrared radiation focused at the crystal. While internal reflection occurs at the solid/crystal interface, radiation can penetrate into the sample layer and be attenuated, allowing an absorption spectrum to be obtained (Figure 2.9). The advantage of this strategy is that the solid layer can be in contact with an aqueous phase, giving interfacial information without any sample treatment that may change the surface characteristics.

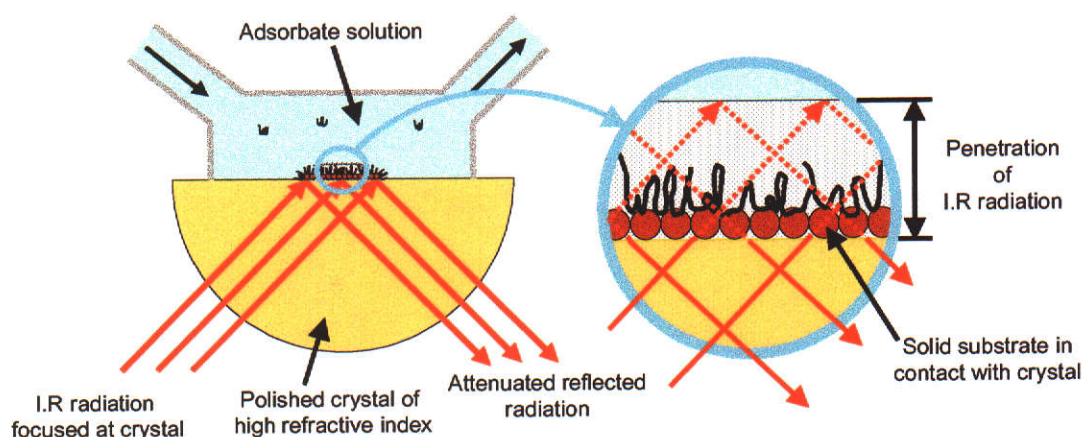


Figure 2.9: FTIR-ATR technique – adsorption onto a coated IRE.

Connor and McQuillan (1999) used coated optics to investigate the adsorption of phosphate on TiO_2 . They were able to monitor the rate of adsorption and by changing the adsorbate concentration, obtain an insight into the adsorption isotherm. Their results indicated that phosphate attached to the TiO_2 surface via a bidentate

surface species, although it could not be determined if it was bridging or chelating complexation.

Hug (1997) used *in situ* FTIR-ATR to measure the adsorption of sulfate onto a hematite coated ZnSe crystal. The author found that for the concentration of sulfate used (1 mM), there was a significant signal enhancement (over 30 times), indicating adsorption and concentration of the sulfate into the hematite layer. He also noted that the spectra of sulfate adsorbed on hematite at pH 3 were clearly different to that of dissolved sulfate. The symmetric IR band of aqueous sulfate (1102 cm^{-1}) was split into two distinct bands (1060 and 1128 cm^{-1}) upon adsorption. This indicated to the author that the symmetry of the adsorbed sulfate had lowered and that it had coordinated with surface Fe(III) sites. Weakly bound or electrostatically attracted sulfate would not be expected to show such significant band shifts. By comparing the spectra of adsorbed sulfate with spectra of compounds with known sulfate coordination, it could be seen that the band positions were similar to those of $[\text{Co}(\text{NH}_3)_5\text{SO}_4]\text{Br}$, $[\text{Co}(\text{en})_2(\text{H}_2\text{O})\text{SO}_4]\text{Br}$ and a solution of mainly $[\text{Fe}^{\text{III}}\text{SO}_4]^+$. Therefore the study concluded that the coordination of sulfate on hematite *in situ* was consistent with monodentate complexation (similar to structure (I) - Figure 2.7).

The mode of carboxylate adsorption onto a variety of mineral surfaces *in situ* has also been deduced successfully using FTIR-ATR. Roddick-Lanzilotta and McQuillan (2000) used coated optics to determine the adsorption mechanism of glutamic and aspartic acid on amorphous TiO_2 . The absorption due to the amine functional group was comparatively weak and gave no evidence of coordinating with the TiO_2 surface, hence the interpretation was based on the stretches associated with the carboxylate groups. At pH 6.9 they found that the spectrum of adsorbed glutamic acid resembled the solution spectrum. The separation of the symmetric (1404 cm^{-1}) and antisymmetric (1583 cm^{-1}) stretches of the carboxylate ion was not significantly changed upon adsorption. This implies either electrostatic interaction or, in agreement with the rules outlined by Deacon and Phillips (1980), bidentate coordination through one or both of the carboxylate groups. Due to electrostatic interactions being unfavoured at pH 6.9, because both TiO_2 and glutamic acid have a net negative charge, the authors proposed that the dominant adsorbed species was

most likely bridging bidentate coordination to the TiO_2 surface (structure (III) - Figure 2.7).

Adsorption at pH 2.9 caused a loss of the absorption band at 1713 cm^{-1} due to the carbonyl stretch of the carboxylic acid group, indicating that glutamic acid was deprotonated on adsorption to TiO_2 . Similar to pH 6.9 adsorption, an antisymmetric carboxylate stretch at approximately 1600 cm^{-1} was consistent with an electrostatic interaction, or bidentate coordination through one or both of the carboxylate groups. The presence of a second antisymmetric carboxylate band arising at 1537 cm^{-1} represents a significant decrease in the separation between the symmetric and antisymmetric carboxylate stretches, indicating bidentate chelation to a single surface titanium ion (structure (II) - Figure 2.7). The authors suggested that the results supported a mixture of bidentate bridging and bidentate chelating coordination of the carboxylate groups to the TiO_2 surface.

At approximately pH 7, the spectrum of adsorbed aspartic acid strongly resembled that of the solution spectrum. In a similar argument to that for adsorption of glutamic acid at pH 6.9, the authors suggested that the dominant coordination was bidentate bridging through one or both carboxylates to two surface titanium ions (structure (III) - Figure 2.7). Steric considerations would suggest that coordination through one rather than both carboxylates is more likely.

Dobson and McQuillan (1999) used a TiO_2 or Al_2O_3 coated ZnSe ATR element to examine the adsorption profile of a range of aliphatic mono- and di-carboxylic acids from aqueous solutions. Mono-carboxylic acids (formic and acetic) were found not to adsorb, but dicarboxylic acids did. The spectrum of succinic acid adsorbed onto TiO_2 and Al_2O_3 was clearly different to that of dissolved sodium succinate. For the dissolved sodium succinate spectrum the symmetric and antisymmetric stretch of the carboxylate ion were at 1393 cm^{-1} and 1550 cm^{-1} , respectively ($\Delta\text{COO}^- = 157\text{ cm}^{-1}$). In the adsorbed spectrum the equivalent modes were at 1539 cm^{-1} and 1413 cm^{-1} ($\Delta\text{COO}^- = 126\text{ cm}^{-1}$) on TiO_2 at 1553 cm^{-1} and 1420 cm^{-1} ($\Delta\text{COO}^- = 133\text{ cm}^{-1}$) on Al_2O_3 . Due to the lack of any carbonyl stretch and the molecular flexibility of the adsorbate, it was proposed that coordination was through both carboxylate groups of the molecule. The authors suggested that a bridging bidentate complex was formed, but because of the reduction in the separation of the carboxylate stretches, use of the

rules outlined by Deacon and Phillips (1980) would actually indicate bidentate chelation coordination. Adipic acid behaved in the same manner as succinic acid and hence should be considered to also adsorb via bidentate chelation coordination to TiO_2 and Al_2O_3 .

Specht and Frimmel (2001) have characterised the adsorption of malonic and succinic acids onto kaolinite. In the spectrum of malonic acid adsorbed onto kaolinite at $\text{pH} < 6$ the presence of a weak carbonyl stretch (1722 cm^{-1}), characteristic of the free protonated acid group, indicated that a small fraction of the molecules were adsorbed through one carboxylate group. The authors suggested that a strong peak at 1600 cm^{-1} was due to a shift of the carbonyl stretch to lower energy, which is indicative of a weakened double bond, due to bonding of the other oxygen atom (C-O whose stretch occurred at 1380 cm^{-1}) to the kaolinite surface. They proposed that the adsorption mode was dominated by monodentate complexation of both carboxylate groups of the molecule to surface aluminium atoms. This proposed mode is in agreement with the rules outlined by Deacon and Phillips (1980), where the separation between the adsorbed molecule frequencies (220 cm^{-1}) is greater than the separation (208 cm^{-1}) between the symmetric (1356 cm^{-1}) and antisymmetric (1564 cm^{-1}) stretch of the carboxylate ion of fully ionised malonic acid. It is also favoured on steric grounds, as bidentate binding from only one carboxylate group would force the second carboxylate to be non-binding and hence lead to nearer equal intensities of free and bound carboxylate stretches. At $\text{pH} > 6$, only the symmetric and antisymmetric stretching vibrations of the carboxylate ion were present, at similar positions to those in the unadsorbed solution spectra. The authors proposed, in agreement with the Deacon and Phillips rules, a bidentate bridging complexation. It is also possible that the ionised carboxylate group of malonic acid was electrostatically attached to the kaolinite surface, as this interaction would exhibit the same stretching frequencies as those shown in the study. Steric considerations would once again suggest only one carboxylate is bound, with the other carboxylate unbound and deprotonated, exhibiting the same stretching frequencies associated with the bound carboxylate group.

Succinic acid was found to adsorb onto kaolinite in a similar manner to malonic acid at low pH, but differed significantly at higher solution pH. At pH 6.5 and 11.5, the

adsorbed spectra developed near equal intensities of frequencies characteristic of the carboxylate ion and the carbonyl functionality. The symmetric and antisymmetric stretching of the carboxylate ion (1552 and 1396 cm^{-1} , respectively) were at similar positions to those in the unadsorbed solution spectra, while the carbonyl stretch (1650 cm^{-1}) remained unshifted from that exhibited by adsorption of succinic acid at low pH. This indicates that monodentate complexation persists in going from low to high pH, and further indicates that one of the bound carboxylate groups becomes non-bonding, is deprotonated and hence exhibits the characteristic stretching frequencies of the carboxylate ion.

FTIR-ATR studies using the coated IRE strategy have advantages over studies where adsorption is onto particulate matter followed by contact with the IRE. The latter strategy relies on the settling of adsorbed slurries onto the ATR element, while adsorption onto coated optics can give quantitative surface excess results equivalent to those obtained by solution depletion (Sperline and Freiser, 1995) and offers considerable potential for characterising adsorption kinetics.

In addition, the coated optics strategy has been shown to be successful in characterising adsorption, particularly for carboxylate species onto mineral surfaces. Therefore, coated optics were used in this study as they clearly provide higher quality information.

2.4.2 Adsorption Isotherms and Adsorption Kinetics

Irving Langmuir was the first to describe an isotherm for adsorption (Langmuir, 1918). His relationship (Equation 2.10) describes adsorption as a function of the equilibrium bulk concentration, with a limiting adsorption value associated with monolayer coverage on a homogenous surface. In reality, surfaces are generally not homogeneous, with the more energetically favourable sites occupied first and the adsorption decreasing with increasing surface coverage. There have been a number of theoretically derived isotherms that consider this. The Freundlich isotherm (Equation 2.11) takes into account that adsorption decreases with increasing surface coverage. The Langmuir-Freundlich isotherm (Equation 2.12) extends this to include the limiting adsorption value associated with monolayer coverage (Tien, 1994, pp20).

- Langmuir isotherm: $\theta = \frac{x}{m} / \left(\frac{x}{m} \right)_{\max} = \frac{Kc}{(1+Kc)}$ (Equation 2.10)

- Freundlich isotherm: $\frac{x}{m} = Kc^{1/n}$ (Equation 2.11)

- Langmuir-Freundlich isotherm: $\theta = \frac{x}{m} / \left(\frac{x}{m} \right)_{\max} = \frac{Kc^n}{(1+Kc^n)}$ (Equation 2.12)

where θ is the fraction adsorbed in relation to the maximum, x is the amount of solute adsorbed by a mass m of solid, c is the solution equilibrium concentration, and K and n are constants.

Adsorption isotherms for polymers onto substrates are approximated by the Langmuir isotherm and are typically characterised as high affinity isotherms. They show an almost concentration independent nature, where there is high adsorption at low concentrations and a plateau is obtained (La Mer and Healy, 1963). The occurrence of low affinity isotherms, which are more rounded and exhibit no clear plateau, have generally been attributed to polydispersity (wide molecular weight distribution). This has been explained by larger molecular weight polymer fractions preferentially adsorbing and removing smaller molecular weight polymer molecules from the surface, resulting in an increase in polymer adsorption with increasing polymer concentration (Cohen Stuart, Fleer and Bijsterbosch, 1982).

Contrary to this, Papenhuijzen, Fleer and Bijsterbosch (1985) showed that low affinity type isotherms were indicative of weak adsorbate-substrate interactions, while high affinity isotherms were indicative of strong adsorbate-substrate interactions. This was supported by the findings of Adam and Robb (1983) who found that the adsorption of a polydispersed poly(styrene sulfonate) polymer onto calcium carbonate exhibited a high affinity isotherm.

Hence it would appear that the curvature of the isotherm, represented by the K value in the Langmuir isotherm (Equation 2.10), can be a measure of polymer affinity for the substrate surface. As expressed by the Langmuir isotherm, K is the equilibrium constant for the adsorption-desorption reaction. The ability to define it in this way for polymer adsorption is limited by the fact that polymer adsorption is considered

irreversible, although it may be an indication of the ratio of rate constants for the adsorption of individual polymer segments from solution (La Mer and Healy, 1963).

Rigorous interpretation of adsorption kinetics for a polymer adsorbing system is limited by the fact that the system is in no way ideal or homogeneous. For this reason, polymer adsorption kinetics is normally discussed in a more qualitative rather than quantitative manner. In modelling polymer adsorption kinetics, Hogg (1999) assumed that the polymer molecules act as monodispersed spheres and adsorb irreversibly in a simple collision process similar to coagulation. He found that polymer adsorption occurs rapidly and for a typical flocculated system, adsorption is essentially complete within seconds.

Polymer adsorption densities and kinetics of adsorption have been investigated by the usual solution depletion method in some studies (Bajpai and Bajpai, 1995a; 1995b). Alternatively, the adsorption process is monitored by adsorbing the polymer from solution onto a flat substrate and detecting the adsorbed polymer spectroscopically, typically by means of ellipsometry or attenuated total reflection, utilising infrared, uv/visible or fluorescence. Though used successfully, fluorescence has the disadvantage of the need for the adsorbate to be intrinsically fluorescent, which is not common in flocculant molecules, or be capable of being labelled with a suitable fluorophore, which obviously modifies the polymer.

Kuzmenka and Granick (1988) studied the kinetics of adsorption of polymethylmethacrylate onto a germanium prism from carbon tetrachloride solution. They found that adsorption proceeded rapidly over the first few minutes but took four hours to plateau. Neivandt and Gee (1995) obtained similar results for the adsorption of a cationic polymer onto silica. However, Parsons, Harrop and Mahers (1992) found that for an amphoteric polymer adsorbed onto a quartz surface, the rate of adsorption exhibited a double-exponential rate equation. They suggested that initial adsorption was dominated by mass transfer while there was an excess of available adsorption sites, and the later adsorption rate was due to the reduced number of available sites and limited by the rate at which the polymer molecules rearrange on the surface to give an optimum configuration. Alternatively, they suggested that it was possibly due to the molecular weight distribution of the polymer leading to a range of mass transfer rates.

Filippova (1999) studied the adsorption of cationic polyelectrolytes onto silicon wafers under controlled flow conditions. Adsorption was governed at short times by adsorption kinetics for low polymer concentration, at medium times by convective-diffusive mass transfer for medium and high polymer concentrations, and at long times by adsorption kinetics and convective-diffusive mass transfer for medium and high polymer concentrations.

There have been many studies investigating the adsorption of polyacrylate or acrylamide/acrylate copolymers onto hematite in aqueous systems (Bajpai and Bajpai, 1995a; Bajpai and Bajpai, 1995b; Drzymala and Fuerstenau, 1987; Khangaonkar and Bala Subramani, 1993; Lee and Somasundaran, 1989), with all results exhibiting Langmuir-like adsorption isotherm behaviour. Adsorption densities were assessed through a pH range of 2-12, collectively, and showed that increasing the pH decreased the amount of polymer adsorbed. This was attributed to changes in polymer properties and the surface charge of hematite at varying pH.

Bajpai and Bajpai (1995b) observed that for hydrolysed polyacrylamide, the variation of the initial rate of adsorption with pH followed the same trend as that for the adsorption density. In a pH range of 4 to 8.4, they found that the adsorption rate increased until pH 5.4 and then decreased thereafter. They explained the increase by an initial electrostatic attraction between ionised polymer groups and the positively charged hematite surface, while the decrease was attributed to polymer extension and consequent changing of the hematite surface to negatively charged beyond the pzc. In addition, they observed that the rate of adsorption was independent of the agitation intensity and hence concluded that the attachment of the molecule to the hematite surface, rather than transport of the molecule to the surface, governed the rate of adsorption. At pH 4, where the hematite surface is positively charged, the authors found that the initial rate of adsorption increased with an increasing degree of hydrolysis of the polymer. Once again, this mirrored the trend of adsorption density and was explained via an increased electrostatic interaction.

In characterising polymer adsorption in the Bayer process, Jones, Farrow and van Bronswijk (1998a) studied the adsorption density of a polyacrylate flocculant onto hematite in synthetic Bayer liquor as a function of flocculant remaining in solution at equilibrium. The best fit for their data was obtained with a Langmuir-Freundlich

isotherm, with the isotherm exhibiting a low plateau adsorption coverage (0.164 mg m^{-2}). Plateau adsorption densities for polymers characteristically lie between 1.5 and 3 mg m^{-2} (Lyklema, 1989). The K value was 0.01 , indicating a very low affinity isotherm, while the n value was 1.90 , ($n = 1$ for a Langmuir isotherm). The authors calculated that at plateau adsorption coverage, less than 15% of the hematite surface was occupied by flocculant. The plateau coverage was calculated assuming the hematite surface and flocculant were uniform and the flocculant adsorption was flat. Flocculant molecules that partake in the bridging mechanism are known not to adsorb in this manner but rather form loops and tails that protrude into the liquor. This would seem to indicate that the surface coverage was much lower than 15% . In addition, the authors found that optimum flocculation, as measured by settling tests, corresponded to 20% of the plateau coverage. All these results would appear to suggest that the polyacrylate flocculant has a very low affinity for the hematite surface under the conditions tested.

The molecular weight is an important property of a flocculant and this has been highlighted by many studies (Walles, 1968; Bajpai and Bajpai, 1995a; Misra, 1996; Santhiya *et al.*, 1998; and Jones, Farrow and van Bronswijk, 1998a). While affecting its ability to act as a bridging polymer, the molecular weight of the polymer will also affect the adsorption density and the rate of adsorption. Bajpai and Bajpai (1995a) observed that the rate of adsorption of polyacrylamide onto hematite in an aqueous medium decreased with increasing molecular weight of the polymer. The authors attributed this to the larger molecular weight polymers needing a greater length of time to attach to the surface in addition to having a slower rate of diffusion within the solution.

Santhiya *et al.* (1998) have found that for an alumina suspension in the presence of polyacrylic acid, increasing molecular weight ($2\ 000$ to $90\ 000$) increased the adsorption density. The same effect was noted by Misra (1996) for the adsorption of lower molecular weight ($2\ 100$ and $5\ 100$) polyacrylates onto hydroxyapatite. This was attributed to the longer chain molecules being irreversibly bound to the substrate surface and hence not being in equilibrium with the free molecules in solution.

Results obtained by Misra (1996) showed that higher molecular weight polyacrylates ($60\ 000$ and $170\ 000$) adsorbed to the same extent. Similarly, Jones, Farrow and van

Bronswijk (1998a) observed that two polyacrylates of significantly different molecular weights (150 000 and 14 000 000) adsorbed to the same extent on hematite. Of the two polyacrylates, only the higher molecular weight polymer showed significant flocculation effectiveness, indicating that the chain length of that polymer was sufficient to form aggregates by bridging. This further indicates that both polymers adsorb on the surface with an equivalent ratio of unadsorbed to adsorbed polymer segments, i.e. essentially the same fraction of 'train' segments and therefore the same fraction projecting into the solution as loops and tails. This would suggest that for particular polymers, when varying the molecular weight, there is a correlation between the maximum adsorption density and the conformation of the adsorbed polymer.

2.4.3 Quantitation of Adsorbed Species by FTIR-ATR

Adsorption densities and adsorption kinetics have been examined *in situ* using FTIR-ATR. Sperline, Muralidharan and Freiser (1987) first proposed and applied the following FTIR-ATR adsorption density equation (Equation 2.13) for adsorption onto a reactive IRE element:

$$\Gamma = \frac{(A / N) - \epsilon c_b d_e}{2000 \epsilon (d_e / d_p)} \quad (\text{Equation 2.13})$$

where A is the integrated absorbance (cm^{-1}), N is the number of internal reflections, ϵ is the molar absorptivity ($\text{L g}^{-1} \text{cm}^{-2}$), c_b is the bulk solution concentration (g L^{-1}), d_e is the effective thickness (cm), and d_p is the depth of penetration (cm).

In adsorbing cetylpyridinium chloride onto ZnSe from dichloromethane and water, assuming that the adsorbed cetylpyridinium chloride layer was $\ll d_p$, they were able to show that the adsorption densities determined were in good agreement with the solution depletion method employed.

Free and Miller (1997) also employed the FTIR-ATR adsorption density equation (Equation 2.13) to examine the adsorption density as a function of time in their kinetic study of oleate adsorption onto a CaF reactive IRE. Utilising this technique and through a thorough consideration of flow conditions, they were able to show that oleate adsorption onto CaF was under kinetic control and that it was first order in

respect to surface sites when the solution surfactant concentration was maintained constant.

Sperline, Song and Freiser (1992) and Sperline and Freiser (1995) have shown that the same equation applies to coated optics, although if the coated film is more than a few nanometers thick, the optical properties of the film must be considered. Using this approach they assumed that there were three phases, the IRE (n_1), $\sim 2 \mu\text{m}$ thick alumina coating (n_2), and the aqueous solution (n_3). The rf sputter coated alumina coating was assumed to be uniform and exhibit the same optical properties as crystalline alumina. Also, it was again assumed that the adsorbate layer thickness (sodium dodecyl sulfate) was $\ll d_p$. In characterising the effective path length and the depth of penetration of the evanescent wave in the aqueous phase (phase three), their equation (Equation 2.14) takes into account the decay of the evanescent wave through the alumina coating and leads to a modified version of the previously developed adsorption density equation:

$$\Gamma = \frac{(A/N) - \epsilon c_b d_{e,3}}{1000 \epsilon (d_{e,3} / d_3)} \quad (\text{Equation 2.14})$$

where A is the integrated absorbance (cm^{-1}), N is the number of internal reflections, ϵ is the molar absorptivity ($\text{L g}^{-1} \text{cm}^{-2}$), c_b is the bulk solution concentration (g L^{-1}), $d_{e,3}$ is Beer's law 'effective path length' in the third phase (cm) (defined by Hansen (1965) as b_{eff}), and d_3 is the decay constant for the time average of the square of the electric field in the third phase and is similar to the depth of penetration (cm).

Sperline, Song and Freiser (1992) have demonstrated that for adsorption of sodium dodecyl sulfate onto alumina coated optics, adsorption isotherms constructed using the modified adsorption density equation agreed well with those at similar conditions by other authors using solution depletion.

Thus, in addition to the *in situ* FTIR-ATR technique providing high quality information in mechanistic studies, it has also been shown to be applicable to characterising adsorption isotherms and adsorption kinetics. Both aspects of the technique were utilised in this study.

2.4.4 Multi-Angle Laser Light Scattering (MALLS)

The pH and ionic strength of a polyacrylate solution influences the degree of ionisation, and the amount of shielding experienced by the ionisable carboxylate groups, and ultimately determines the conformation of the polymer in solution. Therefore, an extended or more tightly coiled conformation is reflected in the size of the polymer in solution.

Light scattering is one of the few absolute methods for the determination of molecular mass and structure of macromolecular solutions. It has the additional advantage of being non-invasive, with laser light being projected into the polymer solution through a flowcell or scintillation vial. Multi-angle laser light scattering (MALLS) involves the simultaneous measurement of the scattered light through an array of detectors, allowing measurements to be made in a matter of seconds.

Wyatt (1993) has given a thorough review of light scattering in relation to the absolute characterisation of macromolecules. It is possible to determine the weight-average molecular weight (M_w) and the root-mean-square-radius ($\langle r_g^2 \rangle^{1/2}$) by measuring the light scattering behaviour of molecules simultaneously at various angles. For high molecular weight molecules, the usual method for determining M_w and $\langle r_g^2 \rangle^{1/2}$ is by preparing a Debye plot (Figure 2.10), which is achieved by plotting $R_\theta/(K^*c)$ versus $\sin^2(\theta/2) + Sc$ at each scattering angle. K^* is the physical constant for vertically polarised incident light, c the concentration, R_θ the excess Rayleigh ratio of the light scattered from the dilute suspension, θ the angle between the incident and scattered rays and S is a stretch factor. The stretch factor S is applied to spread the data points to produce a well-defined plot. It gives approximately equal weighting to angular and concentration terms and does not affect the final results. A polynomial function is used to fit the non-linear Debye plot. The angular fit is extrapolated to $\theta = 0^\circ$ for each concentration, and the data at each angle extrapolated to zero concentration. The common intercept of the two extrapolated curves yields the molecular weight, while the slope of the $c = 0$ curve near $\sin^2(\theta/2) = 0$ yield the square mean radius. The order of polynomial used for angular fitting, which increases with molecular weight, is chosen to minimise the error and remains constant for the analysis (Wyatt, 1993).

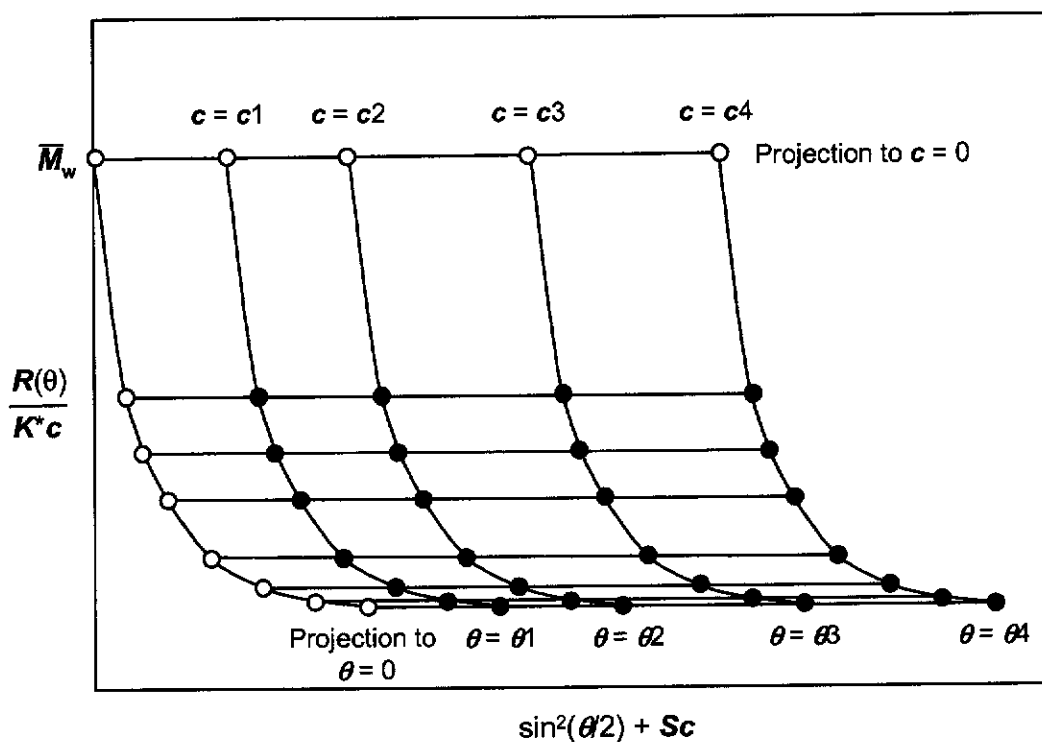


Figure 2.10: Typical Debye plot for a high molecular weight polymer.

The ratio of slope to intercept, necessary for computing $\langle r_g^2 \rangle$, is independent of instrument calibration, consequently independent of molecular weight. The root mean square radius $\langle r_g^2 \rangle^{1/2}$ is simply the square root of the mean square radius, and this is also termed the radius of gyration (r_g). For linear molecules the root mean square radius is proportional to the hydrodynamic radius (Wyatt, 1993).

The mean-square-radius ($\langle r_g^2 \rangle$) is, in general, determined when each mass element of the molecule is weighted by the square of its distance from the molecule's centre of gravity, with this quantity integrated over all the mass elements. For a homogenous sphere and a spherical shell, both of radius a , the mean square radius will be equal to $3/5a^2$ and a^2 , respectively. Therefore the mean square radius depends on the internal mass distribution of the molecule and for this reason is not generally the same as the square of the molecule's mean diameter (r_h - hydrodynamic diameter) (Wyatt, 1993).

For a polymer in solution, spherical in shape and assuming a random coil conformation, the relationship between the hydrodynamic radius (r_h) and the radius of gyration (r_g) is given by Equation 2.15 (Adolphs and Kulicke, 1997) and is shown schematically in Figure 2.11.

$$r_g = 0.778 \cdot r_h \quad (\text{Equation 2.15})$$

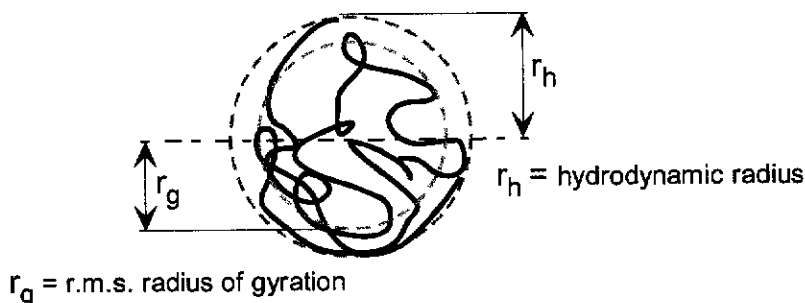


Figure 2.11: Relationship between r.m.s radius of gyration and hydrodynamic size.

Light scattering is thus an invaluable tool for determining the solution dimensions of polymeric molecules. This is particularly important for polyelectrolyte macromolecules, where the solution dimensions of a particular polymer can vary dramatically, depending on the properties of the solvent. In this way, light scattering is a direct way of measuring the effect that pH and ionic strength of the solution has on the polymer.

There have been a number of studies carried out to investigate polyacrylate or acrylate copolymer flocculant solution characteristics by light scattering. Table 2.3 gives the general range that their radius of gyration has been determined to fall in, at relatively benign solution pH and relatively low solution ionic strength.

The data corresponding to the copolymers correlates fairly well with the results obtained by Reed (1995) for sodium polyacrylate. Based on the results in Table 2.3, when polyacrylate is approximately half ionised (pH 6) and in a solution medium of relatively low ionic strength, its radius of gyration will vary from approximately 150 to 400 nm for a molecular weight range of approximately 10^5 to 10^6 .

Table 2.3: Solution size and molecular weight of some selected polyacrylate and hydrolysed polyacrylamide polymers.

Reference	M_w	r_g (nm)	Polymer Type/Solvent
Kulicke and Kniewske (1981)	$17 - 18.3 \times 10^6$	~ 345	17% hydrolysed polyacrylamide (0.5 M NaCl)
Kulicke and Horl (1985)	$6.0 - 6.4 \times 10^6$	213 - 279	45 - 95% hydrolysed polyacrylamide (0.1 M Na_2SO_4)
Kheradmand and Francois (1988)	6×10^6	~ 250	17% hydrolysed polyacrylamide (~ 0.85 M NaCl, pH 6.5)
Crees, Senogles and Whayman (1991)	$3 - 28 \times 10^6$	337 - 433	23 - 41% hydrolysed polyacrylamide (0.3 M NaNO_3 , 0.005 M Ca^{2+})
Reed (1995)	$\sim 10^5 - 10^6$	$\sim 150 - 400$	Sodium polyacrylate (0.1 M NH_4NO_3 , pH 6)

As the technique used to characterise polymer adsorption in this study is FTIR-ATR, which is a very shallow penetration sampling technique, it is essential to know both the depth of penetration of the sampling infrared beam and the size of the polymer in solution, as they are of similar magnitude. MALLS is versatile technique able to measure polyacrylate solution dimensions over an extensive range of solution pH and ionic strength, and hence at conditions that reflect those used to characterise the adsorption of polyacrylate onto hematite in this study.

2.4.5 Electrophoretic Mobility

In characterising the adsorption of polyacrylate onto hematite, it is essential to understand how solution properties affect the hematite surface. The typical measure for determining the manner in which solution conditions such as pH and ionic strength influence the surface of a substrate is to determine its surface potential.

When characterising the surface potential of a substrate, the relevant measure is the effective potential on the particle, because this is the potential that is 'seen' by another approaching particle (or polyelectrolyte). The best estimate of the effective

potential is the Stern potential (Section 2.1) because it is the relevant measure in characterising the way in which charged species interact. In practice this can only be approximated by measurement of the zeta potential, which in itself is measured indirectly from the electrophoretic mobility.

Charged particles will migrate under the influence of an electric field, with the direction of migration indicative of the sign of the charge of the particles. The electrophoretic mobility is defined as the velocity the particles attain within an applied electric field. The zeta potential (ζ) is derived from the electrophoretic mobility (μ) via Equation 2.16 (Tscharnuter, 2001):

$$\mu = \frac{f(\kappa a) \zeta \epsilon}{\eta} \quad (\text{Equation 2.16})$$

where $f(\kappa a)$ is a function of the particle size (of radius a), $1/\kappa$ the thickness of the double layer, ϵ the dielectric constant of the dispersing medium, and η the viscosity.

For polar media such as aqueous-based dispersions of moderate ionic strength and containing a particle size that is not too low, κa is 100 or more, $f(\kappa a) = 1.5$ and the above equation becomes the Smoluchowski relationship. For particles in nonpolar media, $f(\kappa a) = 1$ and the above equation becomes the Hückel relationship. For aqueous colloids that obey the Smoluchowski relationship, a zeta potential range of -80 mV to 100 mV is common (Tscharnuter, 2001).

Generally, as the ionic strength increases, the zeta potential and the mobility both approach zero, due to the shielding effect ions have on the surface charge of the dispersed particles. It is in these types of environments, where the conductivity is very large, that conventional Laser Doppler electrophoretic (LDE) measurements are limited.

With conventional LDE, the scattered light from a colloidal suspension moving in an electric field is frequency shifted by the Doppler effect. This is then optically mixed with the unshifted reference beam, which leads to a beating at a frequency dependent on the speed of the particles. As the direction of the electric field is defined, the sign and magnitude of the electrophoretic mobility can be determined (Tscharnuter, 2001).

The displacement of the particles in a given time can be related to the scattering vector (K), which is defined in Equation 2.17:

$$K = 4\pi n / \lambda_0 \sin(\theta / 2) \quad (\text{Equation 2.17})$$

where λ_0 is the wavelength of the monochromatic light source (laser) in vacuum, θ the scattering angle, and n the refractive index of the suspending liquid.

The limitation of the LDE method occurs when the mobility is low, because there is only a very small displacement of the particles in a given time. When the displacement is less than K^{-1} , the signal will not produce a complete frequency cycle of 2π and hence cannot be measured accurately. While small displacements can be measured by waiting sufficiently long times, this is not a realistic option in electrophoretic measurements, as the continual application of the field in one direction leads to electrode polarisation. Increasing the field could also be an option, but this leads to sample heating and other undesirable effects such as dielectrophoresis (when there is a large difference in particle and medium dielectric constant) and Brownian motion (which can add to the electrophoretic motion and hence decreases the precision of any measurement) (Tscharnutter, 2001).

It has been shown that the limitations of conventional LDE can be overcome by applying the principles of phase analysis light scattering (PALS) to electrophoretic mobility measurements. This enables very low mobilities to be measured in media that are very high in ionic strength and hence conductivity, and has been reported to have a sensitivity of up to three orders of magnitude better than conventional LDE (Tscharnutter, McNeil-Watson and Fairhurst, 1998).

A schematic of an instrument used to determine electrophoretic mobility by phase analysis light scattering is given in Figure 2.12. Laser light is scattered by charged particles that are moving due to an applied electric field and this scattered beam is mixed with a reference beam at the detector (a photomultiplier tube) (Brookhaven Instrument Corporation internet site).

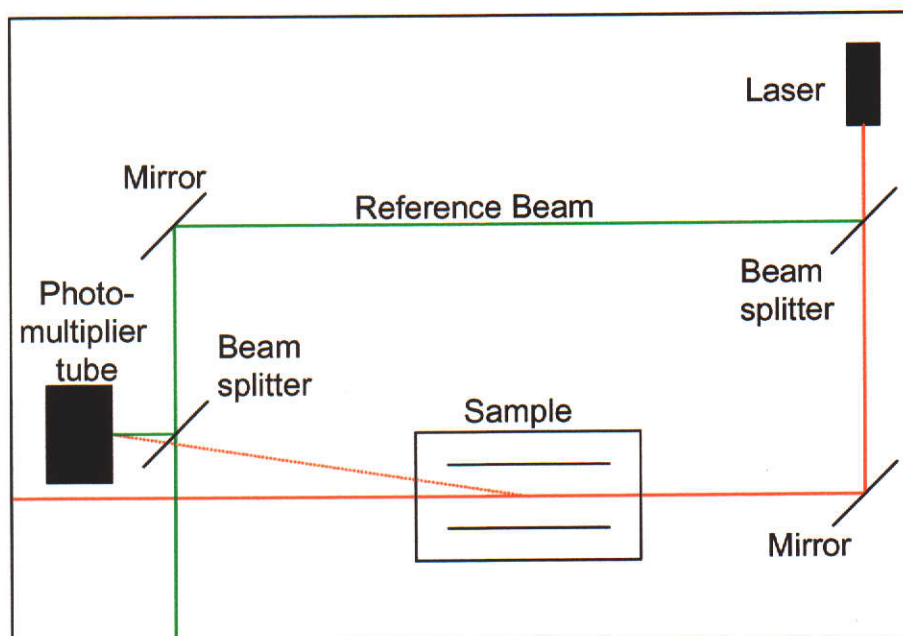


Figure 2.12: Schematic representation of the Brookhaven ZetaPlus instrument (Brookhaven Instrument Corporation internet site).

The reference beam is modulated and phase modulation is applied so that the Doppler frequency of a zero mobility particle is equal to the modulation frequency ω_0 . Any deviation from the modulation frequency present in the scattered light is measured by phase comparison of the modulation frequency and the detected signal. If the mobility is actually zero, then the relative phase of the two will be constant, whereas if there is a small phase shift, this can be measured by a phase separator. The advantage of the phase separator is that phase comparison takes place over many cycles of the respective waveforms and hence only a fraction of the Doppler cycle is required. The average phase change as a function of time is given in Equation 2.18:

$$\langle Q(t) - Q(0) \rangle = \langle A \rangle K [\langle \mu \rangle E(t) + V_c t] \quad (\text{Equation 2.18})$$

where the mobility, μ , is extracted as the mean mobility $\langle \mu \rangle$ for all phase changes due to the many particles being detected; K is the scattering vector (as defined above); $Q(t)$ the amplitude weighted phase at time t , A the signal amplitude, $E(t)$ the electric field, and V_c the collective motion due to variables such as temperature gradients.

V_c is assumed to be constant over the time scale of the measurement. By suitable data treatment the collective motion can be virtually eliminated. In typical electrophoretic measurements, the sample is confined to a capillary and an electric field is applied to the ends. The complication this introduces is that the applied field

causes not only movement of the particles (electrophoresis) but also a movement of the suspension medium (by electro-osmosis). It is essential that both processes are taken into account to obtain useful information (Hunter, 1993, pp241, 242). The design of the sample cell in Figure 2.12 is such that the electrodes are entirely within the cell, remote from any cell wall. Therefore the electric field does not cut across the cell walls, focus and cell position are not critical, there is no effect from sedimenting particles and importantly, it avoids the troubling electro-osmotic effect (Tscharnuter, McNeil-Watson and Fairhurst, 1998).

Tscharnuter, McNeil-Watson and Fairhurst (1998) carried out a comparison study on several samples, including a NIST standard reference material, and found that results obtained by utilising the principles of phase analysis light scattering were in excellent agreement with results obtained by conventional LDE. In addition, measurements were carried out on samples that were beyond the capability of conventional LDE, which included a ferrite colloid (believed to be stabilised by a low molecular weight polymer) in silicone oil that had been diluted in dodecane. A very low mobility ($0.013 \pm 0.0015 \times 10^{-8} \text{ m}^2\text{V}^{-1}\text{s}^{-1}$) could be measured reproducibly and the authors felt that this was consistent with what might be expected for a sterically stabilised system. In addition, the authors measured the electrophoretic mobility of quartz spheroids in deionised water containing different concentrations of potassium chloride. All the measured mobilities were negative, and for KCl concentrations ranging from 0.0001 M to 2.0 M, the general trend in the mobility and hence zeta potential was one of approaching zero. The exception was a minimum found at 0.001 M KCl, which the author attributed to a possible slight specific adsorption of chloride ions.

The mobility of particles suspended in high ionic strength environments has also been measured using an electroacoustic device. The device measures an electroacoustic effect called the electrokinetic sonic amplitude (ESA) and has been applied to measure the zeta potential of aluminium hydroxide particles in solutions ranging up to 3 M NaCl and pH 12.8 (Rowlands *et al.*, 1997) and alumina as a function of monovalent salt concentration (up to 1 M and pH 12) (Johnson, Scales and Healy, 1999). To achieve this the authors had to modify a commercially available instrument that is typically limited to mobility measurements in a pH range

of 1 to 13 and conductivity range of 0 to 5 S m⁻¹ (approximately 0.5 M NaCl) (Colloidal Dynamics internet site).

Calibration is required with electroacoustic measurements and the instrument modifications made by Rowlands *et al.* (1997) involved specific calibration for solutions of high conductivity. To qualify as a calibration standard, an electrolyte must have a strong ESA signal, and for this to be the case one of the ions should be large, hence the instrument was calibrated using CsCl. The electrolyte calibration involves the assumption that the ionic mobilities are independent of frequency, which is less likely at high electrolyte concentrations due to the ionic mobility being affected by ion interactions with the possibility of these interactions being frequency dependent. It was found that the assumption was approximately valid for CsCl, BaCl₂ and KCl, but not for NaCl. This was attributed to an 'electrode effect' which is more pronounced for NaCl because it has a small ESA signal (Rowlands *et al.*, 1997).

At high electrolyte concentrations, the ESA signal from the colloidal particle is small in comparison to the background electrolyte. The ESA signal attributable to the particle is extracted by measuring the ESA signal of solutions of identical conductivity and pH as those of the suspensions (Rowlands *et al.*, 1997). Measuring mobilities at high ionic strength using electroacoustics would appear to be near or at the limit of this technique, while the extraction of the ESA signal that contributes to the particle mobility would at best be expected to have large errors associated with it.

In characterising the surface charge of hematite, the solution conditions to be used in this study are likely to be beyond the limitations of conventional surface potential determination and inappropriate for examination by electroacoustics. Hence electrophoretic mobility measurements derived by utilising phase analysis light scattering present the best option for characterising zeta potentials over a wide range of pH and ionic strength.

3. OBJECTIVES

There is a wealth of literature discussing the adsorption of polyelectrolytes onto oxide surfaces, but such studies are generally limited to conditions of rather benign pH and low ionic strength. In addition, there has been little research carried out to examine the mechanism of polyelectrolyte adsorption *in situ*. The Bayer process operates under high caustic and high ionic strength conditions and this presents quite a unique set of conditions with regards to the study of polyelectrolyte adsorption onto oxide surfaces.

As the flocculation of bauxite residue material is commonly achieved using flocculants containing the carboxylate functionality, the principle aims of this study were to obtain a fundamental understanding of the adsorption mechanism of polyacrylate onto hematite (a model Bayer residue solid) *in situ* and under conditions that relate as nearly as possible to the Bayer process. Hence, the focus of this study has obviously been to examine the flocculant-substrate interaction at high pH. In addition, examinations have been carried out at low pH, to contrast the high pH results and investigate any significant differences. The following strategy was used to accomplish these aims:

- Establishment of an FTIR-ATR technique able to examine polyelectrolyte adsorption onto hematite *in situ*.
- Mechanistic studies to characterise the mode of adsorption of polyacrylate onto hematite at low and high solution pH.

Studies derived using FTIR-ATR rely primarily on the speciation changes of the carboxylate functional groups of the polymer when going from unadsorbed to adsorbed. This can be simplified by noting the fact that at low pH, polyacrylic acid is totally protonated, while at high pH it is totally deprotonated and hence at both pHs there exists as only one carboxylate species. Hence, intermediate pHs have not been examined because the polymer will be only partially deprotonated and the complexity of signals due to protonated and deprotonated carboxylate groups will unnecessarily complicate any FTIR-ATR study.

The study also sought to investigate parameters that affect this adsorption process. Strategies used to accomplish this aim include:

- Examination of the effects that variables such as polymer molecular weight, pH and ionic strength have on adsorption of polyacrylate onto hematite, by measurement of adsorption isotherm and adsorption kinetic information.
- A MALLS investigation to measure solution dimensions of polyacrylate as a function of solution pH and ionic strength.
- Electrophoretic mobility measurements (derived using phase analysis light scattering) to derive zeta potentials of colloidal hematite samples to investigate the surface charge of hematite as a function of pH and ionic strength.

4. MATERIALS AND METHODS

4.1 Samples and Reagents

4.1.1 General Reagents

- FeCl_3 : BDH Chemicals, AR Grade.
- HCl : BDH Chemicals, 33.0 – 33.5%, AR Grade.
- AgNO_3 : Ajax Chemicals, AR Grade.
- NaOH : Rowe Scientific, AR Grade.
- $\text{LiOH}\cdot\text{H}_2\text{O}$: Sigma Chemicals, minimum 99%, LR Grade.
- $\text{CsOH}\cdot\text{H}_2\text{O}$: Sigma Chemicals, minimum 99% (99.5% on basis of metal content), LR Grade.
- NaCl : BDH Chemicals, AR Grade.
- LiCl : Rhone – Poulenc LTD, LR Grade.
- CsCl : Sigma Chemicals, minimum 99%, LR Grade.
- NaNO_3 : Ajax Chemicals, AR Grade.
- LiNO_3 : Rowe Scientific, AR Grade.

4.1.2 Aqueous Solutions

- Water (general): Deionised water passed through a Millipore Mill-Q₁₈₅plusTM system fitted with a final 0.2 μm filter.
- Water (used in MALLS preparations): As above but passed through an additional 0.1 μm filter.
- pH measurements: All pH measurements were carried out using a Ross[®] Sure-Flow (Model No. 8165) pH probe attached to an Orion (Model 520) pH meter. The pH of aqueous solutions was decreased using HCl or increased using the

corresponding alkali hydroxide (NaOH, LiOH or CsOH). An exception was pH 14 solution conditions, which were prepared volumetrically.

- The ionic strength of aqueous solutions was adjusted by using the corresponding alkali chloride or alkali nitrate (NaCl, KCl, CsCl, NaNO₃ or LiNO₃).

4.1.3 Colloidal Hematite Preparation

Aqueous hematite colloids were prepared through an adaptation of the method described by Kan *et al.* (1996). Equal volumes of FeCl₃ (0.01 M) and HCl (0.004 M) were mixed in a round-bottomed flask fitted with a water-cooled reflux condenser. The mixture was heated to boiling, and the heat adjusted to maintain a constant reflux, for 48 hours. Once refluxed, the colloid was cooled to room temperature and dialysed (Spectra/Por[®] CE Membrane, MWCO: 500) against water for 7 days to remove any residual salts. The water in which the dialysis tubes were placed was changed daily.

A portion of the resultant colloid was analysed for iron by digesting it in HCl and analysing by ICP-AES (sequential ICP, Varian, Liberty 220). The final dialysis water (5 mL) was analysed for chloride ions, whereby the chloride ion concentration was determined turbidimetrically as AgCl, precipitated by the addition of AgNO₃ (0.09 M, 50 mL).

The particle size distribution of the hematite particles in the colloid was determined by laser diffraction (Malvern Instruments Mastersizer MS2000 – dual laser source giving two size ranges, which the software blends to report a size range of 0.02 to 2000 µm).

The colloid was also characterised by X-ray diffraction (XRD) on a Philips X'pert X-ray Automated Powder Diffractometer. XRD of the colloid was achieved by casting several layers of the colloid onto a zero background silicon XRD slide, then air drying and running the sample for 4 hours (cobalt K α : 40 kV and 30 mA, scan angle: 5 – 90° 2 θ , step size: 0.02°, time per step: 5 s, spinner on and continuous scan).

Transmission electron microscopy (TEM) images of the colloidal particles were acquired by depositing a drop of the colloid (diluted to 50%) onto a carbon coated copper TEM grid and air drying. The TEM examination was then made using a Philips 430 TEM at an acceleration voltage of 300 kV.

4.1.4 Adsorbates and Adsorbate Solutions

Details of the adsorbates used in this study, together with the codes used to identify them, are shown in Table 4.1. All were used as received.

Table 4.1: Adsorbates used in this study.

Adsorbate	Manufacturer	Molecular Weight	Code
Pimelic Acid	Aldrich, 98%, LR Grade	160	-
Polyacrylic Acid	Aldrich (powder)	~2 000	PAA2K
Polyacrylic Acid	Aldrich (powder)	~5 100	PAA5K
Polyacrylic Acid	Aldrich (powder)	~450 000	PAA450K
Sodium Polyacrylate (ALCLAR 600)	Allied Colloids (powder) (now Ciba Specialty Chemicals)	~13 000 000	PAA13M

Concentrated adsorbate solutions (concentration range: 1 000 – 30 000 ppm) were prepared by the addition of adsorbate to an aqueous solution of the approximate pH required, followed by mixing on a stirrer table (3 days for polymers, 1 day for pimelic acid) until dispersed. Once dispersed, the solution was made up to the required pH and ionic strength and stirred for a further day. The final pH of the solution was then recorded.

Dilutions of the concentrated adsorbate solutions were made with solutions of the required pH and ionic strength. Once again, the solutions were stirred for a further day to ensure dispersion before the pH of the solution was finally recorded.

4.2 FTIR-ATR Spectroscopy

4.2.1 Instrumentation

FTIR-ATR spectra were obtained using a Bruker IFS 66 instrument, MCT (mercury cadmium telluride) detector and Harrick 'Seagull' variable angle, single-bounce ATR accessory. Figure 4.1 gives a schematic representation of the experimental set-up for ATR measurements. Test solutions were pumped through the flowcell of the Seagull accessory to waste by a peristaltic pump (Masterflex model 7550-92, pump head model 7518-10). The pump was calibrated before each use to accurately deliver $1.0 \pm 0.02 \text{ mL min}^{-1}$ by measuring the mass of water per unit time. The total volume from test solution to waste was 3.05 mL (tubing: Masterflex Tygon tubing number 6409-13) and the volume of the flowcell was 0.75 mL. The ATR element in all experiments was a hemispherical ZnSe crystal (Harrick Scientific Corporation).

Solutions were pumped through the 'Seagull' flowcell at a constant flowrate of 1 mL min^{-1} (unless otherwise stated). A spectral resolution of 4 cm^{-1} was used and the number of scans accumulated ranged from 56 to 256 depended on the intervals between acquiring spectra. The incident angle of the infrared beam was 45° (unless otherwise stated).

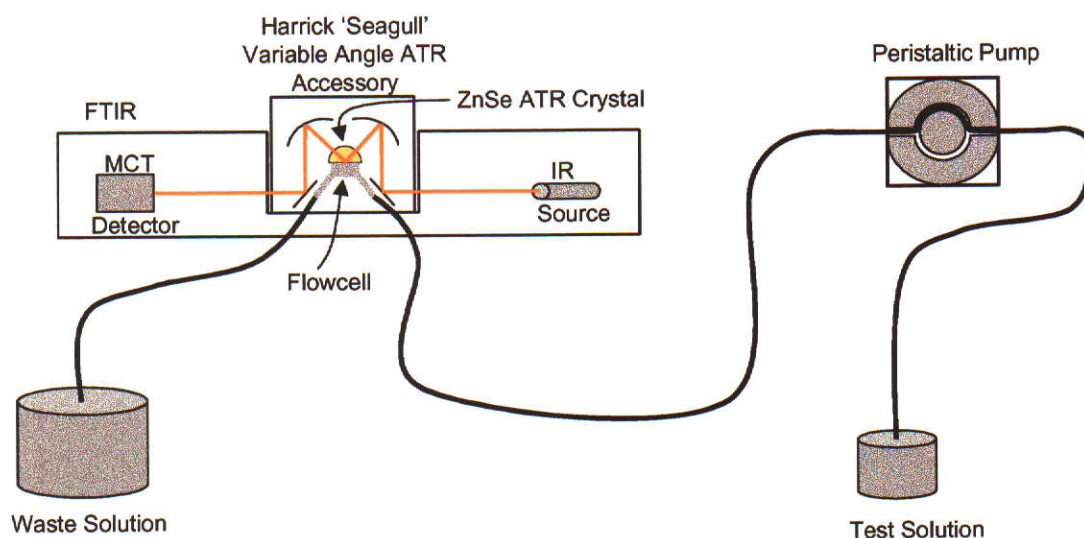


Figure 4.1: Schematic representation of FTIR-ATR experimental set-up.

The Harrick 'Seagull' variable angle ATR accessory is shown schematically in Figure 4.2. Mirrors M1, M2 and M3 direct the infrared beam onto the ellipsoidal mirror (M4), which focuses the beam onto the sample. The sample reflects the attenuated beam onto ellipsoidal mirror M5 and then to mirrors M6, M7, and M8 to the detector. When changing the incident angle, mirrors M3 and M6 are coupled to rotate together, directing the beam to different portions of the ellipsoidal mirrors. This configuration automatically preserves the optical alignment for any selected angle of incidence (Seagull data sheet, Harrick Scientific Corporation).

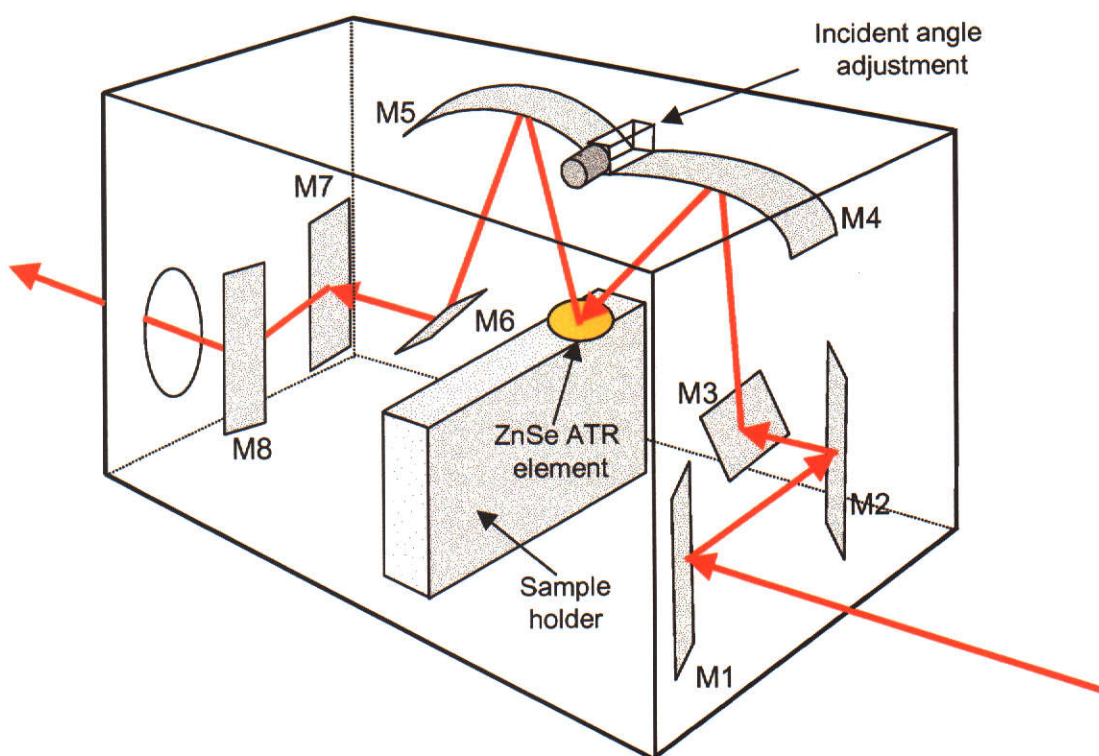


Figure 4.2: Schematic representation of the Harrick 'Seagull' variable angle reflection accessory, showing the mirrors M1 to M8.

4.2.2 *Spectra of Concentrated Adsorbate Solution Species and Adsorbed Species on Hematite*

The background measurement for all spectra was that of the clean dry ZnSe crystal. Because of the time difference between background measurement and sample measurement (1 to 5 days), several backgrounds were recorded at various purge conditions so that the conditions between background and sample could be matched. For the spectra of concentrated adsorbate solution species, no hematite film was cast onto the ZnSe ATR element. For the adsorbed species spectra, once the background

measurements had been acquired, the hematite film was cast onto the ZnSe crystal and left to dry at least overnight.

Initially, a solution containing no adsorbate was introduced and a spectrum recorded (A). For the adsorbed species spectra, the hematite film was equilibrated (approximately 30 minutes) with this solution. Solution containing adsorbate was then introduced and a spectrum obtained (B).

The spectrum of the concentrated adsorbate solution species was obtained by spectral subtraction ($B - A$). For the adsorbed species, spectra were collected as a function of time (C) and the adsorbed species spectra again obtained by spectral subtraction ($C - A$).

Often the resultant species spectrum exhibited peaks attributable to water vapour and carbon dioxide as a result of slight variations in the purge conditions between spectra A and B. The water vapour spans the spectral region of interest in this study and was removed by a weighed subtraction of a difference in two background spectra. The difference in two background spectra is essentially a spectrum of water vapour and carbon dioxide. The carbon dioxide bands ($\sim 2350\text{ cm}^{-1}$) occur in a spectral region that did not interfere and were therefore ignored.

4.2.3 Optical Parameters Study for FTIR-ATR Spectroscopy

Transmission spectra were obtained using a DTGS (deuterated triglycine sulfate) detector. A resolution of 4 cm^{-1} was used and 4 scans accumulated. The path length of the fixed path-length cell was calculated from the interference fringes created by the empty (air) cell with ZnSe windows.

ATR spectra were obtained as described above. Two incident angles of infrared radiation were used (45° and 50°).

The absorbance of the water peak at 2125 cm^{-1} and the weakly absorbing peak at 2210 cm^{-1} for benzene (AR Grade – BDH Chemicals) were determined by a Type 1 integral (see Section 4.2.4) from $2000 - 2250\text{ cm}^{-1}$ and $2200 - 2220\text{ cm}^{-1}$, respectively.

4.2.4 Peak Area Determination

The peak area rather than peak height was used as a measure of peak absorbance in this study. Integrals were calculated using Bruker Opus version 2.0 software. Two types were necessary and are illustrated in Figure 4.3. Type 1 was used for resolved peaks (e.g. 1720 cm^{-1} and 1560 cm^{-1}) and is a valley-valley peak area determination. Type 2 was used for overlapped peaks (e.g. 1410 cm^{-1}) and is a three-valley, perpendicular drop peak area determination.

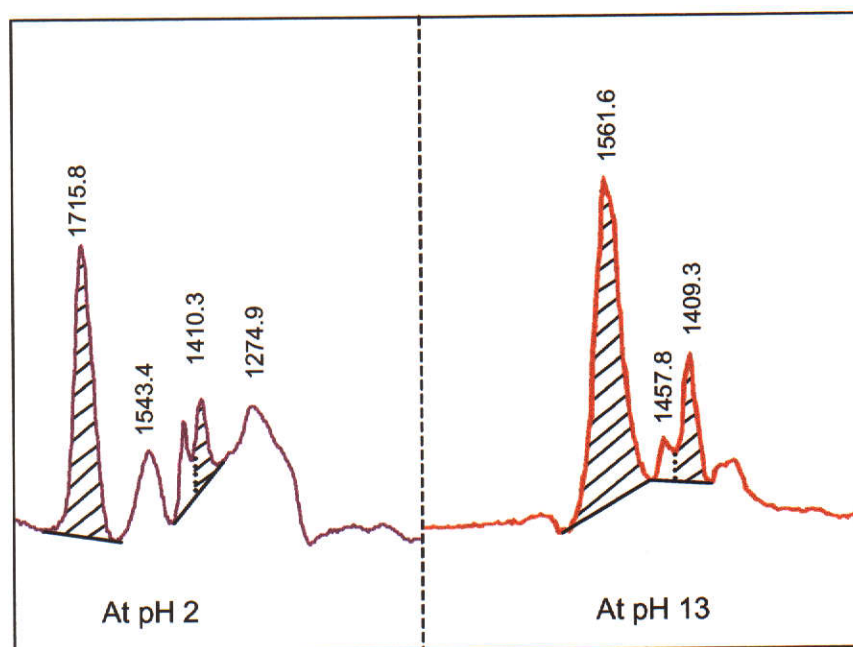


Figure 4.3: Diagram of the peak areas determined in this study. Type 1 (valley-valley) includes: 1720 cm^{-1} ($1630 - 1805\text{ cm}^{-1}$) and 1560 cm^{-1} peaks ($1484 - 1636\text{ cm}^{-1}$); and Type 2 (three-valley, perpendicular drop) includes: 1410 cm^{-1} peak ($1362, 1436$ and 1488 cm^{-1}).

4.3 Multi-Angle Laser Light Scattering (MALLS)

Static light scattering was carried out with a DAWN DSP photometer (Wyatt Technology) fitted with a K5 flowcell and helium-neon laser (632.8 nm). Scattered light was collected at 15 collimated detectors at fixed angles around the flowcell (Figure 4.4b). Each detector observes a fixed angle within the glass flowcell and consequently the scattering angle can be determined. The detector observes an angle that is dependent on the refractive indices of the glass cell, the solvent and also the polymer (Figure 4.4a). The scattering due to the polymer only is determined by the

subtraction of the scattering due to the cell and the solvent. This is performed internally by the instrument software (DAWN 3.30 software).

A 1 wt% dextran solution (0.2 μm filtered - Acrodisc 4652, Gelman Sciences) was used for normalisation of the detectors. PAA450K (200 ppm) and PAA13M (40 ppm) were analysed. Background solutions were generally water at the required ionic strength, except at pH 13, where a pH 13 solution at the required ionic strength was used. Solutions were introduced into the flowcell at 9.92 mL h^{-1} (Razel, Model A-99 syringe pump) through a 5 μm filter (Acrodisc 4199, Gelman Sciences), except for PAA13M at pH 9, 11 and 12 where no filter was used due to the viscosity of the solutions.

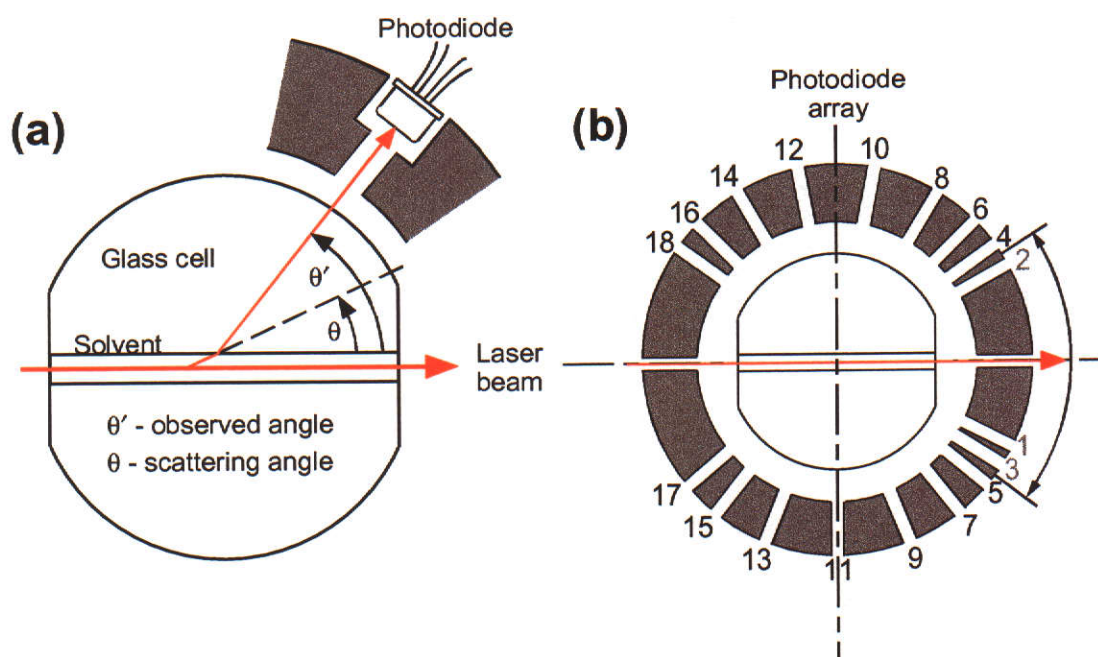


Figure 4.4: Schematic representation of DAWN DSP photometer flowcell, showing relationship between (a) observed angle and scattering angle, and (b) the detectors array around the flowcell. Detectors 1, 2 and 3 can not be used with aqueous solutions due to the solvent scattering.

Light scattering is very sensitive to particulates and air bubbles and the associated scattering is an additive effect. To avoid incorporating these effects, 40 - 60 scans were collected over approximately 30 minutes, of which most were rejected due to excessive scattering. Approximately 10% of the lowest, most reproducible scans were kept to construct the Debye plot and subsequent determination of the radius of gyration.

The collection of data and determination of the radius of gyration was conducted through the use of DAWN 3.30 software using the Debye formulation. A consequence of Debye formulation is the requirement of fitting a polynomial, which is user selectable. A 5th order polynomial equation was required to achieve a suitable fit of the data from the Debye plot and was used in all cases.

4.4 Electrophoretic Mobility

Electrophoretic measurements were obtained using a Brookhaven ZetaPlus instrument at the University of NSW. Measurements were recorded at 23°C using an applied field of 3 V and a frequency of 2 Hz. A total of three sub-samples (5 mL sample cell volume) were analysed for each sample and the error taken as the standard deviation. Each sub-sample was subject to three analytical runs by the instrument at 5 cycles per run. The Smoluchowski model was used to calculate the zeta potential (Tscharnuter, McNeil-Watson and Fairhurst, 1998).

The hematite colloid (prepared as in Section 4.1.3) was used as the substrate and was diluted to a solids concentration of 30 ppm. The pH of samples was adjusted using an alkali hydroxide solution and the ionic strength using the corresponding alkali nitrate salt (NaNO_3 or LiNO_3). The chloride salt was not used because chloride ions have been found to react with the palladium electrode to form a red palladium chloride precipitate, giving erroneous results. The nitrate salt has been found not to interfere (Brookhaven ZetaPlus technician UNSW - Personal Communication). Once prepared, the solutions were stirred for a day and the pH tested. The solutions were then stirred for a further day and the pH tested again to ensure there was no drift. The specific pH of the solution was then recorded. Prior to measurement, samples were vigorously shaken and then placed in an ultrasonic bath for approximately 1 minute to aid dispersion of particles.

4.5 Other Techniques

In characterising the cast hematite film, an optical microscopy (Nikon Optiphot microscope) equipped with a Pulnix Scan Video Camera (interfaced to Optimas 6.2 software) and atomic force microscopy (AFM) (Digital Instrument, Dimension 3000; Scan area $80 \times 80 \mu\text{m}$; Scan rate 2.289 Hz; Setpoint 0 V) were used.

5. MATERIALS CHARACTERISATION

5.1 Colloidal Hematite Characterisation

5.1.1 Chemical and Physical Properties

Effective use of the FTIR-ATR technique requires that the substrate particles be small and relatively constant in size. Initially, adsorption was examined using FTIR-ATR by placing adsorbed hematite slurries in contact with the ZnSe ATR element (adsorption of particulate matter in contact with the IRE strategy). A number of commercial (Fluka; d_{50} : 0.46 μm ; Aldrich; d_{50} : 1.02 μm) and natural (Mt Newman; d_{50} : 3.68 μm) hematite samples were examined, however no adsorption was detected and even the finest was found to be coarser than desirable. While the hematite samples were considered pure ($> 99\%$), there was also a possibility of surface contamination. The possible presence of surface impurities and the larger than desirable particle size were also issues for zeta potential determinations. For these reasons pure hematite colloids were prepared as outlined in Section 4.1.3. Due to the dilute nature of the colloid, it was advantageous to cast the hematite onto the ZnSe crystal rather than use it as a slurry. This strategy also has the advantage that adsorption gives quantitative surface excess results equivalent to those obtained by solution depletion (Sperline and Freiser, 1995).

To avoid agglomeration and hence destabilisation, the hematite colloids prepared during this study were stored in a refrigerator. While the colloidal solutions remained relatively stable, agglomeration of the aggregates was apparent over time, with the colour change of the colloidal solutions from red to orange indicating an increase in effective particle size. Hence, it was necessary to prepare a number of hematite colloids over the course of the research. The chemical and physical properties of the prepared hematite colloids were reproducible and are summarised in Table 5.1.

Table 5.1: Physical and chemical properties of prepared hematite colloids.

Cl ⁻	Less than 1 µg L ⁻¹ . Below detection limit of AgNO ₃ technique used
Fe	162 – 189 mg L ⁻¹ Fe equivalent to 232 – 270 mg L ⁻¹ Fe ₂ O ₃
XRD (Appendix A)	Indicative of hematite – no contaminant peaks
Particle Size (Colloid 2 - Appendix B)	d ₁₀ = 56 nm d ₅₀ = 96 nm d ₉₀ = 152 nm

The only solution contaminants expected as a consequence of the mode of colloid preparation were hydrogen and chloride ions. The use of a AgNO₃ titration, whereby a AgCl precipitate is formed (Kolthoff *et al.*, 1971, pp716-719), established that chloride ions could not be detected in the dialysis water (i.e. no precipitate formed). The initial concentration of chloride ions in the colloid was approximately $6.03 \times 10^{-1} \text{ g L}^{-1}$. The concentration of Ag⁺ in the mixture was 0.09 M and the solubility product of AgCl is 1.77×10^{-10} (CRC Handbook of Chemistry and Physics, Section 8, Table 159). If it is assume that the detection limit is when the concentration of chloride ions is such that the solubility product is exceeded, then the concentration of chloride ions in the dialysis water must be less than 1 µg L⁻¹. Due to the dialysis technique used it could be expected that the concentration of chloride ions in the colloid would be the same as that in the dialysis water. Therefore the results indicate that the dialysis of the colloid removed almost all chloride ions initially present. The measured pH of the colloid was 5, indicating that the hydrogen ion concentration was also very low.

The XRD analysis of all the colloids was indicative of hematite, with no peaks in the XRD traces indicating the presence of any crystalline contaminant. A typical XRD trace is given in Appendix A. All the colloids were found to be similar in colour and solids concentration (ranging from 232-270 mg L⁻¹ Fe₂O₃), and hence particle size (colour being indicative of particle size for similar solids concentrations). Analysis of the particle size of the second colloid prepared showed the colloid to be relatively monodispersed, with a measured d₅₀ of approximately 100 nm (Appendix B).

5.1.2 Transmission Electron Microscopy (TEM)

The morphology of colloidal ferric oxide particles can be easily manipulated depending on the mode of preparation. Such morphologies include spherical, cubic, rod-like, and ellipsoidal. To minimise potential contamination, the colloids in this study were prepared from dilute FeCl_3/HCl solution according to Kan *et al.* (1996), which was expected to give cubic $\alpha\text{-Fe}_2\text{O}_3$ single crystals of approximately 100 nm in size. The shape and size of the particles formed was confirmed by TEM analysis, and typical images of deposited colloid are shown in Figure 5.1.

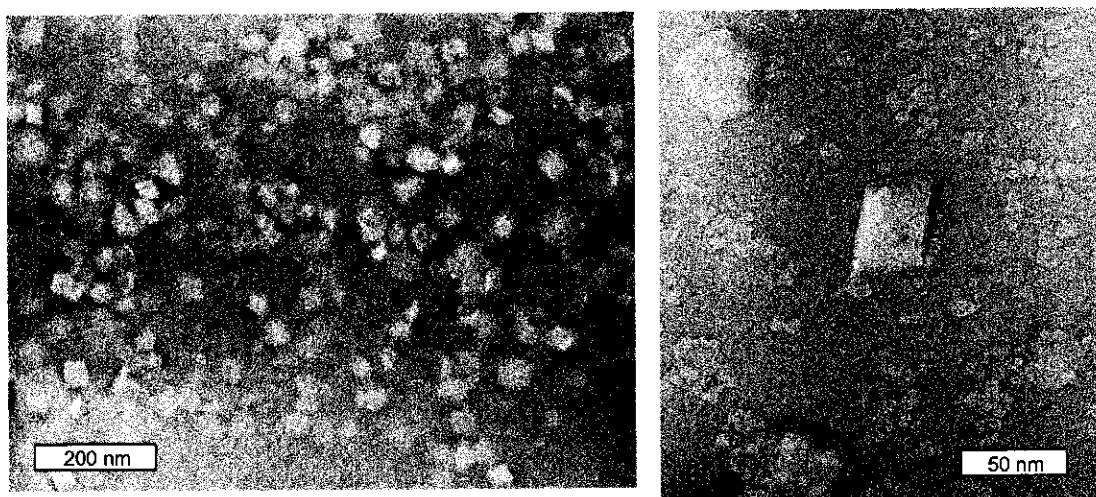


Figure 5.1 TEM images of colloidal hematite particles.

The smaller amorphous material that can be seen more clearly in the right image can possibly be attributed to the sputtered carbon applied to the copper grids that the colloid was cast onto for TEM imaging. The TEM images complement the particle size analysis results in that the particles appear to have a relatively narrow size distribution, although they do indicate that the average size of the discrete particles is probably closer to 50 - 100 nm rather than 100 nm determined by the Malvern Mastersizer. This is probably due to a degree of agglomeration of the samples determined by Malvern Mastersizer. In addition, the low solids concentration in the colloid led to a very low obscuration in the Malvern Mastersizer that was close to the detection limit of the instrument, which is a possible source of error.

5.2 Concentrated Polymer Solution Characterisation

Absorption of infrared radiation associated with molecular vibrations is often used as a means of characterisation and identification. In addition, monitoring spectral changes in the substrate surface and/or that of the adsorbate before and after adsorption is often how the mode of adsorption is elucidated in spectroscopic investigations. It was anticipated that the mode of adsorption of polyacrylate onto hematite could be determined by analysing spectral changes in the adsorbate before and after adsorption. To achieve this, the chemical environment of the polymer in solution was first characterised by recording the infrared spectra of concentrated polymer solutions using a clean, uncoated ZnSe crystal.

The acrylate functionality of polyacrylate has characteristic absorption bands in the 1000 to 2000 cm^{-1} region of the infrared spectrum and Figure 5.2 shows the absorption bands of PAA450K solution species in this region in pH 2 and in pH 13 plus 1 M NaCl electrolyte solution media.

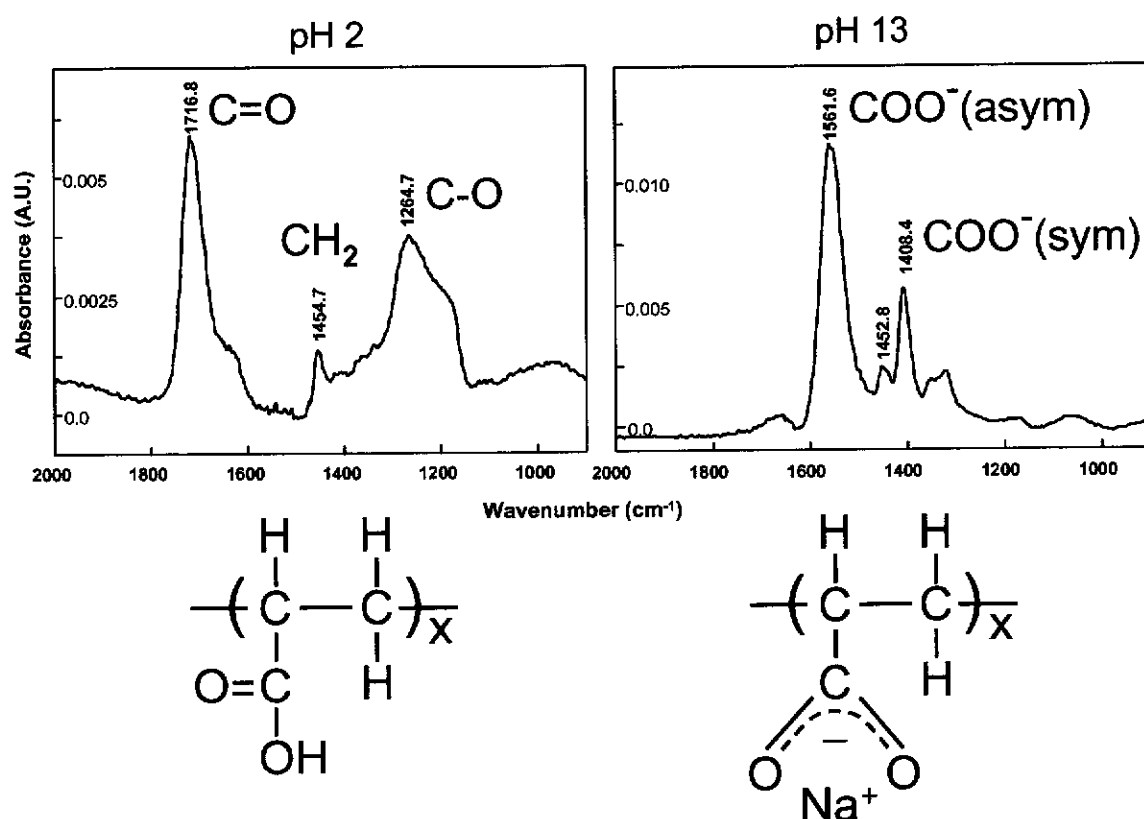


Figure 5.2: Spectra of concentrated PAA450K (1 wt%) solution species at pH 2 and pH 13 (1 M NaCl).

A polymer concentration of 1 wt% was used, which generates a peak absorbance of approximately 0.006 A.U. at 1717 cm^{-1} and 0.012 A.U. at 1562 cm^{-1} for solution pH values of 2 and 13 (1 M NaCl), respectively. At pH 2, the carboxylate functional group is completely protonated, whereas at pH 13 the carboxylate functional group is fully ionised. These results complement those of Boisvert *et al.* (2002), who found that polyacrylate was totally protonated below pH 3 and totally deprotonated above pH 9.

At pH 2 the characteristic stretching frequencies include the carbonyl stretch ($\text{C}=\text{O}$) at 1717 cm^{-1} , CH_2 stretching at 1455 cm^{-1} , and C-O stretch at 1265 cm^{-1} . At pH 13 (1 M NaCl), the characteristic stretching frequencies include the symmetric and antisymmetric stretching frequencies of the carboxylate ion (COO^-) at 1408 cm^{-1} and 1562 cm^{-1} , respectively, and once again the CH_2 stretching frequency 1453 cm^{-1} . These values compare quite well with those of Kulicke and Horl (1985) who carried out *ex situ* FTIR-ATR measurements on polyacrylate and polyacrylic acid ($M_w > 5$ million) by drying 0.5 wt% solutions onto a ZnSe crystal. Polyacrylic acid was found to exhibit the carbonyl stretch ($\text{C}=\text{O}$) at 1704 cm^{-1} and the CH_2 stretch at 1450 cm^{-1} (no mention of the C-O stretch was made). Polyacrylate was found to have the symmetric and antisymmetric stretching frequencies of the carboxylate ion (COO^-) at 1410 cm^{-1} and 1560 cm^{-1} , respectively, and the CH_2 stretching frequency at 1450 cm^{-1} .

It must be stressed that the spectra in Figure 5.2 are those of concentrated polyacrylate solutions species, not adsorbed polyacrylate species spectra, and are the spectra used for a comparison to the hematite adsorbed polyacrylate species spectra. It should also be noted that additional electrolyte (NaCl) to the pH 13 polymer solution does not effect the position of the spectral bands and hence it was taken to be indicative of the sodium salt solution species spectrum.

6. ADSORPTION MODE OF POLYACRYLATES ON HEMATITE

The challenge with *in situ* studies is often that the signal from the bulk solution floods that of the surface signal, making it impossible to detect and deconvolute. It was anticipated that polyacrylate adsorption onto hematite could be detected *in situ* by FTIR-ATR utilising the experimental design outlined in Section 4.2.1. Essentially, a dilute polymer solution at a concentration below the infrared detection limit is flowed over the hematite film that is cast on the ZnSe ATR element. The very small primary particles of the hematite enable the cast film to have a uniform surface area, with the amount of polymer adsorbed directly related to the surface area exposed for polymer adsorption. Therefore, as the polymer adsorbs it concentrates onto the surface of the hematite film with the signal detected attributable to adsorbed polymer, unbiased by the polymer in the bulk solution. A similar signal enhancement has been described by Hug (1997) for the *in situ* FTIR-ATR study of the adsorption of sulfate onto hematite.

6.1 Adsorption Mode at pH 2

The spectra of PAA450K adsorbed onto hematite *in situ* at pH 2 as a function of time are shown in Figure 6.1. When the polyacrylic acid solution used for the adsorption (50 ppm) is analysed on a clean, uncoated ZnSe crystal, the resulting signal of the polyacrylic acid solution species is below the infrared detection limit. The fact that there is a signal for the adsorbed spectra (Figure 6.1) is in itself indicative of polymer adsorption, as the polymer concentrates onto the hematite surface. This is highlighted by the fact that the concentration of unadsorbed PAA450K solution shown in Figure 5.2, which had an absorbance of approximately 0.006 at 1720 cm^{-1} , was 1 wt%. Comparing the maximum absorption of the 1720 cm^{-1} peak ($\sim 0.015\text{ A.U.}$) in the adsorbed species spectra (Figure 6.1) shows that it has an absorbance equivalent to $\sim 2.5\text{ wt\%}$ unadsorbed concentrated polymer solution. The adsorbed species spectral results are summarised and compared with solution spectra (Figure 5.2) in Table 6.1.

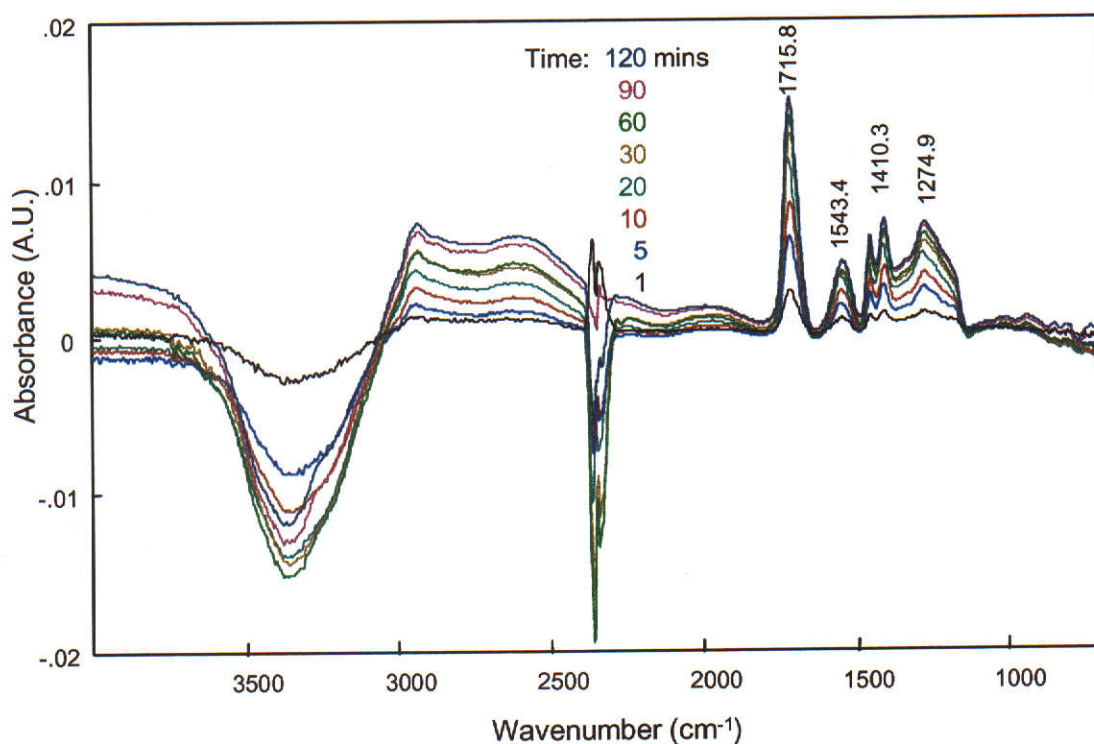


Figure 6.1: Adsorption of PAA450K (50 ppm) onto hematite at pH 2 as a function of time.

Table 6.1: Comparison of FTIR-ATR peak assignments for PAA450K (1 wt% - 10 000 ppm) at pH 2 and pH 13 (1 M NaCl), and after adsorption of PAA450K (50 ppm) at pH 2.

Peak Assignment	pH 2 solution spectrum (cm ⁻¹)	pH 13 (1 M NaCl) solution (cm ⁻¹)	pH 2 adsorbed spectra (cm ⁻¹)
-C=O	1717	-	1716
-COO ⁻ (asym)	-	1562	1543
-CH ₂ scissor	1455	1453	1455
-COO ⁻ (sym)	-	1408	1410
-C-O	1265	-	1275
ΔCOO ⁻	-	154	133

As noted previously (Section 2.4.1.1), of most interest are the stretching vibrations associated with the carboxylate functional group and these form the basis for the interpretation of the adsorption mode. In the adsorbed species spectra, the occurrence of spectral bands at 1410 cm⁻¹ and 1543 cm⁻¹ are indicative of the

symmetric and antisymmetric stretching frequencies of the carboxylate ion. These peaks are absent in the solution spectrum at pH 2 (Figure 5.2) and hence indicate that they are primarily associated with the adsorption process.

For the sodium salt of polyacrylic acid in solution, $\Delta\text{COO}^-_{(\text{salt})}$ was 154 cm^{-1} , while $\Delta\text{COO}^-_{(\text{complex})}$ at pH 2 is significantly lower at 133 cm^{-1} . On this basis, as argued by Deacon and Philips (1980), an adsorbed species involving bidentate chelation (structure (II) - Figure 2.7) is proposed. Only a fraction of the polymer functionalities will actually adsorb onto the surface, with the remainder free to form loops and tails that extend into the solution. Thus, other peaks present in the adsorbed spectra that are characteristic of the carboxylic acid functionality (1717 cm^{-1} and 1275 cm^{-1}) are due to the unadsorbed loops and tails. The shift in the C-O peak from 1265 cm^{-1} in the solution spectrum to 1275 cm^{-1} in the adsorbed spectrum was not considered significant due to the broad and unresolved nature of the peak. The same adsorption behaviour was exhibited by all the polymers (PAA2K, PAA5K, PAA450K, and PAA13M) at pH 2. A schematic representation of the adsorption of polyacrylic acid onto hematite at pH 2 is given in Figure 6.2.

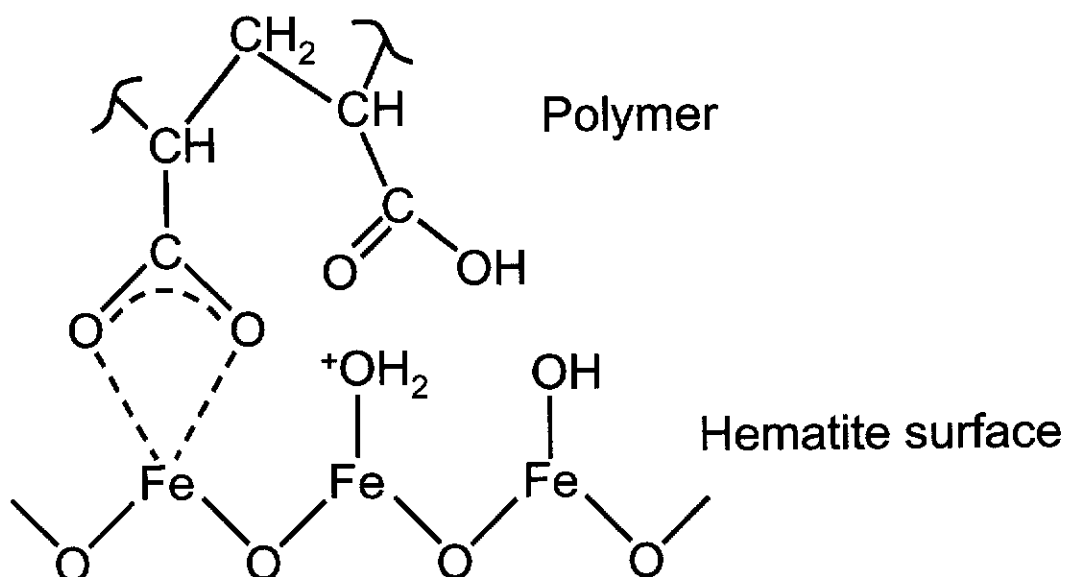


Figure 6.2: Schematic representation of the proposed mode of adsorption of polyacrylic acid onto hematite at pH 2.

Vermohlen *et al.* (2000) examined polyacrylic acid coated alumina using an *ex situ* DRIFT approach. Their results showed peaks associated with the symmetric and antisymmetric stretch of the carboxylate ion, indicating that the polymer was coordinated to the alumina. Due to the poor resolution the peak, as a result of the *ex situ* approach, it was not possible to distinguish bidentate bridging coordination from bidentate chelation. Similarly, in their results a peak attributable to the carboxyl stretch indicated that not all of the polymer chain was adsorbed, however the polymer was coated to the alumina rather than adsorbed and this result may have been due to multi-layer coverage rather than unadsorbed polymer segments.

Apparent in the adsorbed species spectra at pH 2 for all the polymers in this study was the increasingly negative peak at approximately 3300 cm^{-1} . The bidentate chelate surface adsorbed structure proposed requires that a binding carboxylic acid functional group becomes deprotonated and binds directly to a surface ferric ion. In this process of binding to a surface ferric ion, surface hydroxyl groups of the hematite must be removed. This may be achieved by protonation of the surface hydroxyl group that can then leave as a water molecule, and this loss would generate a negative signal in the O-H stretching region at 3300 cm^{-1} . In addition, as the polymer adsorbs onto the surface, some of its non-bonded segments may displace solvent from the surface and this would also contribute a further signal loss. This is supported by the findings of Connor and McQuillan (1999), who in a study of phosphate adsorption onto TiO_2 attributed a similar negative peak (3150 cm^{-1}) to the displacement of terminal hydroxyl groups from the TiO_2 surface and a contribution from adsorbed water molecule displacement.

To identify both the origin of the negative hydroxyl stretching frequency and confirm the adsorption mode proposed for polyacrylic acid, pimelic acid was adsorbed onto hematite at pH 2. Pimelic acid ($\text{C}_7\text{H}_{12}\text{O}_4$ – shown schematically in Figure 6.3) is a dicarboxylic acid with an aliphatic chain of 5 saturated carbons.

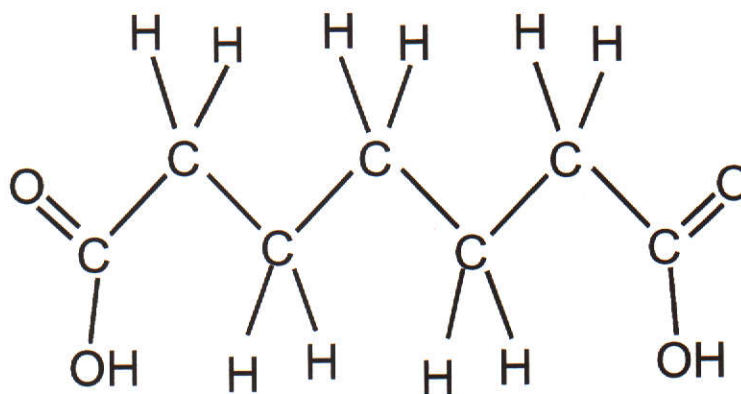


Figure 6.3: Schematic representation of pimelic acid molecule.

It was considered that this molecule would mimic a small segment of polyacrylate, with a chain length long enough to allow the molecule to bind through both carboxylic acid groups, if that proved most favourable. The spectra of adsorbed pimelic acid (100 ppm) onto hematite at pH 2 are given in Figure 6.4. The concentrated solution spectra of pimelic acid (3 wt%) at pH 2 and 13 (1 M NaCl) are given in Figure 6.5.

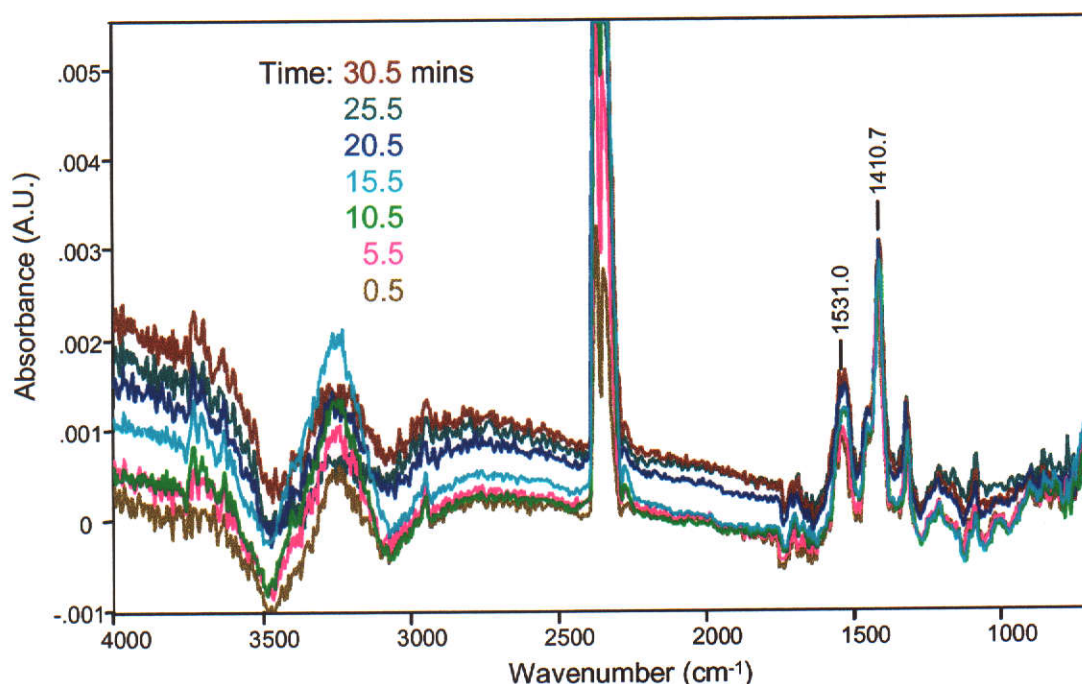


Figure 6.4: Adsorption of pimelic acid (100 ppm) onto hematite at pH 2 as a function of time.

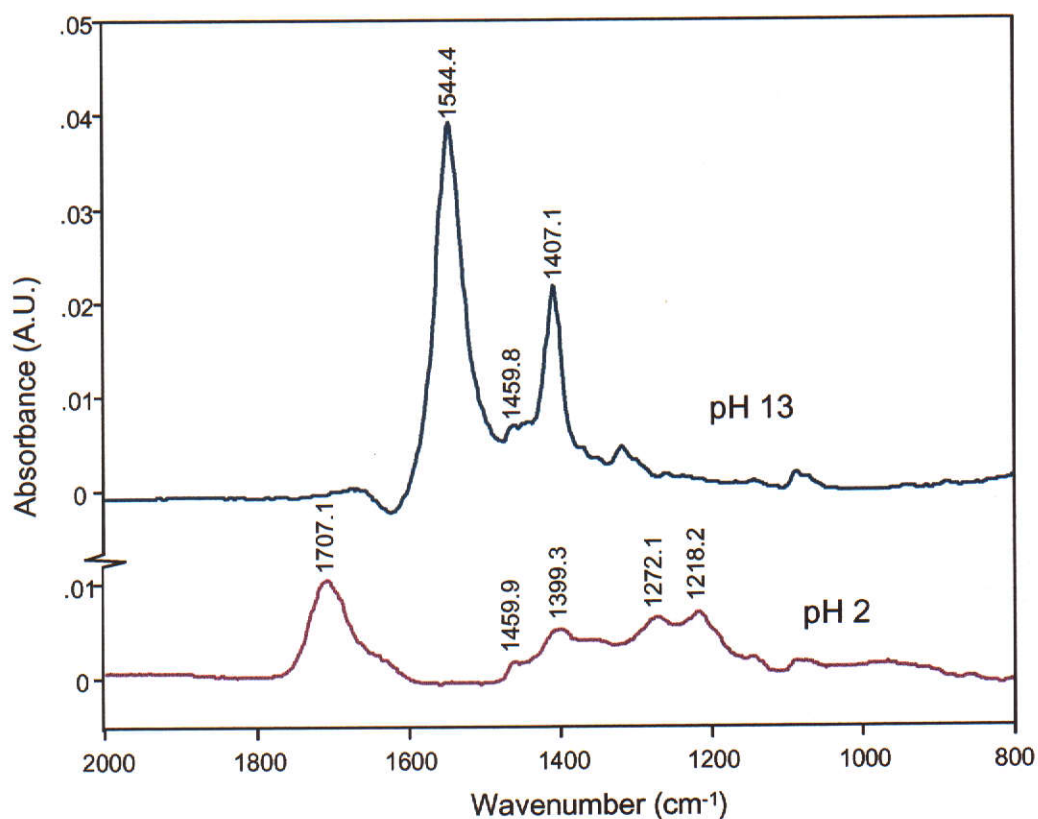


Figure 6.5: Spectra of concentrated pimelic acid (3 wt%) solution species at pH 2 and pH 13.

The principle features of the adsorbed species spectra (Figure 6.4) are summarised in Table 6.2, together with those for the corresponding concentrated solution spectra (Figure 6.5). Like those of adsorbed polyacrylic acid, these results show peaks that are attributable to the symmetric and antisymmetric stretch of the carboxylate ion. A comparison of $\Delta\text{COO}^-_{(\text{salt})}$ (137 cm^{-1}) to $\Delta\text{COO}^-_{(\text{complex})}$ (120 cm^{-1}) once again indicates a bidentate chelate complexation, because $\Delta\text{COO}^-_{(\text{complex})}$ is significantly smaller in value than $\Delta\text{COO}^-_{(\text{salt})}$. Also the absence of a signal due to a carbonyl stretch suggests that pimelic acid was bound to the hematite surface through both carboxylate groups, as a free protonated carboxylate group would have shown peaks at $\sim 1710\text{ cm}^{-1}$ and $\sim 1270\text{ cm}^{-1}$.

Table 6.2: Comparison of spectral peak position for adsorption of pimelic acid at pH 2.

Peak Assignment	pH 2 solution spectrum (cm ⁻¹)	pH 13 solution spectrum (cm ⁻¹)	pH 2 adsorbed spectra (cm ⁻¹)
-C=O	1707	-	-
-COO ⁻ asym	-	1544	1531
-COO ⁻ sym	-	1407	1411
-C-O	1272	-	-
Δ COO ⁻	-	137	120

This is similar to the results found by Dobson and McQuillan (1999) for their *in situ* FTIR-ATR study using molecules from the same homologous series as pimelic acid. They characterised the adsorption of the dicarboxylic acids succinic (C₄H₆O₄) and adipic (C₆H₁₀O₄) onto TiO₂ and Al₂O₃ from aqueous solutions. For concentrated sodium succinate solution species, Δ COO⁻_(salt) was 157 cm⁻¹ while for adsorbed succinic acid species, Δ COO⁻_(complex) for was 126 cm⁻¹ and 133 cm⁻¹ for TiO₂ and Al₂O₃, respectively. Once again, this indicates a bidentate chelate complexation because Δ COO⁻_(complex) is significantly smaller in value than Δ COO⁻_(salt). Adipic acid was found to behave in the same manner to succinic acid and hence also adsorbed via bidentate chelation coordination to TiO₂ and Al₂O₃. In addition, the absence of a signal due to a carbonyl stretch in all adsorbed species spectra suggests that both succinic and adipic acid was bound to the TiO₂ and Al₂O₃ surfaces through both carboxylate groups, as was found for pimelic acid adsorption onto hematite.

These results differ though from those of Specht and Frimmel (2001). In their *in situ* FTIR-ATR study they characterised the adsorption of malonic (C₃H₄O₄) and succinic dicarboxylic acids onto kaolinite as a function of pH. At low pH, the authors proposed a type of surface complexation different to the bidentate chelate adsorption mode proposed for pimelic acid on hematite.

These authors suggested that a shift of the carbonyl stretch to lower energy was indicative of a weakened double bond caused by bonding of the other oxygen atom (from the carboxylate functional group) to the kaolinite surface. They proposed that

the adsorption mode was dominated by monodentate complexation (structure (I) – Figure 2.7) of both carboxylate groups of the molecule to surface aluminium atoms.

The similarities between the adsorption mode for hematite, TiO_2 and Al_2O_3 may be due to their comparative surface charge properties, namely their similar pzc (8.2 and 6 and 9.5, respectively) and surface hydration (Amhamdi, Dumont and Buess-Herman, 1997; Berube and de Bruyn, 1968; Johnson, Scales and Healy, 1999). This differs significantly from that of kaolinite, which does not have a pzc and is heterogeneous in surface charge. It exhibits negative charges on the cleavage or basal planes at all pHs and positive charges around the crystal edges (up to approximately pH 7) (Hunter, 1993, pp17, 230). The relationship between surface charge properties, pzc/iep and surface hydration is discussed in more detail in Section 8.2.2.

Interestingly, there was no negative peak at approximately 3300 cm^{-1} in the pimelic acid adsorbed spectra, perhaps indicating that this negative peak in the adsorbed polyacrylic acid spectra was due to displaced solvent from the surface, rather than displaced surface hydroxyl groups. This may indicate that the hydrophobic aliphatic chain of pimelic acid tends to keep away from the surface whereas the hydrophilic non-bonded carboxylic acid groups of the polymer may approach more closely and displace water from the surface region. It may also be that this occurs because adsorbed polyacrylic acid occupies a much greater volume (at the expense of solvent) within the measured interaction volume of the evanescent wave compared to pimelic acid, as shown schematically in Figure 6.6.

In addition, there was no signal due to a carbonyl stretch, suggesting that pimelic acid was bound to the hematite surface through both carboxylate groups. This supports the assertion that in the adsorbed polymer spectra, the presence of the carbonyl stretching frequency is attributable to the unadsorbed loops and tails of the adsorbed polymer molecules.

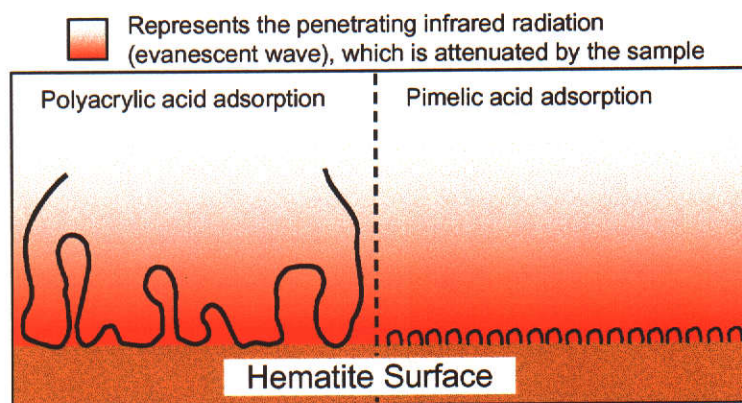


Figure 6.6: Diagrammatic representation of the large volume occupied by adsorbed polyacrylic acid in the measured interaction volume of the evanescent wave resulting in detection of solvent displacement. In comparison, adsorbed pimelic acid occupies a small volume and no solvent displacement is detected.

In summary, polyacrylic acid and pimelic acid were found to complex to hematite in the same manner (bidentate chelation – structure (II) – Figure 2.7) with adsorption to the hematite surface through carboxylate groups. Polyacrylic acid adsorption was accompanied by solvent displacement while pimelic adsorption was not. It is suggested that due to the polymer molecule being more hydrophilic than pimelic acid it is able to approach closer to the hematite surface and hence displace water from the surface region. More significantly, it is thought that the volume that the adsorbed polymer occupied at the expense of solvent was much greater than that of adsorbed pimelic acid and thus more of a contributing factor.

The results of this study, and others, suggest that carboxylates complex onto mineral surfaces readily at low pH, but the mode of attachment is dependant on the substrate. Surface bidentate chelate complexation was found for hematite (this study), TiO_2 and Al_2O_3 (Dobson and McQuillan, 1999) and monodentate complexation for kaolinite (Specht and Frimmel, 2001). The similarities between the adsorption mode for hematite, TiO_2 and Al_2O_3 may be due to them exhibiting similar pzc and surface hydration properties (Amhamdi, Dumont and Buess-Herman, 1997; Berube and de Bruyn, 1968; Johnson, Scales and Healy, 1999), which is significantly different from that of kaolinite (Hunter, 1993, pp17, 230), hence leading to a different adsorption mechanism.

The results also indicated that the mode of attachment for poly-carboxylate molecules at low pH was not dependent on chain length, with a small dicarboxylic

acid molecule (pimelic acid) adsorbing onto hematite in the same manner as polyacrylic acid.

6.2 Adsorption Mode at pH 13

The adsorption mechanism at pH 13 was investigated using the same experimental design as described above. Once again, an adsorbing polyacrylate solution concentration of 50 ppm was used. It was found that polyacrylate did not adsorb at pH 13 unless there was an excess of sodium ions present. For PAA13M (50 ppm) at pH 13 (no added salt) there was no adsorption observed for times up to 30 minutes (Figure 6.7). The pH 13 electrolyte concentration alone represents 0.1 M sodium ions, but an additional 1 M sodium (as NaCl) was required to achieve the adsorption data shown in Figure 6.8.

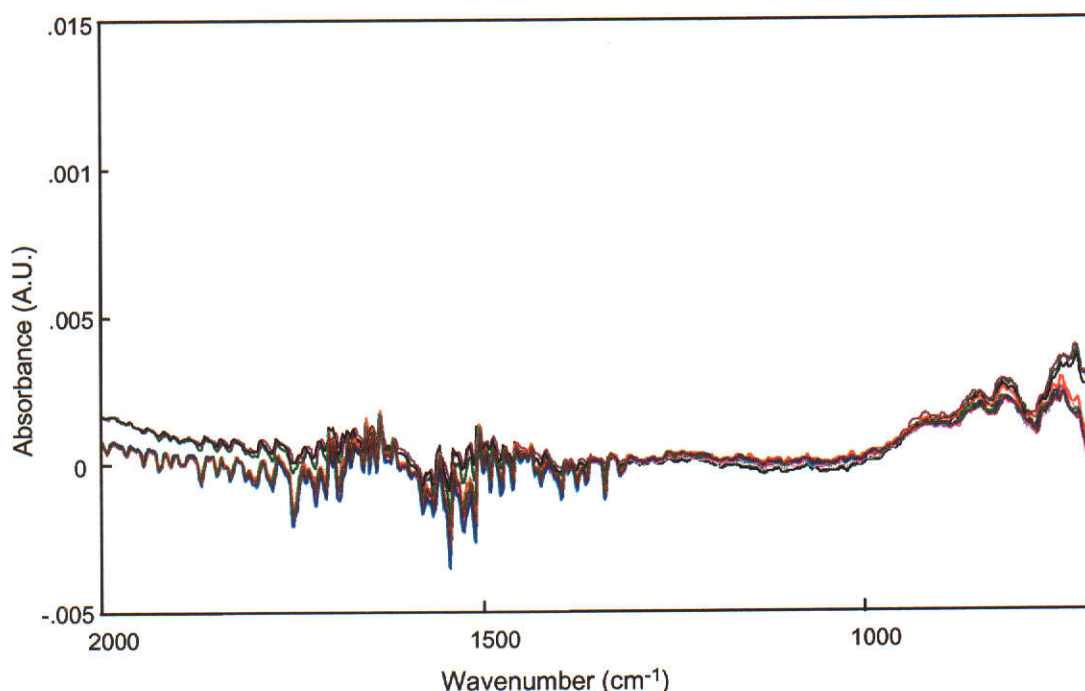


Figure 6.7: Adsorption of PAA13M (50 ppm) onto hematite at pH 13 (no added salt) for 30 minutes.

This result indicates that the sodium ion plays a crucial role in the adsorption of the carboxylate functionality onto hematite under caustic conditions. The peak absorbance of approximately 0.013 A.U. at 1562 cm^{-1} for the adsorbed spectra (Figure 6.8) is very similar to the absorbance of approximately 0.012 A.U. of the equivalent peak in the concentrated (10 000 ppm) unadsorbed polymer spectra

(Figure 5.2). This again highlights that the polymer is adsorbing and concentrating onto the hematite film.

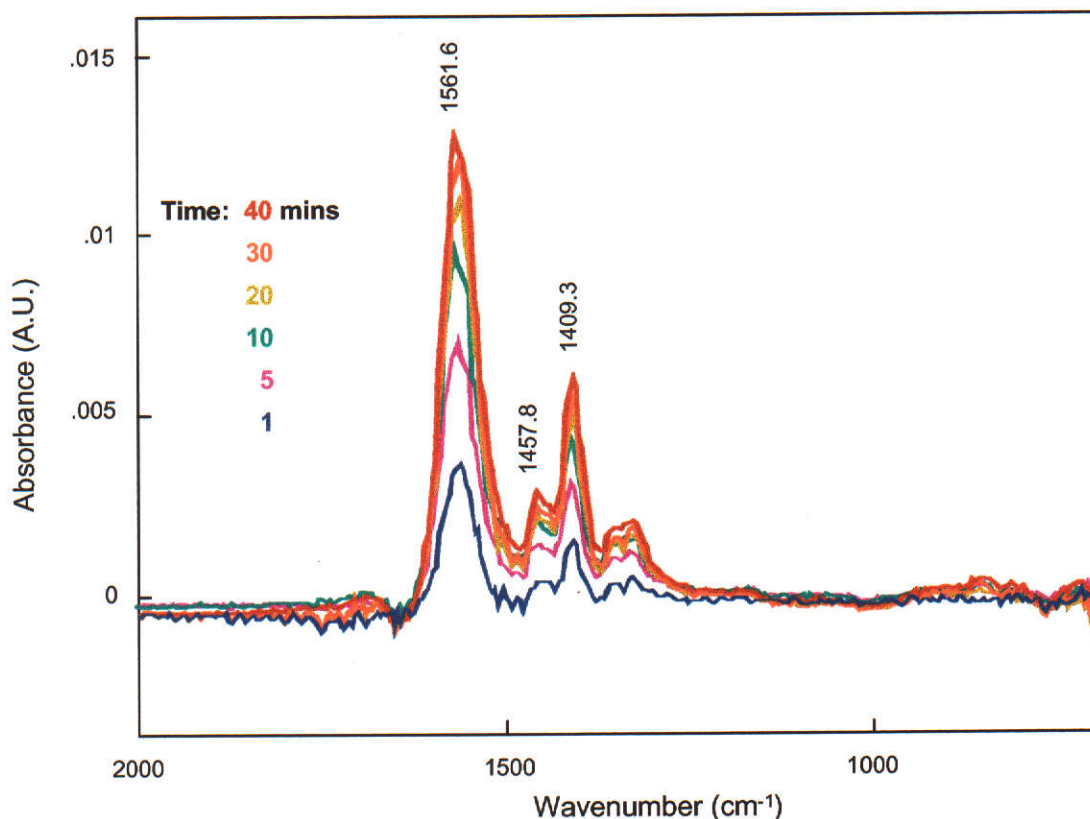


Figure 6.8: Adsorption of PAA450K (50 ppm) onto hematite at pH 13 (1 M NaCl) as a function of time.

The adsorbed spectral results are summarised and compared with the corresponding unadsorbed solution spectra (Figure 5.2) in Table 6.3. It can be seen that $\Delta\text{COO}^-_{(\text{salt})}$ for the sodium salt of polyacrylic acid in solution is almost identical to the $\Delta\text{COO}^-_{(\text{complex})}$ at pH 13 and 1 M NaCl (154 and 153 cm^{-1} , respectively). Use of the Deacon and Phillips (1980) rules outlined in Section 2.4.1.1 would indicate a bidentate bridging structure for adsorption (structure (II) – Figure 2.7). However, this does not take into account the role of the sodium ions, which clearly play a role in the attachment of the negatively charged polyacrylate to the negatively charged hematite surface. In this instance, the adsorption process could be likened to the coagulation of two negatively charged particles by the addition of electrolyte, similar to that described by Hogg (1999) when modelling polymer adsorption kinetics.

Table 6.3: Comparison of spectral peak positions for polyacrylate (PAA450K) at pH 13 (1 M NaCl) in solution and after adsorption onto hematite at pH 13 (1 M NaCl).

Peak Assignment	pH 13 Na salt solution spectrum (cm ⁻¹)	pH 13, 1 M NaCl adsorbed spectra (cm ⁻¹)
COO ⁻ asym	1562	1562
COO ⁻ sym	1408	1409
ΔCOO ⁻	154	153

The adsorbed spectrum at pH 13 (1 M NaCl) was effectively indistinguishable from the unadsorbed solution spectrum under the same conditions. As a consequence, it was not possible to discriminate between the adsorbed and unadsorbed polymer segments, in contrast to the situation at pH 2 (Section 6.1).

In addition, there was no negative peak at 3300 cm⁻¹ associated with polymer adsorption at pH 13, regardless of molecular weight. This is attributed to sodium polyacrylate being much more hydrophilic than polyacrylic acid, as evident from the observation that sodium polyacrylate has a significantly higher solubility than polyacrylic acid in water. This results in more solvent being incorporated into the sodium polyacrylate structure and hence no net displacement of solvent from the interfacial region when the polymer adsorbs onto the hematite. This may also indicate that the relative amount of polymer adsorbed is much greater at pH 2 than at pH 13 (1 M NaCl).

Jones, Farrow and van Bronswijk (1998c) studied the adsorption of polyacrylate onto hematite at pH 13, using an *ex situ* DRIFT approach. Their results indicated an asymmetric bidentate bridging complexation of the carboxylate directly to surface ferric ions (Figure 2.6a). This is obviously contrary to the results found above, where adsorption was not found to occur at pH 13 unless there was added electrolyte and even then, the mode of adsorption was found not to involve chemisorption. The mode of adsorption that they proposed was drawn from spectral interpretation without the consideration that the spectra obtained was actually an average of all interactions that could possibly be occurring. This would seem to be inaccurate because generally there is a greater amount of the polymer unadsorbed than

adsorbed. No consideration was given to unadsorbed polymer or to the possibility that unadsorbed polymer may have collapsed onto the hematite surface and be interacting in a way that was different to the primarily adsorbed polymer. The fact the authors detected adsorption at all may be due to the polymer being forced onto the surface rather than being adsorbed. To separate the hematite from the adsorbate solution for *ex situ* analysis, the samples were centrifuged, decanted and dried under vacuum. Such treatment could be enough to have polymer precipitate onto the hematite surface or interact with the surface even though in the aqueous environment tested, there was little to no affinity, and lead to the spectral shifts they observed.

While it could be considered that the individual electrostatic type interactions proposed for the adsorption at pH 13 (represented schematically in Figure 6.9) would not contribute greatly to any adsorption strength, it is via the sheer number of interactions per polymer molecule that the adsorption occurs and is considered to be irreversible.

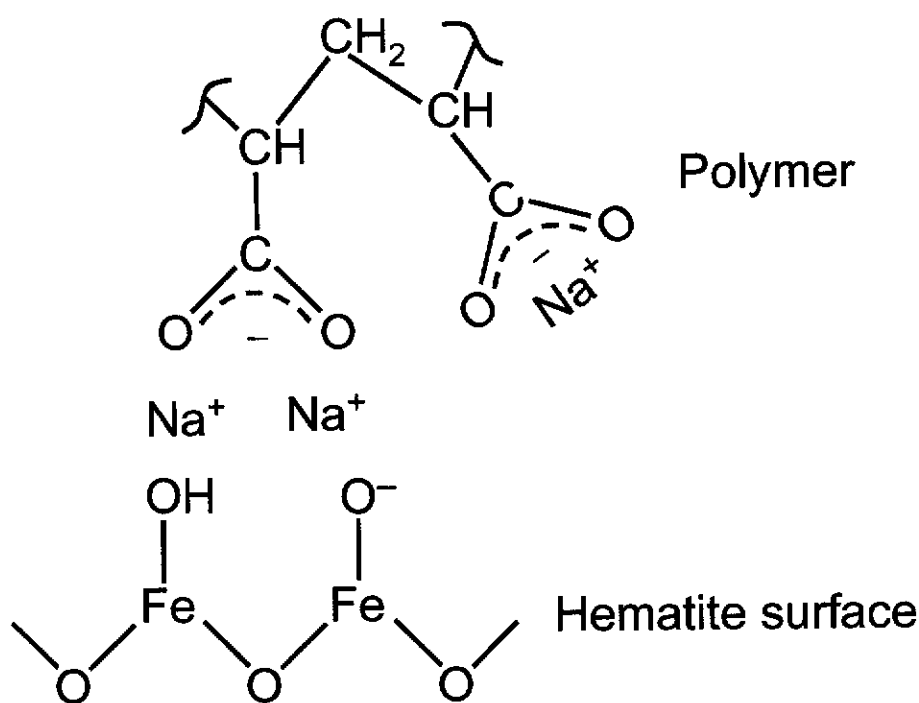


Figure 6.9: Schematic representation of the proposed mode of adsorption of polyacrylate onto hematite at pH 13 in the presence of excess Na⁺ ions.

Irreversible adsorption was observed for all polymers (PAA2K, PAA5K, PAA450K and PAA13M) with the number of carboxylate groups on the polymers ranging from approximately 30 for PAA2K to 140 000 for PAA13M. The irreversible nature of polymer adsorption is demonstrated in Figure 6.10 where PAA5K (50 ppm) was adsorbed onto hematite at pH 13 (1 M NaCl) for 60 minutes and then flushed with pH 13 solution containing no polymer or salt for an additional 15 minutes. By monitoring the adsorption of polyacrylate, and using the area of the 1560 cm^{-1} peak, it was found that there was an initial small amount of desorption but the majority of the polymer remained irreversibly adsorbed, even after 15 minutes of flushing. However, it is plausible that there was little or no desorption and the apparent decrease in adsorption is attributable to the wash solution containing no added electrolyte. This would cause the adsorbed polymer to expand its conformation and hence have more polymer segments further from the surface, resulting in the apparent decrease in the absorbance readings.

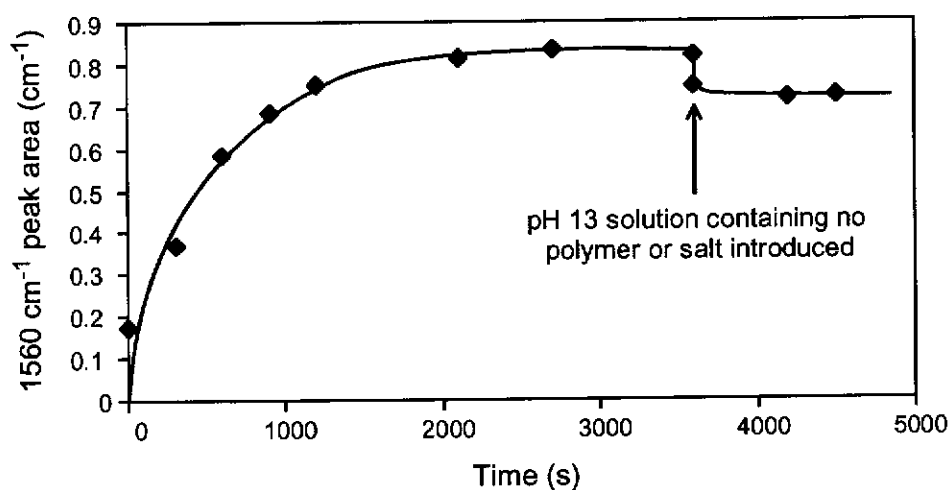


Figure 6.10: Desorption experiment for PAA5K (50 ppm) adsorbed onto hematite at pH 13 (1 M NaCl).

The proposed weak electrostatic mechanism is further reinforced by the observation that pimelic acid (100 ppm) was found to not adsorb at pH 13 (1 M NaCl) even after 20 minutes (Figure 6.11). This would suggest that the electrostatic interaction between the two carboxylate groups on pimelic acid with the hematite surface is not strong enough to allow the molecule to remain adsorbed on the surface. However, polyacrylate has many closely spaced carboxylate groups along the chain and the sum of these electrostatic interactions with the hematite surface, along with having to

desorb all attached segments simultaneously, contributes to each polymer molecule having a strong enough interaction to facilitate irreversible adsorption.

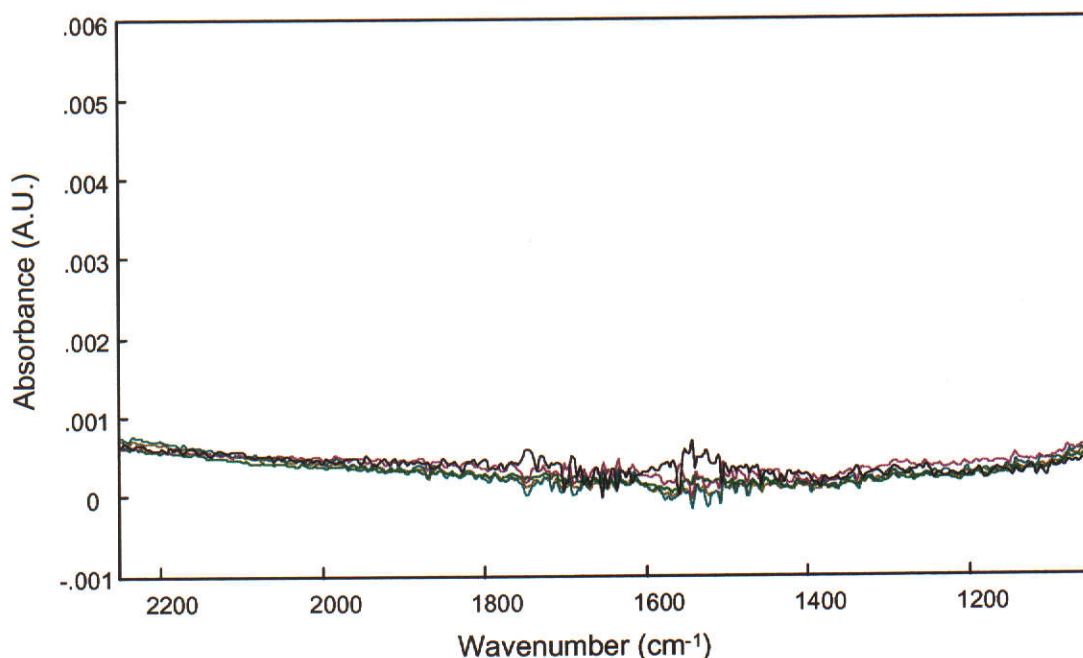


Figure 6.11: Adsorption of pimelic acid (100 ppm) onto hematite at pH 13 (1 M NaCl) for 20 minutes.

Interestingly, this is contrary to what Specht and Frimmel (2001) found *in situ* for the adsorption of dicarboxylic acids onto kaolinite up to pH 11.5. For malonic acid adsorption at pH 7.4, only the stretching vibrations of the carboxylate ion were present, at similar positions to those in the unadsorbed solution spectra. The authors proposed, in agreement with the rules outlined by Deacon and Phillips (1980), a bidentate bridging complexation. However, it is also possible that the ionised carboxylate group of malonic acid was electrostatically attached to the kaolinite surface, as this interaction would exhibit the same stretching frequencies. Steric considerations suggest only one carboxylate is bound, with the other carboxylate group unbound, deprotonated and also exhibiting those same stretching frequencies.

Succinic acid was found to adsorb onto kaolinite in a similar manner to malonic acid at low pH, but differed significantly at higher solution pH. At pH 6.5 and 11.5, the adsorbed spectra developed near equal intensities of frequencies characteristic of the carboxylate ion and the carbonyl functionality. The symmetric and antisymmetric stretching of the carboxylate ion (1396 cm^{-1} and 1552 cm^{-1} respectively) were at similar positions to those in the unadsorbed solution spectra, while the carbonyl

stretch (1650 cm^{-1}) remained unshifted from that exhibited by adsorption of succinic acid at low pH. This would indicate that monodentate complexation persists going from low to high pH, and suggests that one of the bound carboxylate groups becomes non-binding, is deprotonated and hence exhibits the characteristic stretching frequencies of the carboxylate ion.

There are several possibilities as to why pimelic acid did not adsorb onto hematite, while malonic and succinic acids did onto kaolinite. The study by Specht and Frimmel (2001) only went to a pH of 11.5, with no indication of the effects of going to more forcing caustic conditions. Pimelic acid was found not to adsorb onto hematite at pH 13, a caustic concentration almost two orders of magnitude greater. This will obviously have a significant effect on the surface of the substrate and hence the affinity that the molecules may have with it. In addition, the substrates in the two studies were different, and it can be expected that molecules will interact with them differently. This would depend on such factors as substrate surface charge as a function of solution pH, the degree of surface hydration under the conditions tested, and the position and identity of the interacting surface atoms.

The mode of adsorption of polyacrylate at pH 2 and pH 13 are thus radically different. At pH 2 the polymer is uncharged and was found to chemisorb to the hematite surface by bidentate chelate coordination. At pH 13, both the hematite surface and the polymer are expected to carry a net negative charge and adsorption was found to be facilitated by addition of electrolyte, indicating that the adsorption mechanism was an electrostatic process similar to that of coagulation, and promoted by cations.

While all polymer adsorption was found to be irreversible, at high pH adsorption was dependent on chain length or carboxylate spacing with pimelic acid not adsorbing, regardless of the amount of electrolyte added. This is due to the weak individual electrostatic interaction at pH 13, with pimelic acid not having enough points of attachment, and they are too widely separated, for it to adsorb. Polyacrylate, which has closely spaced carboxylate groups along the entire polymer chain, has many weak electrostatic interactions taking place to facilitate molecular adsorption. This results in a high net bond strength and irreversible adsorption.

7. COLLOID DEPOSITION AND CHARACTERISATION

Because of the irreversible nature of polymer adsorption, a fresh hematite film needed to be cast for each adsorption experiment. To fully utilise the potential of the ATR technique there was a need to be able to cast a reproducible hematite film. Knowledge of the analysis area for the infrared beam is essential, because if the hematite film is cast to a diameter that is smaller than the infrared beam area, then there could be variation in the amount of hematite exposed for adsorption in each experiment. Such variations would remove the possibility of quantitative comparisons. Similarly, it was necessary to establish that the colloid was deposited in such a way that a continuous film was presented to each polymer solution.

7.1 Infrared Analysis Area

The analysis area of the infrared beam was determined by monitoring the absorbance of the 3300 cm^{-1} peak associated with water as a function of the diameter of a water droplet that was applied to the clean, dry, uncoated ZnSe crystal (background spectrum was the clean, dry ZnSe crystal). Absorbance was determined as the area of the 3300 cm^{-1} peak measured by a Type 1 integral (see Section 4.2.4) from $2630 - 3746\text{ cm}^{-1}$. The thickness of the water droplet was not relevant, because for a ZnSe–water interface at a wavelength corresponding to 3300 cm^{-1} , the depth of penetration of the evanescent wave is only 345 nm. The analysis area of the infrared beam was found to have a diameter of 3 mm (Figure 7.1) giving an analysis area of $7.07 \times 10^{-6}\text{ m}^2$. Therefore to avoid analysis area variation, the hematite film was cast to a consistent 5 mm diameter.

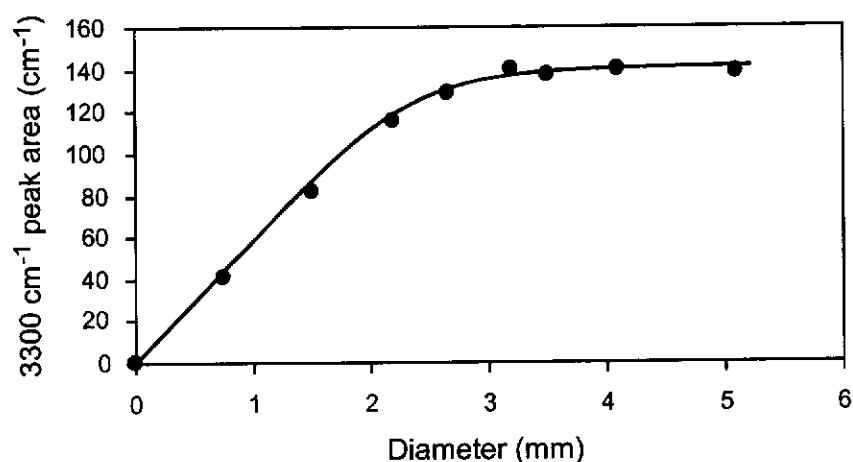


Figure 7.1: Determination of infrared analysis area: 3300 cm^{-1} water peak area versus water droplet diameter.

7.2 Cast Hematite Film Deposition and Characterisation

A template was constructed by punching a hole 6 mm in diameter into a piece of clear plastic overhead projector film. The template was then placed on the ZnSe crystal with the hole centred over the analysis area of the infrared beam. A thin hematite layer was formed on the ZnSe crystal of the ATR accessory by carefully dispensing a selected volume of the colloid from a micropipette (Gilson, Pipetman, P10) to within half a millimeter of the edge of the template and allowing the slurry to dry. This resulted in a cast film with a diameter of 5 mm, which is greater than the analysis area of the infrared beam.

The aim when casting the hematite film was to obtain a film that was thin, uniform and continuous in coverage. The polymer molecules examined were expected to be sufficiently large to only adsorb onto the outer surface of the cast film. Hence by monitoring adsorption as a function of the volume of colloid used to cast the film, it was anticipated that a plateau peak area would be observed, representing complete coverage of the ZnSe crystal surface.

PAA2K (50 ppm) was adsorbed onto the hematite film at pH 2 and a flowrate of 1 mL min⁻¹, with its absorbance (1720 cm⁻¹ peak area) after 20 minutes monitored as a function of the cast colloid volume (Figure 7.2). This figure shows that plateau adsorption was not achieved, presumably because PAA2K is a small enough molecule to achieve some degree of diffusion into the hematite film. Hence the experiment was repeated using the much larger PAA450K.

Figure 7.3 shows the 1720 cm⁻¹ peak area after 30 minutes as a function of cast colloid volume for PAA450K (50 ppm) adsorbed onto the hematite film at pH 2 and at flowrate of 1 mL min⁻¹. The plateau adsorption was achieved at 30 μ L (3×10 μ L) of colloid, and this volume (cast to in a 5 mm diameter) was used for all quantitative studies. Larger volumes were not used to ensure minimum film thickness and hence maximum penetration of the infrared radiation.

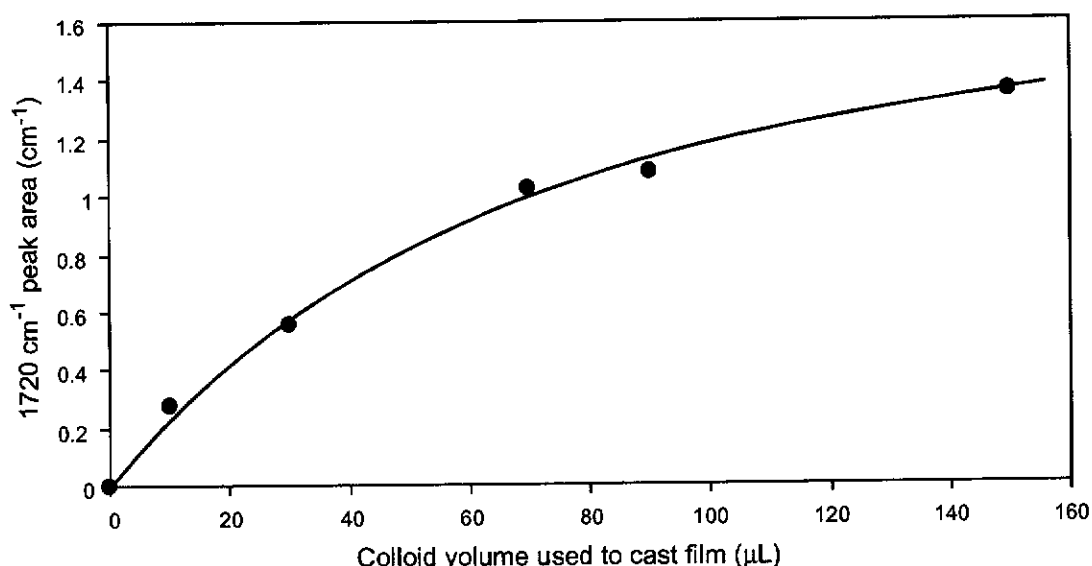


Figure 7.2: Adsorption of PAA2K (50 ppm) onto hematite after 20 mins (monitored by the 1720 cm^{-1} peak area) as a function of colloid volume used to cast the hematite film (flowrate 1 mL min^{-1}).

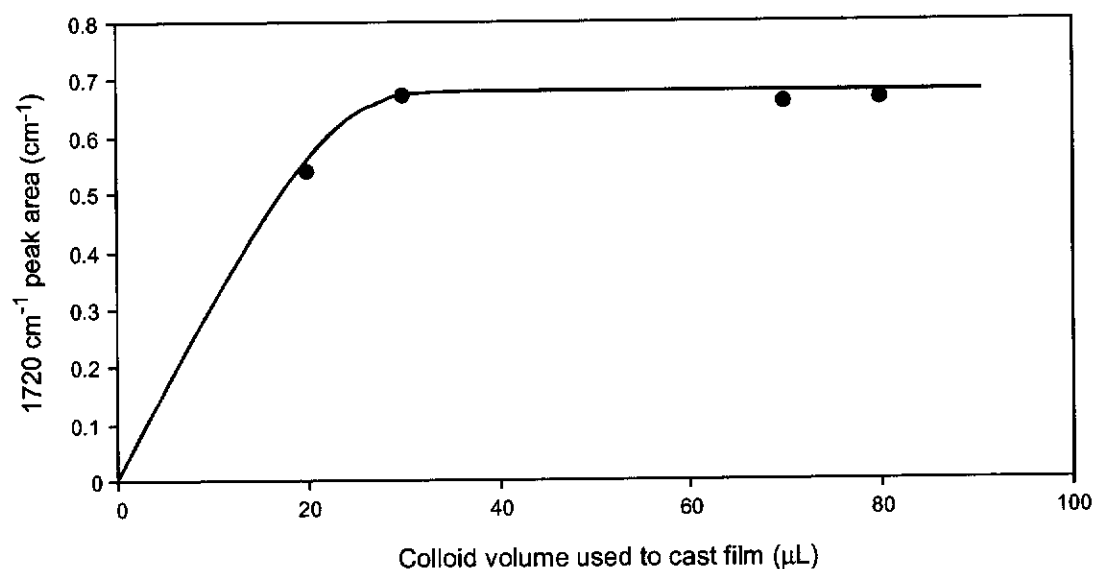


Figure 7.3: Adsorption of PAA450K (50 ppm) onto hematite after 30 minutes (monitored by the 1720 cm^{-1} peak area) as a function of colloid volume used to cast the hematite film (flowrate 1 mL min^{-1}).

The uniformity of the film coverage was examined using optical microscopy. A total of six overlapping images (each representing of an area $1.25 \times 1.25\text{ mm}$) that depicted the entire width of the film were acquired. The monochrome images obtained (Figure 7.4a) show that the film was continuous, as evident by the contrast between the relatively light coloration of the ZnSe crystal and the dark coloration of the hematite film. The high contrast between the ZnSe and the outer rim of the cast

film indicates a dense coverage of colloid in this area. This high contrast is also evident throughout the film, concentrating towards the centre.

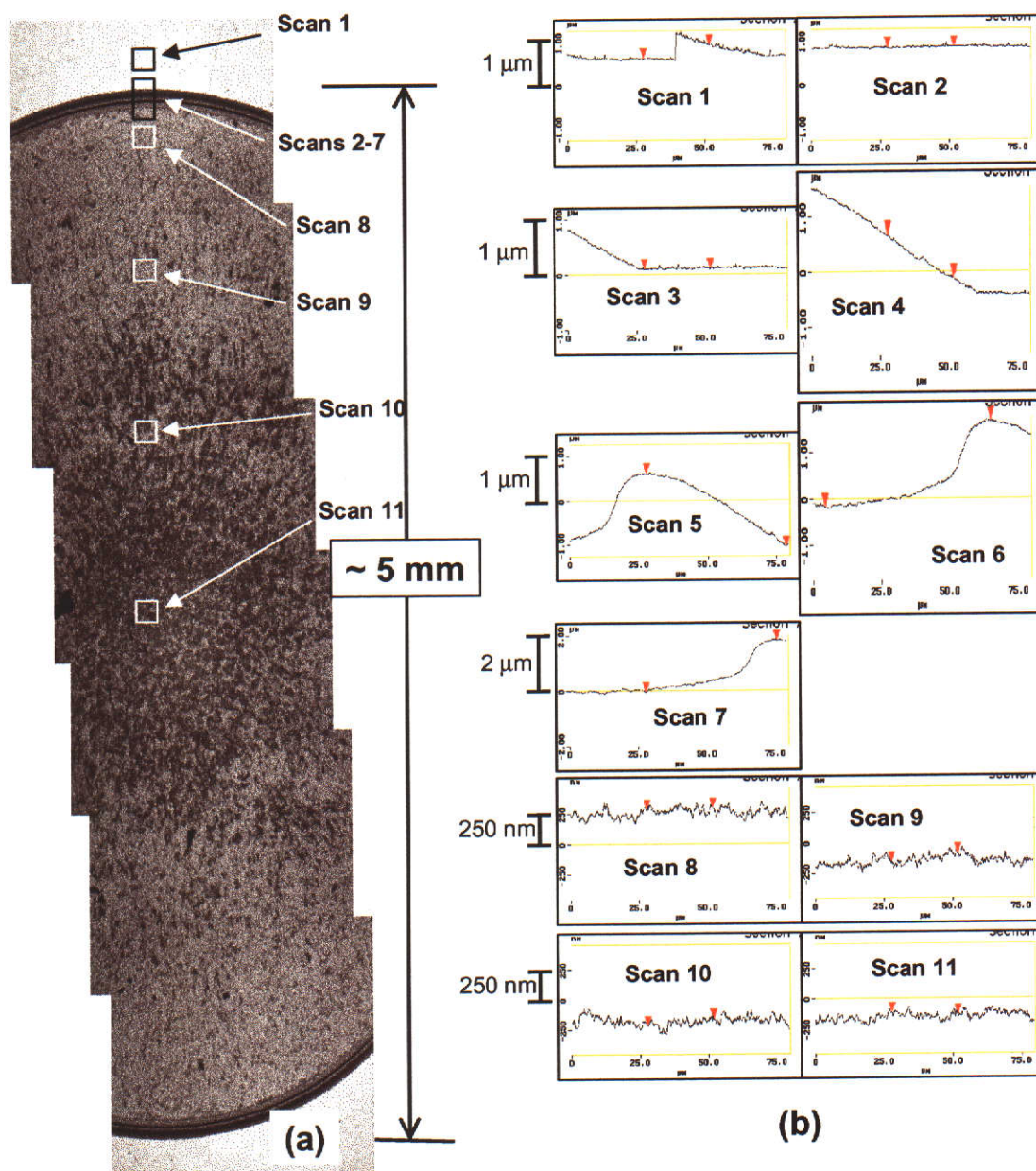


Figure 7.4: Cast hematite film: (a) optical microscopy; and (b) AFM scan data.

Atomic force microscopy (AFM) (Figure 7.4b) was used to determine the variation in the topography and film thickness of the cast hematite film. AFM scans can measure the variation in the z direction within a particular scan but a direct comparison between scans is not possible. This is because there is no set zero point in the z direction and hence no particular measurement of the height above zero can be obtained. To combat this, some overlapping scans were taken. Scans 1 and 2

were of the uncoated ZnSe crystal near the edge of the cast hematite film. Overlapping scans of the uncoated ZnSe crystal interfacing with the hematite coated ZnSe crystal were then taken (scans 3-7) and then onto the hematite film proper (scans 8-11). Scan 8 was close to the edge of the film, while scan 9 was positioned approximately 1/3 of the way to the centre of the film, scan 10 positioned 2/3 of the way and scan 11 at approximately the centre of the cast film.

Scan 2 indicates that the surface of the polished ZnSe crystal is relatively flat, although scan 1 indicates there are some large etches on the surface. This is most likely attributed to a scratch on the ZnSe surface. Close inspection of the bare ZnSe surface at the top of Figure 7.4a confirmed there were indeed several quite significant scratches on the ZnSe crystal surface.

From scans 3 – 5, which measure from the uncoated ZnSe crystal surface to edge of the hematite coating, it was apparent that the rim of the hematite film was in fact raised and was approximately 2000 nm in height. Once past the rim, the rest of the film appeared fairly uniform locally, as evident by the small deviation in the z direction of scans 8-11. This is not necessarily contrary to what the optical microscope indicated and it would appear that the variation in the z direction was consistent for each local scan but may in fact vary across the film. Taking into account the results from both optical microscopy and AFM, the film would appear to be continuous but variable in thickness. Scans 6 and 7 show the decrease in film thickness from the raised outer rim onto the film proper. The scans show that the reduction is less than but close to 2000 nm, indicating that the thickness of the film near the outer edge, inside the raised outer rim, is in the order of approximately 100 nm.

If we assume that the coloration contrast in the optical microscope images of the film (Figure 7.4a) is indicative of film thickness, an estimate of the film thickness can be made (Figure 7.5) using image analysis software (ImageJ). The clean uncoated ZnSe surface was found to have an average grey value of 187 (0 nm thick hematite film), while the edge, which was found to be 2000 nm thick, exhibited a minimum grey value of 38. The film was shown to be uniform across the crystal with an average grey value across the entire hematite film (5 mm diameter) of 124, which equates to an average thickness of 840 nm. The average grey value for the analysis area of the

infrared, which is centred on the film with a diameter of approximately 3 mm, was 116, which represents an average film thickness of 950 nm.

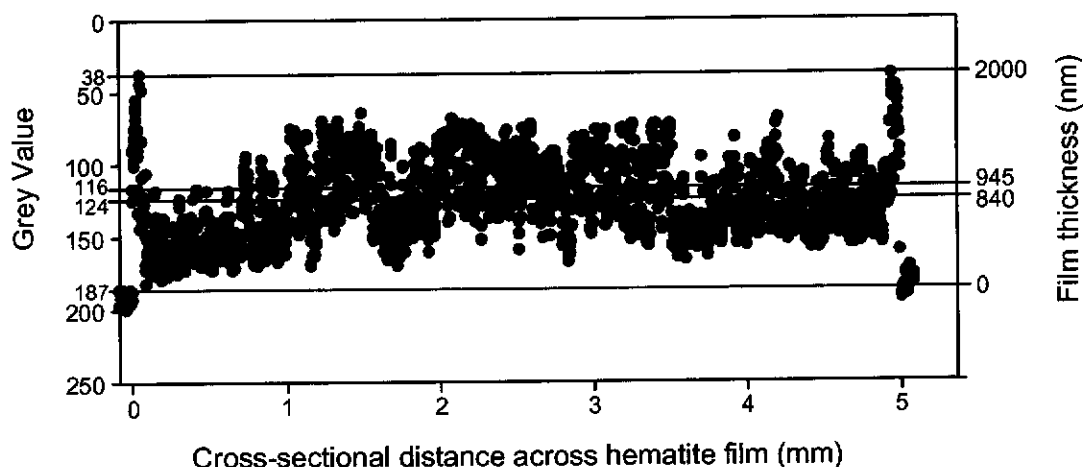


Figure 7.5: Image analysis of hematite film cross-section, showing the grey value and corresponding film thickness.

7.3 Effect of Flowrate and Film Reproducibility

As outlined in Section 4.2.1, a flowcell was utilised to contact the adsorbate solution with the hematite coated ZnSe ATR element. Not only was it deemed necessary to be able to achieve a consistent hematite coating on the ATR element, it was also important to determine the optimum flowrate for the adsorbate solution.

To achieve this, the adsorption of a 50 ppm PAA450K solution onto fresh hematite at pH 2 was monitored by the 1720 cm^{-1} peak area as a function of time for flowrates of 0.17, 0.50, 1.0 and 2.0 mL min^{-1} (Figure 7.6).

The adsorption rate increased with flowrate up to 1.0 mL min^{-1} and then decreased at 2.0 mL min^{-1} . It was thought that the relatively small volume of the flowcell and the flow patterns developed within it may have contributed to the latter effect. A 2.0 mL min^{-1} flowrate represents quite forcing conditions for the design of the flowcell and this may affect the flocculant molecules in several ways. Excessive mixing may lead to shear degradation of the long polymer chains (Scott *et al.*, 1996). Alternatively, flocculant chains that are only in the initial stages of adsorption could conceivably be forced away from the surface. Therefore 1.0 mL min^{-1} represented the most rapid flowrate for adsorbate delivery, which should minimise diffusion effects, and hence was used throughout the remainder of the study.

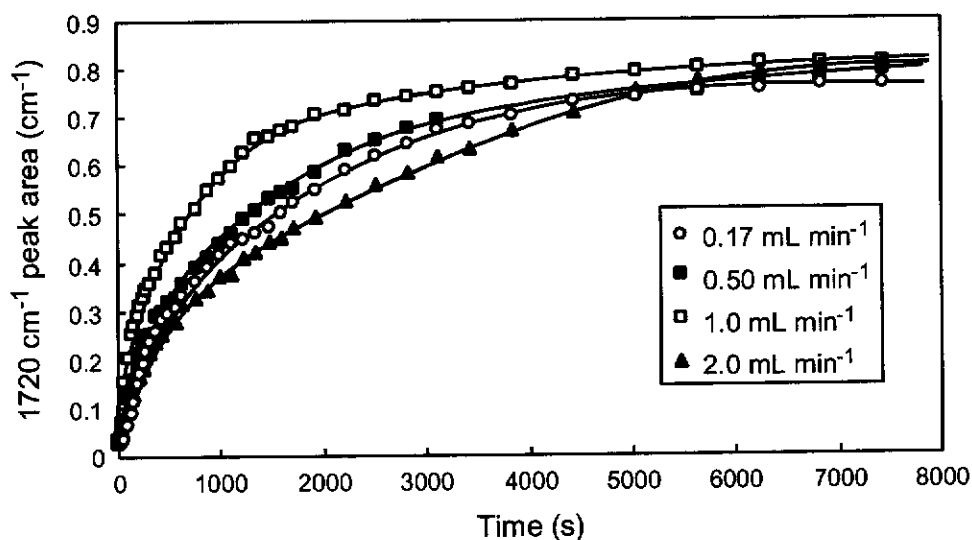


Figure 7.6: Adsorption of PAA450K (50 ppm) at pH 2 as a function of time and flowrate (monitored by the 1720 cm^{-1} peak area).

Figure 7.6 also shows that the adsorption plateau is reasonably consistent regardless of flowrate, indicating that the available surface area per cast film was also consistent. To examine this further, the adsorption of 50 ppm PAA2K, PAA450K and PAA13M solutions onto hematite at pH 2 was monitored, once again by the 1720 cm^{-1} peak area, as a function of time. The experiments were carried out in duplicate using a freshly cast hematite film for each adsorption experiment (Figure 7.7).

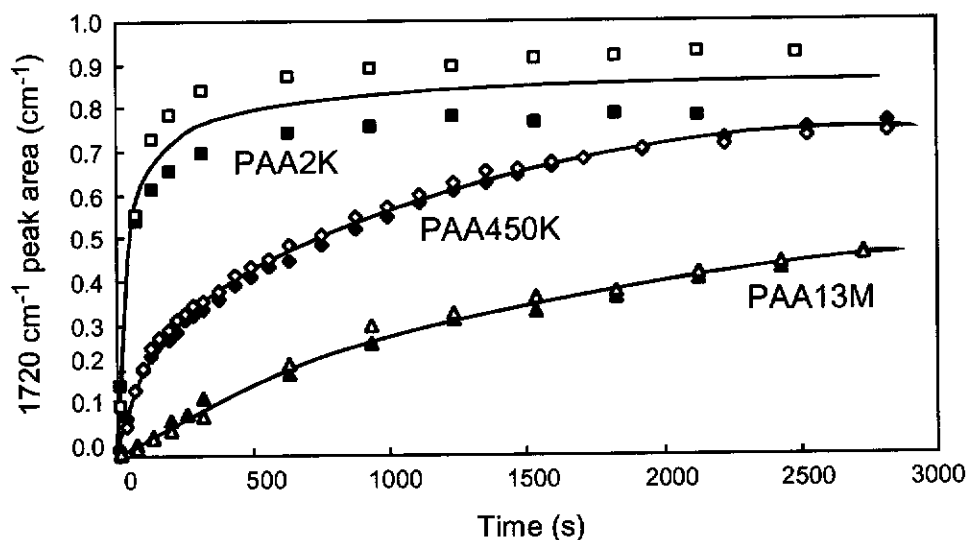


Figure 7.7: Adsorption of polyacrylic acid at pH 2 as monitored by the area of the carbonyl stretching peak (1720 cm^{-1}) as a function of time and polymer molecular weight.

The reproducibility of the results for the adsorption of PAA450K and PAA13M indicates that these polymers were presented to a consistent effective surface area of hematite. In contrast, the adsorption of PAA2K was much less reproducible. PAA2K is expected to have a solution diameter of less than 20 nm and hence would be quite small in comparison to the size of the hematite particles ($d_{50} \sim 100$ nm) in the cast film. As a consequence, the individual polymer chains may readily penetrate into the hematite film and access the surface of hematite particles below the outer surface layer. Diffusion into the film would be quite different from that through the solution and may lead to the observed irreproducibility. The two higher molecular weight polymers have much larger dimensions in solution and would both therefore only have the outer surface of the hematite film on which to adsorb, with little penetration to the particles beneath.

From the results in Figure 7.7 it would appear that the amount and relative rate of PAA13M adsorption is less than PAA450K. However, this result must be viewed with caution, as the molar absorptivity coefficient of the 1720 cm^{-1} peak may not be equivalent for PAA13M and PAA450K. Quantification of relative rates and densities of adsorption are discussed further in Chapter 9.

An examination of the full spectra associated with Figure 7.7 shows that it is also possible to estimate the relative amounts of unadsorbed (loops and tails) and adsorbed (trains) polymer. While the data in Figure 7.7 is constructed from the 1720 cm^{-1} peak area, which represents the unadsorbed segments of the polymer, the spectra also contained the 1410 cm^{-1} peak, which represents the adsorbed fraction of the polymer. The ratio of the unadsorbed (1720 cm^{-1}) to the adsorbed (1410 cm^{-1}) peak areas for the spectra represented in Figure 7.7 is given in Figure 7.8.

For the three polymers the ratio of unadsorbed:adsorbed peaks was found to be approximately 4:1. The PAA13M data appears to have the greatest variability, but all exhibit a trend whereby the ratio starts small and increases. Initially the 1410 cm^{-1} peak provides the strongest relative contribution, indicating that the signal is dominated by peaks associated with the adsorption mode, but with time more unadsorbed polymer sections collapse toward the surface as the polymer finds its optimum configuration.

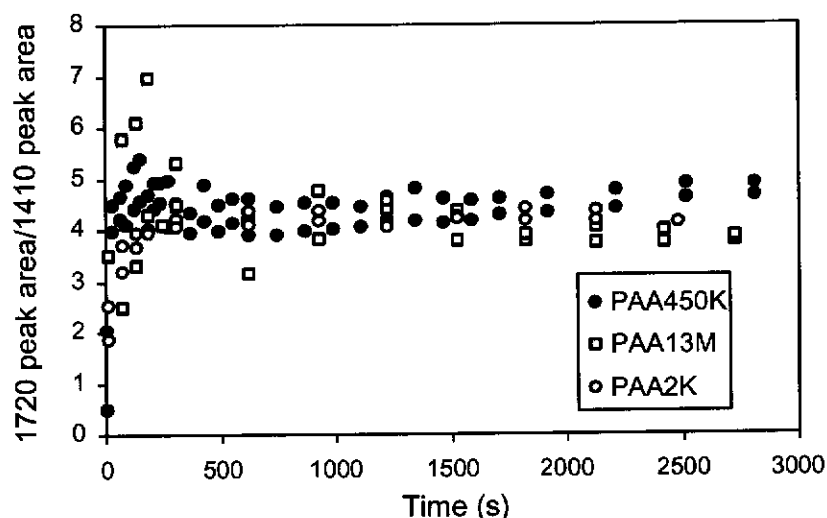


Figure 7.8: Ratio of the unadsorbed carbonyl stretching peak (1720 cm^{-1}) area to the adsorbed symmetric carboxylate ion stretching peak (1410 cm^{-1}) area for polymers adsorbed with varying molecular weight at pH 2, as shown in Figure 7.7.

By comparing the relative intensity of the 1410 cm^{-1} ($\text{COO}^-_{(\text{asym})}$) stretch for PAA450K at pH 13 and 1 M NaCl) and the 1720 cm^{-1} (C=O stretch for PAA450K at pH 2) peaks in the unadsorbed concentrated polymer spectra in Figure 5.2, we can determine the relative molar absorptivity coefficient of the two peaks. The very similar intensities of these two peaks for the 1 wt% solutions (0.006 A.U.) indicates that their molar absorptivity coefficients are comparable and gives confidence that the two can be related directly. Therefore the ratio of unadsorbed:adsorbed polymer of approximately 4:1 (Figure 7.8) suggests that 20% of the polymer segments are adsorbed.

This estimate is possibly a little higher than what is generally accepted and may be due to the shallow penetration of the ATR technique (discussed in Section 2.4.1.2). The absorbance of the infrared radiation is biased toward absorption by components closer to the hematite film, with less emphasis placed on those components further from the hematite surface, as the radiation intensity of the sampling evanescent wave decays exponentially from the surface. This would result in a signal biased towards adsorbed parts of the polymer from that of the unadsorbed loops and tails of the polymer that are extended into the solution away from the hematite surface.

8. FACTORS AFFECTING ADSORPTION AT HIGH pH

8.1 Effect of Electrolyte (NaCl) at pH 13

As described in Section 6.2, the adsorption of polyacrylate onto hematite at pH 13 could not be achieved unless there was added electrolyte. To define the effect of electrolyte concentration on polyacrylate adsorption onto hematite, solutions of fixed polymer concentration (50 ppm) but varying in electrolyte concentration (0.1 to 3 M NaCl) were monitored. Figure 8.1 shows the results for the adsorption of PAA450K, as monitored by the area of the antisymmetric stretching peak of the carboxylate ion (1560 cm^{-1}).

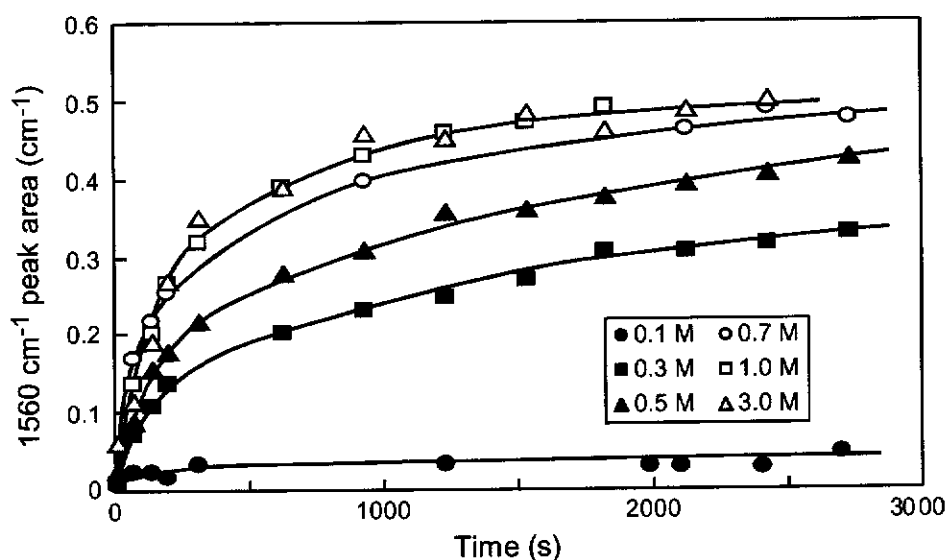


Figure 8.1: Adsorption of PAA450K (50 ppm) onto hematite at pH 13, as a function of NaCl concentration and monitored by the 1560 cm^{-1} peak area.

The estimated maximum adsorption values achieved for each electrolyte solution may then be plotted as a function of the electrolyte concentration. Figure 8.2 shows that the adsorption of polyacrylate at pH 13 increases with increasing NaCl concentration up to a concentration of approximately 1 M, where the effect then plateaus. This plateau indicates that monolayer adsorption has been achieved, and that a considerable sodium ion concentration is required to achieve it.

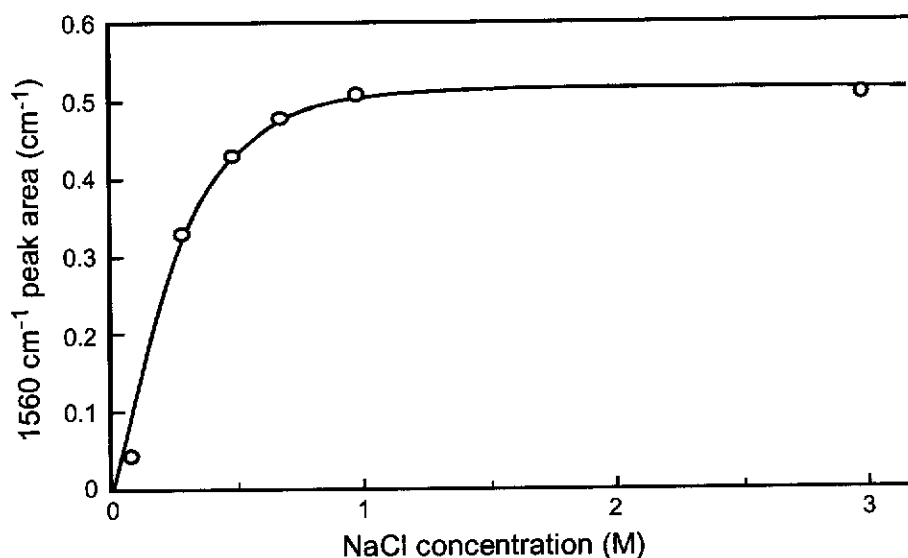


Figure 8.2: The plateau adsorption of polyacrylate (PAA450K) at pH 13 from Figure 8.1 as a function of NaCl concentration.

As shown previously, at pH 13 the carboxylate functional groups on the polymer are deprotonated. The negative charge of the deprotonated carboxylate groups of the polymer cause a repulsion between the polymer segments, leading to an extended chain conformation. Increasing the electrolyte concentration of the polymer solution will result in the added cations screening the negative charge of the deprotonated carboxylate groups. As a consequence of the reduced repulsions along the chains, the polyelectrolyte should then take on a less extended conformation in solution.

The effect of increasing the electrolyte concentration alone would be expected to increase the adsorption of polyelectrolyte onto the hematite surface, because the smaller polymer coils would be able to pack more densely onto the substrate surface. This is similar to the findings of Cosgrove, Obey and Vincent (1986) who observed no adsorption for a negative poly(styrene sulfonate) onto a negatively charged polystyrene latex in zero added salt, but found adsorption increased with increasing salt. They did not specify an adsorption mechanism and attributed the increase in adsorption with ionic strength to only a change in the adsorbed polymer conformation (the development of loops made possible by the suppression in the intersegmental electrostatic repulsions associated with high ionic strength media), without considering the effect that the ionic strength may have had on the charge of the substrate.

Also, at pH 13 the shielding of the negative carboxylate functionalities of the polymer by the additional cations in solution would be expected to give the polymer a greater affinity for the negative hematite surface. In addition, if the cations have an affinity for the hematite, they may shield the negative charge of the hematite surface, also facilitating adsorption. Thus, the increase in adsorption with increasing electrolyte concentration at pH 13 could be attributed to a decrease in polymer size in solution, and a shielding of the negative charge of both the polymer and hematite surface charges. This is represented schematically in Figure 8.3.

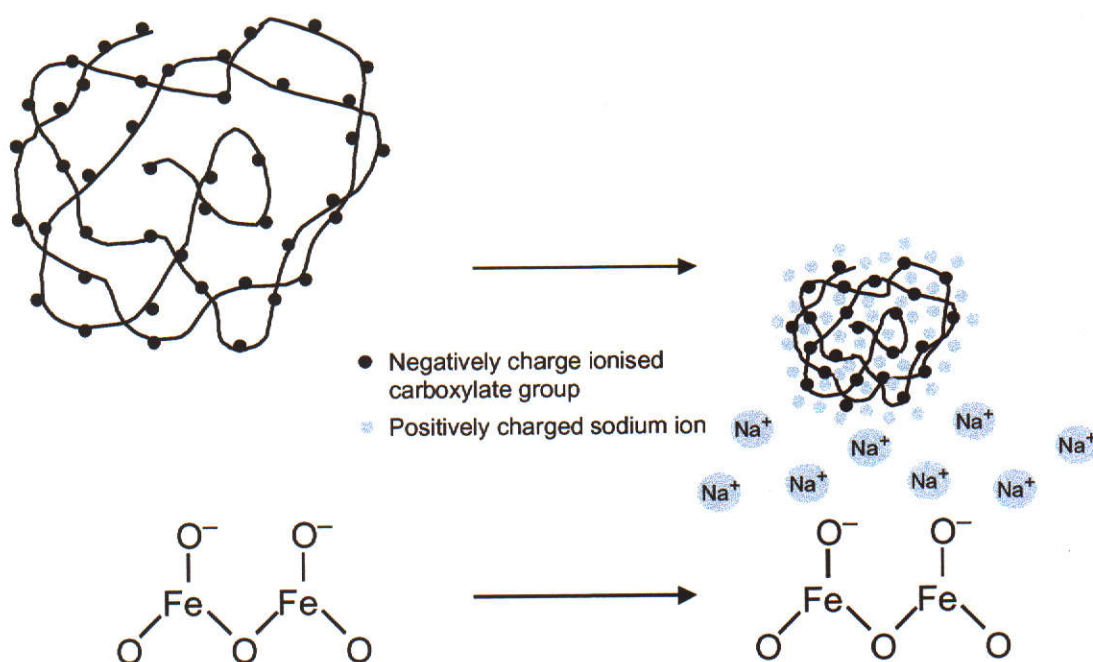


Figure 8.3: Schematic representation of how increasing the electrolyte concentration affects both the dimensions of polyacrylate in solution and the hematite surface at pH 13. The electrolyte shields the negative charge of both the hematite surface and the carboxylate groups on the polymer.

At pH 13 (1 M NaCl), the ionic strength of the solution is similar to pH 14 (with no added salt). Although pH 14 represents more forcing caustic conditions, if it is the ionic strength of the solution media that is a determining factor in facilitating adsorption, then it would be anticipated that adsorption would take place at pH 14, without added electrolyte. The spectra for the adsorption of PAA13M (50 ppm) onto hematite at pH 14 (without added salt) are given in Figure 8.4.

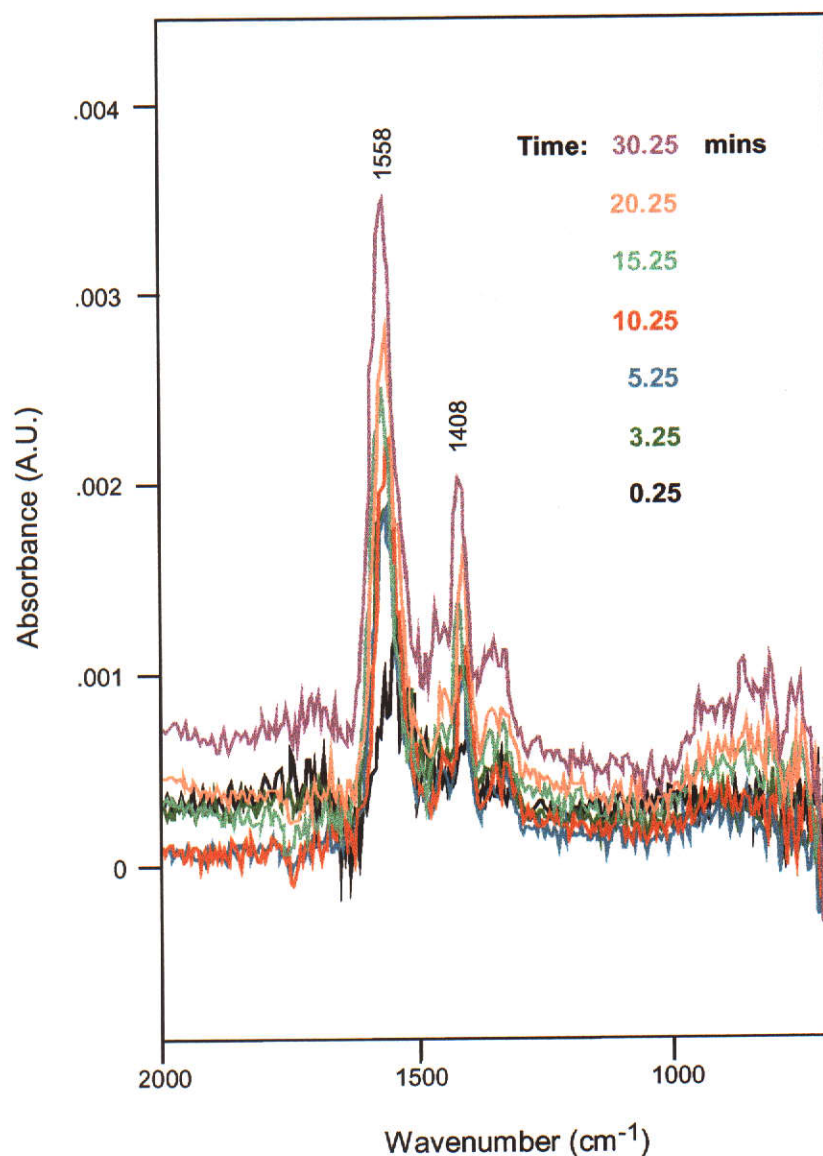


Figure 8.4: Adsorption of PAA13M (50 ppm) at pH 14.

The 1560 cm^{-1} peak area after 30 minutes (1800 seconds) of approximately 0.003 in Figure 8.4 is similar to that of polyacrylate adsorption at pH 13 and 0.3 M NaCl (after 1800 seconds) in Figure 8.1. If we assume that the molar adsorption coefficient of the 1560 cm^{-1} peak is the same for both polymers, then the adsorption density at pH 14 is similar to that at pH 13 (0.3 M NaCl).

8.1.1 Effect of Electrolyte (NaCl) on Polyacrylate at pH 13

The manner in which polyacrylate dimensions change as a function of solution properties was examined via multi-angle laser light scattering (MALLS – discussed in Section 2.4.4). Figure 8.5 shows the change in radius of gyration (r_g) of PAA450K as a function of pH.

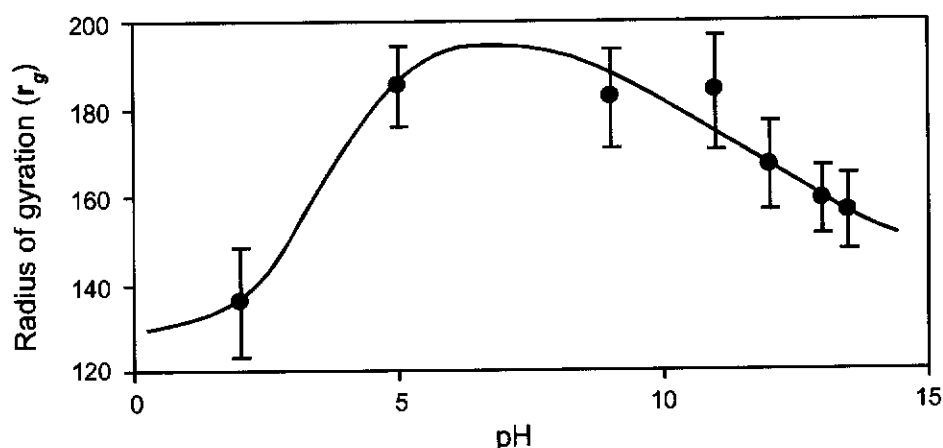


Figure 8.5: The radius of gyration (r_g) of PAA450K (200 ppm) as a function of solution pH.

At pH 2, where the carboxylate groups of the polymer are totally protonated, the polymer has a small radius of gyration and its most coiled conformation in relation to the other values measured. As the pH is increased, the radius of gyration increases up to a maximum near pH 7 and then steadily decreases.

Polyacrylic acid begins to ionise at pH 3 and as the pH increases it becomes more ionised, reflecting a pK_a of approximately 6 (Boisvert *et al.*, 2002). Due to the repulsion between the negatively charged ionised carboxylate groups, the polymer has an more extended conformation in solution, hence r_g increases with pH (up to approximately pH 7). However, as the pH increases so does the sodium ion concentration, which shields the charge of the ionised carboxylate groups, and hence counteracts the repulsion that the ionised carboxylate groups exert on each other. As polyacrylate is fully ionised at pH 9 (Boisvert *et al.*, 2002), the decrease in r_g with increasing pH beyond approximately pH 10 is due only to shielding by sodium ions. If we assume that the size of the polymer at pH 2 represents its most coiled conformation, then the results in Figure 8.5 indicate that even at pH 13.5, which represents a significant ionic strength, there still remains a slight degree of an extended conformation.

For a polymer in solution that is spherical in shape and has a random coiled conformation, then the relationship between r_g and the hydrodynamic radius (r_h) is given by Equation 2.15 (Section 2.4.4).

i.e.
$$r_h = \frac{r_g}{0.778}$$

Using this equation, the results in Figure 8.5 show that at pH 2 the hydrodynamic diameter of PAA450K is approximately 350 nm and at pH 13.5 is 400 nm. If we estimate the maximum r_g value to be 195 nm, then this gives a hydrodynamic diameter of approximately 500 nm. Therefore, in solution the hydrodynamic diameter of PAA450K ranges from 350 – 500 nm.

For sodium polyacrylate at pH 6 in relatively low ionic strength, Reed (1995) found that the radius of gyration (r_g) varied from approximately 150 to 400 nm for a molecular weight range of approximately 10^5 to 10^6 . At pH 6, PAA450K (molecular weight – 450 000) was found to have a radius of gyration of approximately 195 nm (Figure 8.5), which falls within the range of values determined by Reed (1995). However, when Reed (1995) plotted the radius of gyration versus the molecular weight on a log scale, the relationship between the two was linear, and that would predict that at a molecular weight of 450 000 (PAA450K), the radius of gyration should be approximately 285 nm. As size increases at low concentrations, this difference is likely due to the samples determined by Reed (1995) being more dilute, as they were passed through a fractionating column prior to analysis. Also, PAA450K may have a larger molecular weight distribution, whilst the samples that were determined by Reed (1995) had a very narrow molecular weight distribution due to the fractionating column. Hence the molecular weight of the polymers may not be able to be directly related as the molecular weight distribution may effect the molecular weight determination. In addition, the molecular weight of PAA450K (as received from Aldrich) was determined and quoted as a viscosity determined molecular weight, while that of Reed (1995) was determined by light scattering.

Figure 8.6a shows the radius of gyration for PAA13M through the pH range 9 – 13.5, while Figure 8.6b demonstrates how changing the ionic strength at pH 13 effects its radius of gyration. As would be expected, Figure 8.6a mirrors the behaviour seen for

PAA450K in Figure 8.5 where, as the pH increases in the basic region, the radius of gyration decreases. For PAA13M, the hydrodynamic diameter ranges from approximately 550 nm at pH 9 down to 460 nm at pH 13.5.

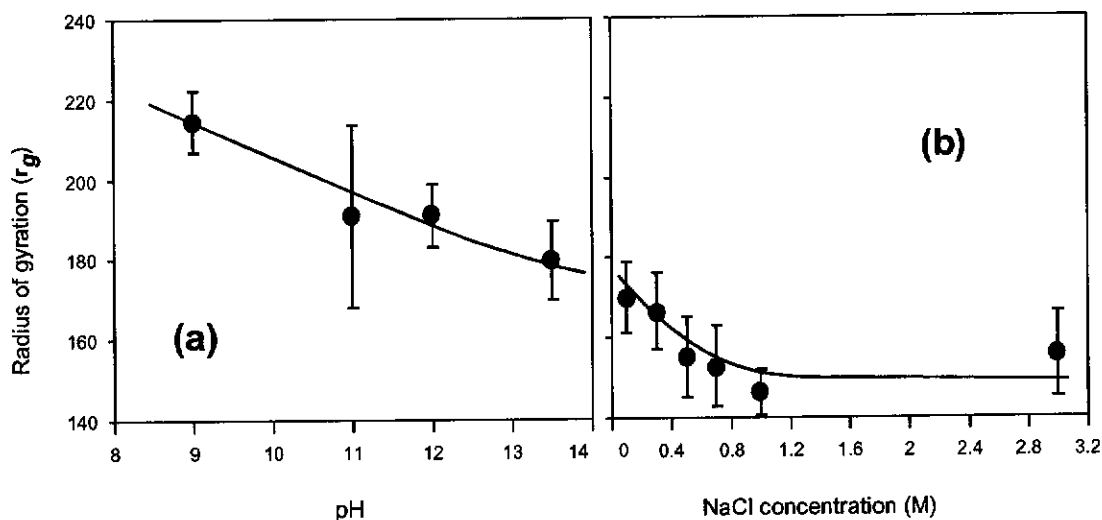


Figure 8.6: The radius of gyration (r_g) of: (a) PAA13M (40 ppm) as a function of pH, and (b) as a function of NaCl concentration at pH 13.

While the measurements of Reed (1995) hold a linear relationship between the logarithm of the radius of gyration and the logarithm of the molecular weight within the molecular weight range 10^5 to 10^6 , extrapolating the data to determine the radius of gyration at a molecular weight of 1.3×10^7 would have a significant uncertainty. It is likely that the linear relationship may not hold at very high molecular weights. Importantly, the results in Figure 8.6 show that PAA13M has a radius of gyration greater than any of the measurements by Reed (1995), although not significantly greater. Obviously the difference in conditions contributes to this, whereby the measurements on PAA13M were carried out in higher caustic and ionic strength environments, causing the polymer to have a more coiled conformation. Once again, difference in concentration may have also contributed.

The results in Figure 8.6b show that when the ionic strength is increased from 0.1 M to 3 M NaCl at solution pH 13, the radius of gyration decreases from 170 nm to a plateau value of approximately 150 nm. The plateau indicates that the polymer is at its smallest possible dimension in solution and is as tightly coiled as it will become, similar to what would be expected at pH 2. The trend in this data is a similar trend to that seen in Figure 8.2 for the adsorption of polyacrylate onto hematite at pH 13,

whereby the adsorption is seen to increase and plateau with increasing electrolyte concentration. In addition, the extent of polyacrylate adsorption at pH 14 (no salt added - Figure 8.4) was found to be similar to that at pH 13 and 0.3 M NaCl. Results in Figures 8.6a and 8.6b suggest that the size of polyacrylate in solution at pH 14 would be comparable to the size at pH 13 (0.3 M NaCl). These findings indicate that the concentration of electrolyte and the effect this has on the polymer solution dimensions is a major factor governing the amount of polyacrylate adsorbed onto hematite at pH 13. However, this should not be viewed in isolation from the potential of the electrolyte concentration to affect the surface charge of the hematite at high pH.

8.1.2 Effect of Electrolyte (NaCl) on the Hematite Surface at pH 13

As described in Section 2.4.5, when a particle has a shell of electrostatically attracted counter-ions, the potential at the surface of shear as the particle moves through the bulk solution is referred to as the zeta potential and is derived from the electrophoretic mobility. While the zeta potential is not the same as the surface potential, due to the presence of counter-ions, it is the relevant measure for the way in which the particles in a dispersion interact.

Figure 8.7 shows the zeta potential of the hematite measured as a function of pH. The results show that from a pH of 4.93 to approximately 8.5 the zeta potential increases from 22.4 to a value just over 40 mV. Above this pH the zeta potential decreases and eventually becomes negative. The most negative value is -44.9 mV at pH 11.92 and above this pH the zeta potential once again starts to approach zero, with the final pH measurement of 13.38 having a zeta potential of -26.9 mV. The iso-electric point (iep) is the pH at which the zeta potential is zero, and was found to be approximately 10 for the hematite colloid.

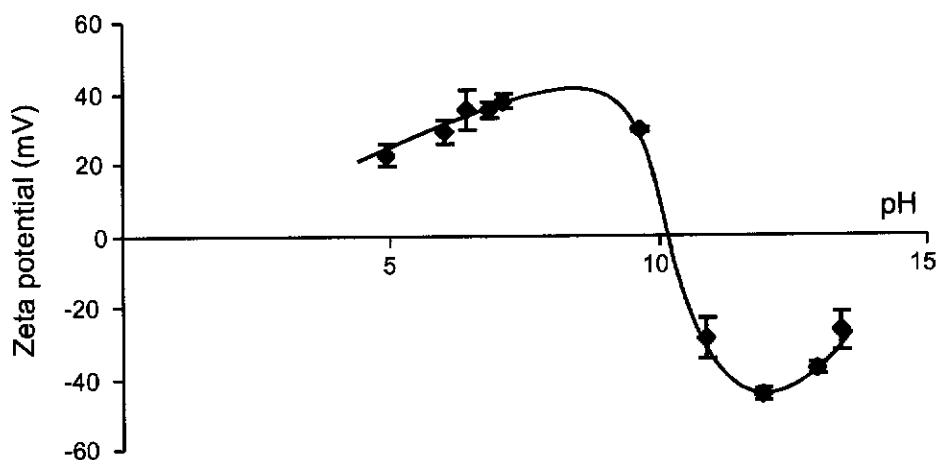


Figure 8.7: Zeta potential of hematite measured as a function of pH.

While the iep for synthetic hematite is generally reported to lie between 8 and 9, a value of 10 is not exceptionally high, as similar values have been reported (Pugh and Lundstrom, 1987).

The hematite colloid is stable at pH 13 by virtue of its net negative charge ($\zeta = -37.5$) and this is one of the main reasons why polyacrylate adsorption onto hematite does not occur at pH 13 without added electrolyte. The electrolyte effect was further examined by assessing how the electrolyte concentration affected the surface charge of hematite at pH 13 (Figure 8.8).

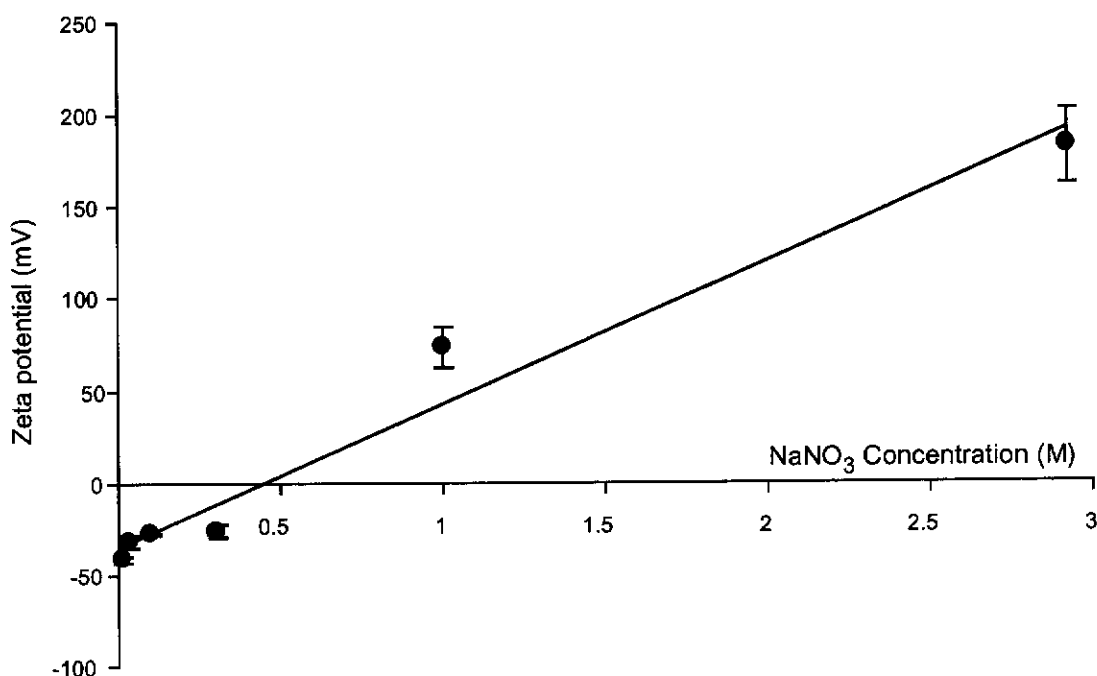


Figure 8.8: Zeta potential of hematite at pH 13 measured as a function of NaNO₃ concentration.

At 0.01 M NaNO_3 and pH 13, the zeta potential was -41.4 mV, and increasing the electrolyte concentration up to 0.30 M increased the zeta potential to -25.9 mV. At an electrolyte concentration of 1.00 M, the zeta potential was found to jump to $+73.7$ mV and further increasing the electrolyte concentration to 2.92 M caused the zeta potential to jump to a surprising $+182.7$ mV. However, the large positive zeta potential values recorded for the colloidal dispersions at 1.00 M and 2.92 M NaNO_3 did not result in the colloids being stabilised, as the samples were found to aggregate over a period of minutes, indicative of zeta potentials closer to zero.

The results for the zeta potential of hematite at high pH as a function of NaNO_3 concentration indicate that the Na^+ ions have a high affinity for the hematite surface and are specifically adsorbed, to the point that at very high salt concentrations this adsorption actually causes the surface to become positively charged. This would indicate that the shear plane is positioned beyond these specifically adsorbed cations. Thus the physical behaviour of the colloidal dispersions appears to be governed by the high ionic strength environment, whereby the high concentration of cations and anions leads to a complex diffuse double layer that facilitates particle aggregation.

This is similar to the finding of Rowlands *et al.* (1997) who published results for the surface properties of aluminium hydroxide in high ionic strength environments based on electroacoustic measurements. In 0.5 M NaCl , they found that the iep shifted from 9.1 to approximately 11, while in 3 M NaCl there was no iep. The authors suggested that under such forcing conditions, while the measured trends in the zeta potential were significant, the normal picture of the diffuse double layer is no longer valid and the absolute value of the measured zeta potentials no longer accurate. They concluded that in alkaline, high ionic strength solution, sodium ions adsorb so close to the particle surface that the net charge at the surface where liquid flow begins to develop is positive.

In a similar study utilising the phase analysis light scattering principle to determine zeta potentials, Tscharnuter, McNeil-Watson and Fairhurst (1998) measured the mobility of quartz spheroids in KCl solutions ranging from 0.0001 M to 4.0 M. In aqueous solutions the zeta potentials of the quartz spheroids was negative and exhibited typical behaviour, with the magnitude of the zeta potential decreasing and approaching zero with increasing electrolyte concentration, never becoming positive,

even at 4 M KCl. The value of the zeta potential at the high electrolyte concentration of 4 M KCl was not published due to irreproducibility. This may also be the case for the hematite samples used in this study, especially at the electrolyte concentration of 2.92 M. This sample exhibits the largest errors, where the three measured zeta potentials for this sample were 183, 203 and 162 mV (average 183 mV) and having a standard deviation of 20.4 mV. Despite this, the results appear reproducible enough to indicate that the trend of the zeta potential becoming positive is legitimate, although the magnitude of the positive potential is questionable.

The results show that under caustic conditions, sodium ions do have an affinity for the hematite surface and shield the negative surface of the hematite, clearly contributing to the increase in polyacrylate adsorption at pH 13 with increasing ionic strength (Figure 8.1). Figure 8.7 indicates that the surface charge of hematite, while still negative, will be much smaller in magnitude at pH 14 than at pH 13. Adsorption at pH 14 (Figure 8.4) was found to be similar to that at pH 13 and 0.3 M NaCl (Figure 8.1) and a comparison of zeta potential values in Figures 8.7 and 8.8 show that the zeta potential at pH 14 would be similar in value to that at pH 13 (0.3 M NaCl). These findings reinforce that the electrolyte affect on the surface charge of the hematite must also be incorporated into the mechanism for the adsorption of polyacrylate onto hematite under caustic conditions.

In summary, at pH 13 and low ionic strength, adsorption is facilitated as a result of increasing the electrolyte (sodium ions) concentration, which has the effect of decreasing the surface charge of the hematite and the size of the polymer in solution by screening the negative charge on both. It would appear that the cations influence both the polymer and substrate in facilitating the adsorption process, whereas at high ionic strength, the adsorption density is limited by the finite size of the polymer in solution.

By either increasing the electrolyte concentration at pH 13 or increasing the pH beyond 13, adsorption is facilitated as a result of increasing the of electrolyte concentration. The maximum adsorption achieved at pH 13 (1 M NaCl) is not expected to be exceeded at higher pH values because adsorption was found to be limited by the finite size of the polymer in solution.

8.2 Effect of Cation Type at pH 13

Results presented in Sections 6.2 and 8.1 are strong evidence for the proposition that the adsorption of polyacrylate in caustic sodium hydroxide media is facilitated by the presence of an excess of sodium ions. That being the case, it could be expected that changing the cation would affect adsorption due to a change in charge density. For this reason lithium, sodium and cesium cation effects were compared. PAA450K was selected as the adsorbate for this study specifically because it exists in its powdered form as a sodium-free polyacrylic acid, compared to the sodium polyacrylate form of PAA13M.

Adsorption of PAA450K at pH 13 and 1 M salt showed that there was no discernable difference in the adsorption density as a function monovalent cation. However, when the electrolyte concentration was decreased to 0.2 M, it was quite apparent that there was a significant effect attributable to the cation type (Figure 8.9).

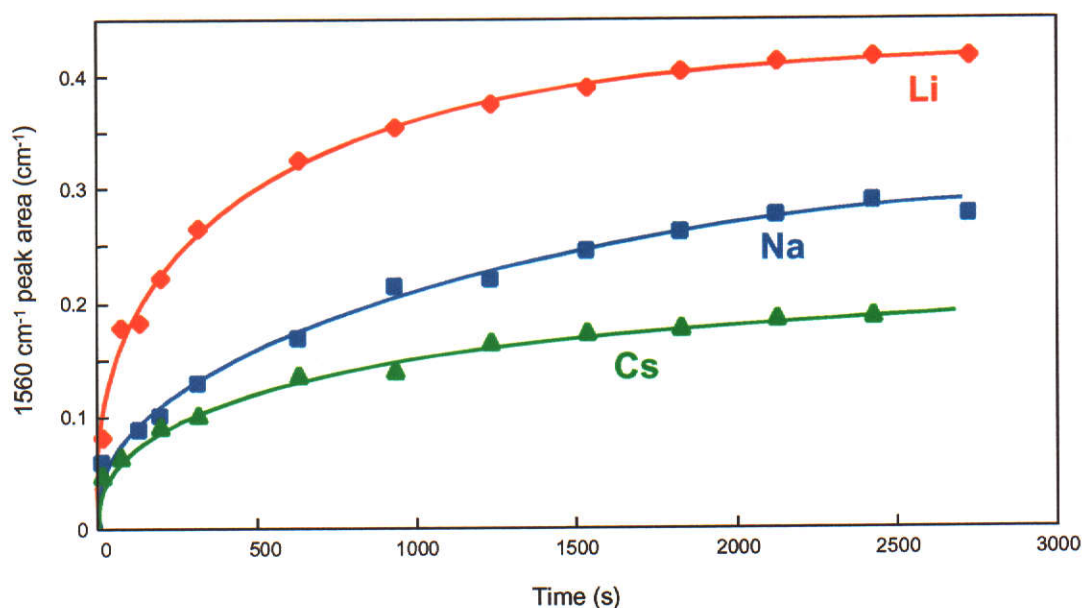


Figure 8.9: Adsorption of PAA450K (50 ppm) at pH 13 (LiOH, NaOH or CsOH) and 0.2 M added electrolyte (LiCl, NaCl or CsCl) as monitored by the area of the 1560 cm^{-1} peak area.

The results in Figure 8.9 show that at an electrolyte concentration of 0.2 M, the lithium system facilitates adsorption to the greatest extent followed by sodium and then cesium. This indicates that lithium is able to shield the negative charge of the carboxylate groups on the polymer and perhaps also the negative surface charge of the hematite more significantly than either the sodium or cesium cation.

8.2.1 Effect of Cation Type on Polyacrylate at pH 13

The effect that the cation type has on the ability to shield the negative moieties of the polymer was examined by measuring the radius of gyration (r_g) for PAA450K at pH 13 in the presence of different chloride salts (0.2 M). Figure 8.10 shows that there is little variation in r_g with cation type and the results indicate that the hydrodynamic diameter of the polymer under these solution conditions is approximately 390 nm. The lack of any trend is in agreement with Boisvert *et al.* (2002), who used osmotic pressure measurements to study the effect of the Li^+ , Na^+ and tetramethyl ammonium (TMA^+) monovalent cations on the effective charge of polyacrylic acid through a pH range of 4 to 9. They found that the effective charge was not dependent on the nature of the monovalent cation and that the interaction between cation and carboxylate functionality was purely electrostatic.

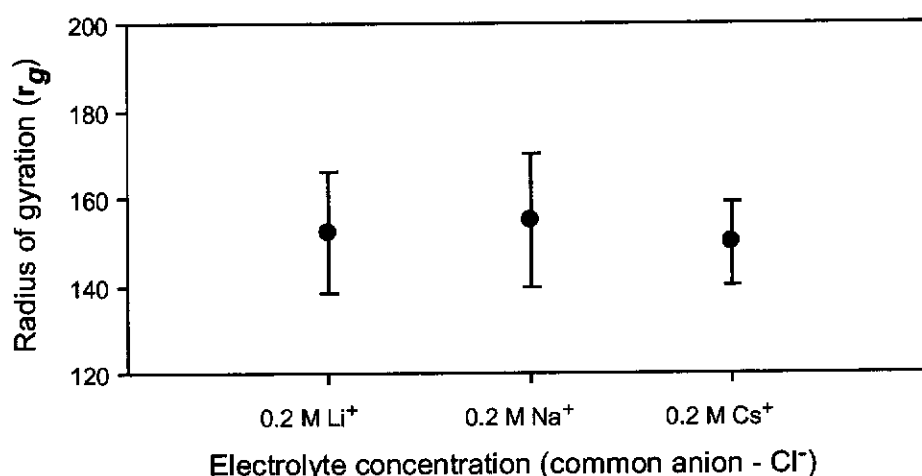


Figure 8.10: The radius of gyration (r_g) of PAA450K (200 ppm) at pH 13 and 0.2 M added salt as a function of cation type.

Although the results in this study were carried out at pH 13, differing considerably from the fairly benign pH conditions of Boisvert *et al.* (2002), the results are comparable and hence the same conclusions must be drawn that the interaction between cation and carboxylate functionality is non-specific and purely electrostatic. Interestingly though, Boisvert *et al.* (2002) did observe a specific interaction of the polymer with divalent cations. This interaction was inversely related to the energy of hydration of the cation, with the magnitude of hydration energy in the order $\text{Mg}^{2+} > \text{Ca}^{2+} > \text{Ba}^{2+}$. Of the three cations, Ba^{2+} is easiest to desolvate and consequently easiest to complex with the carboxylate functionality leading to the formation of a

precipitate. They found that precipitation occurred with Ca^{2+} and Ba^{2+} before all carboxylate functional groups were complexed, indicating that complete neutralisation was not necessary for precipitation to begin. However, Mg^{2+} was so strongly hydrated that precipitation occurred only when there was a slight excess of Mg^{2+} ions with respect to carboxylate functional groups. Hence a high ionic concentration was required to induce desolvation and force precipitation.

If the trend displayed by the divalent cations was extended to the monovalent series, then cesium ions, which are largest and least hydrated (i.e. lowest energy of hydration), would be the most likely to display an affinity for the polymer. In Figure 8.10, the polymer concentration of 200 ppm and 0.2 M salt signifies a large cation excess (approximately 70 cations per carboxylate functional group) and yet no effect was seen, further reinforcing that the monovalent cation interaction is purely non-specific.

8.2.2 Effect of Cation Type on the Hematite Surface at pH 12

The zeta potential of hematite is most negative at a pH of approximately 12 (Figure 8.7), which indicates that the surface charge of hematite is most negative at pH 12. This condition is thus the most appropriate for evaluating the effect that the cation type has on the ability to shield the negative charge of the hematite surface. The zeta potentials of dilute colloidal hematite that had been made up to pH 12 using either sodium hydroxide or lithium hydroxide and the corresponding electrolyte (sodium nitrate or lithium nitrate) are given in Figure 8.11.

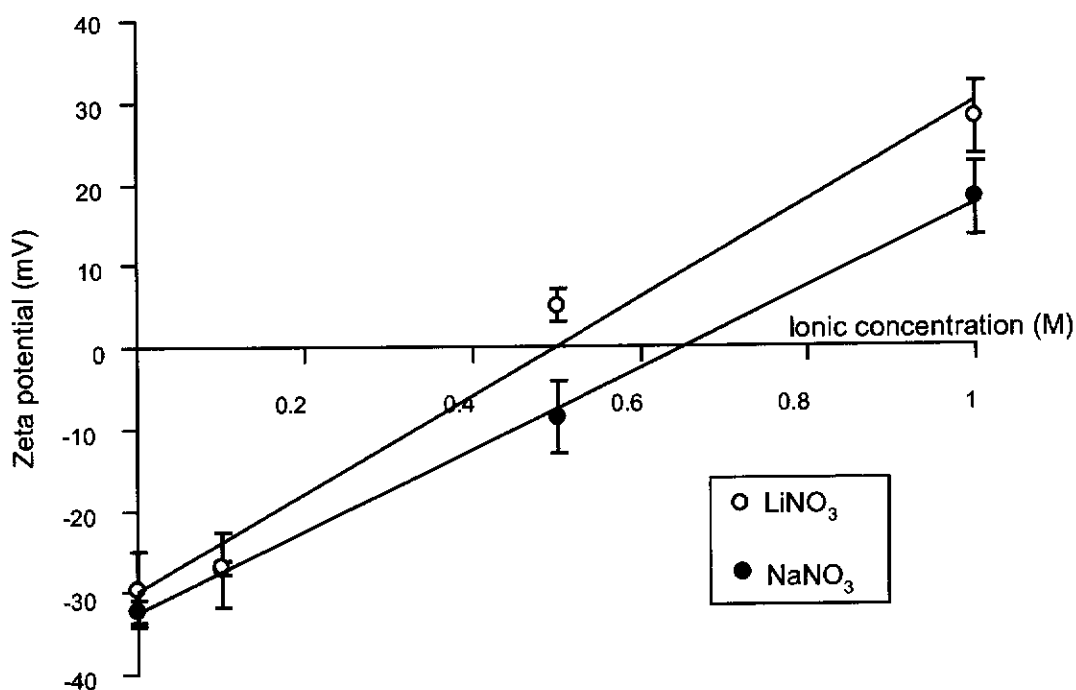


Figure 8.11: Zeta potential of hematite at pH 12 measured as a function of electrolyte (LiNO_3 or NaNO_3) concentration.

The behaviour of hematite as a function of electrolyte concentration at pH 12 is similar to that seen at pH 13 (Section 8.1.2). The results show that for both the Li^+ and Na^+ system at pH 12, an increase in the electrolyte concentration makes the zeta potential less negative. At approximately 0.50 M LiNO_3 and 0.65 M NaNO_3 , the zeta potential becomes zero and beyond these electrolyte concentrations, the zeta potential is positive and increasing in magnitude. Furthermore, LiNO_3 reduces the negative surface charge of hematite to a greater extent than NaNO_3 .

Both cations would appear to have a high affinity for the hematite surface, exhibiting a specific interaction, to the point that at very high salt concentrations the surface becomes positively charged. As the lithium cation reduces the negative charge of the hematite to a greater extent it would appear to have a stronger specific interaction with the hematite than the sodium cation. This result is contrary to what is classically accepted for substrates such as mercury, silver iodide and silica, whereby increasing attractive interactions between surface and counter-ion is usually associated with increasing size of counter-ion. The size of counter-ions increases down the periodic table, hence sodium ions would be expected to have a greater attraction to the negative hematite surface than the lithium ions. This is a consequence of larger counter-ions typically having a smaller radius of hydration,

and therefore being able to approach closer to the surface of the colloid. While the above results do not hold to this general trend, they are not unprecedented, with similar observations for hematite being described by Breeuwsma and Lyklema (1971) and Amhamdi, Dumont and Buess-Herman (1997).

Breeuwsma and Lyklema (1971) carried out surface charge measurements on a synthetic hematite substrate in the presence of several electrolytes. For the chloride salt of Li^+ , their results indicated that there was a specific interaction between Li^+ and the hematite surface at pH values above that of the pzc of the hematite. For the K^+ and Cs^+ chloride salts, no difference in affinity was seen at high electrolyte concentrations (0.1 – 1 M) but at low concentrations (0.001 – 0.01 M), K^+ showed a greater affinity for the hematite surface than Cs^+ . Bivalent cations also showed specific adsorption with the hematite surface, following the trend $\text{Mg}^{2+} > \text{Ca}^{2+} > \text{Sr}^{2+} = \text{Ba}^{2+}$. The authors discussed their finding using ‘the porous double-layer model’. The model described that if a substrate is not porous at all, then the affinity of a counter-ion for the surface will follow the classical trend whereby the larger the counter-ion, the smaller the radius of hydration and therefore the closer the counter-ion can approach the surface of the colloid. When the surface is porous, the authors suggested that the affinity of the counter-ion for the surface would increase, as the surface charge is not only confined to the surface but also distributed within some depth of the surface layer. For a silica surface the affinity follows the typical trend $\text{Cs}^+ > \text{K}^+ > \text{Li}^+$. If the silica is porous, then the authors suggest that the trend is amplified because Cs^+ will penetrate into the pores to a greater extent in relation to Li^+ . The reason given is that Li^+ is a much more hydrated ion than Cs^+ , in addition to the Cs^+ being able to dehydrate to some extent, resulting in Li^+ being dimensionally much larger.

In rationalising the opposite trend for hematite, whereby the affinity for the hematite surface follows the trend $\text{Li}^+ > \text{K}^+ = \text{Cs}^+$ the authors suggest that there is little penetration of Cs^+ and K^+ whereas Li^+ penetrates easily. Their explanation is that in its dehydrated form, Li^+ is the smallest ion dimensionally, and hence penetrates preferentially. While not offering a reason why the Li^+ ion should dehydrate, their conclusion is based on the similar size of dehydrated Li^+ to that of the Fe^{3+} ion, suggesting that the Li^+ penetrates in its dehydrated form occupying a vacant Fe^{3+} site.

The bivalent series holds the same trend and is explained in the same manner, i.e. Mg^{2+} has the greatest affinity to the hematite surface because the dehydrated ionic radius of Mg^{2+} is once again very similar to that of Fe^{3+} , whereas Ca^{2+} , Sr^{2+} and Ba^{2+} are not. The authors noted that their work assists in explaining the preference of Li^+ for other oxides, namely the work by Berube and de Bruyn (1968) on TiO_2 , and can be extended to include the work by Johnson, Scales and Healy (1999) on Al_2O_3 . Once again the ionic radii of Ti^{4+} and Al^{3+} are very similar to that of Li^+ .

While there may be some validity in the explanation posed by Breeuwsma and Lyklema (1971), the question remains as to why Li^+ would dehydrate in selected systems but not in others. Hematite is similar to several metal oxides including rutile and alumina in the fact that the surface hydrates quite readily. In their explanation of the preferred affinity of Li^+ to the rutile (TiO_2) surface, Berube and de Bruyn (1968) found it illogical that Li^+ , which is the most highly hydrated alkali cation, would preferentially dehydrate and specifically adsorb onto a surface that is known to have a strong affinity with water molecules. In addition, similar findings (Johnson, Scales and Healy, 1999; Berube and de Bruyn, 1968; and Amhamdi, Dumont and Buess-Herman, 1997) have shown that the trend follows the series $\text{Li}^+ > \text{Na}^+ > \text{K}^+ > \text{Cs}^+$ (inverse lyotropic adsorption sequence) rather than an effect that is exclusive to only Li^+ and Mg^{2+} as suggested by Breeuwsma and Lyklema (1968).

The model of the ionic double layer presented by Berube and de Bruyn (1968) to describe the reason for the inverse lyotropic adsorption sequence has become more commonly known as the 'structure making - structure breaking' model. When a surface has a strong affinity for water then the water molecules associated with the surface exhibit a high degree of order and structure. In an opposing effect, the addition of electrolytes to bulk water is likely to decrease order within the liquid due to the tendency of large ions (e.g. Cs^+) that are not heavily hydrated to destroy the way in which water molecules cluster. However, there is a select group of ions that are small and heavily hydrated (e.g. Li^+ , Na^+) that promote or rather do not destroy such structures. It is thought that these ions may be small enough to be incorporated into the water molecule clusters without destroying them, while larger ions cannot. The authors concluded that when a surface exhibits a strong affinity for water, whereby the water molecules are very ordered and structured on the surface, then

strong specific adsorption by ions is going to be favoured by ions that won't significantly disrupt the surface structure. Hence small, heavily hydrated cations such as Li^+ and Na^+ will preferentially adsorb over larger, less hydrated cations such as K^+ and Cs^+ .

The strength of the water-solid interaction indicates the degree of ordering of the water molecules on the surface for a given oxide. Dumont, Dang Van Tan, and Watillon (1976) suggested that if the structuring properties of ions are directly related to their heat of hydration then the structuring properties of the substrate should be related to the heat of immersion. Their study showed that oxides with surfaces with a pzc less than 4 are structure breakers and this correlates with having heats of immersion less than approximately 400 mJ m^{-2} . Above these values, surfaces are considered to have a strong affinity with water and are regarded as structure makers. The study also incorporated substrates that were not oxides and showed that substrates such as graphite, AgI and Hg, all of which follow the classical lyotropic adsorption series ($\text{Cs}^+ > \text{Li}^+$), all have low heats of immersion. Surprisingly SiO_2 , which is generally considered to be a hydrophilic substrate, is actually a structure breaker, has a relatively low heat of immersion, and follows the classical lyotropic adsorption series.

In summary, it was found that at salt concentrations of 1 M or above, the adsorption of polyacrylate onto hematite at high pH was independent of the solution cation identity. However, there was a distinct cation effect when the salt concentration was reduced to 0.2 M, with polyacrylate adsorption following the order series $\text{Li}^+ > \text{Na}^+ > \text{Cs}^+$. While increasing ionic strength did reduce the solution dimensions of polyacrylate, there was no effect of the cation identity. Therefore the different extent of polymer adsorption for each salt could not be attributed to polymer coil contraction. Instead the trend for polyacrylate adsorption followed that for the adsorption of monovalent cations onto hematite at high pH. This clearly confirmed that the effective surface charge of the hematite colloid was the controlling factor, with the extent of polymer adsorption reflecting the degree to which the negative hematite surface was shielded by the added cations.

9. QUANTIFICATION OF ADSORPTION

9.1 Determining Adsorption Density from Peak Area

As demonstrated in Chapters 6 to 8, FTIR-ATR can be applied successfully to monitoring the adsorption of polyacrylate *in situ*. The adsorption of PAA450K at pH 2 was monitored by the 1720 cm⁻¹ peak area and PAA450K and PAA13M at pH 13 (1 M NaCl) by the 1560 cm⁻¹ peak area. However, in order to relate the peak area to an adsorption density, a thorough understanding of the solution-liquid interface as measured by ATR is needed.

9.1.1 Characterisation of the ATR Solid-Liquid Interface

Generally, FTIR-ATR spectroscopy follows Beer's Law, where there is a linear relationship between increasing concentration and increasing absorbance. This is true for the absorbance of solutes that are evenly distributed through a solution phase. However, sometimes solutes have an affinity for the ATR element, or as in the case of this study, for a substrate that has been cast onto the ATR element. In such cases the absorbance does not obey Beer's Law, as the solute adsorbs and concentrates nearer the ATR element, contributing to a signal that is very much enhanced compared to what would normally be the case if it were evenly distributed in the solution phase.

Concentration of the adsorbed solute towards the ATR element inevitably changes the refractive index of the medium in contact with the crystal, which will in turn affect the depth of penetration of the evanescent wave, as it is dependent on the refractive indices of both media. The depth of penetration is also dependent on the incident angle and the wavelength of the radiation. It is commonly represented by d_p , and is given by Equation 2.3 (Section 2.4.1.2).

i.e.

$$d_p = \frac{\lambda}{2\pi n_1 (\sin^2 \theta - n_{21}^2)^{1/2}}$$

The penetration depth (d_p) is not a measure of the total distance of penetration of the evanescent wave, but rather the depth at which the intensity of the evanescent wave decreases to $1/e$ of the intensity at the boundary (Figure 2.8, Section 2.4.1.2). Mathematically, d_p represents the depth of penetration if it were a box car function and not an exponential decay, as described in the following discussion.

The decay of the evanescent wave is exponential and can be expressed using the electric field amplitude (E) as shown below (Harrick, 1987, pp30):

$$E = E_o \exp(-z / d_p) \quad (\text{Equation 9.1})$$

where: z = distance from surface

d_p = depth of penetration (Equation 2.3, Section 2.4.1.2)

If we assume that $E_o = 1$ then: $E = \exp(-z / d_p)$

Therefore when: $z / d_p = 1$, then: $E = \exp(-1) = 0.367$

and the integral from 0 to 1 (where $z = d_p$) is:

$$\left[e^{-x} \right]_0^1 = e^0 - e^{-1} = 1 - 0.367 = 0.633$$

The integral from 0 to ∞ is: $\left[e^{-x} \right]_0^\infty = e^0 - e^{-\infty} = 1 - 0.0 = 1.0$

This is shown schematically in Figure 9.1.

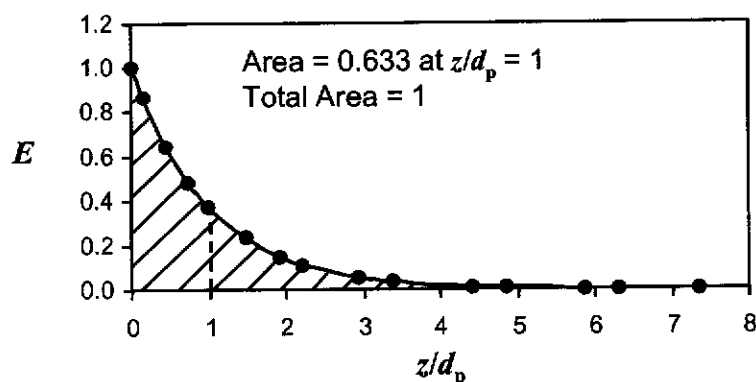


Figure 9.1: Decay of the evanescent wave intensity. Area under curve for $x(0 \rightarrow 1) = 0.633$. Total area under curve is 1.0.

If we assume that the evanescent wave does not decay and only penetrates to a distance of d_p from the surface of the ATR element (i.e. $z/d_p = 1$) as shown in Figure 9.2, we can see that the same total integral is given (i.e. area = 1).

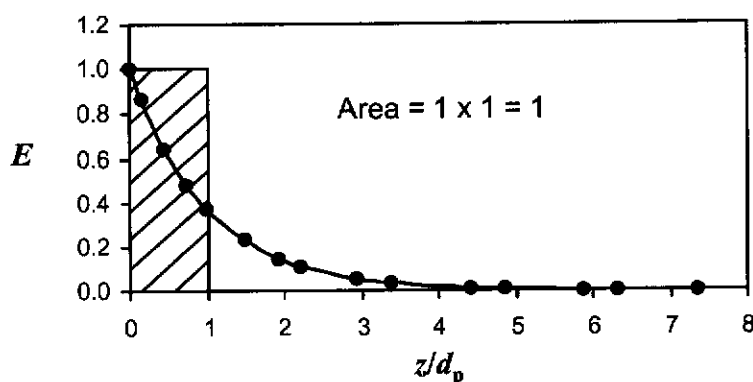


Figure 9.2: Intensity of the evanescent wave, assuming a box car function.

In any given experiment the incident angle and wavelength of the radiation, as well as the refractive index of the ZnSe ATR element, are easily obtained. However, the refractive index of the contacting media, unless uniform and well characterised, is much more difficult to determine. The refractive index of a medium can be derived from the effective thickness (d_e), which in turn can be calculated from the absorbance (A). The effective thickness (d_e) is the thickness required in normal transmission measurements to achieve the same absorbance measured by one internal reflection. However, because the refractive index changes dramatically where there is strong absorbance of the radiation by a medium, a region of weak absorbance must be chosen for this determination. To derive the effective thickness (d_e) from the

absorbance, the molar absorptivity coefficient (ϵ) must be known. This is obtained from absorbance in normal transmission infrared using a fixed path-length cell.

For the refractive index determination to be accurate, the polarisation ratio (the fraction of parallel and perpendicular polarised infrared radiation) needs to be characterised. The polarisation ratio varies markedly between dispersive and Fourier transform infrared instruments, is very dependent on the optics of the instrument and accessory, and hence must be determined specifically for each instrument-accessory set-up. The polarisation ratio is also dependent on the wavelength of the infrared radiation and the incident angle.

9.1.1.1 Polarisation Ratio Characterisation

Determination of the polarisation ratio requires measurements to be taken at two different incident angles. As the FTIR-ATR polyacrylate adsorption measurements were examined at an incident angle of 45° , the two incident angles chosen were 45° and 50° . Initially, the angles of 40° and 50° were considered, to give a greater variation, but the 40° angle was considered to be too near the critical angle ($\sim 33^\circ$). This is even more of an issue when the optics of the 'Seagull' accessory are taken into account, which deliver the infrared beam to the ZnSe crystal from a converging focussed beam. This means that the upper rays of the incident beam, which are closer to the normal with regards to the interface, strike the interface at lower incident angle than the central ray, and the lower rays at a greater incident angle. While this doesn't necessarily incorporate inaccuracies into the experiment, it does mean that as the nominal angle approaches the critical angle, some of the incident beam is at an angle very close to the critical angle. This could lead to a loss of reflectance for part of the beam and hence inaccuracy for measurements carried out at the 40° incident angle (Roger P. Sperline – Personal Communication).

As a first step in determining the polarisation ratio, the molar absorptivity of water was calculated for the weak absorbing region from $2000\text{--}2250\text{ cm}^{-1}$ using transmission infrared, a fixed path-length cell, and applying Beer's Law equation (Equation 2.4, Section 2.4.1.2).

i.e.
$$A = \epsilon \cdot c \cdot \ell$$

$$A = 26.03 \text{ cm}^{-1} \text{ (A.U. – peak integral from 2000-2250 cm}^{-1}\text{)}$$

$$c = 55.56 \text{ mol L}^{-1}$$

$$\ell = 3.015 \times 10^{-3} \text{ cm}$$

Therefore: $\epsilon = 155.4 \text{ L mol}^{-1} \text{ cm}^{-2}$ for the 2000-2250 cm^{-1} spectral range.

For ATR spectroscopy the path length (ℓ) is the effective thickness (d_e), as shown by Equation 2.5 (Section 2.4.1.2) and the effective thickness is constructed from contributions by both parallel and perpendicular polarised radiation (Equation 2.7, Section 2.4.1.2).

i.e.
$$A = \epsilon \cdot c \cdot d_e$$

and
$$d_e = X \cdot d_{e\parallel} + (1 - X) \cdot d_{e\perp}$$

The term X in Equation 2.7 represents the fraction of parallel polarised infrared, $(1-X)$ the fraction of perpendicular polarised infrared radiation. The parallel polarised infrared radiation contribution to the effective thickness is given by Equation 2.8 (Section 2.4.1.2), and the perpendicular component by Equation 2.9 (Section 2.4.1.2).

For the ZnSe/water interface the following known properties were used:

$$n_1 = 2.430 \text{ (ZnSe – 2125 cm}^{-1}\text{)}$$

(Feldman *et al.*, 1979, pp37-38)

$$n_2 = 1.320 \text{ (water – 2125 cm}^{-1}\text{)}$$

(Tickanen, Tejedor-Tejedor and Anderson, 1992)

In determinations of this type, the angle of incidence needs to be known accurately. For the Harrick ‘Seagull’ accessory as used in this study, the angle of incidence is accurate to within $\pm 0.1^\circ$ (Harrick Scientific Corporation –Personal Communication).

An experimental value of d_e can be calculated from measured absorbance (A), and known molar absorptivity (ϵ) and concentration (c) using Equation 2.5 (Section 2.4.1.2) (and is designated $d_{e(\text{expt})}$). It can also be calculated

(designated $d_{e(\text{calc})}$) by substituting Equations 2.8 and 2.9 (Section 2.4.1.2) into Equation 2.7 (Section 2.4.1.2) to give Equation 9.2:

$$d_{e(\text{calc})} = X \cdot \frac{n_{21} \lambda (2 \sin^2 \theta - n_{21}^2) \cos \theta}{n_1 \pi (1 - n_{21}^2) [(1 + n_{21}^2) \sin^2 \theta - n_{21}^2] (\sin^2 \theta - n_{21}^2)^{1/2}} + (1 - X) \cdot \frac{n_{21} \lambda \cos \theta}{n_1 \pi (1 - n_{21}^2) (\sin^2 \theta - n_{21}^2)^{1/2}} \quad (\text{Equation 9.2})$$

Knowing the values of n_1 , n_2 , θ , and λ and assuming a trial value for X , we can then use an iteration program, such as Excel Solver (Microsoft Excel, Microsoft Corporation) to solve for X for the condition that $\Sigma[d_{e(\text{expt})} - d_{e(\text{calc})}]^2$ is a minimum.

The results obtained are given in Table 9.1 and it can be seen that at the incident angles of 45° and 50° the ratio of infrared polarisation remains fairly consistent with approximately 39% of the infrared radiation polarised parallel and 61% polarised perpendicularly. The difference in the degree of polarisation at the two angles is expected to be small because there is only small movement in two of the mirrors (M3 and M6 in Figure 4.2) in the Seagull accessory that the infrared radiation consequently strikes at varying angles, to generate this difference. The accurate determination of the degree of polarisation is essential in determining refractive indices and hence the difference between the 45° and 50° values is regarded as significant.

Table 9.1: Determination of the fraction of parallel (X) and perpendicular ($1-X$) polarised infrared radiation at 45° and 50° incident angles.

Incident Angle	Abs. (cm^{-1})	X	d_e (nm)	d_p (nm)
45°	0.889	0.387	1029	681
50°	0.658	0.392	762	571

For any interface, if we assume that ϵ and c remain constant then:

$$\frac{A_{45}}{A_{50}} = \frac{d_{e45}}{d_{e50}} = \frac{0.387d_{e||} + 0.613d_{e\perp}}{0.392d_{e||} + 0.608d_{e\perp}} \quad (\text{Equation 9.3})$$

Therefore, it is possible to solve for the refractive index of an unknown medium as long as the absorbance at 45° and 50° incident angles is measured and the refractive index of the other medium is known.

To test the validity and accuracy of the approach, the ZnSe/benzene interface in the weakly absorbing region from 2200 - 2220 cm⁻¹ was examined. The absorbance at 45° and 50° incident angles was 0.0198 and 0.0129, respectively.

While the polarisation ratio does change with wavelength, particularly in dispersive instruments, in the following calculations it was assumed that the polarisation ratio remained constant over a narrow range and hence that the X value determined at 2125 cm⁻¹ could be used at 2210 cm⁻¹.

The ratio of the absorbance (A) at 45° and 50° incidence angle was assigned $A_{(45)}/A_{(50)(\text{expt})}$. Knowing the values of X , n_1 , θ , λ , and assuming a value for n_2 , a value can also be calculated (assigned $A_{(45)}/A_{(50)(\text{calc})}$) using Equations 9.3, 2.8 (Section 2.4.1.2) and 2.9 (Section 2.4.1.2).

Excel Solver was used to solve for n_2 so that the condition:

$$\Sigma [(A_{(45)}/A_{(50)(\text{expt})}) - (A_{(45)}/A_{(50)(\text{calc})})]^2 \text{ is a minimum is satisfied.}$$

It was found that for benzene at 2210 cm⁻¹, $n_2 = 1.52$, which is higher than the value of 1.48 reported in the literature (Goplen, Cameron and Jones, 1980).

Using FTIR-ATR for the accurate determinations of refractive index is usually carried using a circular rod ATR element rather than a flat plate. The reason for this is that the polarisation of the infrared radiation using a circle cell is scrambled and hence the degree of parallel and perpendicular polarised radiation is equal. In addition, studies using circle cells have highlighted that accurate refractive index determinations rely heavily on knowing the incident angle accurately, and hence a

method to calibrate the angle of incidence for circle cells has been developed (Sperline, Muralidharan and Freiser, 1986). The polarisation of the infrared radiation being scrambled is also a requirement in calibrating the incident angle by this method. Unfortunately, independent characterisation of the polarisation of the infrared radiation was not possible for a flat plate without knowing an accurate incident angle, and vice versa.

The high value obtained here for the refractive index of benzene is most likely due to inaccuracies in the incident angle, which has a more significant effect on the refractive index determination than slight variations in the X value. While there was an assurance that the incident angle could be determined to within $\pm 0.1^\circ$ (Harrick Scientific Corporation - Personal Communication), this is more likely to be the reproducibility or precision of the incident angle, rather than its absolute accuracy.

While a more accurate result would have been welcome, the result has demonstrated that the technique is accurate enough for the purpose of this study. Refractive indices of benzene of 1.52 and 1.48 for the ZnSe/benzene interface represents an error of less than 3%, which is more than satisfactory for this study. The technique can be used as an approximate but effective means of determining refractive indices and hence can be utilised as a tool for determining the effect that a hematite film has on the way the evanescent wave is attenuated, i.e. determining d_p and d_e .

9.1.1.2 Effect of Hematite Coated Optics

When a thin film is in contact with an ATR element then attenuation of the evanescent wave is governed by the medium beyond thin film, rather than by the thin film itself. This is commonly referred to as the three-layer model, as distinct from the usual two-layer model. As a general rule, when the thickness of the film medium is much greater than d_p , a two-layer model is appropriate, whereas if there is a film that is much thinner than d_p ($d \ll d_p$), a three-layer model is appropriate (Harrick, 1987, pp51). The hematite film thickness here was approximately 950 nm, which almost certainly represent a significant fraction of d_p , and therefore doesn't fall neatly into either of these categories.

Alternatively, an approach similar to that used by Sperline, Song and Freiser (1992) in determining the adsorption density of sodium dodecyl sulfate on alumina coated

optics could be considered. In this approach, they assumed that there were three phases, which were the IRE (n_1), the $\sim 2\ \mu\text{m}$ thick alumina coating (n_2) and the aqueous solution (n_3), and used the FTIR-ATR adsorption density (Γ) equation modified for coated optics (Equation 2.14, Section 2.4.3).

i.e.
$$\Gamma = \frac{(A/N) - \epsilon_c d_{e,3}}{1000\epsilon(d_{e,3}/d_3)}$$

The alumina coating was assumed to be uniform and to exhibit the same optical properties as crystalline alumina (i.e. 1.761, CRC Handbook of Chemistry and Physics, pp4-140) and it was also assumed that the adsorbed layer thickness of sodium dodecyl sulfate was $\ll d_p$. In characterising the effective path length and the depth of penetration of the evanescent wave in the aqueous phase (phase three), this equation takes into account the decay of the evanescent wave through the alumina coating.

However, in this study such assumptions cannot be made, because the hematite film, which is significantly thick (950 nm), has a refractive index (2.91) (CRC Handbook of Chemistry and Physics, pp4-141) greater than that of ZnSe (2.43). Hence, the infrared radiation will be refracted by the hematite film, then reflected by the solution phase (lower n) beyond the hematite film, but also reflected again by the ZnSe (lower n). It would thus be retained in the hematite layer (highest n), indicating that total internal reflection should not occur. This is obviously not the case, as evident from the spectra showing absorption presented in Chapters 6 to 8. As the hematite film is cast from colloidal particles, it may be expected to act more like a porous film than a thin piece of solid hematite. Therefore, assuming that the entire film has the refractive index of hematite would be erroneous, as air or solution would inevitably occupy a certain fraction of the film. In addition, the refractive indices of ZnSe and the hematite film are similar, especially if porosity is taken into account, indicating that the hematite may have a minor or insignificant influence on the evanescent wave.

To assess the effect of the hematite coating, a ZnSe-hematite/water interface was used and the value of n_2 was assumed to be that of water (1.320 at $2125\ \text{cm}^{-1}$). Absorption values were recorded at 45° ($A = 0.896$) and 50° ($A = 0.645$) incident

angles. The value for n_1 (due to the ZnSe-hematite interface) was then determined in the same manner as n_2 for the ZnSe/benzene interface, and found to be 2.319.

The presence of the hematite thus slightly reduces the value of n_1 . This suggests that because of the higher refractive index of hematite (2.91), the presence of the porous hematite film acts like an extension of the lower refractive index ZnSe (2.43) crystal, such that total internal reflection and creation of the evanescent wave happens within the hematite film rather than the ZnSe crystal.

If we assume that the pores of the hematite are filled with water ($n = 1.320$) and that the apparent refractive index (2.319) is due to a mixture of water and hematite components, then the refractive index could be described by Equation 9.4:

$$n_1(obs) = n_{hematite} \cdot x + n_{H_2O} \cdot (1 - x) \quad (\text{Equation 9.4})$$

where: x = mole fraction of hematite

$$2.391 = 2.91x + 1.32(1 - x)$$

$$x = 0.67$$

The void fraction for a set of mono-sized close packed spheres is 26% (Atkins, 1988, pp 567), which would indicate that a porous film with approximately 33% water is a reasonable value, particularly considering that the hematite film is not made up exclusively of uniform spherical particles. Therefore it can be concluded that the two-layer model is appropriate for describing the solid-liquid interface for a hematite film cast on a ZnSe ATR element.

9.1.1.3 Effect of Adsorbed Polymer

As the adsorption of polymer onto a hematite-coated ZnSe crystal follows the behaviour expected for adsorption onto a reactive IRE, with an effective refractive index of 2.319, the adsorption density (Γ) can be characterised by Sperline, Muralidharan and Freiser's (1987) equation (Equation 2.13, Section 2.4.3):

$$\text{i.e.} \quad \Gamma = \frac{(A/N) - \epsilon_c d_e}{2000\epsilon(d_e/d_p)}$$

Similar to Equation 2.14, Equation 2.13 requires the thickness of the adsorbed layer to be $\ll d_p$, a condition that may not be met for adsorbed layers of high molecular weight polymers. The hematite layer is cast from a colloid that has a relatively narrow size distribution and a d_{50} of approximately 100 nm (Section 5.1.1), while the adsorbing polymers have a hydrodynamic diameter in solution of ~ 400 nm (Section 8.1.1) and will thus adsorb onto the outer surface of the cast hematite film only. The adsorption of high molecular weight cationic polymers onto negatively charged surfaces has been found to give an adsorbed layer thickness of approximately 100 nm (Wang and Audebert, 1988; Aksberg *et al.*, 1991). Charged polymers typically adsorb onto oppositely charged surfaces in a flat conformation at low ionic strength. This is dissimilar to the adsorption processes in this study, hence a flat adsorption conformation is not expected. A reasonable minimum estimate of the adsorbed layer thickness is 200 nm, which represents a 50% flattening of the hydrodynamic diameter in solution.

The adsorbed polymer layer could be modelled in a similar way to that expressed by Sperline, Song and Freiser (1992) in Equation 2.14 (Section 2.4.3), but only if a specific refractive index and thickness of the adsorbed polymer layer is known. This was not feasible for this study, as there are several complications in investigating the refractive index for the ZnSe-hematite/adsorbed polymer solution system, hence a more qualitative approach needed to be taken.

Whilst characterising the refractive indices of ZnSe/solvent and ZnSe-hematite/solvent systems is relatively simple, the addition of an adsorbed polymer layer significantly complicates the situation. Assuming that the ZnSe-hematite film has the same refractive index as that determined for the ZnSe-hematite/water interface, is likely to be erroneous as that refractive index incorporated a contribution from solely water filling the pores of the hematite film. For the adsorbed polymer system the pores are likely to be filled by solutions of various ionic strength and possibly some polymer in the case of low molecular weight species. The refractive index of these components would be expected to be significantly greater than that of water and would increase the effective refractive index of the film.

The other complication is the difficulty of dealing with the adsorbed polymer layer. A three-layer system would be ZnSe-hematite/adsorbed polymer/solution, with the adsorbed layer thickness estimated to be at least 200 nm. Once again, this thickness would likely represent a significant fraction of d_p , and is thus too significant to be considered for a three-layer model.

Therefore, in a similar argument to that used to describe the ZnSe-hematite/water system, the refractive index of the adsorbed polymer has been taken to be the same as that of a concentrated polymer solution. The refractive index of the adsorbed polymer layer and the solution beyond the adsorbed polymer is thus described in a simple manner, i.e. one layer with a specific refractive index. This is a reasonable approximation as the evanescent wave decays exponentially from the surface. The refractive index of the porous hematite film, which will be expected to change from the previously determined value for the ZnSe-hematite/water system with changes in solution ionic strength, can then be determined.

The ZnSe/concentrated polymer solution interface characterisation is relatively straight forward, because there is no complication associated with the presence of the hematite film, and is equivalent to the ZnSe/benzene calculations (Section 9.1.1.1). As a concentrated polymer solution was required for the determination, a 1 wt% solution of PAA450K made up at pH 13 in 1 M NaCl was selected, the value of n_1 was assumed to be that of ZnSe (2.430 at 2125 cm^{-1}) and absorption values were recorded at 45° (0.875) and 50° (0.637) incident angles. The value for n_2 (the concentrated polymer solution) was found to be 1.360.

The result shows that the presence of polymer and electrolyte in the pH 13 solution medium increases the refractive index from that of water (1.320). While there is no direct literature data to compare this value to, measurements at a wavelength of 589 nm (16978 cm^{-1}) show that 1 wt% acetic acid has a refractive index of 1.33 and 1 M NaCl has a refractive index of 1.34 (CRC Handbook of Chemistry and Physics, pp8-57 and 8-77, respectively). Both show a trend of increasing refractive index with increasing concentration in solution, therefore it would be expected that the above polymer solution would have a refractive index greater than that of water and that a result of $n_2 = 1.360$ is reasonable.

In the proposed model, the adsorbed polymer is assumed to have equivalent optical properties to a concentrated polymer solution in contact with an uncoated ATR crystal (i.e. $n_2 = 1.360$ at 2125 cm^{-1}). The refractive index of the ZnSe-porous hematite film was determined from absorbances measured after 45 minutes contact with a 50 ppm polymer solution (PAA13M at pH 13 and 1 M NaCl) that was pumped at a rate of 1 mL min^{-1} past the cast hematite film. The measured absorbances at 45° (0.829) and 50° (0.602) incident angles lead to a value of 2.417 for n_1 (ZnSe-porous hematite film).

Using Equation 9.4 and the calculated n_1 (2.417, ZnSe-porous hematite film) and n_2 (1.360, adsorbed polymer) indicates a film porosity of 32%.

$$\begin{aligned} \text{i.e.} \quad & 2.417 = 2.91x + 1.36(1 - x) \\ & x = 0.68 \quad (32\% \text{ porosity}) \end{aligned}$$

The result shows that the porosity of the film has remained essentially consistent for both the ZnSe-hematite/water system (33%) and the ZnSe-hematite/adsorbed polymer system (32%). This indicates that the model of the adsorbed polymer system, whereby the adsorbed polymer has the same refractive index as the concentrated polymer solution and that this solution fills that the pores of the hematite, is sound. This is consistent with the refractive index of the solution filling the pores being determined by the electrolyte rather than the polymer concentration, as the high molecular weight polymer used does not penetrate the film (Section 7.3).

9.1.2 Adsorbed Polymer Quantification

To relate a peak area to an adsorption density, the absorptivity coefficient of the peak area needs to be characterised. Typically, it is calculated via transmission infrared by measuring the absorbance at a particular concentration in a fixed path-length cell (Equation 2.4, Section 2.4.1.2). However, due to the very small path-length cell needed ($< 10\text{ }\mu\text{m}$) because of the intense water absorption bands, and the viscosity of the polymer solutions studied here, it was not possible to inject the polymer solutions into a conventional transmission flowcell. As the absorptivity coefficients could not be determined by transmission, they were instead derived using ATR measurements with a clean ZnSe crystal.

The d_e at 1720 cm^{-1} was calculated using Equation 9.2 (Section 9.1.1.1) for a concentrated PAA450K solution at pH 2. The polarisation ratio of the infrared radiation (i.e. $X = 0.387$) and the refractive index of the polymer solution ($n_2 = 1.36$) used were those determined for the concentrated polymer/ZnSe interface examined above. The refractive index for ZnSe is 2.426 (Feldman *et al.*, 1979, pp37,38) and an incident angle of 45° was used. The same procedure was used to determine d_e at 1560 cm^{-1} ($n_1 = 2.424$, Feldman *et al.*, 1979, pp37-38) for concentrated PAA450K and PAA13M solutions at pH 13 (1 M NaCl). The calculated values of d_e are given in Table 9.2.

Table 9.2: Effective thickness (d_e) calculation for 1 wt% polymer ($n_2 = 1.360$) and ZnSe ($n_1 = 2.426$ at 1720 cm^{-1} and 2.424 at 1560 cm^{-1}) interface. d_e was determined at 1720 cm^{-1} for adsorption at pH 2 and 1560 cm^{-1} for adsorption at pH 13 (1 M NaCl).

Adsorbing Polymer and Conditions	d_e (Peak)
PAA450K at pH 2	1419 nm (1720 cm^{-1})
PAA450K at pH 13 (1 M NaCl)	1571 nm (1560 cm^{-1})
PAA13M at pH 13 (1 M NaCl)	1571 nm (1560 cm^{-1})

These d_e values can then be used to determine ϵ from the concentration response trends (Figures 9.3 and 9.4). These were found to obey Beer's Law, being linear and passing through the origin, and hence their slopes were equal to ϵd_e .

A comparison of the relationship shown below for polymers PAA450K and PAA13M indicates that the gradient for the PAA450K polymer was almost twice as large, i.e. at equivalent solution concentrations, the 1560 cm^{-1} peak area for PAA450K will be approximately double that of PAA13M. The slope is equivalent to ϵd_e and d_e is the same for both polymers, thus the absorptivity coefficient ($\epsilon = \text{slope}/d_e$) of the 1560 cm^{-1} peak for the PAA450K polymer ($\epsilon = 0.566/(1.57 \times 10^{-4}) = 3602\text{ cm}^{-2}\text{ wt\%}^{-1} = 3.60 \times 10^2\text{ L g}^{-1}\text{ cm}^{-2}$) is 1.925 times greater than that for the PAA13M polymer ($\epsilon = 187.1\text{ L g}^{-1}\text{ cm}^{-2}$).

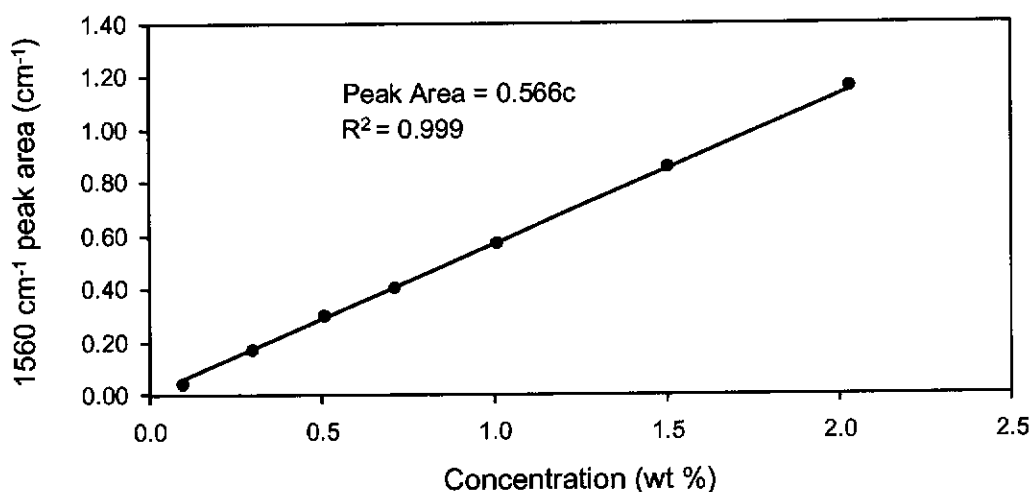


Figure 9.3: The 1560 cm⁻¹ peak area as a function of polymer solution concentration (wt%) for PAA450K at pH 13 (1 M NaCl).

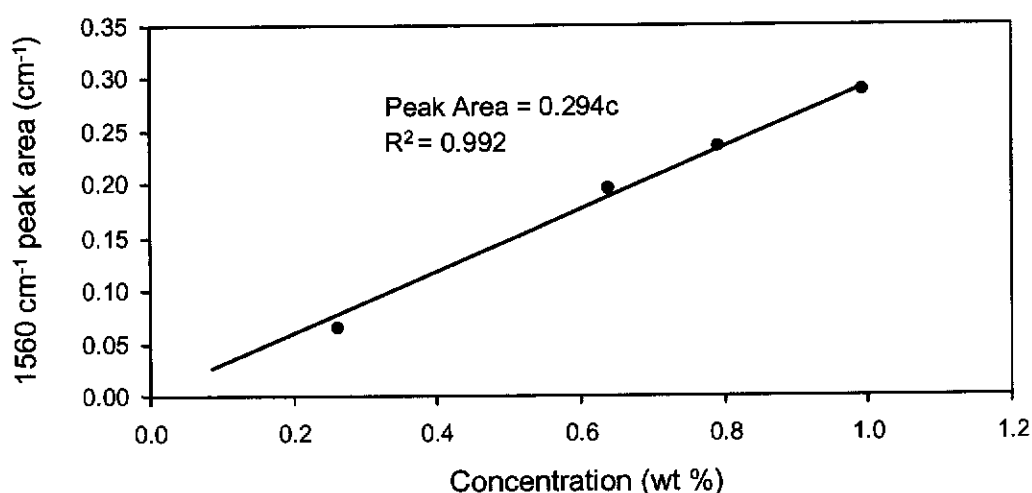


Figure 9.4: The 1560 cm⁻¹ peak area as a function of polymer solution concentration (wt%) for PAA13M at pH 13 (1 M NaCl).

This difference can most likely be attributed to the depth of penetration of the FTIR-ATR technique, which is approximately 1 μm from the surface of the ZnSe ATR element for polymer solutions. At the same concentration, there are approximately 30 times more polymer molecules in the PAA450K solution but the size of these molecules is not 30 times smaller (Section 8.1.1). Therefore, within the d_p there would be expected to be a greater number of PAA450K molecules, which would result in a greater absorbance when compared to that of PAA13M at similar solution concentrations.

Figure 9.5 shows the corresponding calibration for concentrated PAA450K solutions of known concentration at pH 2, monitored using the integral of the 1720 cm^{-1} peak. Due to the significantly reduced solubility of PAA13M at pH 2 it was not feasible to examine its corresponding concentration response curve.

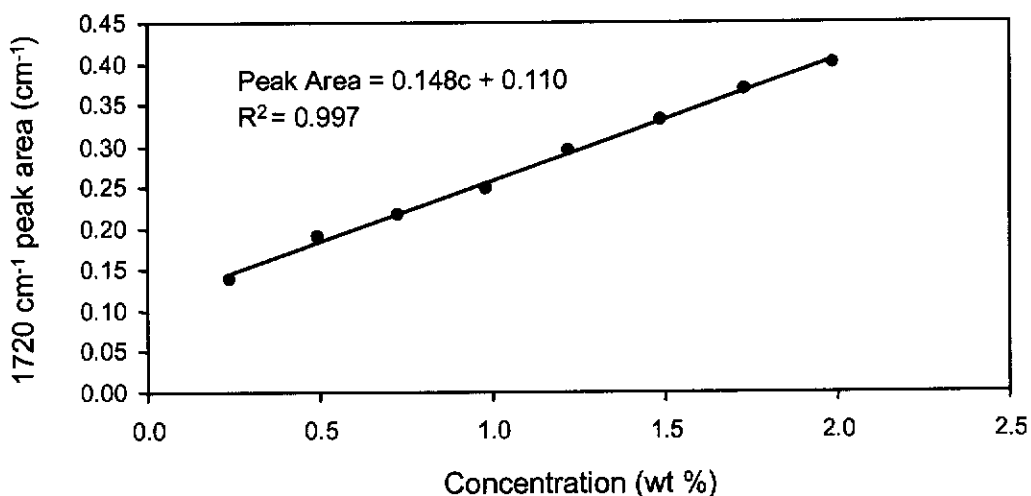


Figure 9.5: The 1720 cm^{-1} peak area as a function of polymer solution concentration (wt%) for PAA450K at pH 2.

The plot shows that there is a linear relationship between absorbance and polymer concentration, but the line of best fit does not pass through the origin, and is offset by 0.110, i.e. the absorbance of PAA450K at pH 2 as a function of concentration does not follow Beer's law. Such behaviour suggests that the polymer has an affinity for the ZnSe surface.

It was noted from these tests that the polymer was removed from the ZnSe surface very easily by flushing with solvent (water), returning the peak area to zero, indicating that the interaction is probably through weak physisorption. At a polymer concentration of 0.25 wt% polymer the offset contributes 80 % of the absorbance, and at 2.0 wt% it contributes 25 %. As there are no spectral shifts discernable, it suggests that the interaction is not only weak but also does not affect the polymer spectrum. Thus the coefficient of absorptivity ($\epsilon = \text{slope}/d_e = 0.148/(1.42 \times 10^{-4}) = 1.04 \times 10^2\text{ L g}^{-1}\text{ cm}^{-2}$) can be determined directly from the slope, by ignoring the 0.110 cm^{-1} offset, i.e. **Peak Area** = $0.148c$, and can be used to quantify the polymer in solution, in the absence of adsorption to the ZnSe surface.

When adsorbing polyacrylic acid onto hematite at pH 2, the hematite acts as a physical barrier between the polymer and the ZnSe surface. Therefore the signal for the adsorption of polyacrylic acid onto hematite is indicative only of that associated with the adsorption onto hematite and not that onto the ZnSe crystal, as polymer does not penetrate the hematite film to that extent. The integrated peak area obtained for the adsorption of polyacrylic acid onto hematite can thus be compared directly, using the coefficient of absorptivity, with that of the integrated peak area obtained from the calibration curve. The absorptivity coefficients for the integrated peak areas are given in Table 9.3.

Table 9.3: Calculated absorptivity (ϵ) for the 1720 cm^{-1} integrated peak area of PAA450K at pH 2 and the 1560 cm^{-1} integrated peak areas of PAA450K and PAA13M at pH 13 (1 M NaCl).

Adsorbing Polymer and Conditions (Peak)	Integrated Peak Range (cm^{-1})	Absorptivity ($\text{L g}^{-1}\text{ cm}^{-2}$)
PAA450K at pH 2 (1720 cm^{-1})	1630 - 1805	104
PAA450K at pH 13 and 1 M NaCl (1560 cm^{-1})	1484 - 1636	360
PAA13M at pH 13 and 1 M NaCl (1560 cm^{-1})	1484 - 1636	187

9.2 Adsorption Isotherms

Adsorption isotherms are used to determine the relationship between fractional coverage of the surface and the concentration of the adsorbate solution. Such isotherms are typically constructed by the solution depletion technique, where a powdered substrate and an adsorbate of specific concentration are mixed together. The solution concentration of the adsorbate decreases as it adsorbs onto the substrate and the amount adsorbed is calculated by the change in adsorbate concentration in the solution. The amount adsorbed is assumed to be in equilibrium with the concentration of the adsorbate left in solution.

The adsorption isotherms in this study were constructed by flowing polymer solution past the cast hematite film. The polymer solutions were of a fixed concentration, ranging from 5 to 56 ppm, and were added sequentially in order of increasing concentration without re-running the polymer-free solution and without applying a new hematite film to the ZnSe crystal. This strategy thus provides a consistent surface area for each polymer concentration.

The polymer solutions flowed from the source, past the hematite film and then to waste. Therefore the concentration of the polymer adsorbate solution remained fixed, and known, throughout the adsorption. This is different from the solution depletion approach, in that it involves the application of the higher concentrations to surfaces that are already partially covered. However, it was found that equivalent adsorption was achieved for a polymer adsorbate concentration, regardless of whether it was obtained directly by application at the higher concentration or by sequential addition of increasing concentrations, as shown in Figure 9.6.

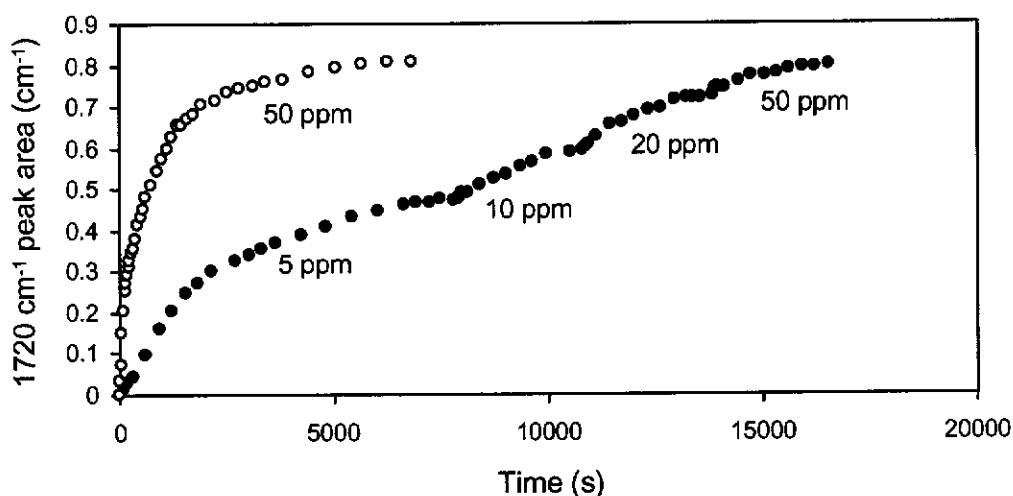


Figure 9.6: PAA450K adsorption at pH 2 (monitored by the 1720 cm^{-1} peak area), demonstrating equivalent adsorption achieved by either direct application of 50 ppm polymer solution or by sequential addition of increasing polymer solution concentration up to 50 ppm.

The adsorption profiles as a function of time for PAA450K at pH 2 and at pH 13 (1 M NaCl) are given in Figure 9.7, while that for PAA13M at pH 13 (1 M NaCl) is shown in Figure 9.8. The results show that the lowest initial polymer solution concentration takes the longest time to reach an equilibrium adsorption state. For all adsorption conditions this was approximately 7500 seconds (125 minutes). Subsequent application of polymer solutions of increasing concentration took much

less time to reach equilibrium adsorption. This is mainly a reflection of the method used to obtain the adsorption isotherm. The initial polymer concentration fills a certain number of adsorption sites, as determined by the concentration of the polymer in solution. These adsorption sites stay essentially filled, so that when a greater concentration of polymer is introduced into the system, additional sites are filled but the time taken to achieve equilibrium adsorption is less.

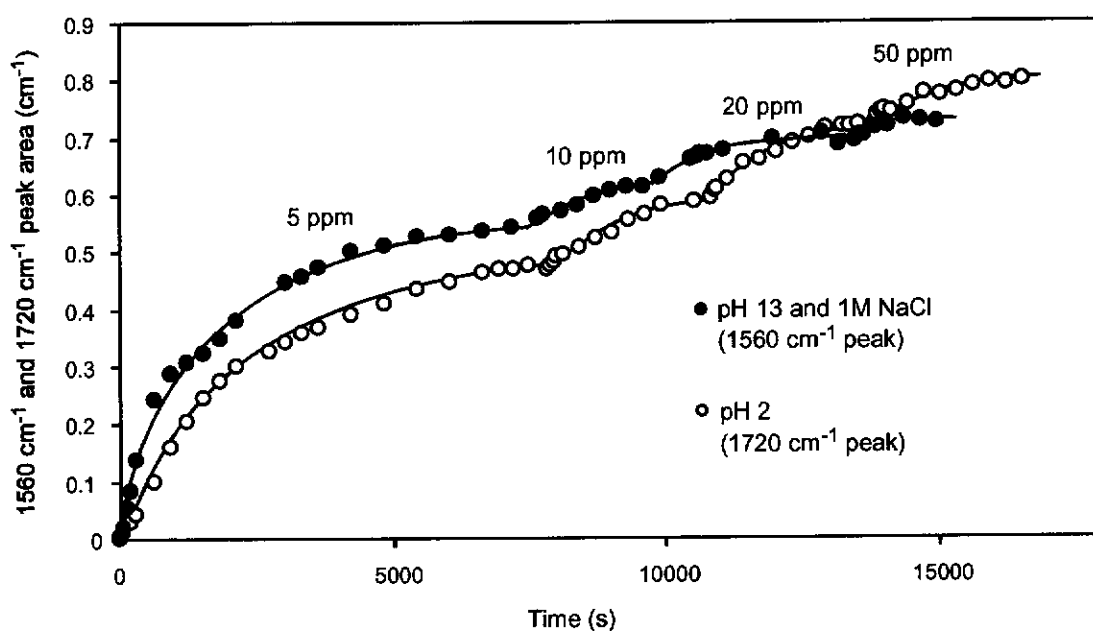


Figure 9.7: Adsorption of PAA450K at pH 2 (monitored by 1720 cm⁻¹ peak area) and at pH 13 and 1 M NaCl (monitored by 1560 cm⁻¹ peak area) at polymer concentrations of 5, 10, 20 and 50 ppm.

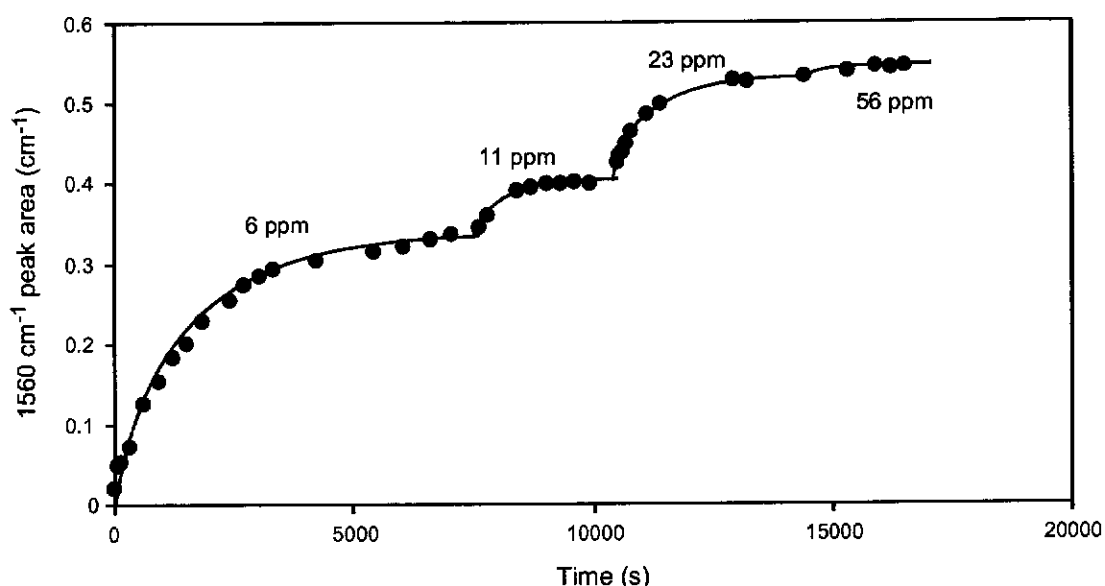


Figure 9.8: Adsorption of PAA13M at pH 13 and 1 M NaCl (monitored by 1560 cm⁻¹ peak area) at polymer concentrations of 6, 11, 23 and 56 ppm.

9.2.1 Langmuir Isotherm Fit

The plateau integrated absorbances as a function of polymer solution concentration for each adsorption profile above was fitted to Freundlich, Langmuir and Langmuir-Freundlich functions (Section 2.4.2), using a non-linear least squares curve fitter (Nonlinear Least Squares Curve Fitter). The Langmuir function (Equation 2.10, Section 2.4.2) was found to fit the experimental data best (i.e. lowest residual value). In applying this function, the fraction coverage θ was taken to equal the ratio of the integrated peak area (at concentration = c) relative to that of the maximum integrated peak area (at infinite concentration).

The Langmuir isotherm fits to the data are shown in Figure 9.9 (PAA450K) and Figure 9.10 (PAA13M), and summarised in Table 9.4.

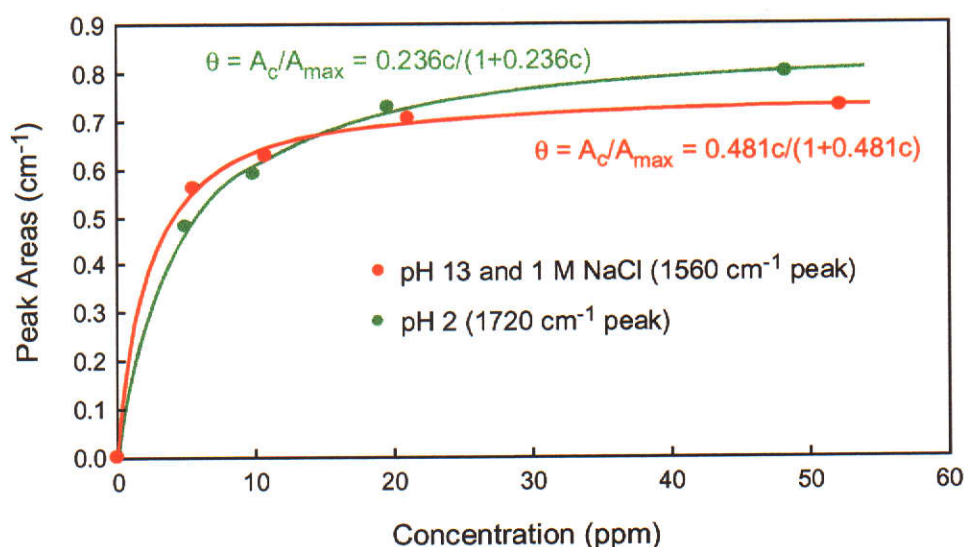


Figure 9.9: Plot of plateau absorbance values as a function of polymer concentration in Figure 9.7 for PAA450K adsorption at both pH 2 and pH 13 (1 M NaCl) and the subsequent Langmuir adsorption isotherm fit to the data.

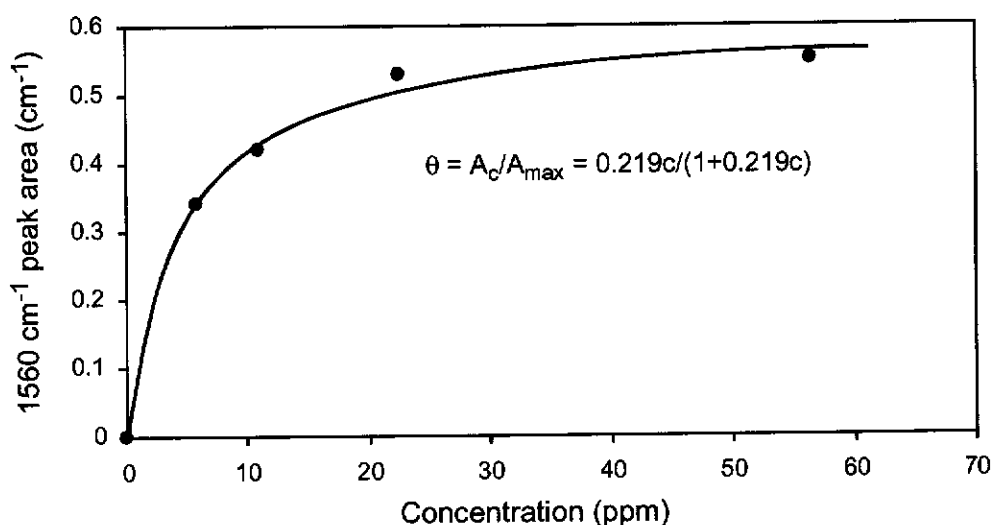


Figure 9.10: Plot of plateau absorbance values as a function of polymer concentration in Figure 9.8 for PAA13M adsorption at pH 13 (1 M NaCl) and the subsequent Langmuir adsorption isotherm fit to the data.

Table 9.4: The maximum integrated peak area and K as determined by Langmuir isotherm fit of the data in Figures 9.9 and 9.10.

Adsorbing Polymer and Conditions (Peak)	Maximum Integrated Peak Area, A_{\max} (cm^{-1})	K
PAA450K at pH 2 (1720 cm^{-1})	0.873	0.236
PAA450K at pH 13 and 1 M NaCl (1560 cm^{-1})	0.765	0.481
PAA13M at pH 13 and 1 M NaCl (1560 cm^{-1})	0.609	0.219

The maximum integrated peak area may be used to estimate the maximum adsorption density, and is discussed in the following Section. Interpretation of the equilibrium constant (K) is discussed in Section 9.2.3.

9.2.2 Maximum Adsorption Densities

The refractive index of the hematite coated ZnSe crystal was found to be 2.417 and that of the adsorbed polymer to be 1.360 (Section 9.1.2). Once again we can calculate d_e for each polymer adsorbing system by applying Equation 9.2

(Section 9.1.1.1). From these d_e values, the absorptivities as determined in Section 9.1.2, and including the maximum integrated absorbance as determined from the isotherms (Table 9.4), the equivalent solution concentration of polymers can be calculated using Equation 2.5 (Section 2.4.1.2) and are given in Table 9.5.

Table 9.5: The maximum adsorption of PAA450K at pH 2 and at pH 13 (1 M NaCl) and PAA13M at pH 13 (1 M NaCl) onto hematite, expressed as an equivalent solution concentration.

Adsorbing Polymer and Conditions (Peak)	Equivalent Solution Concentration (wt%)	Absolute Mass Adsorbed (μg)
PAA450K at pH 2 (1720 cm^{-1})	5.83	0.294
PAA450K at pH 13 and 1 M NaCl (1560 cm^{-1})	1.34	0.093
PAA13M at pH 13 and 1 M NaCl (1560 cm^{-1})	2.05	0.143

For the peaks at 1720 cm^{-1} and 1560 cm^{-1} , and using Equation 2.3 (Section 2.4.1.2), the concentrations determined above represent infrared penetration depths of 894 nm and 986 nm, respectively. The infrared analysis area is $7.07 \times 10^{-6}\text{ m}^2$ (Section 7.1), hence the interaction volumes are $5.04 \times 10^{-12}\text{ m}^3$ and $6.97 \times 10^{-12}\text{ m}^3$, respectively. Taking these interaction volumes into account, the equivalent solution concentrations can be converted (assuming a solution density of 1) into the corresponding absolute masses adsorbed, which are shown in Table 9.5.

The adsorption density is ideally described in terms of the mass of polymer adsorbed per unit surface area. Therefore a reliable estimate of the available hematite surface area is required. Due to the large size of the polymer in solution in comparison to the particle size of the cast hematite, it was evident that the polymer would adsorb only onto the outer surface of the cast hematite film (discussed in Section 7.3). This means that the available surface area of the hematite film would only be a fraction of the total surface area represented by all the particles that constitute the hematite film. Therefore, techniques normally used to determine the total surface area of the colloid

as a powder, such as BET (nitrogen adsorption), are inappropriate in this situation. Similarly, the use of a probe molecule, under specific conditions where the amount of adsorption is well characterised, is also inappropriate as the typically small probe molecules would undoubtedly adsorb into the pores of the hematite film and hence be exposed to a much greater available surface area than that of the adsorbing polymers. Therefore a purely geometric approach was used to determine the effective surface area of the film.

In calculating the surface area, it was assumed that the film consisted of spherical hematite particles in a close packed arrangement, as shown in Figure 9.11. While the particles are known to be cubic in shape (Section 5.1.2), their regularity suggests that on average this assumption should not introduce a significant error. In addition, it was assumed that the polymer only adsorbs onto the outer surface of the hematite film and hence only the top half of the hematite particles are available for adsorption. The particles in the hematite colloid were found to have a narrow size distribution with a d_{50} of approximately 100 nm. These form a continuous film greater than the analysis area of diameter 3 mm (Sections 7.2 and 7.1, respectively).

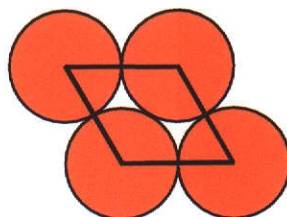


Figure 9.11: Close packed arrangement of spherical particles.

The minimum repeating unit within such close packed spherical particles has an area of $8.66 \times 10^{-15} \text{ m}^2$ and effectively contains one sphere. The 3 mm diameter analysis area of the infrared beam would thus contain:

$$(1 \times 7.07 \times 10^{-6}) / 8.66 \times 10^{-15} = 8.16 \times 10^8 \text{ particles.}$$

The surface area of each particle is: $4 \times \pi \times (50 \times 10^{-9})^2 = 3.14 \times 10^{-14} \text{ m}^2$

Therefore the total surface area of all the particles is $2.56 \times 10^{-5} \text{ m}^2$. As at most only the top half of the particles are available for adsorption, the maximum available surface area is estimated as $1.28 \times 10^{-5} \text{ m}^2$.

Taking into account the amount of polymer adsorbed and the available surface area, the adsorption densities can be determined. As an alternative approach, results from the interface characterisation can also be incorporated into the FTIR-ATR adsorption density equation (Equation 2.13, Section 2.4.3) proposed by Sperline, Muralidharan and Freiser (1987). For example, for PAA450K adsorption at pH 2:

$$\begin{aligned}
 A &= 0.873 \text{ cm}^{-1} && \text{(Section 9.2.1)} \\
 N &= 1 && \text{(single bounce accessory)} \\
 \epsilon &= 104.0 \text{ L g}^{-1} \text{ cm}^{-2} && \text{(Section 9.1.2)} \\
 c_b &= 0.050 \text{ g L}^{-1} && \text{(bulk polymer concentration)} \\
 d_e &= 1.441 \times 10^{-4} \text{ cm} && \text{(Equation 9.2, Section 9.1.1.1)} \\
 d_p &= 8.94 \times 10^{-5} \text{ cm} && \text{(Equation 2.3, Section 2.4.1.2)}
 \end{aligned}$$

where: $\lambda = (1/1720) \text{ cm}$, $n_1 = 2.417$ (Section 9.1.2) and $n_2 = 1.360$ (Section 9.1.2).

The adsorption density results obtained by the two approaches are given in Table 9.6. The results show that the trends are the same for both methods and the magnitudes similar, suggesting that the approach taken in this study is reasonable.

Table 9.6: Adsorption densities determined using porous hematite film model and by applying the FTIR-ATR adsorption density equation (Sperline, Muralidharan and Freiser, 1987).

Polymer and Conditions	Maximum adsorption density (mg m^{-2}) determined by:	
	Porous hematite film model	FTIR-ATR adsorption density equation (2.13, p 39)
PAA450K at pH 2	23.0	26.0
PAA450K at pH 13 (1 M NaCl)	7.27	6.56
PAA13M at pH 13 (1 M NaCl)	11.2	10.1

Table 9.6 shows that adsorption of PAA450K at pH 2 is much higher than for either polymer at pH 13 (1 M NaCl). Furthermore, this adsorption density at pH 2 is

determined using the 1720 cm^{-1} peak integral, which is indicative of the loops and tails from the adsorbed polymer chains, with no contribution from the 1410 cm^{-1} or 1545 cm^{-1} peaks for the adsorbed segments. For 1 wt% unadsorbed concentrated polymer solutions, the intensity (peak height) of the 1410 cm^{-1} peak (from a pH 13 solution spectrum), compared to the 1720 cm^{-1} peak intensity (from a pH 2 solution spectrum) suggests a 1:1 relationship (Section 7.3). Results of adsorbed polyacrylic acid at pH 2 in Section 7.3 (Figure 7.8) show that the polymer unadsorbed:adsorbed ratio is 4:1. Therefore this indicates that 80% of the polymer is unadsorbed while 20% is adsorbed. The above adsorption density of 23.0 mg m^{-2} would therefore only represent 80% of the polymer functionalities and the entire adsorption density would in fact be closer to 28.8 mg m^{-2} .

If peak areas are used instead of peak intensities to compare the relative infrared activity of the 1410 cm^{-1} and 1720 cm^{-1} peaks, then the error associated with the affinity that PAA450K had with the ZnSe crystal at pH 2 can be avoided. Using the peak area from the calibration curve in Figure 9.5 (Section 9.1.2), we see that the integral for the 1720 cm^{-1} peak is 0.295 at 2 wt% (using the function Peak Area = $0.148c$) and the integral is 0.187 for the 1410 cm^{-1} peak at 2 wt% (Figure 9.12). The unadsorbed:adsorbed ratio determined for the adsorption experiment at pH 2 then becomes 2.5:1. This indicates that 28% of the polymer is adsorbed, and that consideration of the unadsorbed segments now increases the above adsorption density from 23.0 mg m^{-2} to 32.1 mg m^{-2} .

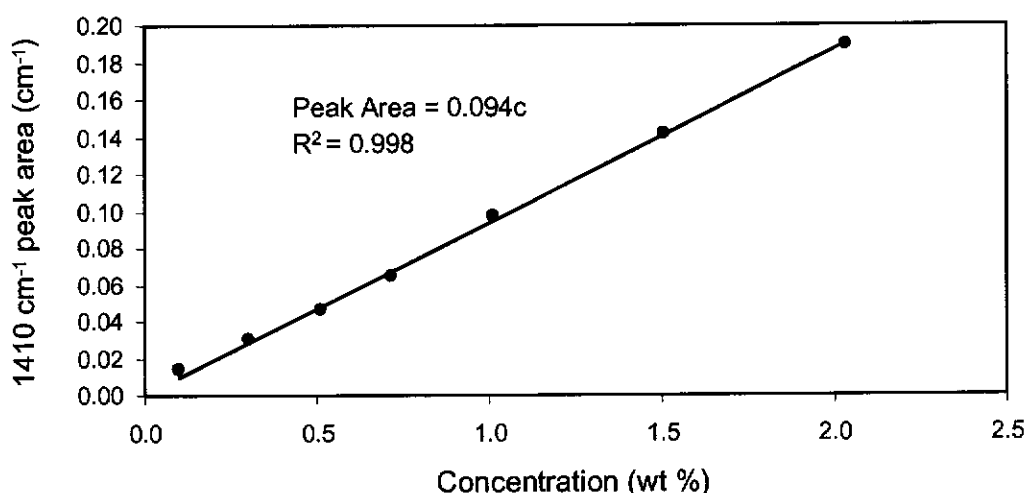


Figure 9.12: The 1410 cm^{-1} peak area as a function of polymer solution concentration (wt%) for PAA450K at pH 13 (1 M NaCl).

The most notable characteristic of the results in Table 9.6 is that the adsorption densities are much higher than expected. Typically, reported plateau adsorption densities for polymers lie between 1.5 and 3 mg m⁻² (Lyklema, 1989), while Jones, Farrow and van Bronswijk (1998a) found that polyacrylate had an even lower plateau coverage of 0.164 mg m⁻² on hematite when adsorbed from synthetic Bayer liquor. This is likely due to the different techniques used, solution depletion in the above two studies and ATR in this study.

While the two ATR approaches represented in Table 9.6 gave comparable results, several differences also exist between them. The use of the FTIR-ATR adsorption density equation (Equation 2.13, Section 2.4.3) includes the term $\epsilon_c d_c$ in the numerator, which represents the contribution to the absorbance from the bulk solution. In the porous hematite film model, this contributes less than 0.5% of the measured absorbance, and hence was ignored. The main difference is that Equation 2.13 assumes the adsorbed layer thickness is $\ll d_p$ and that the refractive index of the solution beyond the adsorbed layer is 1.360. This has the effect of increasing the adsorption density if it is assumed that the solution beyond the adsorbed layer would have a refractive index closer to that of water (1.320). While for the porous hematite film model, the solution refractive index of 1.360 is assumed to represent an infinitely thick (i.e. $\gg d_p$) adsorbed polymer layer, which also has the effect of increasing the adsorption density if the adsorbed polymer layer is less than d_p .

The thickness of the adsorbed polymer layer is in fact estimated to be 200 nm (Section 9.1.1.3), which is only about a quarter the depth of penetration. A correction for this can be introduced into the porous hematite film model, with the adsorption detected for an adsorbed polymer layer with a thickness of approximately $0.25d_p$ equivalent to an infinitely thick solution at a concentration some 4.5 times more dilute. Therefore, this would represent a discrepancy in the adsorption densities of a factor of 4.5 from those determined by the porous hematite film model. Table 9.7 presents adsorption densities corrected for this factor, which are considerably lower than the uncorrected values.

If it is assumed that the entire available hematite surface is accessible to the polymer, which adsorbs flat on the surface, then an equivalent monolayer coverage can be

estimated from knowledge of the area per monomeric unit. Misra (1996) quotes an area per monomer unit for polyacrylate of 0.154 nm^2 , and therefore the equivalent monolayer coverage for polyacrylic acid (pH 2) and sodium polyacrylate (pH 13) are 0.776 mg m^{-2} and 1.01 mg m^{-2} , respectively. The monolayer values in relation to the maximum adsorption densities are also given in Table 9.7.

Table 9.7: Adsorption density values for PAA450K at pH 2 and PAA450K and PAA13M at pH 13 (1 M NaCl), and the number of equivalent monolayer coverages that these adsorption densities represent.

Polymer and Conditions	Corrected Maximum Adsorption Density (mg m^{-2})	No. of Equivalent Monolayer Coverages
PAA450K at pH 2	7.10	9.15
PAA450K at pH 13 (1 M NaCl)	1.61	1.59
PAA13M at pH 13 (1 M NaCl)	2.48	2.45

These maximum adsorption density values are more realistic, however it would appear that the ability of the technique to measure adsorption densities is limited by the accuracy of the determination of the adsorbed polymer layer thickness. Table 9.7 also shows that the number of equivalent monolayer coverages exceeds 1 in all cases. This is not uncommon for polymer adsorption onto mineral particles, as it is typically characterised by 'trains' of adsorbed polymer with 'loops' and 'tails' of unadsorbed polymer (Figure 2.4, Section 2.2.2.1) that extend into the solution. Hence, flocculant adsorption characteristically reaches a limiting value, corresponding to a large excess over that expected for monolayer coverage of polymer adsorbed flat on the solid surface (Eirich, 1977; Misra, 1996). Misra (1996) has shown that for adsorption of polyacrylic acids and sodium polyacrylates ranging in molecular weight from 2000 to 250 000 onto hydroxyapatite, the number of equivalent monolayer coverages ranged from 0.45 to 6.29.

A contributing factor to the particularly high adsorption of PAA450K at pH 2 may have been due to an erroneous determination of the absorptivity coefficient of the polymer solution. That determination was complicated by the polymer actually

having an affinity for the ZnSe crystal. However, even if the calibration curve represented by Figure 9.5 (Section 9.1.2) had exhibited no affinity (i.e. obeyed Beer's Law and passed through origin) and the slope was such that the 1720 cm^{-1} peak area of 0.406 cm^{-1} at 2.0 wt% remained, this would equate to an absorptivity coefficient of $143.1\text{ L g}^{-1}\text{ cm}^{-2}$, and give a corrected maximum adsorption density of 5.23 mg m^{-2} , demonstrating that adsorption of PAA450K at pH 2 would still have been significantly higher than that achieved at pH 13.

The major uncertainty for quantifying adsorption densities is the assumption that the integrated peak absorbance used to monitor adsorption can be related to an equivalent peak in a concentrated polymer solution through the absorptivity coefficient. If the volume occupied by each polymer in the adsorbed state differed significantly from that in the solution state, then the absorptivity coefficients of the peak area being monitored may no longer be comparable.

If it is assumed that each polymer molecule adsorbed to the hematite surface covered an area with a diameter equivalent to the diameter of gyration (Section 8.1.1), this would equate to monolayer coverages of 0.013 mg m^{-2} , 0.012 mg m^{-2} and 0.201 mg m^{-2} for PAA450K at pH 2, at pH 13 (1 M NaCl), and PAA13M at pH 13 (1 M NaCl), respectively. These values are obviously much smaller than the determined maximum adsorption densities and hence would indicate that in the adsorbed state, the polymer is much more condensed than the voluminous coil structure it assumes in solution. Therefore the quoted adsorption densities in Table 9.7 indicate that, in addition to allowing for the possibility of considerable polymer overlap, there must also be considerable compaction of the polymer at the surface and condensation of the polymer coils to dimensions significantly smaller than the solution diameter.

While the porous hematite film model has been treated in a quantitative manner, several simplifications and assumptions were made. Despite this, it has demonstrated that for polymer adsorption onto a porous layer, whose average refractive index is close to those of the ATR element, a simplified model leads to useful results that compare very well with those obtained using the FTIR-ATR adsorption density equation proposed by Sperline, Muralidharan and Freiser (1987).

It would appear that the FTIR-ATR technique is not appropriate for obtaining absolute polymer adsorption densities. It is limited by the accurate determination of the adsorbed polymer layer thickness and knowledge of how the conformation of the polymer changes from solution to the adsorbed state. However, these uncertainties remain relatively constant for each polymer adsorbing system, therefore comparisons of the trends within the data can be made with confidence.

Previous studies of the adsorption of polyacrylate or acrylamide/acrylate copolymers onto hematite through a pH range of 2-12 at low ionic strength (Bajpai and Bajpai, 1995b; Drzymala and Fuerstenau, 1987; Khangaonkar and Bala Subramani, 1993; Lee and Somasundaran, 1989) have found that increasing the pH decreased the amount of polymer adsorbed. The decrease in adsorption was attributed to changes in the polymer properties and the surface charge of the hematite at varying pH.

In the present study, a similar result was found, where the adsorption density for PAA450K decreased from pH 2 to pH 13 (1 M NaCl). However, the mode of adsorption is completely different from low to high pH. The mode at low pH is chemisorption and the results suggest that there are many more favourable adsorption sites for this process compared to that for the electrostatic adsorption mode occurring at pH 13 (1 M NaCl).

The results in Table 9.7 also show that at pH 13 (1 M NaCl), increasing the molecular weight from 450 000 to 13 000 000 has the effect of increasing the adsorption density. This is similar to the findings of Santhiya *et al.* (1998) for the adsorption of polyacrylic acids (2 000 to 90 000) on alumina suspension at pH 3. Misra (1996) noted the same effect for the adsorption of lower molecular weight (2 100 and 5 100) polyacrylates onto hydroxyapatite. These results were attributed to the longer chain molecules being irreversibly bound to the substrate surface and hence not forming an equilibrium with the free molecules in solution. Obviously in this study, both polymers exhibit a much higher molecular weight and hence longer chain length, with both expected to adsorb irreversibly.

For the adsorption of such high molecular weight polymers, some workers have suggested that the maximum adsorption achieved is independent of molecular weight. Results obtained by Misra (1996) showed that higher molecular weight

polyacrylates (60 000 and 170 000) adsorbed to the same extent. Similarly, Jones, Farrow and van Bronswijk (1998a) observed that two polyacrylates of significantly different molecular weights (150 000 and 14 000 000) adsorbed to the same extent on hematite from synthetic Bayer liquor. These results indicate that maximum polymer adsorption may be fairly consistent once the molecular weight exceeds approximately 60 000.

While this is contrary to the results obtained for adsorption at high pH in this study, it is consistent with results for the adsorption of polyacrylic acid at low pH. In Figure 7.7 (Section 7.3) the adsorption of PAA450K at pH 2 appears to be approximately double that of PAA13M. The absorptivity coefficient of the 1720 cm^{-1} peak area of PAA13M could not be characterised due to solubility restrictions, but would be expected to be approximately half that of the equivalent PAA450K peak (i.e. demonstrates a similar behaviour as the 1560 cm^{-1} peak at high pH – Section 9.1.2), hence the extent of adsorption would be essentially the same. In addition, it was shown that the ratio of unadsorbed:adsorbed polymer segments remained consistent, regardless of molecular weight (Section 7.3). These results indicate that the adsorbed conformation and hence maximum adsorption were independent of molecular weight for polymers of significant size.

At high pH, the increase of the maximum adsorption with molecular weight indicates that the conformation that the polymer takes up when adsorbing onto the hematite may change as a function of molecular weight. The results suggest that under such conditions polyacrylate may have a greater proportion of adsorbed polymer segments, taking a flatter and more extended adsorbed conformation at lower molecular weights.

Therefore, it may be concluded that if conditions favour the adsorbed conformation remaining the same, then for polyacrylates with molecular weights over approximately 60 000, the extent of adsorption will be independent of molecular weight. If conditions are such that the adsorbed conformation does change as a function of molecular weight, then the trend of maximum adsorption will increase with increasing molecular weight.

9.2.3 *Interpreting the Langmuir 'K' Value*

The Langmuir isotherm assumes that the sites where adsorption occurs are all thermodynamically equivalent and that the adsorption is independent of whether or not nearby sites are occupied. When the adsorption has reached equilibrium for a specific concentration, this normally indicates that the rate that surface sites are filled due to adsorption is equal to the rate at which they are vacated by desorption.

While the plateau adsorption value can be related to monolayer coverage and ultimately a maximum adsorption density (Section 9.2.2), the other information that can be derived from the Langmuir isotherm data prior to the plateau is the K value (Table 9.4, Section 9.2.1). In true equilibrium systems, this value is equal to k_a/k_d , where k_a and k_d are the rate constants for adsorption and desorption, respectively.

The above interpretation of the K value cannot be applied in this study where polymer adsorption is irreversible. Irreversible adsorption occurs because high molecular weight polymer molecules will have many attachments to the substrate surface and it is therefore statistically unlikely that all of these attachments will simultaneously detach resulting in desorption.

The implication from this is that monolayer coverage could potentially be achieved by applying any concentration of polymer, as it would only ever accumulate onto the surface and adsorption would not exhibit equilibrium type behaviour (i.e. K would approach an infinite value). However, the results obtained clearly show that adsorption does in fact increase as a function of concentration, indicating that the driving force for polymer adsorption is related to the concentration of polymer in solution. This driving force increases with increasing polymer concentration, with equilibrium adsorption at a particular concentration essentially being the maximum adsorption that the particular driving force can impart. However, the driving force for adsorption is not competing with a simultaneous desorption process.

Generally, adsorption isotherms for polymers are approximated by the Langmuir function and are typically characterised as high affinity isotherms. They show an almost concentration independent nature, where there is high adsorption at low concentrations and a plateau is obtained (La Mer and Healy, 1963).

The occurrence of isotherms that are more rounded and exhibit no clear plateau have in the past generally been attributed to polydispersity (wide molecular weight distribution) and classified as low affinity isotherms. This shape has been explained in terms of larger molecular weight polymer fractions preferentially adsorbing and removing smaller molecular weight polymer molecules from the surface, resulting in an increase in polymer adsorption with increasing polymer concentration (Cohen Stuart, Fler and Bijsterbosch, 1982). However, contrary to this, Papenhuijzen, Fler and Bijsterbosch (1985) have shown that low affinity type isotherms were indicative of weak adsorbate-substrate interactions, while high affinity isotherms were indicative of strong adsorbate-substrate interactions. This was supported by the findings of Adam and Robb (1983) who showed that the adsorption of a polydispersed poly(styrene sulfonate) polymer onto calcium carbonate exhibited a high affinity isotherm.

Hence, it would appear that K , describing the curvature in a Langmuir isotherm, may be a measure of polymer affinity to a substrate surface. For all the isotherms solved above, the K values are all less than 1 and are indicative of very low affinity isotherms.

Due to polymer adsorption being irreversible, if we assume some low constant value for the rate of desorption, then K becomes directly proportional to the rate of polymer adsorption. The results in Table 9.4 therefore suggest that the rate of polymer adsorption increases from pH 2 to pH 13 (1 M NaCl) for PAA450K, and that the rate of PAA13M adsorption at pH 13 (1 M NaCl) is comparable to that of PAA450K at pH 2. The relative rate of polymer adsorption is discussed in more detail in the following Section.

9.3 Adsorption Kinetics

Kinetic studies of adsorption using *in situ* FTIR-ATR have in the past been limited to those involving reactive IREs (Free and Miller, 1997). The molecules examined are normally dimensionally so small that diffusion into the film coating would complicate any kinetic study on coated optics. In this study, it has been shown that high molecular weight polymers are dimensionally large enough in solution to only

adsorb onto the outer surface of the cast hematite film and hence diffusion of the polymer into the pores of the cast film is not an issue.

The kinetics for the rate of adsorption can be expressed as:

$$R_{ads} = k_a [P][V] - k_d [P_v] \quad (\text{Equation 9.5})$$

where k_a is the rate constant for adsorption, $[P]$ is the concentration of polymer at the surface, $[V]$ relates to the number of vacant surface sites, k_d the rate constant for desorption, and $[P_v]$ is the concentration of adsorbed species.

If we assume that there is very little desorption and that the desorption rate is insignificantly low, i.e. an irreversible reaction, then the expression becomes:

$$R_{ads} = k_a [P][V] \quad (\text{Equation 9.6})$$

i.e. the rate is dependent on both the solution concentration and the number of surface sites available.

9.3.1 Effect of Flowrate

The flow properties of the ATR flowcell used in this study are not well characterised, hence accurate predictions of the absolute concentration of polymer within the surface region under specific conditions cannot be made. However, Figure 7.6 (Section 7.3), which shows the adsorption of PAA450K (50 ppm) at pH 2 as a function of flowrate, indicates that the rate of adsorption increases with flow (0.17 to 1.0 mL min⁻¹). This suggests that mass transport is a major factor in the adsorption process. The decrease in adsorption rate at 2.0 mL min⁻¹ was attributed to changes in the flow patterns of the flowcell and the subsequent effect of this on the adsorbing polymer molecules (discussed in Section 7.3). As the plateau absorbance (A_{max}) is a measure of the sites available for adsorption, Figure 7.6 also shows that A_{max} and hence the number of surface sites available for carboxylate coordination to be essentially the same for all hematite films used. As a consequence, relative rate data can be obtained from such adsorption data.

Because the flow of polymer, $[P]$, is constant under a given set of experimental conditions, the k_a and $[P]$ terms in Equation 9.6 can be combined and the rate

equation thus becomes first order, i.e. $\text{Rate} = k'[V]$. The rate of adsorption is monitored from the increase in carboxylate peak area as a function of time, and a relative rate of adsorption can therefore be expressed as:

$$\frac{dA}{dt} = k'(A_{\infty} - A) \quad (\text{Equation 9.7})$$

where A is the integrated peak area of the adsorbing polymer at time t , A_{∞} is the plateau adsorption value, and k' is the pseudo first order relative rate constant.

Hence:

$$A = A_{\infty} \left(1 - \frac{1}{e^{k't}} \right) \quad (\text{Equation 9.8})$$

The linear form of Equation 9.8 is given by Equation 9.9:

$$\ln \frac{A_{\infty}}{(A_{\infty} - A)} = k't \quad (\text{Equation 9.9})$$

For any particular polymer bulk concentration, A_{∞} can be determined from the adsorption isotherms (Section 9.2.1) and incorporated into Equation 9.9. Graphing of $\ln(A_{\infty}/(A_{\infty} - A))$ versus time (t) thus yields a slope equivalent to k' , and the standard error associated with k' can be determined. For the adsorption data in Figure 7.6, after an initial fast relative rate of adsorption that occurs for less than 500 seconds in all cases, the rate slows (Figures 9.13 to 9.16). The k' value corresponding to the initial rate of reaction was used with A_{∞} in Equation 9.8 to give calculated values of A . These have been included in Figures 9.13 to 9.16, and a comparison of the raw adsorption profile data compared to the calculated response demonstrates that the rate of polymer adsorption slows significantly after an initial high rate of adsorption.

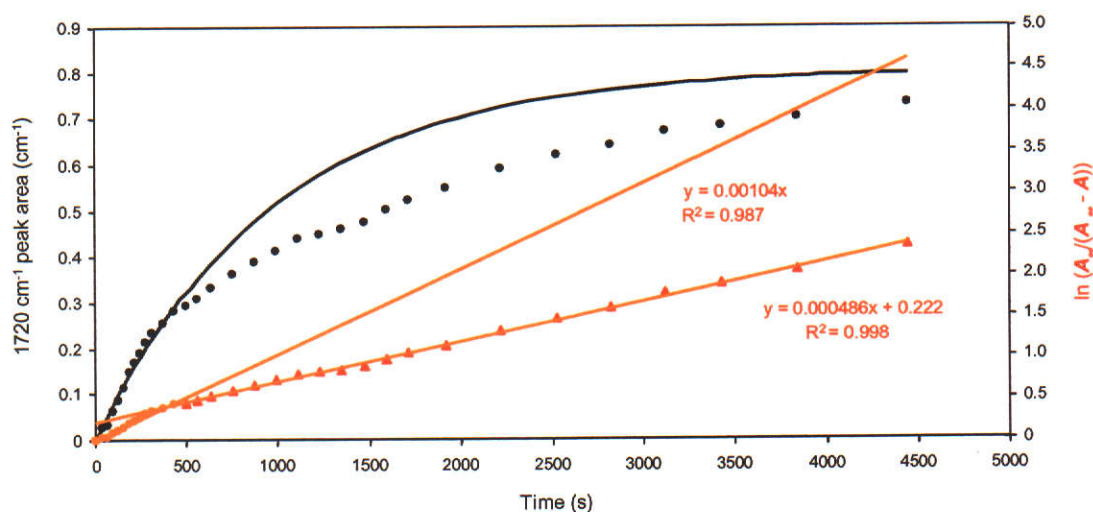


Figure 9.13: Adsorption of 50 ppm PAA450K at pH 2 (monitored by 1720 cm^{-1} peak area) and at a flowrate of 0.17 mL min^{-1} , together with the predicted response, as determined using Equation 9.8, for the initial relative rate of reaction. Also shown is the relative rate as determined from the slope of the plot of $\ln(A_{\infty}/(A_{\infty} - A))$ as a function of time. Both the fast relative rate of adsorption at initial times and the slower relative rate of adsorption at longer times are given.

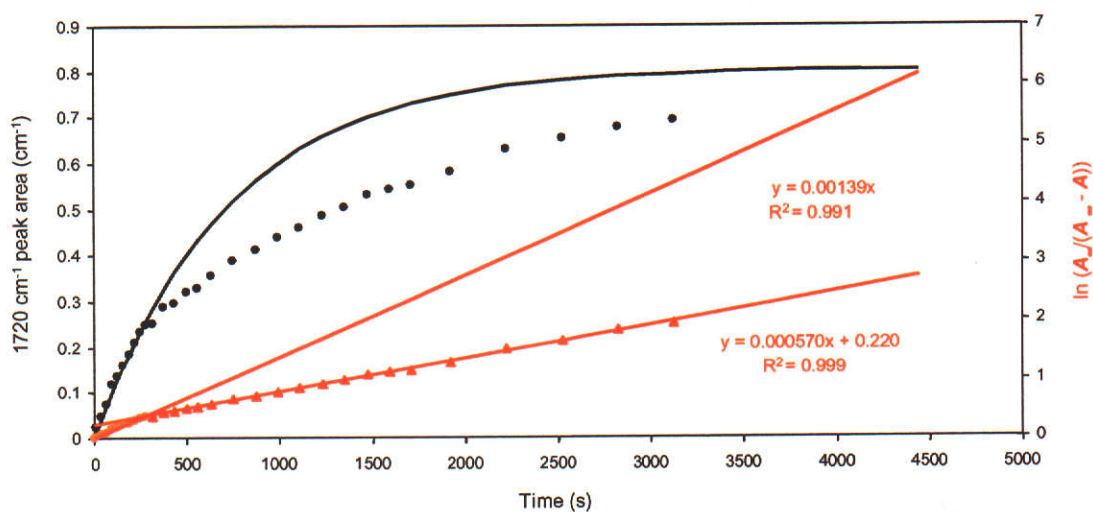


Figure 9.14: Adsorption of 50 ppm PAA450K at pH 2 (monitored by 1720 cm^{-1} peak area) and at a flowrate of 0.5 mL min^{-1} , together with the predicted response, as determined using Equation 9.8, for the initial relative rate of reaction. Also shown is the relative rate as determined from the slope of the plot of $\ln(A_{\infty}/(A_{\infty} - A))$ as a function of time. Both the fast relative rate of adsorption at initial times and the slower relative rate of adsorption at longer times are given.

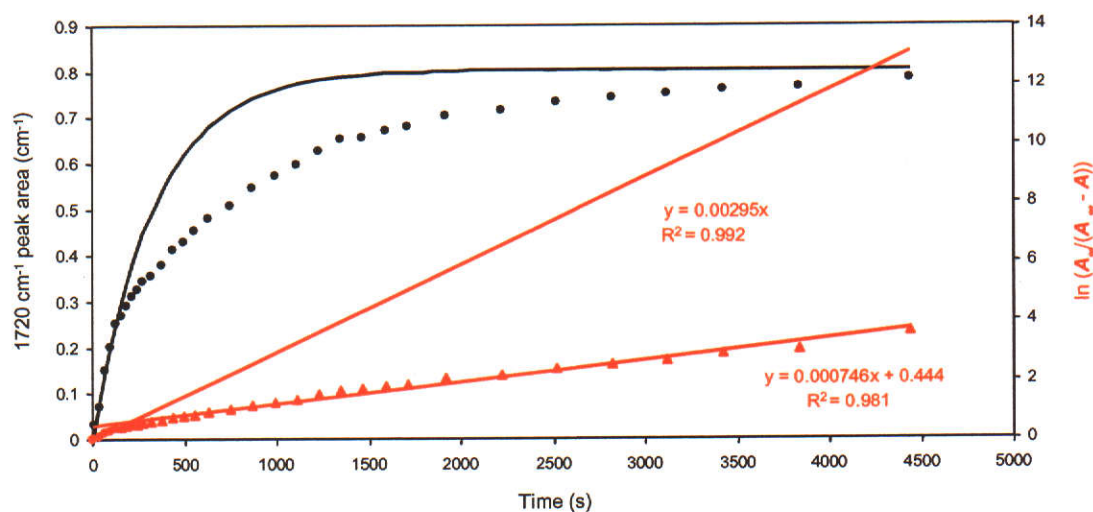


Figure 9.15: Adsorption of 50 ppm PAA450K at pH 2 (monitored by 1720 cm^{-1} peak area) and at a flowrate of 1.0 mL min^{-1} , together with the predicted response, as determined using Equation 9.8, for the initial relative rate of reaction. Also shown is the relative rate as determined from the slope of the plot of $\ln(A_{\infty}/(A_{\infty} - A))$ as a function of time. Both the fast relative rate of adsorption at initial times and the slower relative rate of adsorption at longer times are given.

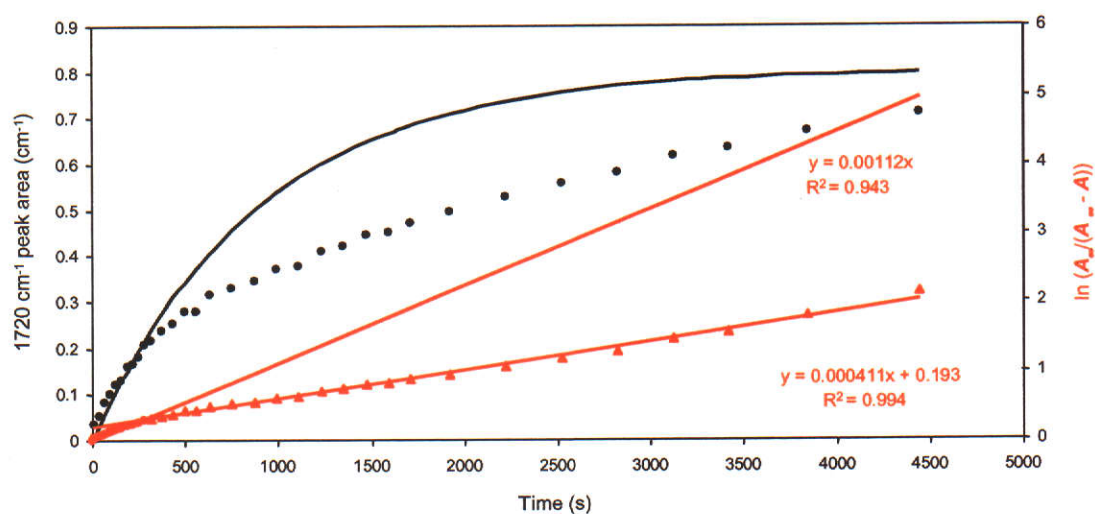


Figure 9.16: Adsorption of 50 ppm PAA450K at pH 2 (monitored by 1720 cm^{-1} peak area) and at a flowrate of 2.0 mL min^{-1} , together with the predicted response, as determined using Equation 9.8, for the initial relative rate of reaction. Also shown is the relative rate as determined from the slope of the plot of $\ln(A_{\infty}/(A_{\infty} - A))$ as a function of time. Both the fast relative rate of adsorption at initial times and the slower relative rate of adsorption at longer times are given.

The initial high relative rate of adsorption shown in Figures 9.13 to 9.16 confirms that there is an excess of available adsorption sites and that adsorbate-adsorbate interaction is minimal. The decrease in the rate at later times is typical for polymer adsorption and indicates that adsorption is limited by reconfiguration of adsorbed polymer, and possibly polymer-polymer interactions.

This is similar to the findings of Parsons, Harrop and Mahers (1992), who found a double-exponential rate equation for the adsorption of an amphoteric polymer onto a quartz surface. Their explanation was that the initial fast adsorption rate appeared to be dominated by an excess of available adsorption sites, while the later slower adsorption rate was due to the reduced number of available sites and limited by the rate at which the polymer molecules can rearrange onto the surface and adopt an optimum conformation.

An examination of the initial relative rates as a function of flowrate (Table 9.8) shows that the rate of adsorption does in fact increase up to 1 mL min^{-1} . As mentioned previously, the decrease observed on going to a flowrate of 2 mL min^{-1} has been attributed to changes in the flow patterns of the flowcell (discussed in Section 7.3).

Table 9.8: Relative rates of 50 ppm PAA450K adsorption at pH 2 as a function of flowrate and derived from the slope of the graph of $\ln(A_{\infty}/(A_{\infty} - A))$ versus time (t) (Equation 9.9) for initial adsorption times as shown in Figures 9.13 to 9.16.

Flowrate (mL min^{-1})	k' ($\text{mg L}^{-1} \text{ s}^{-1}$)
0.17	$1.04 (\pm 0.02) \times 10^{-3}$
0.50	$1.39 (\pm 0.02) \times 10^{-3}$
1.00	$2.95 (\pm 0.07) \times 10^{-3}$
2.00	$1.12 (\pm 0.04) \times 10^{-3}$

A plot of the initial relative rate against flowrate, up to 1 mL min^{-1} (Figure 9.17), suggests that the value for 0.17 mL min^{-1} is greater than the trend would predict. However, this is almost certainly a reflection of the limiting rate of adsorption being governed by diffusion of the polymer to the surface as in a non-flowing system. Deviation from a linear trend at low flowrates is expected, as diffusion from the bulk solution becomes the dominant factor, i.e. a zero rate of adsorption in the absence of flow is not realistic. At higher flowrates, the rate of adsorption increases, indicating that all the polymer molecules within the surface region are adsorbed and that the adsorption process is mass transport limited. This would suggest that there is a

minimal barrier or activation energy required for adsorption. The relative rates of adsorption are thus indicative of the mass transfer limited rate constant (k_m).

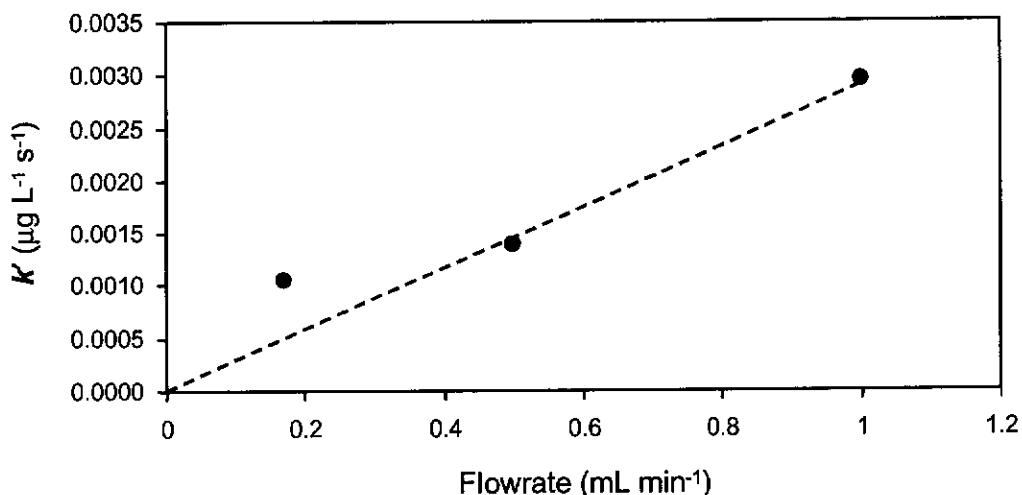


Figure 9.17: Relative rate of adsorption of PAA450K at pH 2 as a function of flowrate up to 1 mL min⁻¹ from Table 9.8.

9.3.2 Effect of Polymer Concentration and Molecular Weight

By using a constant flowrate of 1 mL min⁻¹ in each test, the hydrodynamics of the flowcell should remain fixed, and the effect of varying the bulk polymer concentration on the relative rates of adsorption can be determined. While there is the potential for the hydrodynamics to be influenced by the viscosity of the polymer solutions, the concentrations studied are sufficiently low that the solution viscosities are very close to that of water under all conditions.

Figures 9.18 to 9.23 present the adsorption profiles for the adsorption of PAA450K at pH 2 and PAA450K at pH 13 (1 M NaCl) at 5 ppm and 50 ppm, and PAA13M at pH 2 and pH 13 (1 M NaCl) at 50 ppm. In examining the initial relative rate of adsorption, the data was treated in the same manner as in Figures 9.13 to 9.16.

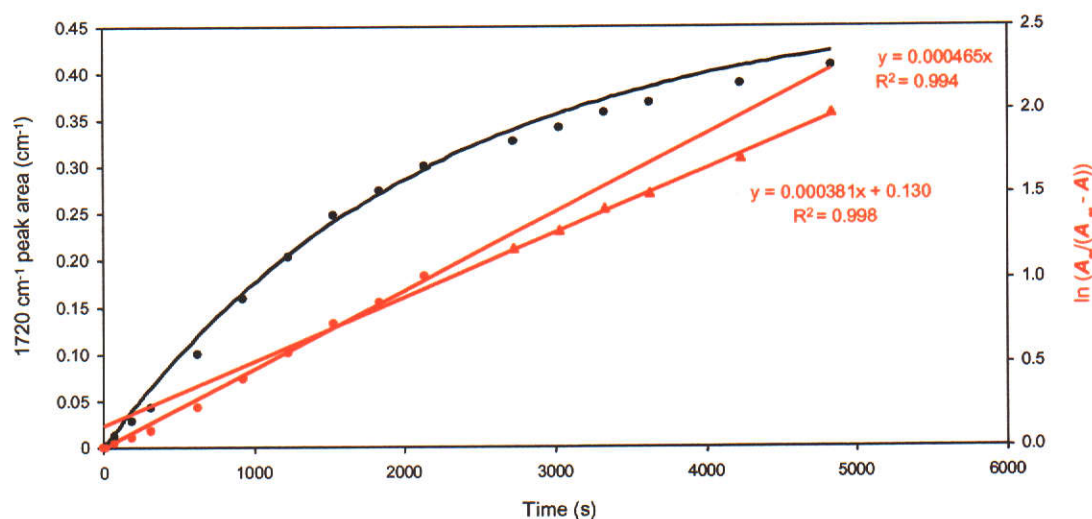


Figure 9.18: Adsorption of 5 ppm PAA450K at pH 2 (monitored by 1720 cm^{-1} peak area), together with the predicted response, as determined using Equation 9.8, for the initial relative rate of reaction. Also shown is the relative rate as determined from the slope of the plot of $\ln(A_{\infty}/(A_{\infty} - A))$ as a function of time. Both the fast relative rate of adsorption at initial times and the slower relative rate of adsorption at longer times are given.

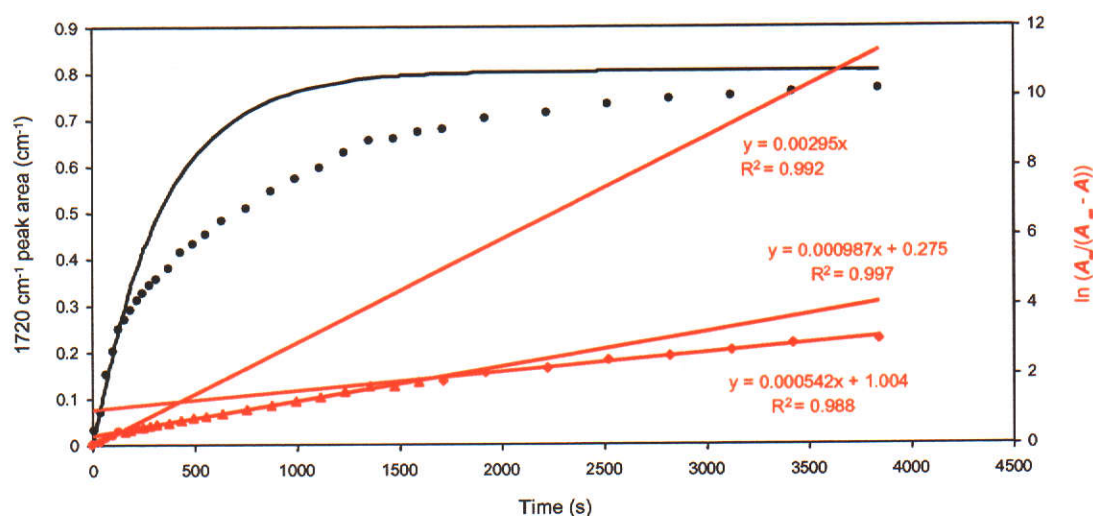


Figure 9.19: Adsorption of 50 ppm PAA450K at pH 2 (monitored by 1720 cm^{-1} peak area), together with the predicted response, as determined using Equation 9.8, for the initial relative rate of reaction. Also shown is the relative rate as determined from the slope of the plot of $\ln(A_{\infty}/(A_{\infty} - A))$ as a function of time. Both the fast relative rate of adsorption at initial times and the slower relative rates of adsorption at longer times are given.

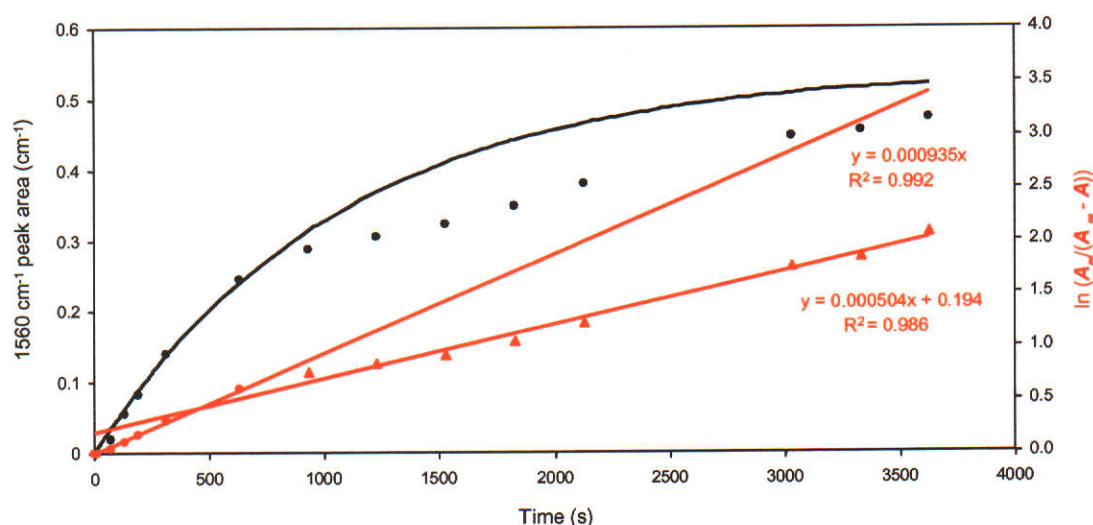


Figure 9.20: Adsorption of 5 ppm PAA450K at pH 13 (1 M NaCl) (monitored by 1560 cm^{-1} peak area), together with the predicted response, as determined using Equation 9.8, for the initial relative rate of reaction. Also shown is the relative rate as determined from the slope of the plot of $\ln(A_{\infty}/(A_{\infty} - A))$ as a function of time. Both the fast relative rate of adsorption at initial times and the slower relative rate of adsorption at longer times are given.

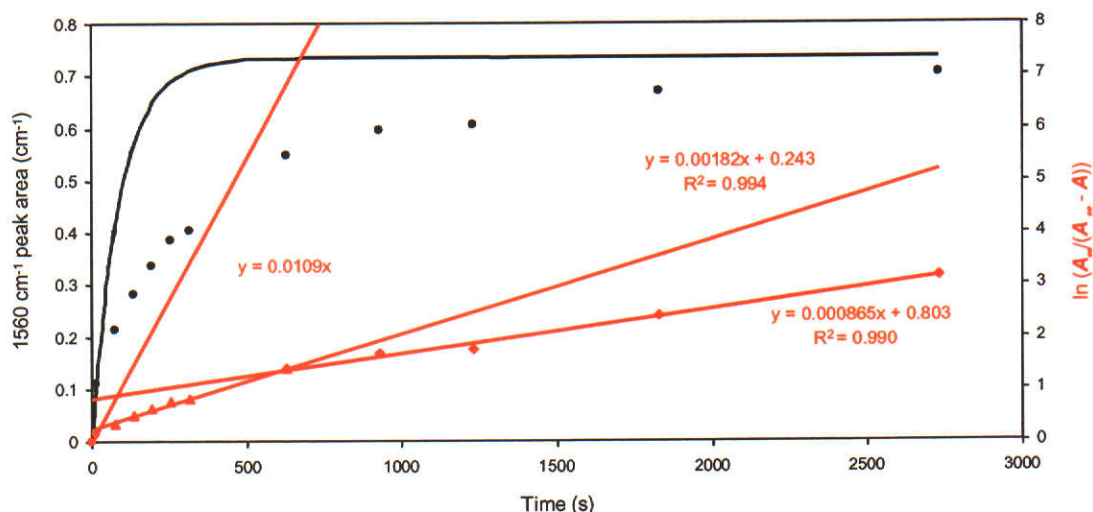


Figure 9.21: Adsorption of 50 ppm PAA450K at pH 13 (1 M NaCl) (monitored by 1560 cm^{-1} peak area), together with the predicted response, as determined using Equation 9.8, for the initial relative rate of reaction. Also shown is the relative rate as determined from the slope of the plot of $\ln(A_{\infty}/(A_{\infty} - A))$ as a function of time. Both the fast relative rate of adsorption at initial times and the slower relative rates of adsorption at longer times are given.

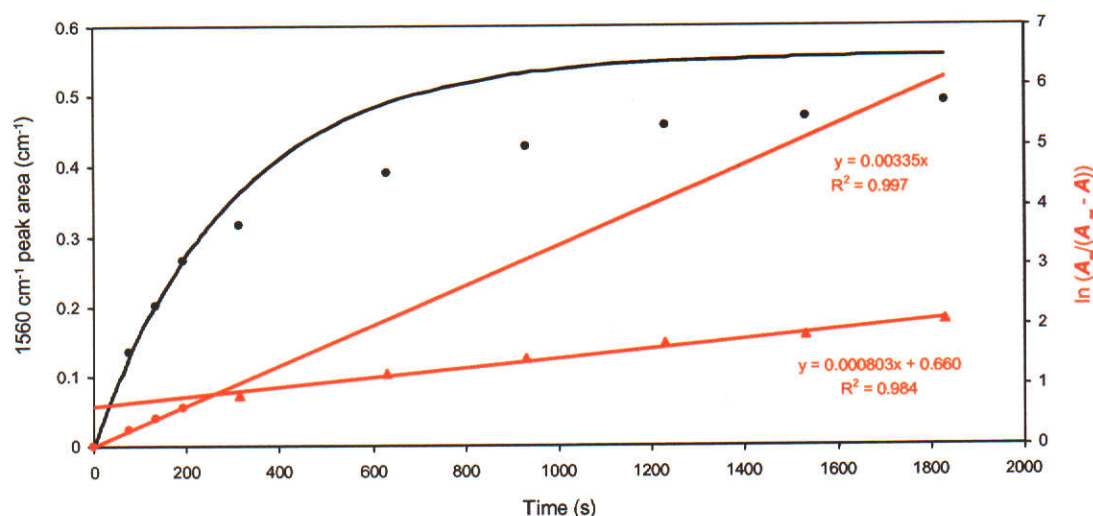


Figure 9.22: Adsorption of 50 ppm PAA13M at pH 13 (1 M NaCl) (monitored by 1560 cm^{-1} peak area), together with the predicted response, as determined using Equation 9.8, for the initial relative rate of reaction. Also shown is the relative rate as determined from the slope of the plot of $\ln(A_{\infty}/(A_{\infty} - A))$ as a function of time. Both the fast relative rate of adsorption at initial times and the slower relative rate of adsorption at longer times are given.

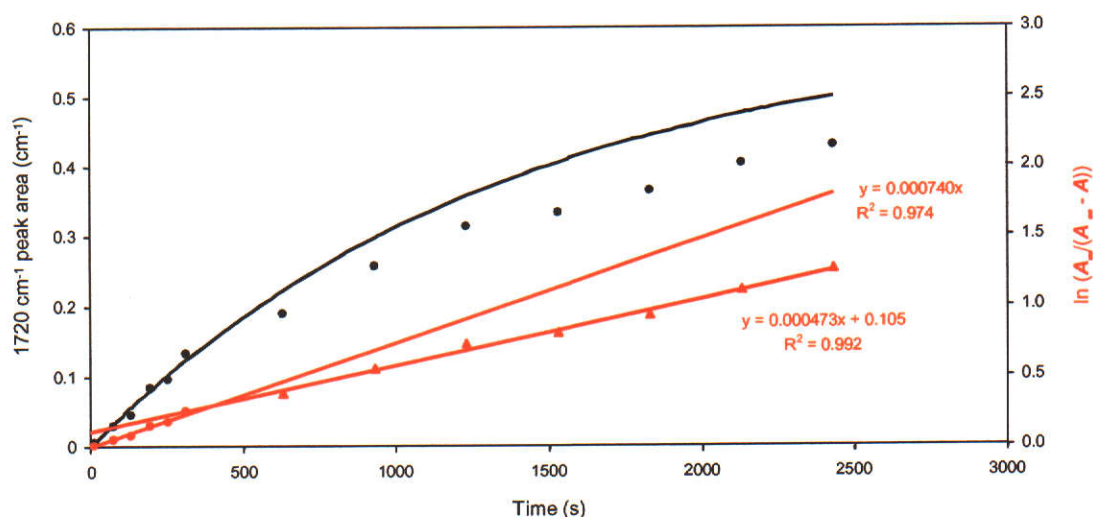


Figure 9.23: Adsorption of 50 ppm PAA13M at pH 2 (monitored by 1720 cm^{-1} peak area), together with the predicted response, as determined using Equation 9.8, for the initial relative rate of reaction. Also shown is the relative rate as determined from the slope of the plot of $\ln(A_{\infty}/(A_{\infty} - A))$ as a function of time. Both the fast relative rate of adsorption at initial times and the slower relative rate of adsorption at longer times are given.

The results in Figures 9.18 to 9.23 again show that there is an initial high relative rate of adsorption, followed by a slower rate. In some instances (Figure 9.19 and Figure 9.21), a third even slower rate is evident, suggesting that even greater rearrangement of adsorbed polymer occurs as the packing of polymer to the surface increases. The initial relative adsorption rates constants (k') are given in Table 9.9,

and are expressed as concentrations per unit of time, as k' incorporates the polymer concentration (Equation 9.7).

Table 9.9: Relative rates of adsorption (k') for polymer adsorption at varying concentration.

Polymer	k' (mg L ⁻¹ s ⁻¹) at 5 ppm	k' (mg L ⁻¹ s ⁻¹) at 50 ppm
PAA450K at pH 2	$0.465 (\pm 0.008) \times 10^{-3}$	$2.95 (\pm 0.07) \times 10^{-3}$
PAA450K at pH 13 (1 M NaCl)	$0.94 (\pm 0.03) \times 10^{-3}$	$\sim 11.0 \times 10^{-3}$
PAA13M at pH 2		$0.740 (\pm 0.028) \times 10^{-3}$
PAA13M at pH 13 (1 M NaCl)		$3.35 (\pm 0.06) \times 10^{-3}$

Table 9.9 shows that the relative rate decreases with increasing molecular weight and is significantly faster at high pH. The results also highlight that there is an increase in the initial rate of adsorption with increasing polymer solution concentration. This is once again consistent with the adsorption process being mass transport limited, and indeed the increase in rate was found to be approximately proportional to the increase in concentration. Variations from proportionality can in part be attributed to the rate of adsorption at 50 ppm for the lower molecular weight polymer being so rapid that there is a scarcity of data points for the determination, as is particularly evident for adsorption of PAA450K at pH 13 (1 M NaCl). The results obtained for adsorption at of PAA450K at 5 ppm are therefore more reliable than those obtained at 50 ppm.

Using the 5 ppm data at PAA450K and the 50 ppm data at PAA13M, the average mass transport limited rate constants were obtained by standardising the relative rates of adsorption to the bulk polymer concentration (i.e. $k_m = k'/c$) and are given in Table 9.10. Assuming the method demonstrated in Section 9.2.2 to determine adsorption densities from peak area is reliable, then the peak area at A_∞ can be related to an adsorption density (Γ_∞). The diffusional flux can then be obtained from the product of the adsorption density at A_∞ and the mass transport rate constant (i.e. $\Gamma_\infty \times k_m$). For a flowrate of 1 mL min⁻¹, the diffusional flux for 50 ppm bulk

polymer solution concentrations are also given in Table 9.10. Due to solubility restrictions, the absorptivity coefficient and hence adsorption density measurements for PAA13M adsorption at pH 2 could not be determined (Section 9.2.2).

Table 9.10: Rate constants for the adsorption of polyacrylate onto hematite at a flow rate of 1 mL min^{-1} and diffusional fluxes that correspond to 50 ppm bulk polymer solution concentration.

Adsorbing Polymer	$k_m (\text{s}^{-1})$	$A_\infty (\text{cm}^{-1})$	$\Gamma_\infty (\text{mg m}^{-2})$	Diffusional flux ($\text{mg m}^{-2} \text{s}^{-1}$)
PAA450K at pH 2	0.930×10^{-4}	0.805	6.55	0.609×10^{-3}
PAA450K at pH 13 (1 M NaCl)	1.88×10^{-4}	0.734	1.54	0.290×10^{-3}
PAA13M at pH 2	0.148×10^{-4}			
PAA13M at pH 13 (1 M NaCl)	0.670×10^{-4}	0.558	2.27	0.152×10^{-3}

These results are consistent with the K values from the adsorption isotherms (Table 9.4, Section 9.2.1), which were considered to be proportional to the forward rate constant (k_m in Table 9.10). Like k_m , the value of K for PAA450K at pH 2 ($K = 0.236$) has a value slightly greater than PAA13M at pH 13 and 1 M NaCl ($K = 0.219$), and a value approximately half that of PAA450K at pH 13 and 1 M NaCl ($K = 0.481$).

Table 9.10 shows that even though the relative rate of adsorption is much slower at pH 2, the amount of polymer adsorbing per unit time (diffusional flux) is considerably greater. This is due to there being many more surface sites available for polymer functional group adsorption and possibly due to the adsorbed polymer conformation exhibiting a greater ratio of unadsorbed (loops and tails) to adsorbed (train) polymer segments. Hence for equivalent initial adsorption times, there will be a greater mass of polymer adsorbed on the surface at pH 2 compared to pH 13

(1 M NaCl). These effects are reflected by the adsorption at pH 2 exhibiting the highest maximum adsorption density (Section 9.2.2).

The much slower relative rate of adsorption at pH 2 compared to pH 13 (1 M NaCl) could indicate a significant activation energy required for adsorption. At pH 2 the attachment of the polymer to the surface is through chemisorption, relying on the breaking of bonds associated with removal of surface hydroxyl groups from the hematite, and the subsequent bidentate chelation coordination of the carboxylate to the hematite. This would be expected to have a higher activation energy than that exhibited by adsorption at pH 13, which is an electrostatic interaction, and hence lead to a slower adsorption rate.

The strong chemisorption of polymer functional groups to the hematite surface at pH 2 may also contribute to the adsorbed polymer molecule being more difficult to reorientate than at pH 13. It may also account for the relative constant ratio of unadsorbed:adsorbed polymer segments regardless of polymer molecular weight for adsorption at pH 2 (Section 7.3). In contrast, the electrostatic adsorption at pH 13 should allow the conformation to be more mobile, enabling the polymer to take a more flat adsorbed conformation relative to that at pH 2.

Table 9.10 also shows that at both pH 2 and pH 13, the higher molecular weight PAA13M exhibits a slower rate of adsorption than PAA450K. This is similar to the findings of Bajpai and Bajpai (1995a) who observed that the rate of adsorption of polyacrylamide onto hematite in an aqueous medium decreased with increasing molecular weight of the polymer. They attributed this behaviour to the larger molecular weight polymers needing a greater length of time to attach to the surface primarily due to the slower rate of diffusion within the solution. The decrease in polymer diffusion coefficient with increasing molecular weight has been demonstrated and utilised by Hecker *et al.* (1999) for the fractionation of high molecular weight polyacrylamides.

While the relative rates of adsorption decrease with increasing polymer molecular weight, the results in this study indicate that the relative rate of adsorption at pH 13 (1 M NaCl) is much less dependent on polymer molecular weight than at pH 2 (Table 9.10). While the reason for this effect is unclear, it may be attributable to

the difference between the polymer-solvent system at high pH (charged polymer/high ionic strength) and low pH (uncharged polymer/low ionic strength). The diffusion coefficient of a polymer is strongly dependent upon the molecular weight and is related by the following expression (Polymer Handbook, 1999, pp VII/88):

$$D = AM_w^b$$

where A and b are empirically determined constants for a given polymer-solvent-temperature system.

The magnitude of b defines the extent at which the diffusion constant will change as a function of molecular weight.

The higher initial rate of adsorption shown by PAA450K over PAA13M at pH 13 (1 M NaCl) is mirrored by the diffusional flux results (Table 9.10), showing that at equivalent initial adsorption times, there would be a greater mass of PAA450K polymer adsorbed on the surface compared to PAA13M. This is not necessarily reflected by the maximum adsorption densities obtained with these polymers, which is higher for PAA13M (Section 9.2.2). At pH 13 (1 M NaCl), the number of sites taken at maximum adsorption by polymer functional group adsorption could be considered constant and independent of polymer molecular weight. Therefore the greater extent of adsorption for the higher molecular weight polyacrylate may be attributed to the adsorbed conformation, with a greater ratio of unadsorbed to adsorbed polymer segments. However, the number of PAA13M molecules adsorbed per unit surface area will be less than for PAA450K, due to their much higher molecular weight.

9.3.3 Factors Affecting Subsequent Flocculation

For any flocculation system, the residence time of slurry particles and flocculant under applied shear is critical because this determines the extent of polymer coverage on the particles, which in turn influences aggregation kinetics. Flocculation performance typically increases with coverage up to a point that represents 50% of the available surface (La Mer and Healy, 1963). Increasing the surface coverage beyond 50% reduces the probability of successful polymer bridging between

particles, resulting in a decrease in flocculation performance. At even higher coverages the particles tend to be stabilised by the adsorbed polymer (i.e. remain dispersed).

For the prediction of aggregation behaviour, a more relevant measurement is the time taken to obtain 50% maximum surface coverage ($t_{0.5A_{\max}}$). The value of A_{\max} can be obtained from the adsorption isotherms (Section 9.2.1). An estimate of the time taken to reach $t_{0.5A_{\max}}$ can then be obtained as follows and is shown for the adsorption of 5 ppm PAA450K at pH 13 (1 M NaCl) in Figure 9.24. A first order kinetic fit is applied by iterative fitting of Equation 9.8 to the total adsorption isotherm, where A_{∞} and k' values are obtained by minimising the difference between the experimental and the calculated A values (Figure 9.24).

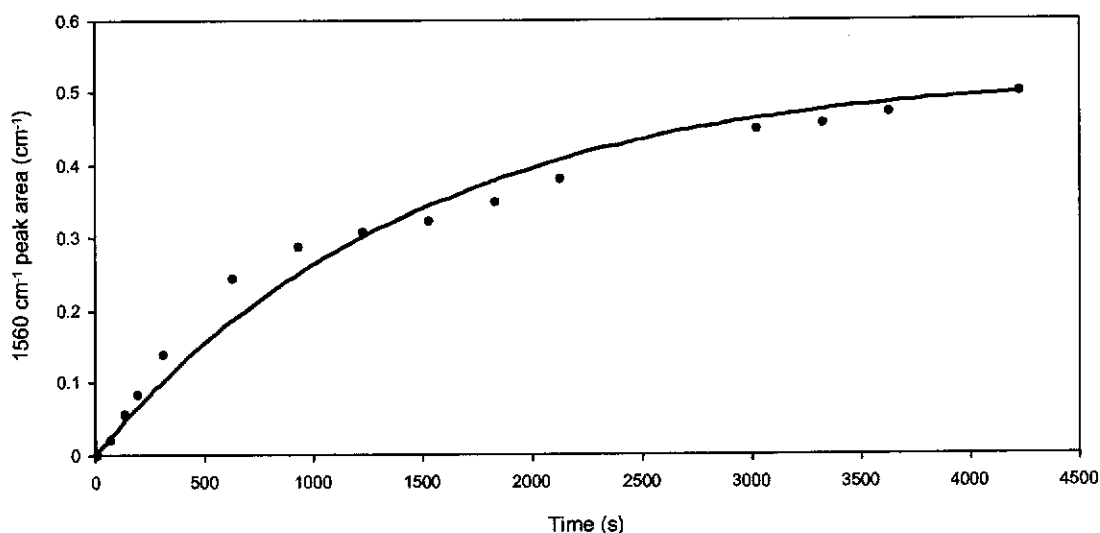


Figure 9.24: Adsorption of 5 ppm PAA450K at pH 13 (1 M NaCl) (monitored by the 1560 cm⁻¹ peak) onto hematite, with the first order fit as determined using Equation 9.8.

While this treatment does not lend itself to examining the initial rate of adsorption, as investigated earlier in this section, it does give an estimate of the rate of adsorption across the entire adsorption profile and enables the time required to reach $0.5A_{\max}$ to be calculated (Table 9.11). Clearly the mixing condition obtained for a flowrate of 1 mL min⁻¹ through the ATR flowcell cannot be related to those experienced by flocculant and feed within a feedpipe or thickener feedwell. However, the information derived from these spectral measurements does provide some insights into flocculation behaviour in practical systems.

Table 9.11: The time taken to achieve 50% maximum surface coverage ($t_{0.5A_{\max}}$) for the adsorption profiles shown in Figures 9.18 to 9.22, determined by a first order fit of the data.

Adsorbing Polymer (conc.)	k' (mg L ⁻¹ s ⁻¹)	A_{\max} (cm ⁻¹)	$t_{0.5A_{\max}}$ (s)
PAA450K at pH 2 (5 ppm)	0.412×10^{-3}	0.873	5428
PAA450K at pH 2 (50 ppm)	1.84×10^{-3}	0.873	475
PAA450K at pH 13 (1 M NaCl) (5 ppm)	0.696×10^{-3}	0.765	1856
PAA450K at pH 13 (1 M NaCl) (50 ppm)	3.69×10^{-3}	0.765	244
PAA13M at pH 13 (1 M NaCl) (50 ppm)	4.00×10^{-3}	0.609	271

The results in Table 9.11 show that $t_{0.5A_{\max}}$ is far greater at the lower polymer concentration, demonstrating that for flocculant adsorption that is mass transport limited, control of the flocculant dosage (concentration) is of great importance. For most flocculation applications, it is accepted that a reduction of the flocculant concentration added to the slurry leads to more efficient flocculation (e.g. Connelly, Owen and Richardson, 1986). This is generally attributed to more efficient distribution of the polymer throughout the slurry particles, with the implication that adding flocculant at a high concentration results in a significant proportion adsorbing onto only a small fraction of the particles. While the better dispersion at lower concentrations in part reflects the greater volume of the added flocculant solution, it is also probable that a reduced rate of adsorption is a contributing factor.

The results also suggest that variations in the flocculant molecular weight will have a relatively insignificant effect on the time taken to achieve 50% surface coverage in comparison to the impact of changes in dosage or mixing regime. The parameter $t_{0.5A_{\max}}$ may potentially be of value in modelling the dynamic process of flocculant distribution throughout a particle system and subsequent adsorption (i.e. determining if the flocculant chains are well-distributed across all particles or preferentially adsorbed onto the first particles they contact). However, it cannot be directly related

to the extent of flocculation achieved with a given product, which is much more a reflection of the polymer's bridging capacity (i.e. molecular weight and chain extension) and the mixing regime.

10. SUMMARY AND CONCLUSIONS

This study has sought to advance the fundamental understanding of flocculant adsorption onto the residue solids formed as a consequence of Bayer processing of bauxite. Because of the mixture of phases typically present in bauxite residue, it was necessary to focus on an appropriate model substrate. Hematite was chosen, as it is the dominant mineral found in Bayer residue, particularly those originating from Australian bauxitic ores. Polyacrylate was chosen as the adsorbate, as this has historically been the dominant Bayer flocculant, and even with the advent of hydroxamated products, the carboxylate functionality is still a common feature in all flocculants used for bauxite residue treatment.

Polymer adsorption onto mineral particles is typically characterised by 'trains' of adsorbed polymer, with 'loops' and 'tails' of unadsorbed polymer that extend into the solution. *Ex situ* studies carried out in the past have been complicated by the way in which the unadsorbed parts of the polymer interacts with the surface of the substrate on drying. In this study, a major goal was to establish an *in situ* technique to specifically examine the interaction of the polymer with a mineral surface.

10.1 FTIR-ATR

The *in situ* investigation of the solid-liquid interface was achieved by using FTIR-ATR, whereby a polymer solution, at a concentration so low that absorbance due to the polymer solution species was not detectable, was adsorbed onto a thin film of hematite that had been cast onto the ZnSe ATR element. As a consequence of adsorption, the polymer was concentrated onto the substrate surface, thereby enabling the acquisition of spectra for adsorbed polymer unbiased by the contribution of the bulk polymer solution.

For the FTIR-ATR technique to work effectively, it is critical that the deposited phase has a very small particle size, with a diameter in the order of 0.10 μm . Coarser particles are unlikely to deposit in a mechanically stable layer that does not change when exposed to a flowing solution, and would be much more difficult to deposit in an even manner across the measurement area. The deposited phase should be non-absorbing in the spectral region of interest and be virtually insoluble in the applied adsorbate solution.

In this study, hematite of small particle size and hence large surface area was achieved by preparation as a colloid. The colloid was found to be pure and have a d_{50} of approximately 100 nm. Characterisation of the deposited films indicated that they were reproducible and gave a continuous coverage, but were quite porous to water, small molecules and ions.

The solution dimensions of the high molecular weight polyacrylates used in this study (as determined by MALLS) were larger than the discrete hematite particles that made up the cast film, and hence only adsorbed onto the outer surface of the hematite film, rather than diffused and adsorbed in the pores of the film.

10.2 Characterisation of the ATR Solid-Liquid Interface

The technique of ATR relies on the total internal reflection of radiation at the interface of two media of differing refractive index. At this interface, the radiation penetrates to a small extent into the optically rarer medium, through what is known as the evanescent wave. To relate the absorbance of adsorbed polymer to an adsorption density, the solid-liquid interface examined using ATR needed to be thoroughly characterised so that depth of penetration and effective thickness determinations could be made. Consequently, a method to measure the refractive indices of the various media placed in contact with the ZnSe crystal was established.

The cast hematite film was found to have a void fraction of approximately one third and behaved as an extension of the ZnSe crystal, similar to a reactive IRE, due to the porous film exhibiting a similar refractive index to ZnSe. The refractive index of the hematite coated ZnSe is dependent on the refractive index of the solution that contacts it, as this solution fills the pores of the film and reduces the refractive index from that of hematite (2.91) to a value nearer that of ZnSe (2.430). Hence, the hematite coated ZnSe could be treated as one interface, exhibiting a specific refractive index.

10.3 Adsorption Mode at pH 2

The spectra of polyacrylic acid adsorbed on hematite showed additional peaks at 1410 cm^{-1} and 1560 cm^{-1} that were not present in the unadsorbed solution spectrum. An interpretation of their peak positions, on the basis of the Deacon and Phillips rules, led to the conclusion that at low pH, polyacrylic acid was adsorbed onto hematite via bidentate chelate complexation directly to a surface ferric ion. The unshifted carbonyl peak (1720 cm^{-1}) apparent in the adsorbed spectrum was indicative of the unadsorbed 'loops' and 'tails' of the adsorbed polymer molecule. A schematic representation of polyacrylic acid adsorption at low pH is given in Figure 10.1.

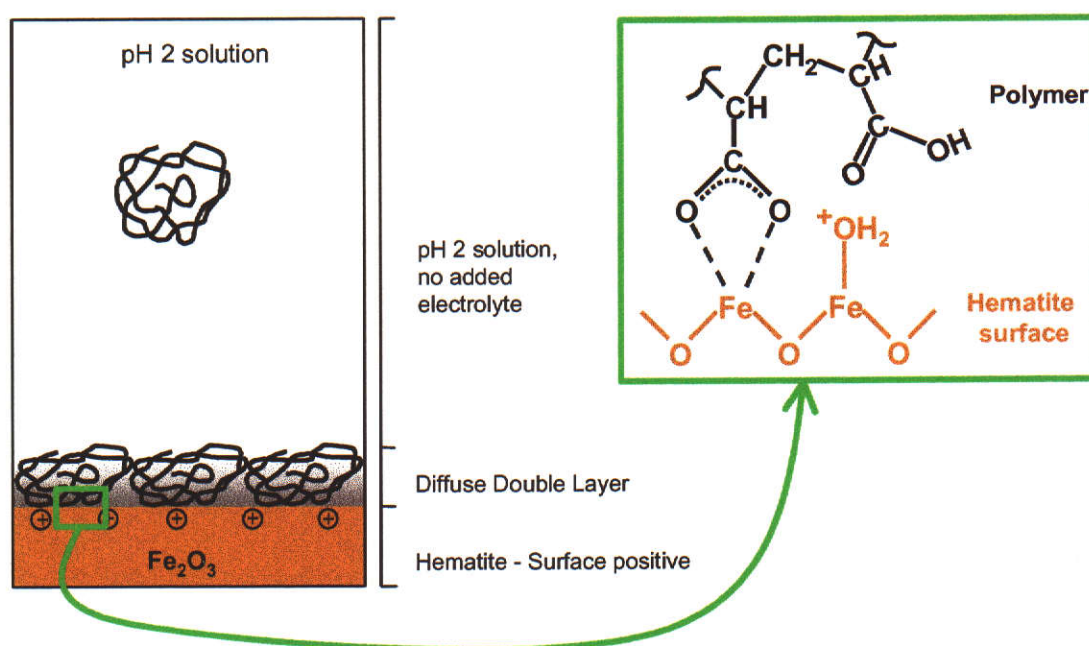


Figure 10.1: Schematic representation of the proposed adsorption mode of polyacrylic acid onto hematite at pH 2.

Other *in situ* FTIR-ATR studies have shown the same coordination by carboxylates onto TiO_2 and Al_2O_3 (Dobson and McQuillan, 1999), while the coordination onto kaolinite was different (Specht and Frimmel, 2001). This suggests that carboxylates complex onto mineral surfaces readily at low pH, with the mode of attachment dependent on the substrate. The similar mode of adsorption for hematite, TiO_2 and Al_2O_3 was probably due to their similar surface charge and heat of hydration properties, which differ significantly from those of kaolinite.

The technique was not only used to determine the adsorption mode of polyacrylic acid *in situ*, but also to discriminate between adsorbed and unadsorbed segments of polymer. Comparing the amount of unadsorbed (1720 cm^{-1}) and adsorbed (1410 cm^{-1}) polymer, taking into account the molar adsorption coefficient of each peak, established a ratio of approximately 2.5:1, indicating that approximately 28% of the polymer was adsorbed. This ratio may actually be higher in reality, because absorbances measured with the ATR technique are biased toward the adsorbed segments close to the hematite film relative to the unadsorbed loops and tails of the polymer that are extended into the solution away from the hematite surface.

The adsorbed spectrum of polyacrylate at pH 2 also exhibited a sizable broad negative peak in the hydroxyl stretching frequency region ($\sim 3300\text{ cm}^{-1}$), indicating a reduction of water or OH^- concentration at the hematite surface. No such negative peak was exhibited by adsorbed pimelic acid (M_w 160), which adsorbed in the same manner as polyacrylic acid, but due to its small size had minimal contribution from tails and loops near the surface. This strongly indicates that the negative peak was due to displaced solvent from the surface, rather than displaced surface hydroxyl groups. In addition, there was little or no signal due to a carbonyl stretch (1710 cm^{-1}) for pimelic acid, suggesting that it was bound to the hematite surface through both carboxylate groups. This finding also supports the assertion that in the polymer adsorbed spectra the presence of the carbonyl stretching frequency (1720 cm^{-1}) is attributable to the unadsorbed loops and tails of the adsorbed polymer.

10.4 Adsorption Mode at pH 13

Adsorption behaviour at high pH provided a distinct contrast to that at low pH. It was found that at pH 13 polyacrylate did not adsorb unless there was an excess of sodium ions present, indicating that the solution cation played a crucial role in the adsorption of the carboxylate functionality onto hematite.

The adsorbed spectra at pH 13 with added electrolyte (NaCl) were found to be indistinguishable from the unadsorbed solution spectrum under the same conditions, and hence it was not possible to discriminate between the adsorbed and unadsorbed segments of the polymer. According to the Deacon and Phillips rules, the spectral band positions suggested a bidentate bridging structure for adsorption, but this does

not take into account the role of the sodium ions. As the attachment of the negatively charged polyacrylate to the negatively charged hematite surface is facilitated by the presence of sodium ions, the adsorption process is likened to the coagulation of two negatively charged particles by the addition of electrolyte.

The proposed electrostatic interaction would not contribute to any great adsorption strength, and this was reinforced by the finding that pimelic acid did not adsorb at pH 13 regardless of the amount of electrolyte added. Thus, the driving force for adsorption of higher molecular weight polyacrylates was the large number of binding contacts per polymer molecule.

Polyacrylate adsorption onto hematite at pH 13 increased with increasing electrolyte concentration (NaCl) up to a concentration of approximately 1 M, which was attributed to changes in both the polymer dimensions and the hematite surface.

Radius of gyration measurements of polyacrylate solutions (MALLS) demonstrated that increasing the electrolyte concentration (up to 1 M NaCl) had the effect of reducing the size of the polymer in solution. While this effect alone would have increased adsorption due to increased packing ability, shielding of the negative moieties of the polymer by added sodium ions would also give the polymer a greater affinity to the negative hematite surface.

The magnitude of the negative surface charge of hematite at pH 13 decreased with increasing electrolyte concentration. At approximately 0.45 M NaCl, the zeta potential was zero and above 0.45 M NaCl there was evidence that the effective surface charge became positive.

Although interpretation of the double layer structure is difficult at such high ionic strength, there is evidence to support the conclusion that at high pH, sodium ions have a high affinity for the hematite surface and are specifically adsorbed, to the point that at very high salt concentrations this adsorption actually contributes to the surface becoming positively charged. This indicates that the shear plane is positioned beyond these specifically adsorbed ions, resulting in a positive measured zeta potential at high ionic strength. The physical behaviour of the colloidal dispersions is thus governed by the high ionic strength environment, whereby the high concentration of cations and anions contribute to a complex diffuse double layer

that facilitates particle aggregation. This complex diffuse double layer is also a major factor in polyacrylate adsorbing on hematite. A schematic representation of the proposed interaction of polyacrylate with hematite at pH 13 and at pH 13 with added electrolyte (NaCl) is given in Figure 10.2.

At high pH and high electrolyte concentration there was no significant difference in the adsorption as a function of monovalent cation. However, at low concentrations the identity of the solution cation had a definite effect, in the order lithium > sodium > cesium.

MALLS measurements demonstrated that the dimensions of polyacrylate in solution did not change with monovalent cation type and that the cation-polyacrylate interaction was purely electrostatic, i.e. not dependent on charge density or cation hydration. The increase can thus not be attributed to a change in polymer size.

Zeta potential measurements for the hematite colloid at high pH established that lithium ions reduced the negative surface charge of hematite to a greater extent compared to sodium ions. This indicates that lithium has a similar but stronger specific interaction with hematite than that exhibited by sodium, and that this leads to greater polymer adsorption.

This conclusion is consistent with the model of the ionic double layer presented by Berube and de Bruyn to describe the same ion adsorption sequence on rutile (the inverse lyotropic adsorption sequence, more commonly known as the 'structure making - structure breaking' model). When a surface exhibits a strong affinity for water, whereby the water molecules are very ordered and structured on the surface, then strong specific adsorption will be favoured by ions that will not disrupt the structural order of the water in the surface region. Hence adsorption will follow the trend of the heat of hydration of the ions, where heavily hydrated cations such as lithium and sodium will preferentially adsorb over larger, less hydrated cations such as potassium and cesium. The model was extended by Dumont, Dang Van Tan and Watillon (1976), who showed that the structuring properties of an oxide surface can be inferred from its heat of immersion and pzc, with high values related to a structure-making surface.

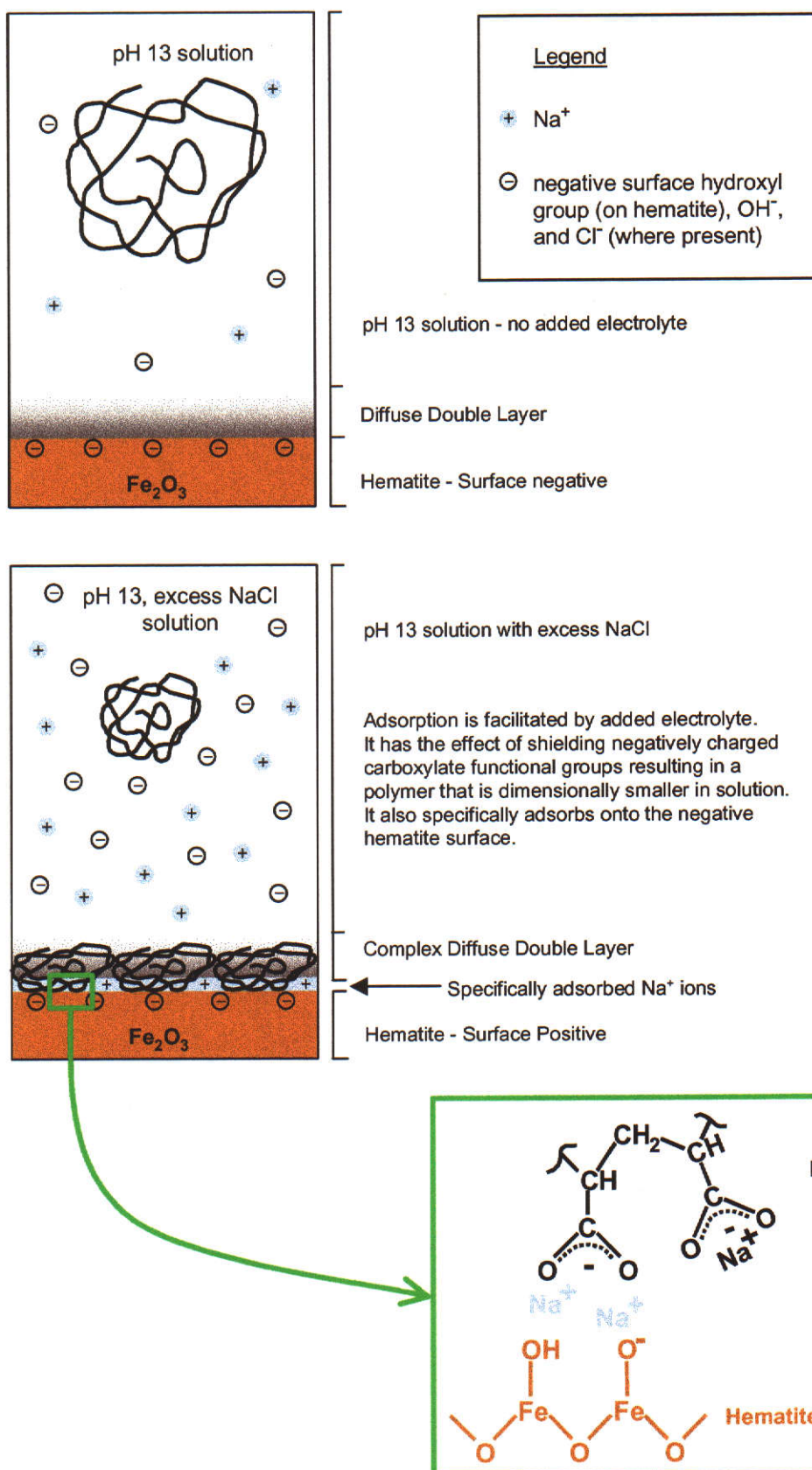


Figure 10.2: Schematic representation of the proposed adsorption mode of polyacrylate onto hematite at pH 13 with and without added electrolyte.

10.5 Adsorption Isotherms and Adsorption Kinetics

The Langmuir isotherm was found to offer the best fit to the adsorption profiles in this study, where the ratio of the plateau integrated absorbance at each concentration (A_c) to that of the maximum integrated peak absorbance (A_{max}) was used in determining the fractional coverage (θ).

The maximum integrated peak absorbances (A_{max}) were translated into a mass of polymer adsorbed by establishing the absorptivity coefficient of the peak areas and the effective thickness at the solid-liquid interface. The mass adsorbed was converted to the maximum adsorption density by calculating the available surface area of the hematite exposed to the IR beam.

The weakness in this approach is that the peak area used to monitor adsorption must be related to an equivalent peak in a polymer solution. It was shown that the conformation of the polymer in the adsorbed state is much more condensed than the voluminous coil structure it assumes in solution. Hence the absorptivity coefficients of the peak area being monitored may no longer be comparable, and the measured adsorption densities are likely to be higher than their true value. The ability of the technique to measure adsorption densities is also limited by the accuracy of the adsorbed polymer layer thickness determination. However, as these limitations are consistent for all the adsorbed polymers studied, the calculated adsorption densities can be used for making valid comparisons.

The maximum adsorption densities of PAA450K at pH 2 and pH 13 (1 M NaCl) and PAA13M at pH 13 (1 M NaCl) were 7.10, 1.61 and 2.48 mg m⁻², respectively. This corresponded to a large excess over that expected for monolayer coverage of polymer adsorbed flat on the solid surface in all cases. Such a result is not uncommon for polymer adsorption that is typically characterised by 'trains' of adsorbed polymer with 'loops' and 'tails' of unadsorbed polymer that extend into the solution.

The maximum adsorption density on hematite was greater at low pH than at high pH. This almost certainly reflects the different modes of adsorption, and indicates there are many more favourable adsorption sites for carboxylate coordination at pH 2 compared to the electrostatic carboxylate association occurring at pH 13 (1 M NaCl).

It also implies that the adsorbed conformation at low pH exhibits a higher degree of unadsorbed polymer segments (loops and tails).

At high pH, the maximum adsorption density increased with increasing polymer molecular weight. This indicates that the conformation of the adsorbed polymer changed as a function of molecular weight, and that polyacrylate had a flatter and more extended adsorption conformation at lower molecular weights.

In contrast, at pH 2 the maximum adsorption density did not change as a function of molecular weight, and the ratio of unadsorbed:adsorbed polymer segments remained constant. This indicates that the adsorbed conformation does not change as a function of molecular weight, which may reflect the strength of the specific chelation relative to the less specific electrostatic adsorption at pH 13.

The Langmuir isotherm offered the best fit to the adsorption data with the curvature of the isotherm, represented by the equilibrium constant (K), being a measure of polymer affinity for the substrate surface. For all the isotherms in this study, K was less than 1, indicating low affinity. The results suggest that there is relatively small individual bond strength, and it was only the number of these per bound polymer molecule that leads to irreversible adsorption. Due to polymer adsorption being irreversible, and the rate of desorption being assumed to be some low constant value, it is proposed that K is directly related to the rate of polymer adsorption. Indeed the K values displayed similar trends to the initial rate constants measured from profiles of adsorption against time.

There are a number of factors that can contribute to the observed rate of adsorption. They include mass transport towards the surface (as determined by diffusion and possibly convection), the rate of attachment to the surface (which depends on the activation energy for the attachment), and reconfiguration of the polymer chains from a coiled solution conformation to an adsorbed structure with trains, loops and tails.

For the polymers examined, adsorption was dominated by mass transport, suggesting there was no appreciable barrier or activation energy to the adsorption process. When there was no longer an excess of available adsorption sites, the rate of adsorption slowed as it was limited by the reconfiguration of adsorbed polymer.

The relative rate of adsorption was much slower at pH 2 than at pH 13 (1 M NaCl), but the diffusional flux (amount of polymer adsorbing per unit area per unit time) was greater. This was attributed to the many more surface sites available for polymer functional group adsorption at pH 2, and the adsorbed conformation exhibiting a greater proportion of unadsorbed polymer segments (loops and tails). Hence for equivalent initial adsorption times, there is a greater mass of polymer adsorbed on the surface at pH 2.

If there is an activation energy contribution of significance to the observed kinetics, it would most likely be a factor at pH 2, and may explain the slower initial relative rate of adsorption at pH 2 compared to pH 13 (1 M NaCl). At pH 2 the adsorption is chemisorption, relying on the breaking of bonds associated with removal of surface hydroxyl groups from the hematite surface, and the subsequent bidentate chelate coordination of the carboxylate to the hematite surface. Contrary to this, the adsorption at pH 13 it is an electrostatic interaction, which would be expected to have a much lower activation energy.

At both high and low pH, the decrease in rate of adsorption with increasing molecular weight is attributed to the larger molecular weight polymers needing a greater length of time to attach to the surface, primarily due to the slower rate of diffusion within the solution.

The relative rate of adsorption at pH 13 (1 M NaCl) was much less dependent on polymer molecular weight than at pH 2. This may be due to differences in the polymer-solvent interactions at high pH (charged polymer/high ionic strength) and low pH (uncharged polymer/low ionic strength), with the polymer likely to be more highly solvated at high pH.

An implication of these results for flocculation is that the aggregation kinetics may not only be governed by the initial rate of polymer adsorption but also by the number of available sites for adsorption. For example, results from this study show that if optimum flocculation was achieved at some low absolute surface coverage, then it is quite likely that this surface coverage would be achieved faster at pH 2 than at pH 13 (1 M NaCl), due to the diffusional flux being greater, despite the fact that the rate constant is lower at pH 2.

In a flocculating system, optimum aggregation rate is usually achieved when there is 50% coverage of the available adsorption sites (although in practice most systems operate at below 50% coverage). The time taken to achieve 50% coverage was far less at a higher polymer concentration, demonstrating the mass transport limited nature of the system and reinforcing the importance of flocculant dosage control.

10.6 Bayer Process Implications

Although the main intention of this study was to advance the fundamental understanding of the polyacrylate adsorption process at high pH, rather than focusing on any specific plant residues or operational conditions, clearly there was an expectation that some practical conclusions would be drawn. Bayer liquor is a highly caustic solution of high ionic strength, and even in the last stages of washing, the caustic concentration is such that the pH is typically in the order of 13.5. This is comparable to the maximum pH values of 14 and 13.5 of the systems studied here by ATR and zeta potential measurements, respectively. While higher caustic levels will clearly influence the extent of adsorption achieved, it is not anticipated that the adsorption mechanism would vary significantly from that proposed. The results obtained therefore should provide a useful insight into a number of factors that may influence bauxite residue flocculation.

10.6.1 Factors Affecting Flocculation

The primary implication from this study to the Bayer process is that it is the high ionic strength environment of Bayer liquors that facilitates the adsorption of polyacrylate flocculants onto residue materials, in particular those residues containing hematite as a major component. The concentration of sodium ions in solution is more than sufficient to favour adsorption. There is no need to postulate calcium bridging between the polymer and surface, as has been suggested previously in other studies. However, it is feasible that the presence of calcium, which would be expected to be in a solid phase under Bayer conditions and be combined with the residue, may influence the surface charge of the residue and contribute to coagulation of the residue material.

Hematite, and minerals with similar surface chemistry to hematite, may exhibit a positive charge due to the specific adsorption of sodium ions, however it would be

anticipated that the residue material in Bayer liquor would be slightly aggregated from the interaction of the complex double layers at the surface of the particles. These aggregation forces are typically very weak, and therefore in slurries under shear such forces may only influence the finest particles (i.e. submicron sized). Flocculant would only be exposed to the reduced “external” surface area of coagulated aggregates, and as a consequence the dosages required to achieve acceptable settling rates would be much lower than that expected for fully dispersed particles. High molecular weight polymers are known to be very inefficient flocculants for the treatment of very fine particles, due to the difficulty of achieving sufficient polymer chains per particle (Hogg, 1999), and without pre-coagulation the requisite flocculant dosages become prohibitively high. This behaviour is exhibited by Jamaican bauxite residue, for which the majority of primary particles are sub-micron sized, but the flocculant dosages within the residue thickeners are not appreciably larger than those for coarser materials.

The ionic strength within the process liquor, even under final washer conditions, will be sufficiently high that flocculant adsorption process will not be greatly influenced by variations in the residue mineralogy. However, the effective surface areas exposed to any applied flocculant will be determined by the extent of particle coagulation, and this represents by far the greater effect on the required dosage and ultimate aggregate properties.

It might be expected that the rate of flocculant adsorption would decrease with increasing molecular weight, and if optimum flocculation occurs at low surface coverage, this would be achieved faster with lower molecular weight polymers. However, any increase in molecular weight would benefit the bridging ability of the flocculant molecule, particularly since it was shown that the bridging component of the molecule (loops and tails) becomes more significant with increasing molecular weight. It would be anticipated that the amount of flocculant adsorbed would increase with molecular weight, although this would not be an important factor, as it was shown that plateau adsorption takes a long time to achieve (over an hour), whereas flocculation of residue material happens very rapidly (less than a minutes).

Comparison of the adsorption isotherms measured at pH 2 and 13 indicates that the maximum attainable surface coverage was significantly greater at the lower pH. This

implies that at the high pH there may be a lower number of sites available for binding, and this could have a potential consequence on the practical range of flocculant dosages. For any flocculation system, the performance achieved typically increases with dosage up to a critical point that represents 50% coverage of the available surface. Higher dosages then serve to reduce the free sites for polymer bridging, leading to a decrease in flocculation performance. In tailings thickening, such dosages are rarely attained prior to the onset of over-flocculation, and are therefore not often a practical consideration. However, a significantly lower critical dosage may be anticipated for bauxite residue flocculation, and in some instances this could affect performance. The most likely experimental observation of this would be a decrease in the slope of the dosage response curve at higher flocculant dosages.

It is likely that there is a similar interaction between polyacrylate and other minerals that have a similar surface chemistry to hematite. This would include other iron oxides that make up Bayer residue, but might not include the silica-based materials in the residue, such as silica, aluminosilicates, etc. Gibbsite with a pzc ranging from 9.8 to 11.2 (Davis and Hem, 1989) would exhibit similar surface charge properties to hematite and possibly interact with polyacrylate in a similar manner.

10.6.2 Aggregation Kinetics

Work within these laboratories is progressing on the use of a population balance model to describe the kinetics of aggregate formation and rupture in mineral tailings flocculation (Heath, 2002), and in particular the flocculation of bauxite residue. This involves the fitting of a series of mathematical equations to experimental data for aggregate size as a function of reaction time. The process currently produces four empirically fitted parameters, but it is hoped that these parameters will ultimately be related to physical and chemical properties of each tailings system.

Within the model, the initial aggregation rate is described only in relation to a mixing parameter, as it is assumed that polymer adsorption is very rapid. Removing or reducing the empirical nature of this parameter will require knowledge of the adsorption kinetics, however, this is almost impossible to achieve under Bayer conditions. The results of this study for adsorption of polyacrylate onto hematite

show that adsorption is mass transport limited and hence strongly dependent on mixing conditions. The adsorption profiles were also not independent of polymer molecular weight nor the solution conditions at which the polymer were adsorbed. This implies that adsorption may be significantly slower for mild mixing and at lower polymer dosages. Conditions may therefore exist under which the assumption within the aggregation kinetics model that adsorption is effectively instantaneous during mixing may not be valid.

Any sub-model that may be developed to better describe adsorption within the kinetics of aggregation will need to incorporate a measure of the plateau adsorption level (representing effective surface coverage) together with at least an indication of the affinity of the flocculant for the surface. The analysis of FTIR-ATR results as described here represents a viable approach to obtain such information under a range of conditions.

11. FUTURE WORK

11.1 Studies of Bayer Systems

This research has focussed on the interaction of hematite and polyacrylate. Hematite was chosen because it is a major component of many refinery residues. In some alumina refineries throughout the world (particularly those processing Jamaican bauxite), goethite is the dominant residue phase, hence a study to examine the polyacrylate-goethite interaction would also be warranted. Whilst the hematite colloid prepared for this study was found to be stable for long periods of time, the stability of a goethite colloid prepared for such a study may be an issue, and the typical needle-like goethite crystals could possibly hinder the reproducible casting of a film to the ATR element. A preliminary investigation of these factors before embarking on such a study would be prudent.

In general, Bayer residues are a complex mixture of many mineral phases. The techniques developed in this study could be extended to examine the interaction of polyacrylate with actual Bayer refinery residue materials, however the particle size of these solids may inhibit such a study. While it may be possible to achieve a suitably fine particle size through grinding or fractionation, extreme care would be required to ensure that the particle properties are not adversely affected by such processes (e.g. selective concentration of one phase). In addition, residues vary quite markedly between refineries, so such studies would likely be refinery specific. At some refineries polyacrylate flocculants are also used to enhance the settling of the gibbsite product from the precipitators. Further work could include examining the interaction of polyacrylate with gibbsite, which can be obtained commercially or prepared in colloidal form, although there may be limitations on the solution conditions that could be used, as gibbsite exhibits a much higher solubility than hematite, in highly caustic solutions.

The surface chemistry of Bayer solids is very complex, due to the high caustic and ionic strength of their environment. Zeta potential measurements of hematite carried out in this study utilised the phase analysis light scattering principle and enabled measurements to be done in high pH and high ionic strength solutions, giving an insight into the surface chemistry of hematite in Bayer liquor. This same technique

could be used to investigate the surface properties of other Bayer substrates under similar conditions.

Synthetic flocculants containing the hydroxamate functional group (typically as terpolymers with acrylamide and sodium acrylate) are now widely used for the flocculation of bauxite residue. Improved performance with hydroxamate flocculants is generally attributed to the ability of the functionality to strongly coordinate with iron, although direct evidence of this occurring with such polymers has not been presented to date. At the same time, natural polysaccharide (starch) flocculants are still used in some refineries for residue flocculation, and remain the preferred reagents for gibbsite flocculation (used either exclusively or in conjunction with polyacrylate flocculants). Therefore extending the research to examine the interaction such flocculants have with Bayer solids would also be advantageous.

In this research it has been demonstrated that MALLS can be used to investigate the solution dimensions of polyacrylate in solution, including conditions of high pH and ionic strength. MALLS could be used to investigate solution dimensions of other Bayer flocculants under equivalent conditions. Such information would also prove valuable in comparisons of the flocculation performance of each product.

Bayer liquor is also known to contain many characterised and uncharacterised organic and inorganic impurities. Depending on the infrared activity of selected solution impurities, their interaction with the hematite surface and the effect on polymer adsorption could either be examined directly, or if they are infrared inactive, the effect of their presence on polymer adsorption could be measured. Impurities such as phosphate and sulfate could be examined, but many of the organic impurities, such as humates and smaller acids like oxalate that contain the carboxylate group, would complicate such studies, as they would absorb in the same spectral region as the flocculant. However, it would be feasible to characterise the adsorption of organics that are suspected to adsorb onto gibbsite and affect the crystallisation process.

In studies involving other substrates and adsorbates, several factors need to be taken into account. The deposited substrate may exhibit too high a solubility in the solution phase or have very high absorbance in the spectral region of interest.

Depending on the interacting functional group of the adsorbate, characterisation of the mode of adsorption will be limited by the presence and interpretation of associated peak shifts.

This study has demonstrated that adsorption isotherms and adsorption kinetics can be measured in high pH and high ionic strength solutions, however adsorption densities are limited to relative values. The main hurdle to being able to quantify adsorption densities is an accurate measure of adsorbed polymer thickness and the relative compaction of polymer from solution to adsorbed state. With further research these variables could possibly be quantified, enabling accurate adsorption densities to be measured. Ellipsometry is typically employed as a technique to measure adsorbed polymer thickness, although the technique relies on optically flat, reflective substrates, making it inappropriate for the cast colloidal hematite substrate. Dynamic light scattering could be employed to measure the solution dimensions of the colloidal hematite particles before and after polymer adsorption to determine polymer layer thickness. However, much care must be taken that measurements are made in a regime that avoids particle aggregation, and this may not necessarily correlate with FTIR-ATR adsorption conditions.

The flowcell attachment for the Seagull accessory used in this study is made of stainless steel and comes with a Viton o-ring resulting in solution conditions restricted to the 1-14 pH range. The ZnSe ATR crystal is usually rated within the same pH range, however other researches have applied full strength Bayer liquor to ZnSe ATR crystals without adverse short-term effects. It is possible to obtain a teflon flowcell with a Kalrez o-ring, thus FTIR-ATR may possibly be applied to Bayer liquors at full strength or at elevated temperatures, offering considerable potential for quantifying and comparing the rate and extent of adsorption for different flocculant products (e.g. polyacrylate, hydroxamate, starch) at close to real conditions. A diamond ATR element may need to be employed for elevated temperature work, although these are not yet commercially available for the Seagull ATR accessory and the cost of obtaining one may be prohibitive.

The mechanism of flocculant adsorption on bauxite residue as proposed here is quite distinct from that seen for other mineral systems, and isotherms obtained from FTIR-ATR have indicated that substantially less flocculant adsorbs at high pH. Both

factors, in addition to the adsorption kinetic information may influence the aggregation process. Information gained using the procedures developed in this study may be applied in refinement of the population balance for bauxite residue flocculation currently under development. Within this model the rate and extent of aggregate formation is related to the surface coverage achieved, and this property may be expected to vary for different flocculants products used in the Bayer process. At present, only the particle surface area and the flocculant dosage are used in fitting the model to experimental profiles of aggregate size against reaction time, i.e. the physical behaviour of the flocculant molecules are not directly considered. In this study, the time taken to achieve 50% coverage of the available surface for adsorption of polyacrylates onto hematite were measured. While only a relative measure, the implication is that different flocculant products could be tested and any significant changes will possibly give insight into the dosage and mixing requirements for optimum flocculation. This may ultimately assist in removing some of the empirical nature of the fitted model parameters.

Of particular interest may be a comparison between flocculants containing the hydroxamate functionality and those containing only the carboxylate functionality. Through laboratory work and mostly plant trials (e.g. Phillips, 1999; Rothenberg *et al.*, 1989) it was found that hydroxamated flocculants had the potential to reduce solids in the overflow and just as importantly increased the density of underflow solids (Kahane and McRae, 1996). In addition, the underflow solids were found to show improved rheological properties (Spitzer and Avotins, 1994).

It has been suggested that hydroxamated flocculants exhibit faster adsorption kinetics than their polyacrylate counterparts (e.g. Hurd, Laviolette and Lewellyn, 1994; Perrier *et al.*, 1999; Rothenberg *et al.*, 1989), and while it is assumed to be due to differences in the adsorption mechanism, there have been no studies carried out to this effect. Obviously the protocols established within this study could be applied to characterise both the differences between the mode and rate of adsorption of polyacrylate flocculants compared to those containing the hydroxamate functional group.

11.2 Studies of Other Systems

FTIR-ATR is a versatile tool, ideal for the examination of the solid-liquid interface, and only limited by the suitability of the substrate and the infrared activity of the adsorbate.

The carboxylate functionality within polyacrylate flocculants has been shown to represent an ideal system for FTIR spectroscopic studies, as the shifts in the carboxylate stretching frequencies can be readily related to the likely surface binding structure. However, there is only a limited range of functionalities that behave similarly, e.g. the peak shifts associated with the loss of symmetry when sulfate or phosphate ions chemisorb.

Coating of the IRE with a colloid was sufficient for the study of polymer adsorption, as little polymer diffused into the pores. While the porosity has no bearing on the ability of the technique to derive the mode of adsorption, the absence of polymer diffusion into the pores is essential for the measurement of adsorption isotherms and adsorption kinetics. To derive such information for adsorption of small molecules, a better strategy may be to use a reactive IRE (if possible) or a sputter coated (less porous) IRE element. However, kinetic studies in the past have been limited to reactive IREs, indicating that perhaps the sputter coated IRE also exhibits a degree of porosity.

Measured peak shifts that enable the mode of adsorption to be determined are not necessarily obtainable from the spectra of other molecular or polymeric functionalities that may be encountered (e.g. amide, quaternary amine cation). While the mode of adsorption may not be able to be derived, as long as there is an active infrared band, then the extent of adsorption can be monitored. In such situations some mechanistic information may be derived indirectly from determining the response to varying adsorption conditions (i.e. response to ionic strength, pH, impurities), and under controlled circumstances, provide an indication of the extent of adsorption. Indeed this has been the focus of many previously published applications of FTIR-ATR to adsorption studies.

FTIR-ATR has been shown to be a powerful tool for the *in situ* characterisation of adsorption. Sum frequency spectroscopy is perhaps the only other technique that can

supply equivalent information. This technique is sensitive to molecules that are orientated in the same manner at an interface, hence could possibly detect the adsorbed components of the polymer adsorbed onto a flat surface rather than the loops and tails. Recent advances in sum frequency spectroscopy have given access to the 800 to 4000 cm^{-1} spectral region, and carboxylates bound to sapphire and silica have been detected. However, in both cases these measurements were performed on densely packed Langmuir-Blodgett monolayers in air and the intensity of these modes was weaker than anticipated (Colin D. Bain – Personal Communication). Therefore detecting adsorbed polymer at the solid-liquid interface *in situ* would probably not be feasible.

Computer modelling offers the potential to be a complementary technique. It has been used in the past in these laboratories to examine the adsorption of decandioate on hematite as a model for comparison to polyacrylate adsorption (Jones, 1998). However, the application of molecular modelling has several limitations at present. Due to the extremely large size of polymers, only small polymer segments or related molecules can be modelled. Also, it is restricted to the modelling of uncharged surfaces, which would make it inappropriate in examining the adsorption of polyacrylate onto hematite at high pH and high ionic strength. However, computer modelling is a rapidly developing field and such examinations may be achievable in the near future.

12. REFERENCES

- Adam, U.S. and Robb, I.D. (1983) 'Adsorption and exchange of polyelectrolytes on crystal surfaces', *Journal of the Chemical Society, Faraday Transactions 1*, **79**, 2745-2753.
- Adolphi, U. and Kulicke, W.-M. (1997) 'Coil dimensions and conformation of macromolecules in aqueous media from flow field-flow fractionation/multi-angle laser light scattering illustrated by studies on pullulan', *Polymer*, **38**, 1513-1519.
- Aksberg, R., Einarson, M., Berg, J. and Odberg, L. (1991) 'Adlayer thickness of 2 cationic polyacrylamides adsorbed onto polystyrene lattices', *Langmuir*, **7**, 43-45.
- Alexander, M., Beamson, G., Blomfield, C., Leggett, G. and Duc, T. (2001) 'Interaction of carboxylic acids with the oxyhydroxide surface of aluminium: poly(acrylic acid), acetic acid and propionic acid on pseudoboehmite', *Journal of Electron Spectroscopy and Related Phenomena*, **121**, 19-32.
- Allara, D.L. and Nuzzo, R.G. (1985) 'Spontaneously organized molecular assemblies. 2. Quantitative infrared spectroscopic determination of equilibrium structures of solution-adsorbed *n*-alkanoic acids on an oxidized aluminium surface', *Langmuir*, **1**, 52-66.
- Amhamdi, H., Dumont, F. and Buess-Herman, C. (1997) 'Effect of urea on the stability of ferric oxide hydrosols', *Colloids and Surfaces A: Physicochemical and Engineering Aspects*, **125**, 1-3.
- Atkins, P.W. (1988) *Physical Chemistry*, 3rd Edition, 2nd Reprinting, Oxford University Press, Oxford.
- Au, K.-K., Penisson, A., Yang, S. and O'Melia, C. (1999) 'Natural organic matter at oxide/water interfaces: complexation and conformation', *Geochimica et Cosmochimica Acta*, **63**, 2903-2917.
- Bain, C.D. (13/05/99) Physical and Theoretical Chemistry Laboratory, Oxford University - Personal Communication.

Bajpai, A.K. and Bajpai, S.K. (1995a) 'Kinetics of polyacrylamide adsorption at the iron oxide - solution interface', *Colloids and Surfaces A: Physicochemical and Engineering Aspects*, **101**, 21-28.

Bajpai, A.K. and Bajpai, S.K. (1995b) 'Dynamic measurements of adsorption of hydrolyzed polyacrylamide (HPAM) onto hematite', *Colloid and Polymer Science*, **273**, 1028-1032.

Basu, P., Nitowski, G.A. and The, P.J. (1986) 'Chemical interactions of iron minerals during Bayer digest and clarification', In *Iron Control in Hydrometallurgy*, (eds. J.E. Dutrizac and A.J. Monhemius), Ellis Horwood Limited, Chichester, pp. 223-244.

Bayer, K.J. (1888), *German Patent*, Patent No. 43,977.

Berube, Y.G. and de Bruyn, P.L. (1968) 'Adsorption at the rutile-solution interface. II. Model of the electrochemical double layer', *Journal of Colloid and Interface Science*, **28**, 92-105.

Bohmer, M., Evers, O. and Scheutjens, J. (1990) 'Weak polyelectrolytes between two surfaces: adsorption and stabilization', *Macromolecules*, **23**, 2288-2301.

Boisvert, J.-P., Malgat, A., Pochard, I. and Daneault, C. (2002) 'Influence of the counter-ion on the effective charge of polyacrylic acid in dilute conditions', *Polymer*, **43**, 141-148.

Breeuwsma, A. and Lyklema, J. (1971) 'Interfacial electrochemistry of haematite (α -Fe₂O₃)', *Discussions of the Faraday Society*, **52**, 324-333.

Brown, R.W. (1942), 'Alumina Recovery Process', *United States Patent*, Patent No. 2,280,998.

Brookhaven Instrument Corporation homepage, world wide web location: <http://www.bic.com/zoper.htm>.

Brookhaven ZetaPlus technician, University of New South Wales - Personal Communication, Jason Scott (16/08/01).

Bublik, E., Happs, C., Odor, G., Revesz, L. and Sartowski, Z. (1986) 'The use of synthetic polymers in alumina production', In *Fifth Yugoslav International Symposium on Aluminium*, pp. 505-517.

Chvedov, D., Ostap, S. and Le, T. (2001) 'Surface properties of red mud particles from potentiometric titration', *Colloids and Surfaces A: Physicochemical and Engineering Aspects*, **182**, 131-141.

Coast, R., Pikus, M., Henriksen, P.N. and Nitowski, G.A. (1996) 'Vibrational spectroscopic observation of acrylic acid coadsorbed in dissociated and molecular forms on oxidised aluminum', *The Journal of Physical Chemistry*, **100**, 15011-15014.

Cohen Stuart, M.A., Fler, G.J. and Bijsterbosch, B.H. (1982) 'The adsorption of poly(vinyl pyrrolidone) onto silica. I. Adsorbed amount', *Journal of Colloid and Interface Science*, **90**, 310-320.

Colloidal Dynamics homepage, world wide web location: <http://www.colloidal-dynamics.com/index.htm>.

Connelly, L.J., Owen, D.O. and Richardson, P.F. (1986) 'Synthetic flocculant technology in the Bayer process', *Light Metals*, 247-261.

Connor, P. and McQuillan, A. (1999) 'Phosphate adsorption onto TiO₂ from aqueous solutions: an *in situ* internal reflection infrared spectroscopic study', *Langmuir*, **15**, 2916-2921.

Cosgrove, T., Obey, T.M. and Vincent, B. (1986) 'The configuration of sodium poly(styrene sulfonate) at polystyrene/solution interfaces', *Journal of Colloid and Interface Science*, **111**, 409-418.

CRC Handbook of Chemistry and Physics, 3rd electronic edition, Editor-in-Chief: David R. Lide, world wide web location: <http://www.hbcpnetbase.com/hbcp/>.

Crees, O., Senogles, E. and Whayman, E. (1991) 'The flocculation of cane sugar muds with acrylamide-sodium acrylate copolymers', *Journal of Applied Polymer Science*, **42**, 837-844.

Davis, J.A. and Hem, J.D. (1989) 'The surface chemistry of aluminum oxides and hydroxides', In *The Environmental Chemistry of Aluminum*, (ed. G. Sposito), CRC Press, Boca Raton, Florida, pp. 185-219.

Deacon, G.B. and Phillips, R.J. (1980) 'Relationship between the carbon-oxygen stretching frequencies of carboxylato complexes and the type of carboxylate coordination', *Coordination Chemistry Reviews*, **33**, 227-250.

Derjaguin, B. and Landau, L. (1941) 'Theory of the stability of strongly charged lyophobic sols and of the adhesion of strongly charged particles in solutions of electrolytes', *Acta Physicochimica U.R.S.S.*, **14**, 633-662.

Dobson, K.D. and McQuillan, A.J. (1999) '*In situ* infrared spectroscopic analysis of the adsorption of aliphatic carboxylic acids to TiO₂, ZrO₂, Al₂O₃, and TaO₅ from aqueous solutions', *Spectrochimica Acta A*, **55**, 1395-1405.

Drzymala, J. and Fuerstenau, D.W. (1987) In *Flocculation in Biotechnology and Separation Systems*, (ed. Y.A. Attia), Elsevier Science Publishers B.V., Amsterdam, pp. 45-60.

Dumont, F., Dang Van Tan, and Watillon, A. (1976) 'Study of ferric oxide hydrosols from electrophoresis, coagulation, and peptization measurements', *Journal of Colloid and Interface Science*, **55**, 678-687.

Eirich, F.R. (1977) 'The conformational states of macromolecules adsorbed at solid-liquid interfaces', *Journal of Colloid and Interface Science*, **58**, 423-436.

Feldman, A., Horowitz, D., Waxler, R. and Dodge, M. (1979) 'Optical materials characterization final technical report, February 1, 1978 – September 30, 1978', *National Bureau of Standards (U.S.) Technical Note #993*, 71 pages.

Filippova, N. (1999) 'Adsorption kinetics of polyelectrolytes on planar surfaces under flow conditions', *Journal of Colloid and Interface Science*, **211**, 336-354.

Free, M.L. and Miller, J.D. (1997) 'Kinetics of 18-carbon carboxylate adsorption at the fluorite surface', *Langmuir*, **13**, 4377-4382.

Golikova, E., Ioganson, O., Duda, L., Osmolovskii, M., Yanklovich, A. and Chernoberezhskii, Y. (1998) 'Aggregation stability of aqueous dispersions of α -Fe₂O₃, α -FeOOH, and Cr₂O₃ under conditions of the isoelectric state', *Colloid Journal*, **60**, 166-171.

Gong, W.Q., Parentich, A., Little, L.H. and Warren, L.J. (1991) 'Diffuse reflectance infrared Fourier transform spectroscopic study of the adsorption mechanism of oleate on haematite', *Colloids and Surfaces*, **60**, 325-339.

Goplen, T.G., Cameron, D.G. and Jones, R.N. (1980) 'Absolute absorption intensity and dispersion measurements on some organic liquids in the infrared', *Applied Spectroscopy*, **34**, 657-691.

Greenwood, R. and Kendall, K. (2000) 'Effect of ionic strength on the adsorption of cationic polyelectrolytes onto alumina studied using electroacoustic measurements', *Powder Technology*, **113**, 148-157.

Hansen, W.N. (1965) 'Expanded formulas for attenuated total reflection and the derivation of absorption rules for single and multiple ATR spectrometer cells', *Spectrochimica Acta*, **21**, 815-833.

Harrick, N.J. (1987) *Internal Reflection Spectroscopy*, 3rd Printing, Harrick Scientific Corporation, New York.

Harrick Scientific Corporation - Personal Communication, Sue Berets (18/04/01).

Heath, A. (2002) *The Simulation of Polymer Aggregation/Breakage Kinetics in Turbulent Flow by Population Balance*, PhD Thesis, Murdoch University.

Hecker, R., Fawell, P.D., Jefferson, A. and Farrow, J.B. (1999) 'Flow field-flow fractionation of high-molecular-mass polyacrylamide', *Journal of Chromatography A*, **837**, 139-151.

Hind, A. and Bhargava, S. (2000) 'The adsorption of sodium oxalate stabilisers to the surface of gibbsite (a Bayer process solid) under high ionic strength, high pH conditions', *Light Metals*, 65-70.

Hind, A., Bhargava, S. and Grocott, S. (1997a) 'Attenuated total reflection Fourier transform infrared spectroscopic investigation of the solid/aqueous interface of low surface area, water-soluble solids in high ionic strength, high alkaline, aqueous media', *Langmuir*, **13**, 3483-3487.

Hind, A., Bhargava, S. and Grocott, S. (1997b) 'Adsorption of quaternary ammonium compounds on the surface of sodium oxalate: FTIR/ATR investigation under high-ionic-strength, highly alkaline conditions', *Langmuir*, **13**, 6255-6259.

Hind, A., Bhargava, S. and McKinnon, A. (2001) 'At the solid/liquid interface: FTIR/ATR – the tool of choice', *Advances in Colloid and Interface Science*, **93**, 91-114.

Hogg, R. (1999) 'The role of polymer adsorption kinetics in flocculation', *Colloids and Surfaces A: Physicochemical and Engineering Aspects*, **146**, 253-263.

Hood, G. and Willemon, G. (1987) 'Dewatering of red mud', In *Flocculation in Biotechnology and Separation Systems*, (ed. Y.A. Attia), Elsevier Science Publishers B.V., Amsterdam, pp. 773-791.

Hug, S. (1997) 'In situ Fourier transform infrared measurements of sulfate adsorption on hematite in aqueous solutions', *Journal of Colloid and Interface Science*, **188**, 415-422.

Hug, S. and Sulzberger, B. (1994) 'In situ Fourier transform infrared spectroscopic evidence for the formation of several different surface complexes of oxalate on TiO₂ in the aqueous phase', *Langmuir*, **10**, 3587-3597.

Hunter, R.J. (1981) *Zeta Potential in Colloid Science*, Academic Press Inc., London.

Hunter, R.J. (1993) *Introduction to Modern Colloid Science*, Oxford University Press, Oxford.

Hunter, T.K., Moody, G.M. and Tran, C.A. (1990), 'Advances in liquor clarification and mud flocculation in the Bayer process alumina industry', In *Proceedings Second International Alumina Quality Workshop*, Perth, W.A., October 14-19, pp. 394-404.

Hurd, M.D., Laviolette, L.H. and Lewellyn, M.E. (1994) 'Making emulsion polymers work better in the Bayer process', *Light Metals*, 117-120.

ImageJ - world wide web location: <http://rsb.info.nih.gov/nih-image/>.

Johnson, S., Scales, P. and Healy, T. (1999) 'The binding of monovalent electrolyte ions on α -alumina. I. Electroacoustic studies at high electrolyte concentrations', *Langmuir*, **15**, 2836-2843.

Jones, F. (1998) *The Mechanism of Bayer Residue Flocculation*, PhD Thesis, Curtin University of Technology.

Jones, F., Farrow, J.B. and van Bronswijk, W. (1998a) 'Flocculation of haematite in synthetic Bayer liquors', *Colloids and Surfaces A: Physicochemical and Engineering Aspects*, **135**, 183-192.

Jones, F., Farrow, J.B. and van Bronswijk, W. (1998b) 'Effect of caustic and carbonate on the flocculation of haematite in synthetic Bayer liquors', *Colloids and Surfaces A: Physicochemical and Engineering Aspects*, **142**, 65-73.

Jones, F., Farrow, J.B. and van Bronswijk, W. (1998c) 'An infrared study of a polyacrylate flocculant adsorbed on hematite', *Langmuir*, **14**, 6512-6517.

Jones, R.L., Marwood, T.M. and Horsley, R.R. (1994) 'Red mud rheology – the behaviour of iron(III) oxide suspensions in strongly alkaline solutions', In *Proceedings of the Fourth European Rheology Conference, Progress and Trends in Rheology IV*, Sevilla, pp. 660-662.

Kahane, R.B. (1992) 'Effective flocculation in a counter current decantation circuit', In *An International Bauxite Tailings Workshop*, November, Perth, Australian Bauxite and Alumina Producers, pp. 13-23.

Kahane, R.B. and McRae, C. (1996) 'Improved bauxite residue settler performance at Worsley Alumina', In *Proceedings of the Fourth Alumina Quality Workshop*, Darwin, pp. 227-237.

- Kan, S., Yu, S., Peng, X., Zhang, X., Li, D., Xiao, L., Zou, G. and Li, T. (1996) 'Formation process of nanometer-sized cubic ferric oxide single crystals', *Journal of Colloid and Interface Science*, **178**, 673-680.
- Khangaonkar, P.R. and Bala Subramani, K.J. (1993) 'Flocculation of hematite fines by anionic polyacrylamide polymers', *Minerals Engineering*, **6**, 765-774.
- Kheradmand, H. and Francois, J. (1988) 'Degradation of acrylamide-sodium acrylate copolymer in aqueous solution', *Journal of Applied Polymer Science*, **36**, 1583-1600.
- Kitchener, J.A. (1972) 'Principles of action of polymeric flocculants', *British Polymer Journal*, **4**, 217-229.
- Kolthoff, I.M., Sandell, E.B., Meehan, E.J. and Bruckenstein, S. (1971) *Quantitative Chemical Analysis*, 4th Edition, 2nd Printing, The Macmillan Company, New York.
- Kulicke W.-M. and Horl, H.-H. (1985) 'Preparation and characterization of a series of poly(acrylamide-co-acrylates), with a copolymer composition between 0-96.3 mol-% acrylate units with the same degree and distribution of polymerization', *Colloid and Polymer Science*, **263**, 530-540.
- Kulicke W.-M. and Kniewske, R. (1981) 'Long-term change in conformation of macromolecules in solution, 2, *Makromolekulare Chemie*, **182**, 2277-2287.
- Kuys, K. and Roberts, N. (1987) 'In situ investigation of the adsorption of styrene phosphonic acid on cassiterite by FTIR-ATR spectroscopy', *Colloids and Surfaces*, **24**, 1-17.
- Kuzmenka, D. and Granick, S. (1988) 'Kinetics of polymer adsorption measured *in situ* at the solid-liquid interface: utility of the infrared total internal reflection method', *Colloids and Surfaces*, **31**, 105-116.
- La Mer, V.K. and Healy, T.W. (1963) 'Adsorption-flocculation reactions of macromolecules at the solid-liquid interface', *Reviews of Pure and Applied Chemistry*, **13**, 112-133.
- Laird, D.A. (1997) 'Bonding between acrylamide and clay mineral surfaces', *Soil Science*, **162**, 826-832.

- Langmuir, I. (1918) 'The adsorption of gases on plane surfaces of glass, mica and platinum', *Journal of the American Chemical Society*, **40**, 1361-1403.
- Leadley, S.R. and Watts, J.F. (1997) 'The use of XPS to examine the interaction of poly(acrylic acid) with oxidised metal substrates', *Journal of Electron Spectroscopy and Related Phenomena*, **85**, 107-121.
- Lee, D.H., Condrate Snr., R.A. and Reed, J.S. (1996) 'Infrared spectral investigation of polyacrylate adsorption on alumina', *Journal of Materials Science*, **31**, 471-478.
- Lee, L.T. and Somasundaran, P. (1989) 'Adsorption of polyacrylamide on oxide materials', *Langmuir*, **5**, 854-860.
- Lentz, E. (1995) In *Infrared and Raman Spectroscopy*, (ed. B. Schrader), VCH, Weinheim.
- Li, L.Y. (1998) 'Properties of red mud tailings produced under varying process conditions', *Journal of Environmental Engineering*, **124**, 254-264.
- Li, L.Y. (2001) 'A study of iron mineral transformation to reduce red mud tailings', *Waste Management*, **21**, 525-534.
- Lorenzelli, V., Busca, G. and Sheppard, N. (1980) 'Infrared study of the surface reactivity of hematite', *Journal of Catalysis*, **66**, 28-35.
- Lyklema, J. (1985) 'How polymers adsorb and affect colloid stability', In *Flocculation, Sedimentation and Consolidation, Proceedings of the Engineering Foundation Conference*, Georgia, pp. 3-21.
- Lyklema, J. (1989) 'The colloidal background of flocculation and dewatering', In *Flocculation and Dewatering*, Engineering Foundation, New York, USA, pp. 1-20.
- Lyklema, J. and Fleer, G.J. (1987) 'Electrical contributions to the effect of macromolecules on colloid stability', *Colloids and Surfaces*, **25**, 369-385.
- Mathur S. and Moudgil, B.M. (1998), 'Mechanism of nonionic polymer adsorption on oxide surfaces', *Minerals and Metallurgical Processing*, **15**, 24-28.

Misra, D.N. (1996) 'Adsorption of polyacrylic acids and their sodium salts on hydroxyapatite: effect of relative molar mass', *Journal of Colloid and Interface Science*, **181**, 289-296.

Moss, N. and Dymond, B. (1978) 'Flocculation: theory and application', *Mine and Quarry Journal*, May, 1-8.

Neivandt, D. and Gee, M. (1995) 'Variable angle of incidence evanescent wave spectroscopy of the adsorption of quaternarized poly(vinylpyridine) on silica', *Langmuir*, **11**, 1291-1296.

Nonlinear Least Squares Curve Fitter – world wide web location:
<http://m2.aol.com/johnp71/nonlin.html>.

Papenhuijzen, J., van der Schee, H. and Fler, G. (1985a) 'Polyelectrolyte adsorption. I. A new lattice theory', *Journal of Colloid and Interface Science*, **104**, 540-552.

Papenhuijzen, J., van der Schee, H. and Fler, G. (1985b) 'Polyelectrolyte adsorption. II. Comparison of experimental results for polystyrene sulfonate, adsorbed on polyoxymethylene crystals, with theoretical predictions', *Journal of Colloid and Interface Science*, **104**, 553-561.

Parker, R.W. and Frost, R.L. (1996) 'The application of DRIFT spectroscopy to the multicomponent analysis of organic chemicals adsorbed on montmorillonite', *Clays and Clay Minerals*, **44**, 32-40.

Parsons, D., Harrop, R. and Mahers, E. (1992) 'The kinetics of particle and polymer adsorption by total internal reflection fluorescence', *Colloids and Surfaces*, **64**, 151-160.

Pearse, M.J. and Sartowski, Z. (1984) 'Application of special chemicals (flocculants and dewatering aids) for red mud separation and hydrate filtration', In *Bauxite: Proceedings of the 1984 Bauxite Symposium*, Los Angeles, California, pp. 788-810.

Perrier, X., Cristol, B., Cuneo-Raffaelli, A. and Dountsis, P. (1999) 'Settler throughput increase at Aluminium de Grece refinery', *Light Metals*, 63-69.

Phillips, E.C. (1999) 'New water-continuous red mud flocculants for the Bayer process', *Light Metals*, 39-43.

Pochard, I., Boisvert, J.-P., Malgat, A. and Daneault, C. (2001) 'Donnan equilibrium and the effective charge of sodium polyacrylate', *Colloid and Polymer Science*, **279**, 850-857.

Polymer Handbook (1999) 4th edition, Editors: Brandrup, J., Immergut, E.h. and Grulke, E.A., John Wiley and Sons, Inc., New York.

Pugh, R.J. and Lundström, H. (1987) In *Flocculation in Biotechnology and Separation Systems*, (ed. Y.A. Attia), Elsevier Science Publishers B.V., Amsterdam, pp. 673-694.

Rangaraj, A., Vangani, V. and Rakshit, A.K. (1997) 'Synthesis and characterization of some water soluble polymers', *Journal of Applied Polymer Science*, **66**, 45-56.

Reed, W. (1995) 'Data evaluation for unified multi-detector size exclusion chromatography – molar mass, viscosity and radius of gyration distributions', *Makromolekulare Chemie*, **196**, 1539-1575.

Rochester, C.H. and Topham, S.A. (1979) 'Infrared study of surface hydroxyl groups on hematite', *Journal of the Chemical Society, Faraday Transactions 1*, **75**, 1073-1088.

Roddick-Lanzilotta, A. and McQuillan, A. (2000) 'An *in situ* infrared spectroscopic study of glutamic acid and of aspartic acid adsorbed on TiO₂: implications for the biocompatibility of titanium', *Journal of Colloid and Interface Science*, **227**, 48-54.

Rothenberg, A.S., Spitzer, D.P., Lewellyn, M.E. and Heitner, H.T. (1989) 'New reagents for alumina processing', *Light Metals*, 91-96.

Rowlands, W., O'Brien, R., Hunter, R. and Patrick, V. (1997) 'Surface properties of aluminum hydroxide at high salt concentration', *Journal of Colloid and Interface Science*, **188**, 325-355.

Sankey, S.E. and Schwarz, R.J. (1984) 'The use of synthetic flocculant polymers in settling red muds derived from high goethite bauxite ores', *Light Metals*, 1653-1667.

Santhiya, D., Nandini, G., Subramanian, S., Natarajan, K.A. and Malghan, S.G. (1998) 'Effect of polymer molecular weight on the adsorption of polyacrylic acid at the alumina-water interface', *Colloids and Surfaces A: Physicochemical and Engineering Aspects*, **133**, 157-163.

Scott, J.P., Fawell, P.D., Ralph, D.E. and Farrow, J.B. (1996) 'The shear degradation of high-molecular-weight flocculant solutions', *Journal of Applied Polymer Science*, **62**, 2097-2106.

Shaw, D.J. (1992) *Introduction to Colloid and Surface Chemistry*, 4th ed., Butterworth-Heinemann, Oxford.

Sibert, F. (1968) 'Process of making alumina', *United States Patent*, Patent No. 3,390,959.

Specht, C.H. and Frimmel, F.H. (2001) 'An *in situ* ATR-FTIR study on the adsorption of dicarboxylic acids onto kaolinite in aqueous suspensions', *Physical Chemistry Chemical Physics*, **3**, 5444-5449.

Sperline, R.P. (12/02/02) Chemistry Department, University of Arizona - Personal Communication.

Sperline, R. and Freiser, H. (1995) 'Infrared attenuated total reflection spectroscopy of surface active species', In *The Handbook of Surface Imaging and Visualization*, (ed. A.T. Hubbard), CRC Press, Boca Raton, Florida, pp. 245-263.

Sperline, R., Muralidharan, S. and Freiser, H. (1986) 'New quantitative technique for attenuated total reflection (ATR) spectrophotometry; calibration of the "CIRCLE" ATR device in the infrared', *Applied Spectroscopy*, **40**, 1019-1022.

Sperline, R., Muralidharan, S. and Freiser, H. (1987) '*In situ* determination of species adsorbed at a solid-liquid interface by quantitative infrared attenuated total reflectance spectrophotometry', *Langmuir*, **3**, 198-202.

Sperline, R., Song, Y. and Freiser, H. (1992) 'Fourier transform infrared attenuated total reflection spectroscopy linear dichroism study of sodium dodecyl sulfate adsorption at the Al_2O_3 /water interface using Al_2O_3 -coated optics', *Langmuir*, **8**, 2183-2191.

Spitzer, D.P. and Avotins, P.V. (1994) 'Effect of polymers on flow properties of Bayer process underflow muds', *Light Metals*, 1225-1230.

Stumm, W. (1992) *Chemistry of the Solid-Water Interface*, Wiley-Interscience Publication, New York.

Subramanian, S. and Natarajan, K.A. (1989) 'Adsorption behaviour of an oxidised starch onto hematite in the presence of calcium', *Minerals Engineering*, **2**, 55-64.

Swift, J.D., Simic, K., Johnston, R.R.M., Fawell, P.D. and Farrow, J.B. (2002) 'A study of the polymer flocculation reaction in a linear pipe with a focused beam reflectance measurement probe', Submitted *International Journal of Mineral Processing*.

Tickanen, L.D., Tejedor-Tejedor, M.I. and Anderson, M.A. (1992) 'Concurrent determination of optical constants and the Kramers-Kronig integration constant (anchor point) using variable-angle ATR/FT-IR spectroscopy', *Applied Spectroscopy*, **46**, 1848-1858.

Tien, C. (1994) *Adsorption Calculations and Modeling*, Butterworth-Heinemann, Boston.

Tscharnutter, W., McNeil-Watson, F. and Fairhurst, D. (1998) 'A new instrument for the measurement of very small electrophoretic mobilities using phase analysis light scattering', In *Particle Size Distribution (III): Assessment and Characterisation*, (ed. T. Provder), American Chemical Society, Washington D.C., pp. 327-340.

Tscharnutter, W. (2001) 'Mobility measurements by phase analysis', *Applied Optics*, **40**, 3995-4003.

- Underhill, R. and Timsit, R.S. (1992) 'Interaction of aliphatic acids and alcohols with aluminum surfaces', *Journal of Vacuum Science and Technology, Part A*, **10**, 2767-2774.
- Vermohlen, K., Lewandowski, H., Narres, H. and Schwuger, M. (2000a) 'Adsorption of polyelectrolytes onto oxides – the influence of ionic strength, molar mass, and Ca^{2+} ions', *Colloids and Surfaces A: Physicochemical and Engineering Aspects*, **163**, 45-53.
- Vermohlen, K., Lewandowski, H., Narres, H. and Koglin, E. (2000b) 'Adsorption of polyacrylic acid on aluminium oxides: DRIFT spectroscopy and ab initio calculations', *Colloids and Surfaces A: Physicochemical and Engineering Aspects*, **170**, 181-189.
- Verrall, K., Warwick, P. and Fairhurst, A. (1999) 'Application of the Schulze-Hardy rule to haematite and haematite/humate colloid stability', *Colloids and Surfaces A: Physicochemical and Engineering Aspects*, **150**, 261-273.
- Verwey, E. and Overbeek, J. (1948) *Theory of the Stability of Lyophobic Colloids*, Elsevier Publishing Company, Inc., New York.
- Walles, W. (1968) 'Role of flocculant molecular weight in the coagulation of suspensions', *Journal of Colloid and Interface Science*, **27**, 797-803.
- Wang, T.K. and Audebert, R. (1988) 'Adsorption of cationic copolymers of acrylamide at the silica-water interface: hydrodynamic layer thickness measurements', *Journal of Colloid and Interface Science*, **121**, 32-41.
- Wyatt, P. (1993) 'Light scattering and the absolute characterization of macromolecules', *Analytica Chimica Acta*, **272**, 1-40.
- Yamada, K., Harato, T. and Shiozaki, Y. (1980) 'Flocculation and sedimentation of red mud', *Light Metals*, 39-50.
- Zhang, J.W. and Buffle, J. (1995) 'Kinetics of hematite aggregation by polyacrylic acid – importance of charge neutralization', *Journal of Colloid and Interface Science*, **174**, 500-509.

Zhou, N.F., Chen, L.-W., Wang, Y.-S. and Jiang, J.-S. (1994) 'Magnetization and Mössbauer spectroscopic study of adsorption of oxalic acid on α -Fe₂O₃ from solutions', *Chemical Physics Letters*, **224**, 595-601.

APPENDIX A

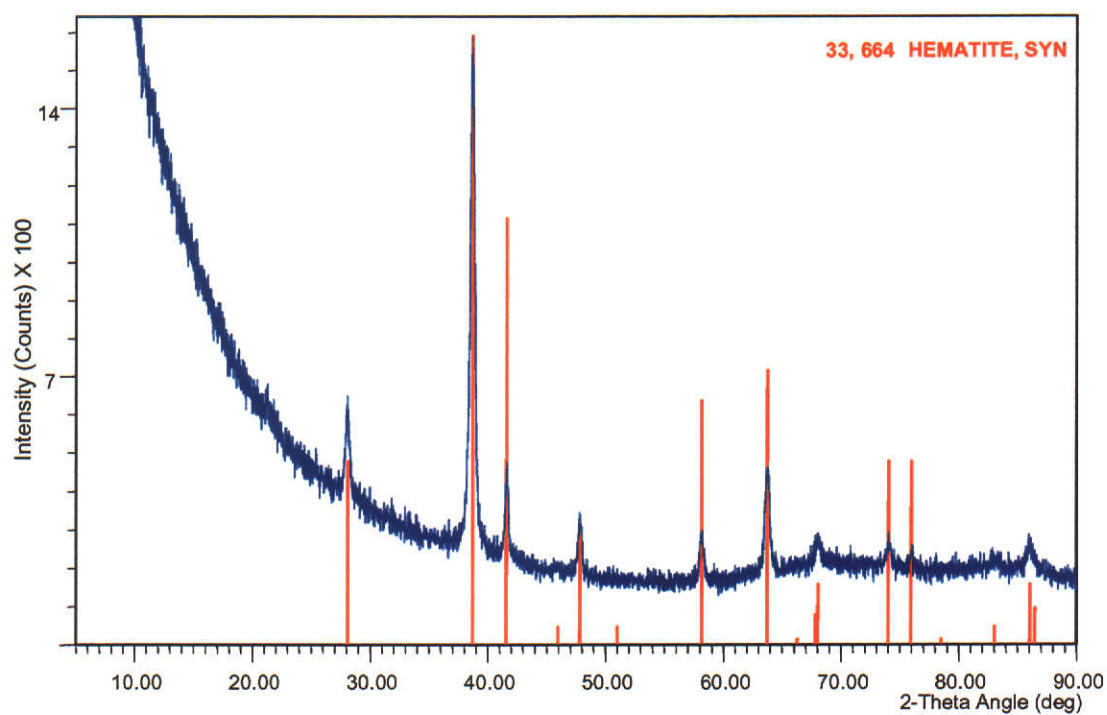
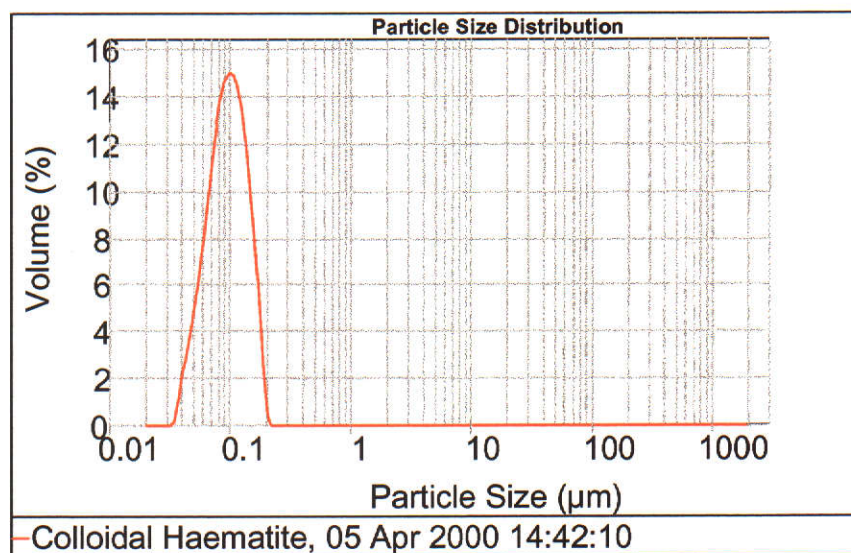


Figure A: Typical X-ray Diffractogram obtained for the colloidal hematite samples prepared in this study. The red lines represent peak positions obtained for a synthetic hematite reference sample (PDF number 33, 664).

APPENDIX B



Size (μm)	Volume In %	Size (μm)	Volume In %
0.010	0.00	0.105	13.25
0.011	0.00	0.120	11.92
0.013	0.00	0.138	9.29
0.015	0.00	0.158	5.84
0.017	0.00	0.182	1.63
0.020	0.00	0.209	0.00
0.023	0.00	0.240	0.00
0.026	0.00	0.275	0.00
0.030	0.00	0.316	0.00
0.035	0.00	0.363	0.00
0.040	0.83	0.417	0.00
0.046	2.44	0.479	0.00
0.052	4.02	0.550	0.00
0.060	5.96	0.631	0.00
0.069	8.24	0.724	0.00
0.079	10.69	0.832	0.00
0.091	12.49	0.955	0.00
0.105	13.39	1.096	0.00

Figure B: Particle size distribution obtained for second hematite colloid prepared (typical of all colloids prepared).